STUDIES OF DEEP-SEA SEDIMENTARY MICROTOPOGRAPHY

IN THE NORTH ATLANTIC OCEAN

by

ROGER DONALD FLOOD

.S.B., Massachusetts Institute of Technology
(1972)

SUBMITTED IN PARTIAL FULFILLMENT OF THE
REQUIREMENTS FOR THE DEGREE OF
DOCTOR OF PHILOSOPHY

at the

MASSACHUSETTS INSTITUTE OF TECHNOLOGY

and the

WOODS HOLE OCEANOGRAPHIC INSTITUTION

January, 1978

Signature of Author . . . .
    Joint Program in Oceanography, Massachusetts Institute
    of Technology/Woods Hole Oceanographic Institution and
    Department of Earth and Planetary Sciences, and Depart-
    ment of Meterology, Massachusetts Institute of Technology,
    January, 1978.

Certified by . . . .
                                            Thesis Supervisor

Accepted by . . . .
    Chairman, Joint Oceanography Committee in the Earth
    Sciences, Massachusetts Institute of Technology/Woods
    Hole Oceanographic Institution

STUDIES OF DEEP-SEA SEDIMENTARY MICROTOPOGRAPHY IN THE NORTH ATLANTIC OCEAN

Roger Donald Flood

Submitted to the Massachusetts Institute of Technology-Woods Hole Oceanographic Institution Joint Program in Oceanography on January 20, 1978, in partial fulfillment of the requirements for the degree of Doctor of Philosophy.

ABSTRACT

Many of the small-scale topographic features (dimensions of centimeters to kilometers) found on the Blake-Bahama Outer Ridge (western North Atlantic, water depth greater than 4000 m) and in the Rockall Trough (northeastern North Atlantic, water depth greater than 2000 m) have been formed as bed forms of deep currents. These bed forms, all developed in cohesive sediments, include current ripples (spacings of tens of centimeters, formed transverse to the flow), longitudinal triangular ripples (spacings of meters, formed in sandy muds and parallel to the flow), furrows (spacings of tens to 100's of meters, formed parallel to the flow and presently either erosional or depositional), and regular sediment waves (spacings of a few kilometers, now found oblique to the flow and migrating either upstream or downstream). The local distribution of any given bed form is influenced by the presence of larger features. Bed forms are often found in zones which strike parallel to the regional contours.

Debris flows, affecting areas of 1000's to 10,000's of square kilometers, are also present in these areas. A debris flow studied in the Rockall Trough is erosional at its shallowest depths and depositional at greater depths. Gravitational flows strike perpendicular to the contours. Pockmarks (tens of meters in diameter, marking fluid seeps) are also found on the Blake-Bahama Outer Ridge.

The larger topographic features (greater than several meters) with steep slopes (greater than about 20°) can be observed on surface echo-sounding profiles either as fields of regular hyperbolic echoes (e.g., echoes from regularly spaced furrows), fields of irregularly spaced, dissimilar hyperbolae (e.g., echoes from blocks, ridges, and folds in debris flows), or as regular features whose structure is often obscured by side echoes (e.g., echoes from sediment waves). Although near-

bottom investigations are required to describe the features, the nature of the sea floor can often be inferred from the character of the echo-sounding profile. Similar echo-sounding records in different areas of the ocean indicate the presence of similar sea-floor features.

The morphology of the bed forms studied and the current and temperature structure of the overlying water column lead to conclusions about bed form origin and present-day inter-actions with deep currents.

Furrows form as erosional bed forms during high-velocity (>20? cm/sec) current events by large, helical secondary circulations in the bottom boundary layer. Once formed, furrows may develop into depositional features, or they may continue as erosional ones, depending on the local currents and the sediment supply.

Large, regular sediment waves may be formed at current speeds of 5 to 10 cm/sec by lee waves generated by topographic irregularities on the sea floor, such as submarine canyons, or by instabilities in the flow of deep, contour-following currents. Sediment waves develop where there is an abundant supply of sediment and steady mean currents. Waves appear to migrate upstream where tidal current fluctuations are smaller than the mean velocity, and downstream where they are larger. Near-bottom currents appear to be faster on the downstream side of upstream-migrating sediment waves than on their upstream side. The resulting variations in bed shear stress lead to higher sedimentation rates on the upstream side and bed form migration in that direction.

Thesis Supervisor: Dr. Charles D. Hollister
Title: Associate Scientist

ACKNOWLEDGEMENTS

were prepared by W.H.O.I. graphic arts and a few by N. Flood.

Finally, I would like to express my appreciation to M.I. Scranton for her continued support throughout this study.

TABLE OF CONTENTS

Page

LIST OF FIGURES

15

LIST OF TABLES

Table		Page
2.1	Cores in BBOR study areas	118
2.2	Carbon-14 dates (KN31 Cores)	133
2.3	Bulk mineralogy of detrital fraction (KN31 Cores)	141
2.4	Clay mineralogy (KN31 Cores)	143
2.5	BBOR current meter summary	162
2.6	Sediment wave temperature profiles: data and results	182
2.7	Bed forms – Blake-Bahama Outer Ridge	209
3.1	Cores in Rockall Trough study areas.	270
3.2	C-14 dates, KN51-19GPC	285
A3.1	Bulk X-ray mineralogy, KN31-GPC 7.	391
A3.2	Bulk X-ray mineralogy, KN31-GPC 8.	391
A3.3	Bulk X-ray mineralogy, KN31-GPC 9.	392
A3.4	Bulk X-ray mineralogy, KN31-GPC 11	393
A3.5	Bulk X-ray mineralogy, KN31-GPC 12 and KC 13 . .	393

CHAPTER I

INTRODUCTION

Sea floor features in abyssal depths with dimensions less than several kilometers are not adequately resolved on conventional surface-ship echo sounders (Appendix I). Also, features larger than a few meters are often missed with conventional bottom photography. As a result, the form and structure of the abyssal sea floor on scales from a few meters to a few kilometers is poorly known. It is important to accurately determine this morphology, since these topographic forms result from processes which occur in the abyss. In addition to learning more about the topographic forms (microtopography), we also seek to derive interpretations about those processes which have occured or which are occuring. Little is known of the range of surface morphologies present in deep-sea sedimentary areas, including the continental margin and other large sedimentary accumulations.

Previous studies of the sea floor have often described the sediment surface in terms of the way it reflects sound (echo character) and how it appears in bottom photographs. Since the development of high-resolution echo-sounding recorders in the 1950's (Luskin et al., 1954; Knott and Hersey, 1956), marine geologists have been characterizing and mapping different types of sea floor features on the basis of their echo returns. The echo return is thought to be some function of both small-scale topography and sediment type, and characteristics of

echo-sounding profiles recorded by conventional wide-beam profilers can be used to discern some properties of the sea-floor relief (Appendix I.D). These short-ping (less than 5 milliseconds) high frequency (3.5 to 12 kHz) echograms have been used as a basis for inferences concerning erosional, depositional, and other processes active on the sea floor. The continental margin is one area where such a technique has proved especially useful for delineating sedimentologically active areas.

Classification of echo types recorded in sedimentary areas is generally based on three criteria. (1) Coherence of the echo return (i.e., whether the echo from a single sound pulse consists of one return or of many closely spaced returns). (2) Presence of side echoes, hyperbolic echoes in particular, from discrete topographic features below the resolution of the echo sounder. (3) Wavelength, height, spacing, and regularity, or lack thereof, of any discernable sea floor relief. Echo character classification schemes have been employed by several investigators, starting with Hollister (1967) and continuing most recently with Clay and Leong (1974) and Damuth (1975). However, the morphology of the sea floor responsible for various echo patterns has been rarely determined.

The hyperbolic echo is perhaps the most perplexing feature described from echo-sounding records (Appendix I.A). Large, regular hyperbolae, presumably originating from sedimen-

tary topography, were first reported from the western North Atlantic by Heezen et al. (1959). Pratt and Heezen (1964) suggested that these hyperbolic echoes resulted from sand dunes. Hyperbolic echoes were reported from an otherwise smooth sea floor near Madeira by Laughton (1962). Clay and Rona (1964) deduced that the hyperbolae on the Blake-Bahama Outer Ridge resulted from a series of parallel linear ridges and suggested that the ridges might be sand dunes. Hollister (1967) and Hollister and Heezen (1972) mapped the distribution of echo types on the Nova Scotian Continental Rise and noted that the zones of hyperbolae were elongated parallel to the contours. The zone of most intense hyperbolic echoes corresponded to the coldest near-bottom potential temperatures, suggesting that the features which produced these hyperbolae were related to the deep, contour-following currents or related water masses. Similar hyperbolic echoes have often been associated with some type of current-produced feature (e.g., Damuth, 1975a), although the nature of the sea floor remained unknown until recently (Hollister et al., 1974a; Flood and Hollister, 1974; Hollister et al., 1976; this study).

Some types of hyperbolic echo returns and hummocky topography have also been associated with down-slope gravitational sediment movements such as slumps, slides, and debris flows (Walker and Messingill, 1970; Embley, 1975;1976; Jacobi, 1976). Hyperbolic echoes, often less distinct than those

associated with deep currents, characterize large areas which strike perpendicular to the regional contours in areas of down-slope sediment movement. Although it has often been assumed that the abundance of side echoes results from the disturbed nature of the sea floor (e.g., references cited above), little evidence has been available on the nature of that disturbance.

Topographic features large enough to be observed on echo-sounding records are also present on the sea floor, although the shape and structure of these features is often obscured by the presence of side echoes (Appendix I.B and I.C). The best known feature is the large sediment wave. These sediment waves are also known as Lower Continental Rise Hills (Heezen et al., 1959), abyssal antidunes (Fox et al., 1968), giant ripples (Ewing et al., 1971), and large mud waves (Hollister et al., 1974). They have been reported from the margins of most of the continents, as well as from the open ocean, and they have been associated with deep, contour-following currents on the basis of their existence in regions of known or suspected deep cur-rents. Due to their limited size and the great water depth in which they are found, few detailed investigations of them have been undertaken, and even such basic characteristics as the orientation of a particular set of waves have been largely unknown.

The small-scale topography and resulting echo character along any given continental margin can result from the influence

of both deep, contour-following currents and down-slope

gravitational movement. Care is often required in order to

correctly determine the origin of the sedimentary topography

present on the basis of echo-sounding profiles alone

(Appendix I.D).

Many questions have arisen as to the actual nature of the

sea-floor topography which corresponds to types of echo traces

found on the deeper portions of the continental margins.

(1) What, in fact, are the features responsible for these

echo traces? What is their structure? What are their dimen-

sions, degree of lineation, orientation with respect to the

regional topography, and, if relevant, to the currents observed

in the area?

(2) Are these features related to current activity, or

do they indicate other processes active on the continental margin?

(3) What process or processes have formed these features?

Are the features now in equlibrium with those processes? How

were they formed by that process? If they are not active now,

when were they last active? How have conditions changed since

that time?

(4) Is the same feature always responsible for the same

echo pattern, or can different features result in the same

pattern?

This study has attempted to address these questions

through a program of detailed surface-ship and near-bottom

investigations with both an unmanned instrument package and a manned submersible.

Many of the observational difficulties described above have been overcome by the use of a deeply-towed instrument package developed by the Marine Physical Laboratory at the Scripps Institution of Oceanography (Spiess and Mudie, 1970; Spiess and Tyce, 1973). This instrument package is towed at a height of 10 to 100 m above the sea floor. With its side-scan sonar, narrow-beam (4°) echo sounder, 4 kHz sub-bottom profiler, stereo photography, continous temperature measurement, and transponder navigation, it can resolve sea floor features of the scale under discussion here (centimeters to kilometers) and can give information on the temperature structure of the overlying water column. This deep tow package has been used successfully to study small features on the sea floor by a number of investigators (e.g., Lonsdale and Spiess, 1977).

Near-bottom investigations were also made in some areas with the Bathyscaphe TRIESTE II (DSV-1). This submersible provided the only means for first-hand observation of the surface morphology on the Blake-Bahama Outer Ridge.

Two areas of the Blake-Bahama Outer Ridge were investigated in detail using the MPL deep tow and DSV TRIESTE II, and a third was studied by a surface ship in order to determine the bottom morphology responsible for the hyperbolic echoes and sediment waves common in this area. Current and temperature

measurements collected at the same time were used to determine
the flow patterns over the features in question. Current-
produced bed forms (furrows) are responsible for the hyperbolic
echoes. These furrows and other current-produced bed forms
are the major topographic elements of the outer ridge. Studies
of the sediments in which the various bed forms are developed
and the structure of the water flow over them permit models to
be advanced for the origins of these bed forms.

Three areas of the Rockall Trough were also investigated
with the deep tow. Surface-ship echo-sounding records indicate
that hyperbolic echoes and sediment waves are common in this
area. These investigations indicate that the sediment waves
are in some ways similar to those on the Blake-Bahama Outer
Ridge, although there are some important differences. One
zone of hyperbolic echoes is the surface of a large gravita-
tional sediment flow (debris flow), while other hyperbolae
appear to be caused by furrows.

CHAPTER II

BED FORMS ON THE BLAKE-BAHAMA OUTER RIDGE

A. *INTRODUCTION*

The Blake-Bahama Outer Ridge is a large sedimentary drift
complex located seaward of the Blake Plateau about 700 km east
of Florida. It is a major topographic feature (over 800 km
in length, 400 km in width and an average 2 km in thickness
with an estimated volume of 6×10^5 km^3). The ridge has long
been recognized as a region characterized by an impressive
array of small-scale topographic features.

Two separate ridges actually form the Blake-Bahama Outer
Ridge: a larger one (over 550 km in length and a maximum
relief of 2900 m) which strikes southeast from the northern
Blake Plateau, and a smaller one (of similar length with a
maximum relief of about 500 m) striking north-south and
located south of the larger ridge (Figure 2.1). Following
the nomenclature of Markl et al. (1970) the larger ridge is
called the Blake Outer Ridge and the smaller, or secondary,
ridge the Bahama Outer Ridge. The term Blake-Bahama Outer
Ridge (BBOR) is used when referring to both features. The
Bahama Outer Ridge is bounded on the west and south by the
Blake-Bahama Basin, a depression at the base of the Blake
Escarpment. The maximum depth of the basin is near 5046 m,

and the shallowest closed contour of the basin is between
4750 and 4800 m. The Blake Outer Ridge is bounded on the
east by the Hatteras Abyssal Plain and on the north by the
continental rise of North America.

Origin of the Outer Ridge

The structure of the BBOR was first studied through the
use of seismic refraction techniques by Hersey et al. (1959).
Later, continuous seismic profiling on the BBOR demonstrated
that the ridge, which is composed entirely of low-velocity
sediments, is not conformable to the basement or to Horizon
A (Ewing and Ewing, 1964), a prominent seismic reflector in
the western North Atlantic. This indicated that the ridge
could not have been caused by the faulting or folding of the
basement rocks and, thus, could not be related to the struc-
ture of the Cape Fear Arch, as suggested by Hersey et al.
(1959). Ewing and Ewing (1964) reported that the ridge
structure was "suggestive of erosion or a most unusual pro-
cess of deposition."

Heezen and Hollister (1964) suggested, on the basis of
bottom photographs which showed evidence of current activity,
that BBOR may have been constructed entirely by sediment
transported along the sea floor by deep bottom currents.
Heezen et al. (1966) stated that the surface sediments

Figure 2.1.   Bathymetry of the Blake-Bahama Outer Ridge.
Contour interval 50 m.   Track lines shown as
bold lines.   Numbered squares are study areas,
numbered line segments are indexed profiles,
and circles are deep-sea drilling sites.

Sources of data: Wood Hole Oceanographic
Institution, Lamont-Doherty Geological
Observatory, U.S. Naval Hydrographic Office
Charts BC805 and BC806 (Bahama Banks, Blake
Escarpment, northwestern BBOR) and Bush (1976;
southeastern flank of BBOR).
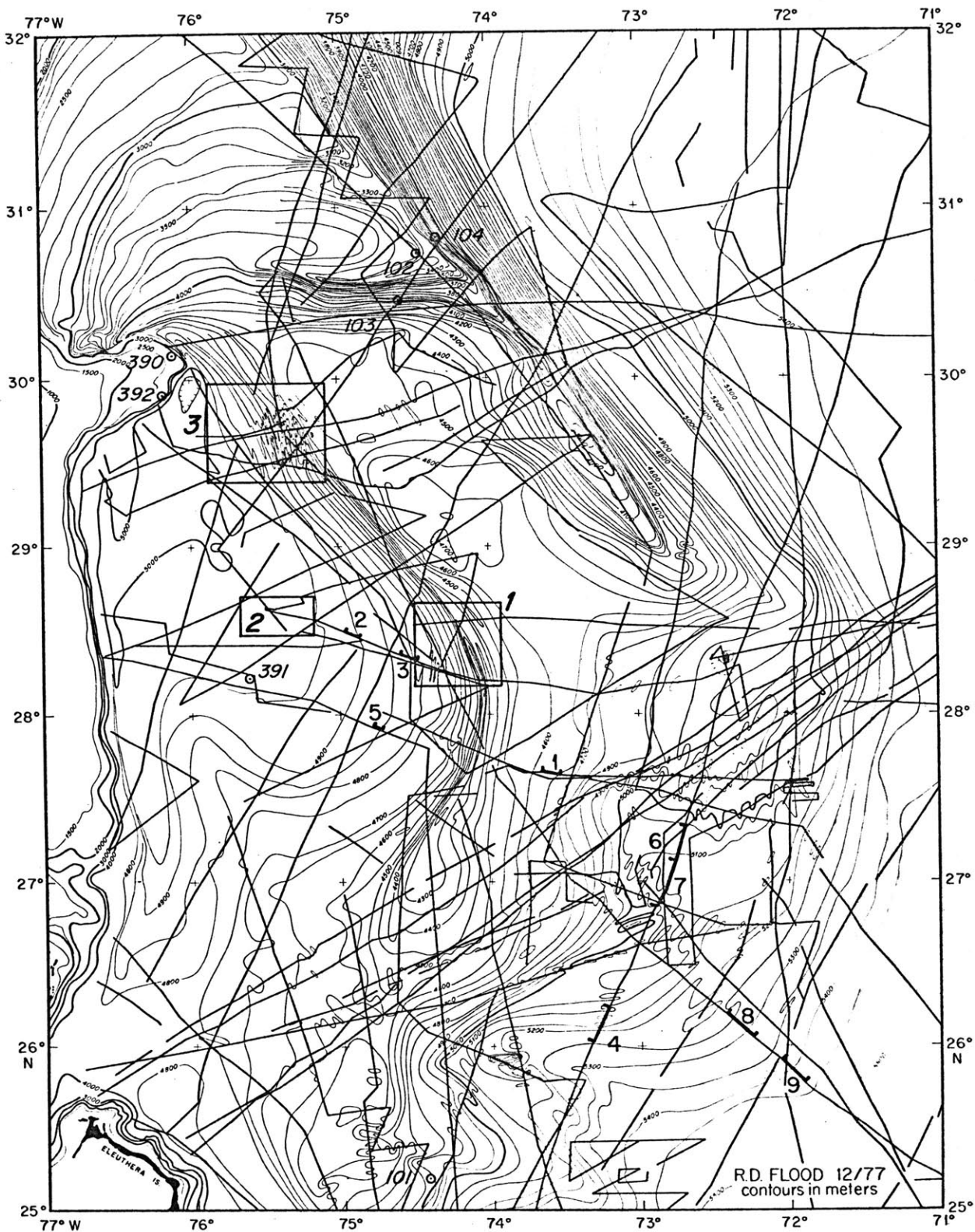
Figure 2.1

originated north of Cape Hatteras and were then transported south and deposited by bottom currents, while Ewing et al. (1966) proposed that the sediments making up the outer ridge were eroded from the Blake Plateau. In contrast, Andrews (1967) suggested that gravitational processes had formed the outer ridge. However, seismic-profiler data compiled by Markl et al. (1970) supported the depositional origin of the outer ridge. Bryan (1970) and Markl et al. (1970) proposed that an interaction between the northward-flowing Gulf Stream and the southward-flowing Western Boundary Undercurrent was responsible for the outer ridge, a "detached continental rise," with the bulk of the sediment coming from the north.

A test of the origin of the BBOR came with the advent of the Deep Sea Drilling Project. Core samples from Sites 102, 103, and 104 drilled on the Blake Outer Ridge demonstrated that at least the upper layers of the ridge are composed of Miocene and younger sediments which were deposited at high sedimentation rates and reflect a northern source area. These fine-grained sediments were transported from the north by southward-flowing currents (Ewing and Hollister, 1972). Sheridan et al. (1974) showed that the Bahama Outer Ridge was constructed on an extensive turbidite deposit of late Miocene age, and suggested that its formation postdated the formation of the Blake Outer Ridge. This finding was later confirmed at

Site 391 (Blake-Bahama Basin), where recovered core samples
indicate that 150 m of Quaternary and uppermost Miocene hemi-
pelagic sediments rest on a 500 m thick section of Miocene
gravity-flow deposits (Benson and Sheridan, 1976). The
Miocene gravity flows unconformably overlie Late Cretaceous
green and black clays. This unconformity corresponds to
Horizon A at this site (Benson and Sheridan, 1976).

Although the detailed history is not yet fully understood,
most of the one kilometer of sediment which make up the Bahama
Outer Ridge appear to have been deposited by bottom currents
during the last ten million years.

Deep Circulation

Studies of the deep circulation along the western margin
of the North Atlantic Ocean have generally confirmed the
existence of a southward-flowing, contour-following current.
The first report of such a current was by Wüst (1936), who
followed a tongue of oxygen-rich North Atlantic Deep Water
throughout the North and South Atlantic and a tongue of cold,
relatively fresh Antarctic Bottom Water north to about 40°N
in the North Atlantic. The existence of strong, deep western
boundary currents was predicted from a theory for the main-
tenance of the thermocline by Stommel (1958) and Stommel and
Arons (1960), and a deep southward-flowing current was sub-

sequently discovered by direct measurement off Cape Fear by

Swallow and Worthington (1961). Subsequent studies (e.g.,

Zimmerman, 1971; Tucholke et al., 1973; Richardson, 1977)

of the Western Boundary Current (WBUC) have generally

confirmed this picture.

The water-mass structure of the WBUC in the vicinity of

Cape Hatteras and on the Blake-Bahama Outer Ridge has been

discussed by Richardson (1977) and Amos et al. (1971) respec-

tively. At the shallowest depths and temperatures which are

a part of the WBUC (approx. 1000 m; 4°C) the water present is

a mixture of fresher water from the Labrador Basin and the

saltier North Atlantic Basin Water (Richardson, 1977). The

Labrador Basin Water can be traced at least as far south as

Cape Hatteras on the basis of a negative salinity anomaly in

a temperature range of 4-6°C (Barrett, 1965; Richardson,

1977). North Atlantic Deep Water (NADW), which makes up the

bulk of the WBUC, is characterized by potential temperatures

ranging from 1.8 to 4.0^{o}C and salinities from 34.89 to

35.00°/$_{oo}$. NADW, found at depths from 2500 to 4000 m off Cape

Hatteras, is a complex mixture of waters from several sources,

including the cold, northern sources of bottom water (Denmark

Straits Overflow (DSOW) and Iceland - Scotland Overflow)

(Worthington, 1976). Richardson (1977) has noted the remnant

of the DSOW at about 2.5°C potential temperature off Cape

Hatteras as a local dissolved silicate minimum (18.6µg-at/1).

At potential temperatures below 1.8° (depths greater than

about 4500 m along the rise off Cape Hatteras) water of

higher silicate (>40 µg-at/1) and lower salinity (<34.98°/$_{oo}$)

is encountered. Since there is no water of northern origin

colder than 1.8°C potential temperature in this region of

the North Atlantic, this water has a southern origin and is

a remnant of Antarctic Bottom Water (AABW) (Worthington and

Wright, 1970; Amos et al., 1971; Richardson, 1977).

Investigations of the deep circulation patterns in the

area of the Blake-Bahama Outer Ridge have been undertaken by

several investigators. Bottom photographs studied by Heezen

et al. (1966) indicated that the deep currents (NADW and AABW)

meander around the various ridges, but always flow so that

the topography slopes up to the right. The first hydro-

graphic studies in the area were carried out by Amos et al.

(1971). This study consisted of an east-west STD (Salinity,

Temperature, Depth sensor) transect across the BBOR. Their

resulting geostrophic velocity calculations supported the

deep circulation pattern proposed by Heezen et al. (1966).

Current directions determined by the east-west transect (Amos

et al.,1971) were to the south along the eastern slopes of

the ridges and along the Blake Escarpment and to the north

along the western slopes of the ridges. Near-bottom velo-

cities calculated by Amos et al. (1971) on the basis of their

STD section reached a maximum of 26 cm/sec towards the south at 4900 m on the eastern flank of the Blake Outer Ridge. Velocities of 2 to 12 cm/sec were calculated for other portions of the transect. Subsequent current-meter measurements of the deep currents in this area (Brundage, personal communication; Biscaye and Eittreim, 1974; Eittreim et al., 1975; Perkins and Wimbush, personal communication; and this study, Section IIB) have largely supported this circulation pattern and the associated velocity calculations. Hydrographic studies presently under way by Rhines (personal communication) also tend to support this circulation pattern.

Echo Character

It has been suggested that many of the small-scale topographic elements present on the BBOR, especially those which are responsible for the common hyperbolic echoes, have been formed by the currents which have built the ridge and which are still active in the area. This a priori statement must, however, be supported by detailed investigations of the actual nature of the sea-floor topography in the region.

The first reports of small-scale topographic elements on the BBOR coincided with the development of precision echo-sounding recorders (Luskin et al., 1954; Knott and Hersey, 1956). Heezen et al. (1959) reported the occurrence of hyperbolic echoes with apices tangent to the sea floor on

the outer ridge and Pratt and Heezen (1964), cited these hyperbolic echoes as partial evidence for the construction of the outer ridge by deep currents. Clay and Rona (1964) reported the existence of hyperbolic echoes in the Blake-Bahama Basin, and, on the basis of 12 kHz echo-sounding records, calculated that the hyperbolae were caused by north-south trending ridges 120 m apart. The amplitudes of the ridges could not be determined, but were thought to be small compared to the spacing. Clay and Rona (1964) speculated that the ridges could be sand waves.

The most extensive study of the distribution of the small-scale topography on the Blake-Bahama Outer Ridge was conducted by Bryan and Markl (1966). They mapped the distribution of three scales of topographic features on the basis of the echo return. The three types of echo character mapped were (1) periodic topography or sediment waves (wavelength of 1 - 7 km, easily resolved on echo-sounding records); (2) "hyperbolic" topography (wavelengths of 100-1000 m, resolved on echo-sounding records only as distinct hyperbolic echoes with apices tangent to the sea floor); and (3) "fuzzy" topography (wavelengths thought to be 10-100 m, observed only as a prolonged echo on echo-sounding records). Regions of fuzzy echoes often showed hyperbolic echo traces when shorter ping lengths were used. Bryan and Markl (1966)

established that the features responsible for both the hyperbolic and periodic topography were generally aligned parallel to the regional contours.

The echo-character map of Bryan and Markl (1966) has been updated on the basis of subsequent echo-sounding records collected by the Woods Hole Oceanographic Institution and some from the Lamont-Doherty Geological Observatory (Figure 2.2). The classification used by Bryan and Markl (1966) has been retained and, also following their usage, the region of fuzzy echoes has been included with the region of hyperbolic echoes. Not enough was known about the nature of the topographic elements on the sea floor to justify a more complicated classification scheme, although some other features of interest were identified.

Most of the outer ridge complex is characterized by the presence of hyperbolic echoes (Figure 2.2). In many cases (Figure 2.3, profiles 1,2), the hyperbolic echoes are just perceptible on the original records, demonstrating the small size of the sea-floor features. However, in other areas, the hyperbolae are quite large and dominate the sea floor relief (Figure 2.3, profile 2). In some instances, hyperbolic echoes are also found developed on the periodic larger features (Figure 2.3, profiles 3 and 4); however, all of the hyperbolic echoes appeared to be similar in character.

Figure 2.2   Echo character of the Blake-Bahama Outer Ridge.
              Data from Bryan and Markl (1966) and echo-
              sounding records of the Woods Hole Oceano-
              graphic Institution.
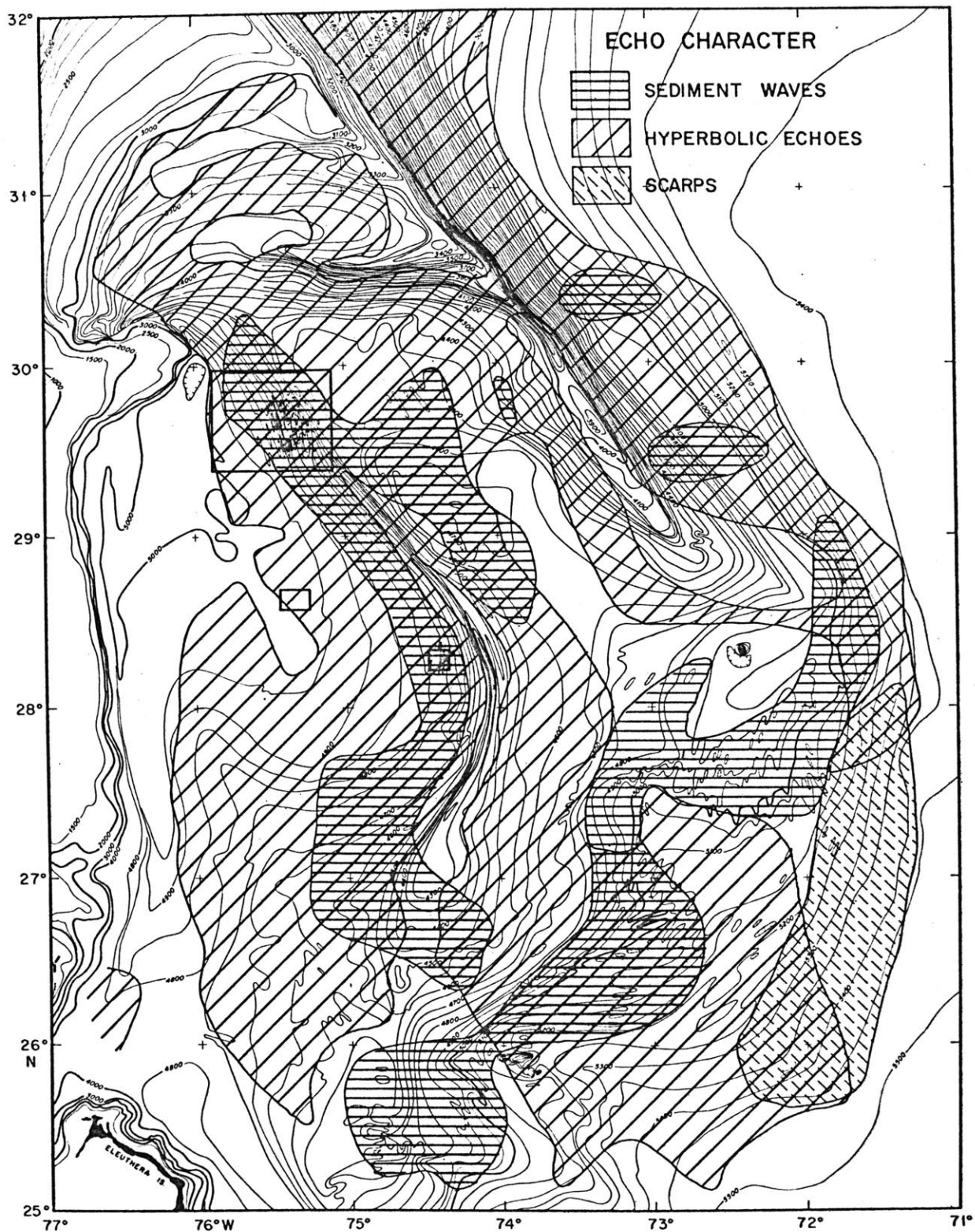
Figure 2.2

Figure 2.3. Hyperbolic echoes and sediment waves on the
            BBOR. Profiles indexed on Figure 2.1.

        Profile 1. Hyperbolic echoes (12 kHz).

        Profile 2. Contact between small hyperbolae and
                    large hyperbolae (3.5 kHz). Hyper-
                    bolae are also developed on sub-
                    bottom reflectors.

        Profile 3. Hyperbolic echoes superimposed on
                    regular sediment waves (3.5 kHz).
                    Hyperbolic echoes are also developed
                    on sub-bottom reflectors.

        Profile 4. Hyperbolic echoes and irregular sedi-
                    ment waves (3.5 kHz).

W   E   — 4.6

  — 4.7

1   2 KM

E   W   — 4.9

  — 5.0

2   2 KM

E   W   — 4.8

  — 4.9

3   2 KM   — 5.0

N   S   — 5.1

  — 5.2

4   5 KM

DEPTH (KM)
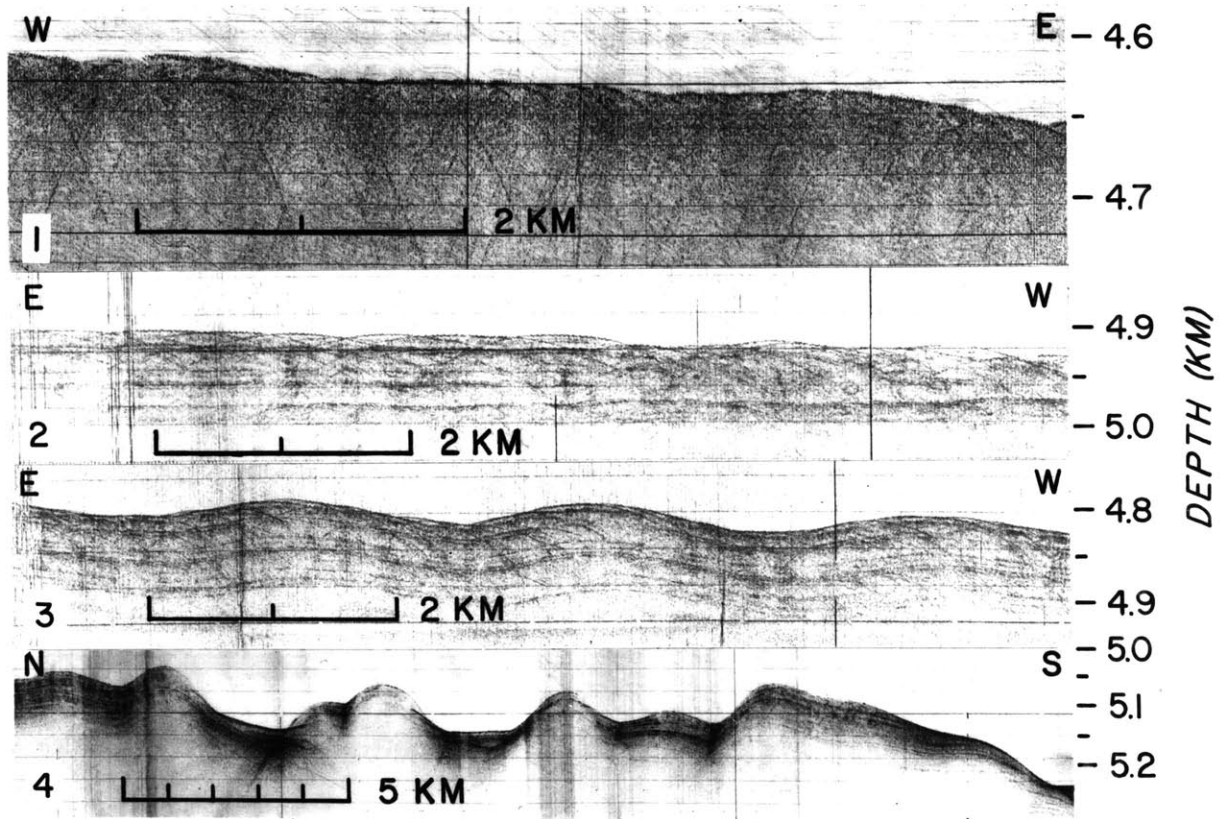
Figure 2.3

The zones of periodic topography (sediment waves) are
often found in lineated zones which extend parallel to the
regional contours (Figure 2.2). The nature of the periodic
topography, however, appears to be different in different
areas of the outer ridge. Some areas, such as the western
flank of the Bahama Outer Ridge, are characterized by the
presence of features which have an almost sinusoidal charac-
ter (Figure 2.2, western zone of sediment waves, Figure 2.3,
Profile 3). Other areas, such as the south eastern margin of
the outer ridge complex, appear to be characterized by a more
irregular periodic topography (Figure 2.2, eastern zone of
sediment waves, Figure 2.3, Profile 4).

In some areas of the Bahama Outer Ridge, hyperbolic
echoes were also observed to occur on sub-bottom reflecting
horizons (Figure 2.3, profiles 2,3 and Figure 2.4), suggest-
ing that the present surface morphology has also existed at
certain times in the past. In many of the records, the
hyperbolic echoes on the deeper layers are directly below
hyperbolic echoes on the sediment surface. This suggests
that these surface and sub-bottom features may be somehow
related.

The nature and origin of the various features responsi-
ble for the small and large hyperbolic and the regular
sediment waves on the western flank of the Bahama Outer
Ridge was determined (Sections II.B and II.D).

Figure 2.4.   Hyperbolic echoes on sediment surface and on sub-
bottom reflectors (3.5 kHz).   Indexed on Figure
2.1 (Profile 5).

E   W

4850 M

4900 M

4950 M

5

0   5 KM
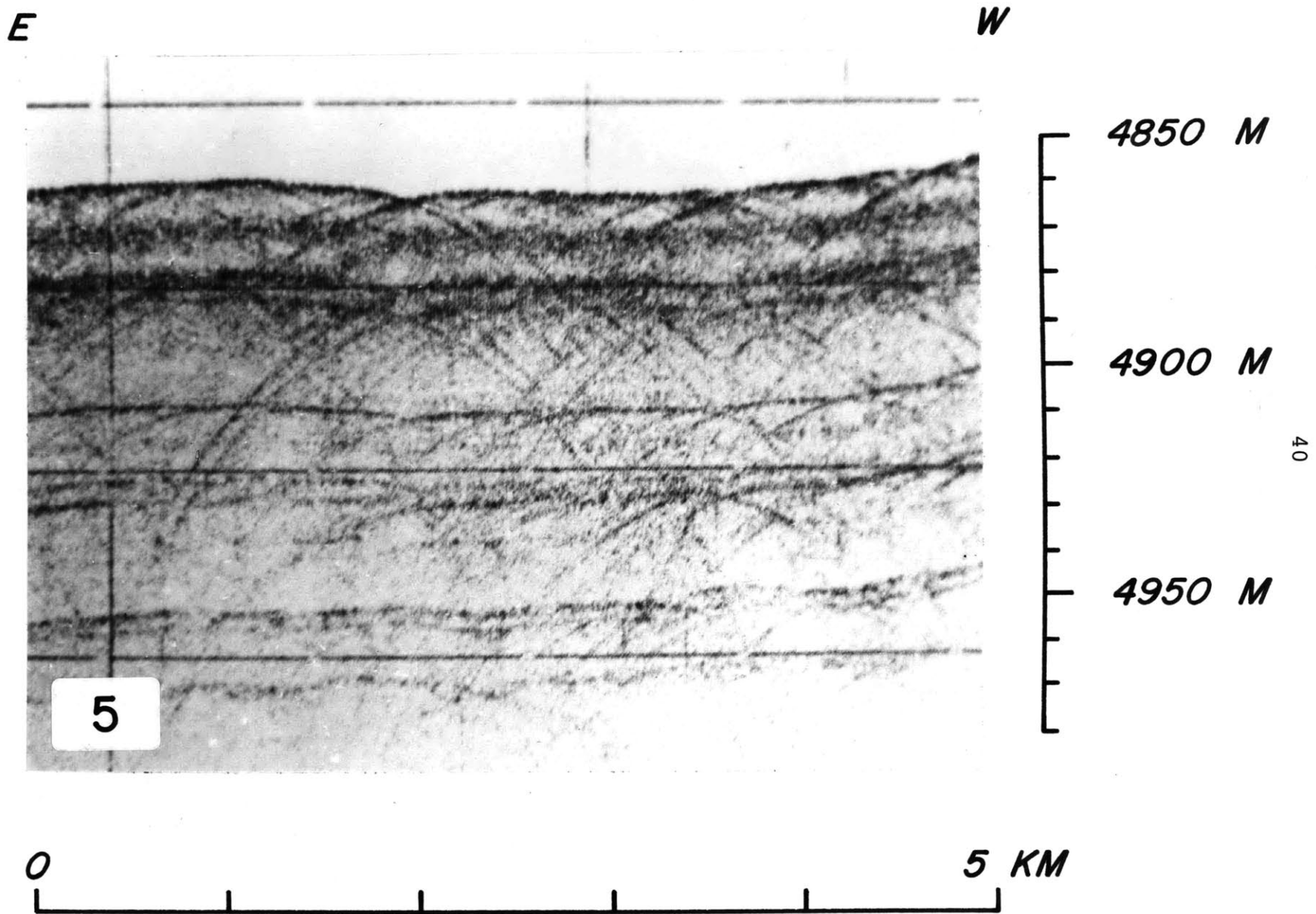
Figure 2.4

A large region (200 km by 400 km) of complicated sea-
floor structure is found on the southeastern margin of the
outer ridge (27°N, 73°W), interrupting the region of irregu-
lar sediment waves. The region corresponds in part to a
pronounced inward bowing of the contours from a depth of
4800 m to 5200 m. This zone appears to be one of sediment
removal, as deeper reflectors can be traced from the north to
where they gradually crop out at the surface (Figure 2.5,
profile 6). Sediments are observed to prograde from the
south over this erosional surface (Figure 2.5, profile 7).

Downslope from this region, there is a zone of topography
characterized by the presence of step-like features (Scarps;
Figure 2.5, profiles 8,9; depth range from ~5200 to ~5450 m).
Many of these features can be correlated from track to track
over short distances and are, in some instances, associated
with small patches of hyperbolic echoes. Where a trend is
determined, the scarps are parallel to the regional contours
(NE-SW). These scarps are also described by Bush (1976). As
the scarps only occur over a distance of about 200 km, and
are located downslope from the area where sediment has been
removed, it is suggested that these features are related.
The U-shaped erosional area at 27°N, 73°W may be the site of
some type of downslope sediment movement. This movement may
have created the scarps. At present, little is known of the
history of the area.

Figure 2.5. Echo-sounding records, southeast flank of BBOR.
Profiles indexed on Figure 2.1.

Profile 6. Erosional area (3.5 kHz). Deeper
layers crop out to the south.

Profile 7. Sediments prograding over erosional
area (3.5 kHz).

Profile 8. Scarps downslope from profiles 6 and
7 (12 kHz). Note hyperbolic echoes
associated with scarps.

Profile 9. Scarps downslope from profiles 6 and
7 (12 kHz).
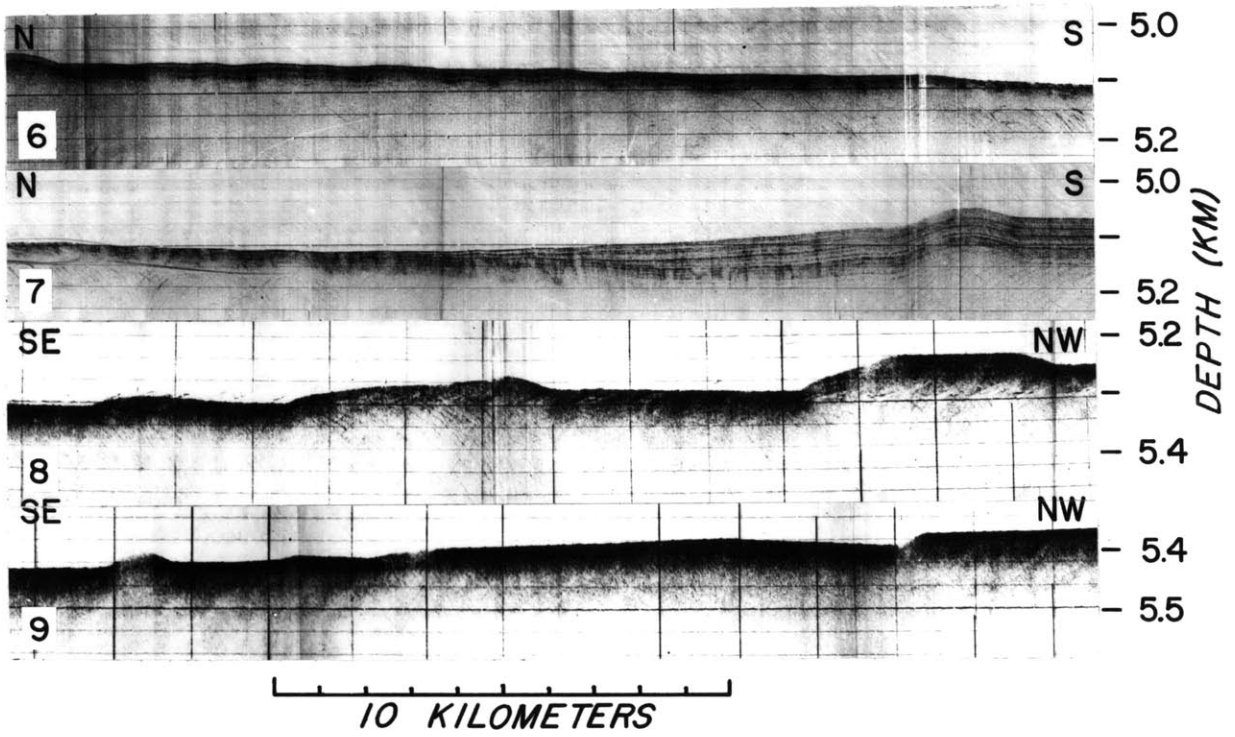
Figure 2.5

B. *RESULTS OF DETAILED INVESTIGATIONS - BAHAMA OUTER RIDGE*

Detailed investigations of the surface morphology, sediments, near-bottom currents, and water column structure were undertaken in three areas of the Bahama Outer Ridge (Figure 2.1). Area 1, centered at 28°17'N, 74°25'W, was designed to study the features responsible for the hyperbolic echoes, the large, regular sediment waves, and the crest of the outer ridge. Area 2, centered at 28°35'N, 75°20'W, was to study the features responsible for the large hyperbolic echoes present in this region, and the contact at the western margin of the outer ridge. Area 3 (RC18-06 area), centered at 29°40'N, 75°22'W, was to study a larger sample of the sediment waves on the western margin of the outer ridge.

Areas 1 and 2 were visited in July and August, 1973, on R/V Knorr Cruise 31, legs 4 and 5, and in September - October, 1977, with the Bathyscaphe TRIESTE II (DSV-1). Area 3 was visited in July, 1975, on R/V Robert D. Conrad Cruise 18, leg 6.

1. Morphology of the Sediment Surface

AREA 1 (SEDIMENT WAVES, SMALL FURROWS, RIPPLES, BAHAMA RIDGE CREST)

This study area, located near the ridge crest, on the western flank of the Bahama Ourter Ridge, includes areas of the sea floor characterized by small hyperbolic echoes and

by sediment waves (Figures 2.1,2.6). Investigations were made in this area with the MPL/SIO deeply-towed instrument package (deep tow) and the Bathyscaphe TRIESTE II. The objectives were to determine (1) the nature and origin of the features responsible for the hyperbolic echoes (furrows), (2) the nature and origin of the large sediment waves, (3) the relationship (if any) between features of different scales, and (4) the structure of the crest of the Bahama Outer Ridge.

One fifty-five hour transponder-navigated deep tow survey (lowering 3 of KN31, leg 5), one giant piston core, three free-fall cores, one bottom-bounce camera station and four current meter records were obtained from within a bottom-mounted transponder array. The center of this transponder-navigated survey is at lat. 28°17'N, long. 74°24'W at a water depth of 4760 m (Figure 2.7). A 27 km long, satellite-navigated deep tow transect was made from the transponder survey area to 28°24'N, 74°05.5'W, over the crest of the ridge.

Three dives (Dives 12-77, 13-77 and 16-77) were made with the Bathyscaphe TRIESTE II within a two-kilometer radius of 28°22'N, 74°12.5'W (depth, 15,000 ft, 4570 m) to study the sea floor features in this area. Along with bottom photographs, three short cores were recovered by DSV TRIESTE II
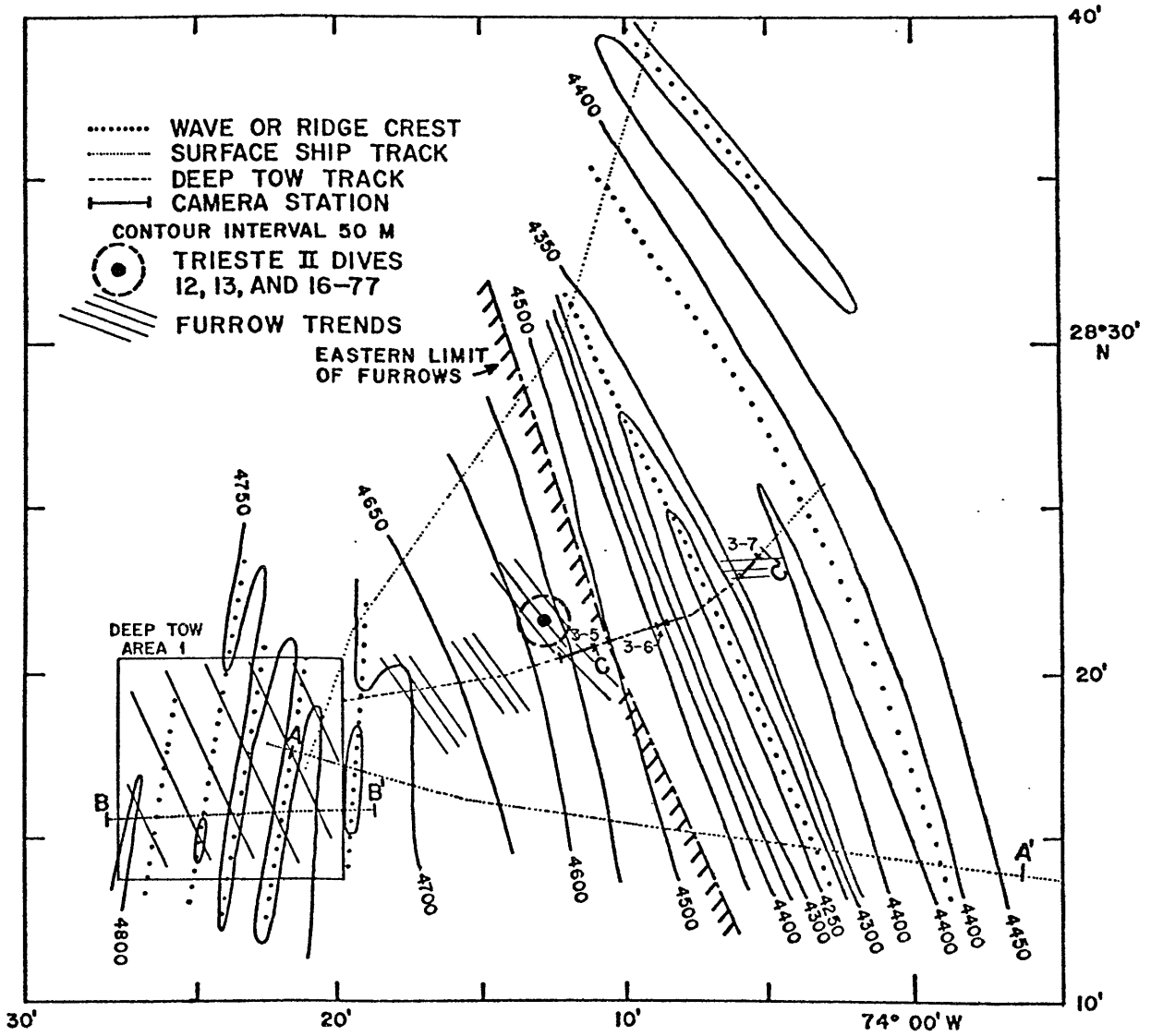
Figure 2.6. Bathymetric map of crest of Bahama Outer Ridge
(Area 1). This map is indexed on Figure 2.1.
Lettered profiles shown in subsequent figures.
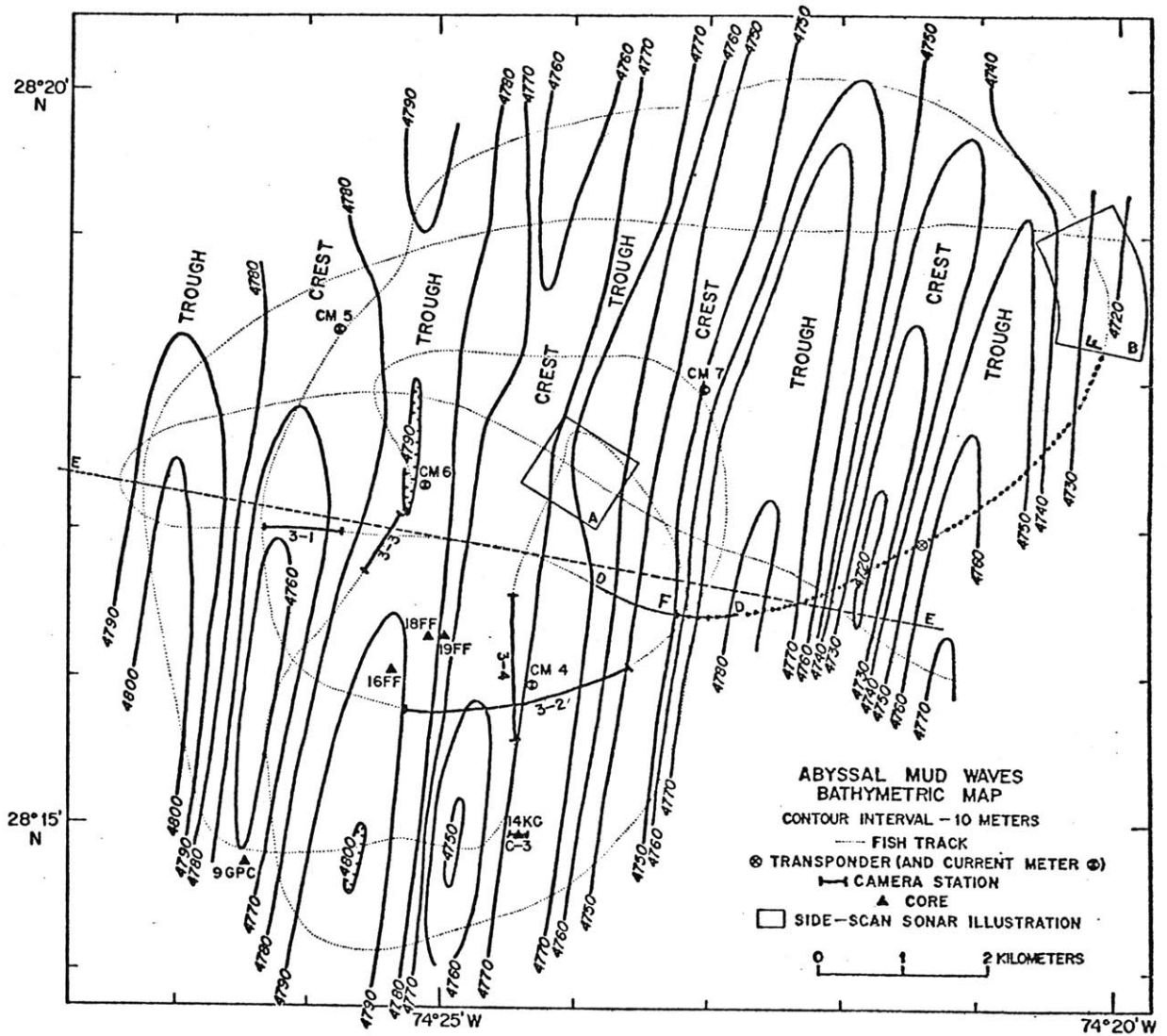
Figure 2.7. Bathymetric map of large sediment waves (Area 1).
Location of profiles, side-scan sonar illustra-
tions, current meters, cores and camera stations
are shown.

from a furrow. Bottom instrument packages, deployed during these investigations, monitored the current velocity in and around the furrows.

Subsequent sections will describe the sediments recovered and the structure of the near-bottom fluid motions.

Sediment Waves

The sediment waves in the transponder-navigated survey area trend N 10° E and have heights of 20 to 60 meters and wavelengths of 2 to 2.5 km (Figure 2.7). The long axes of the sediment waves are at an angle of 35° to the left, looking down stream (in this case looking toward the north), of both the regional contours and the measured currents (Section II.B.3), which trend N 25° W. The four waves in the study area are continuous along strike, but the height of any given wave varies considerably along its axis. Since the wavelengths remain roughly constant, the ratio between the height and wavelength also will vary along strike. This ratio, used by Rona (1969) in an attempt to correlate between sediment waves on echo-sounding profiles, is not generally useful for that purpose.

Comparisons between narrow-beam, near-bottom deep tow bathymetric profiles and wide-beam, surface-ship echo sounding records indicate that the shapes of the sediment waves

are slightly obscured by the presence of side echoes on the
surface echo-sounder records (see Appendix I.) (Figure 2.8).
The surface-ship record suggests that the sediment waves are
almost sinusoidal. S values for those waves range from 0.5
to 1.4, but no overlapping side echoes are observed in the
wave troughs. This is because many waves have sharper peaks
and broader troughs than a sinusoidal wave (Figure 2.8; see
Appendix I.B).

Sub-bottom profiles collected by both the deep tow
(4 kHz) and surface ships (3.5 kHz) indicate that the sedi-
ment waves have migrated with time (Figures 2.8 and 2.9).
These profiles indicate higher rates of sedimentation on the
southeast flank of the wave (the upslope, upcurrent flank)
and lower rates on the northwest flank (the downslope, down-
current flank). These variations in sedimentation rate have
resulted in the upslope, upcurrent migration of the wave
form. Sediment studies indicate that preferential deposition
is continuing to the present (Section II.B.2).

The regular sediment waves are not present at depths
shallower than 4700 m. Instead smaller, more irregular sedi-
mentary features are observed (Figure 2.10).
Small furrows and current ripples
The large sediment waves are decorated with much smaller
features, furrows. These furrows are responsible for hyper-
bolic echoes on the surface-ship echo sounder. Data collect-
ed by the long tow east to the ridge crest and observations

Figure 2.8. Surface and near-bottom profiles of sediment waves.

Upper: Surface-ship 3.5 kHz profile BB$'$. Profile indexed on Figure 2.6.

Lower: Near-bottom bathymetric profile (profile E). Profile indexed on Figure 2.7.

V.E. = 10X.

Figure 2.8

PROFILE D

ONE KILOMETER
▽ = FURROW LOCATION
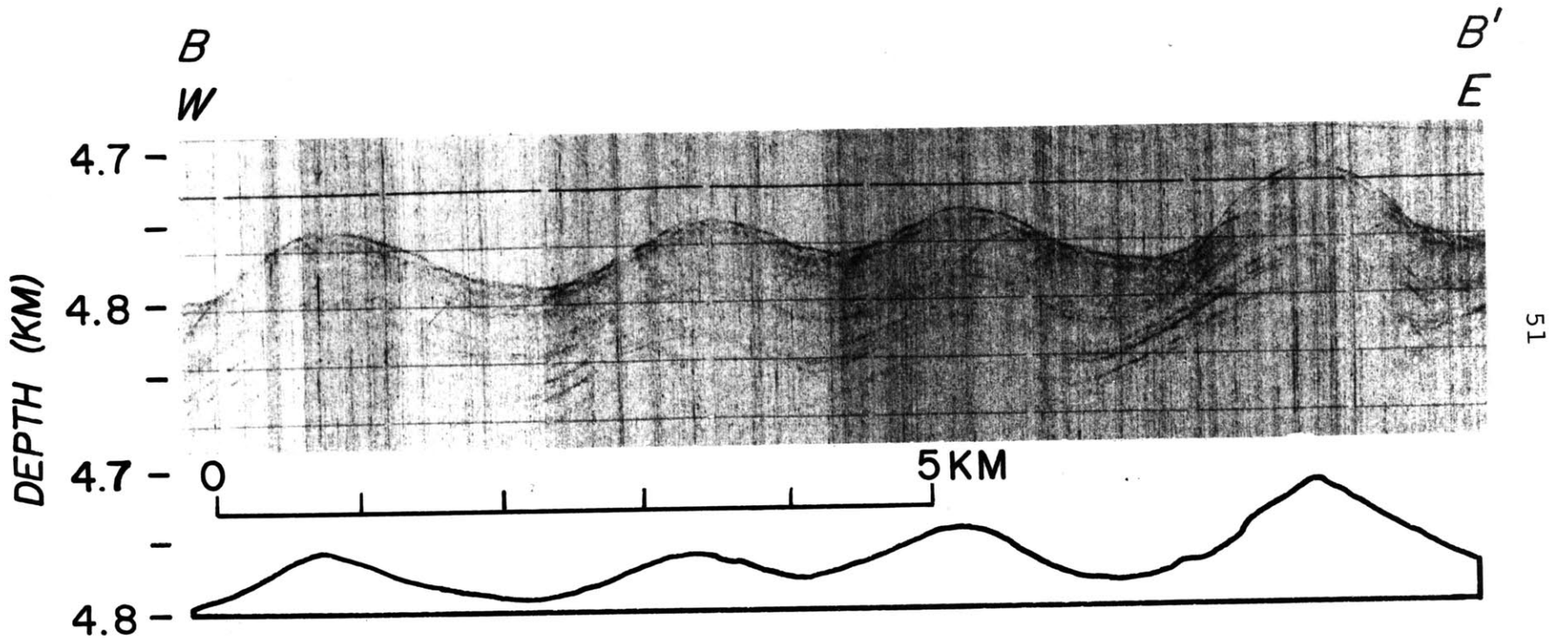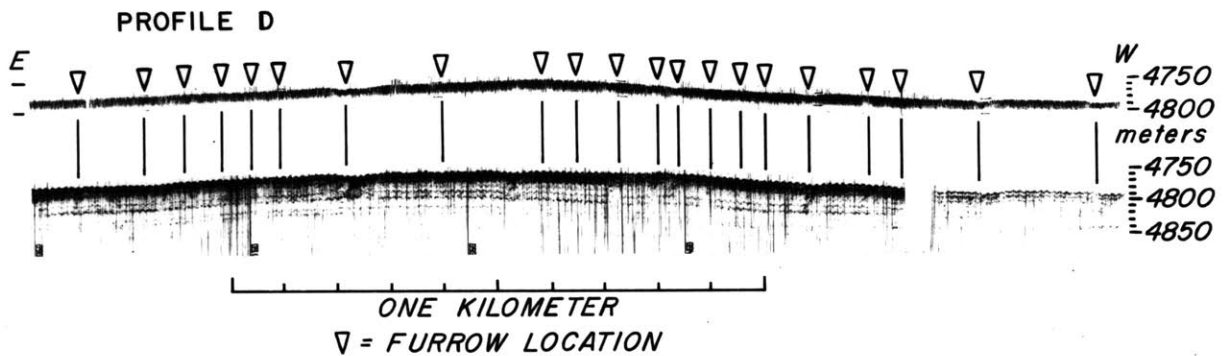
Figure 2.9. Near-bottom profiles across a sediment wave.

Upper: Near-bottom, narrow-beam bathymetric profile.

Lower: Near-bottom 4 kHz sub-bottom profile. Some of the wiggles in the sub-bottom profile are due to deep-tow movement.

Furrow location from side-scan sonar records. Profile indexed on Figure 2.7. V.E. = 1.5

Figure 2.10. Surface-ship 3.5 kHz profile across Bahama
             Outer Ridge crest. Profile indexed on Figure
             2.6. V.E. = 8X.
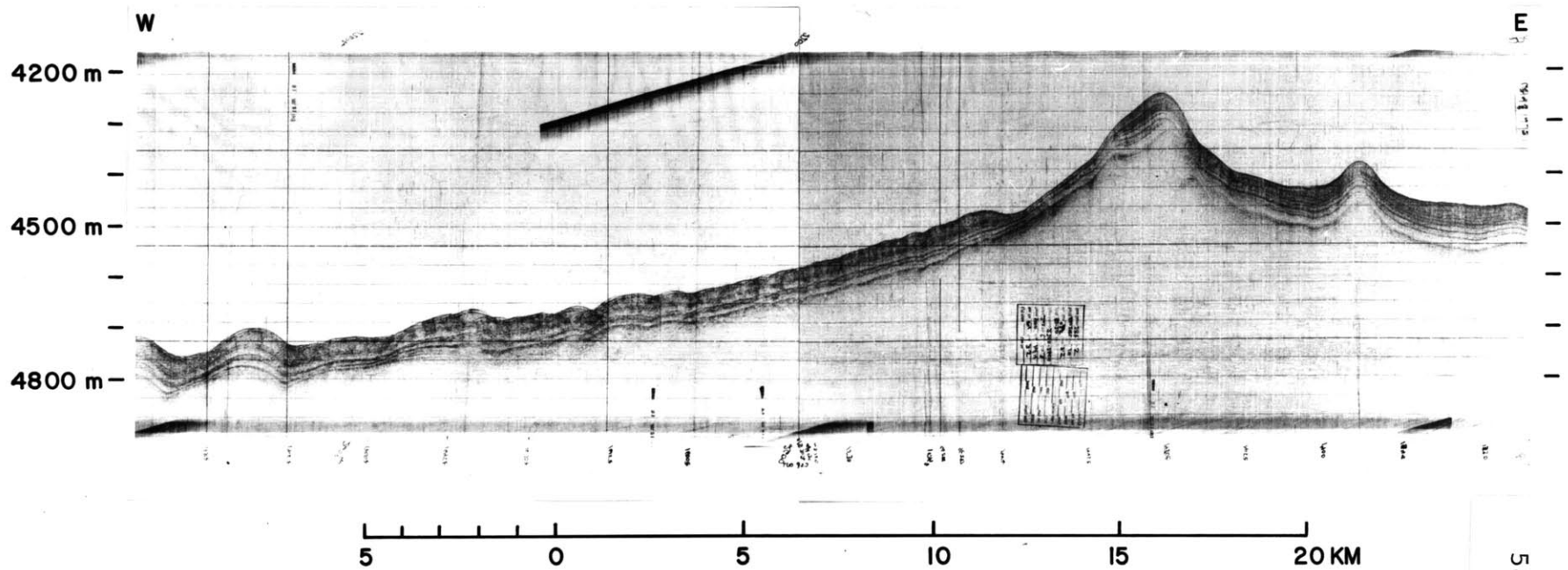
Figure 2.10

from DSV TRIESTE II show that the furrows are well-developed
throughout this area, almost up to the crest of the outer
ridge. The furrows are long, remarkably straight grooves
trending N 25° W in the detailed survey area, parallel to the
regional contours and to the measured currents, but at an
angle of 35° to the strike of the large sediment waves
(Figure 2.11). Closer to the ridge crest, observations from
DSV TRIESTE II determined a trend of N 30° to 40° W (Figure
2.6). The furrows often intersect at shallow angles ("tuning-
fork" junctions) (Figure 2.11,2.12). The tuning-fork
junctions almost exclusively open into the current (i.e.,
furrows come together in the downstream direction, here
toward 335°). Some of the furrows can be traced for at least
5 km on overlapping side-scan sonar images (Figure 2.11).

The spacing between furrows ranges from 10 m to over
200 m with an average of about 50 m and a most common spacing
of about 30 meters (Figure 2.13). In spite of the large
range of furrow spacings, the furrows present in any one
small region appear evenly spaced (Figure 2.11 and 2.12), and
the spacings seem to vary in a systematic way over the sedi-
ment waves. These and other variations in furrow morphology
which are related to the sediment waves are described below.

Figure 2.11. Bathymetric map of Area 1 with furrows super-
imposed. Furrow locations taken from side-
scan sonar records. Arrows near transponders
indicate direction of highest-velocity cur-
rents.

ABYSSAL MUD WAVES
BATHYMETRIC MAP

CONTOUR INTERVAL — 5 FATHOMS

.... FISH TRACK
⊗ NAVIGATION TRANSPONDER

0   1 MILE

Figure 2.11

Figure 2.12. Side-scan sonar record of small furrows (Area 1). Record indexed on Figure 2.7. as "A". Small wiggle superimposed on furrow trend is an artifact due to yaw of deep-tow vehicle.

Figure 2.12

SLANT RANGE (m)

-400

-0

-400

0   1 KM

59
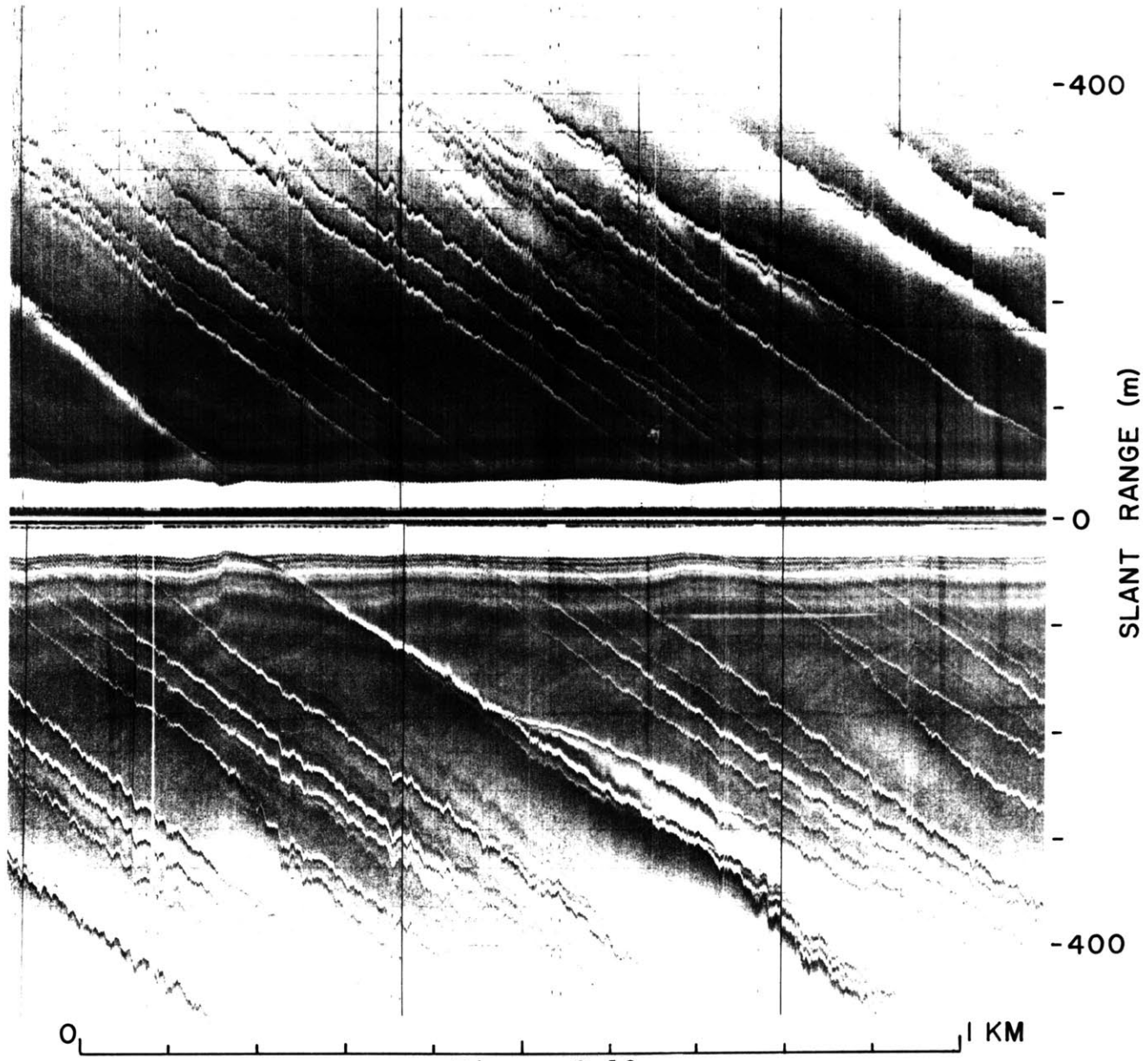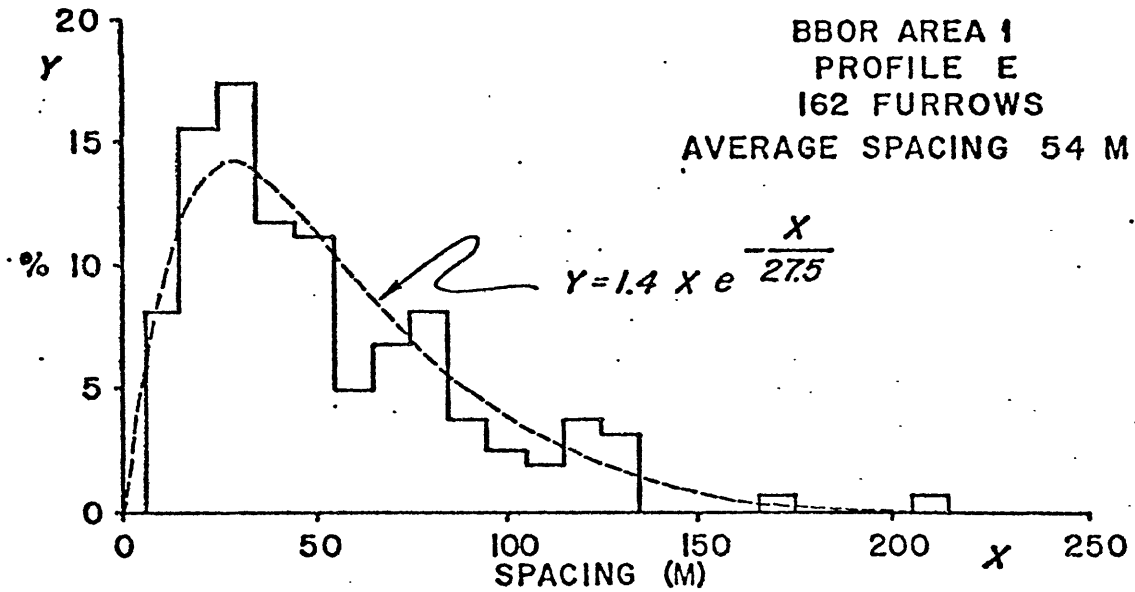
Figure 2.13.   Spacing between furrows in detailed Area 1.
Spacing between furrows crossing profile E
(Figure 2.7). The plot of an equation which
reflects the distribution of spacings is also
shown.

Photographs of the furrows taken by the deep-tow and by DSV TRIESTE II show that the furrows have steep sides (slopes to 50°) and flat floors (Figure 2.14, 2.15 and 2.16). The steepest portions of the walls are decorated with small ripples, and the flat floors often have a small median rise.

The term furrows is used for these features because they have strong morphological similarities to bed forms previously described and known as furrows (e.g., Dyer, 1970). These similarities include a series of parallel troughs aligned with the current, often with steep sides and flat floors. These troughs tend to join in tuning-fork junctions that open into the current.

The furrows cover a wide range of sizes with a given furrow changing size only slowly along its length. DSV TRIESTE II altimeter records shows their lateral expressions range from 5 to 140 m and their depths from one half to eight meters (Figure 2.17). In spite of this wide range, the width of the flat furrow floor varies only from one to three meters and is always seen in its entirety on deep-tow and DSV TRIESTE II photographs (Figure 2.14, 2.15 and 2.16). In the area studied by DSV TRIESTE II, the largest furrows have steep walls on the southwestern side (slopes about 30°) and less steep walls on the northeastern side (slopes about 6°; Figure 2.17). The walls often steepen near the bottom, intersecting the furrow floor with slopes of about 45°. The

Figure 2.14. Cross-section of small furrow (Area 1). Cross-
              section is derived from a deep-tow stereo
              photograph pair. Strongest currents measured
              are parallel to the furrow.
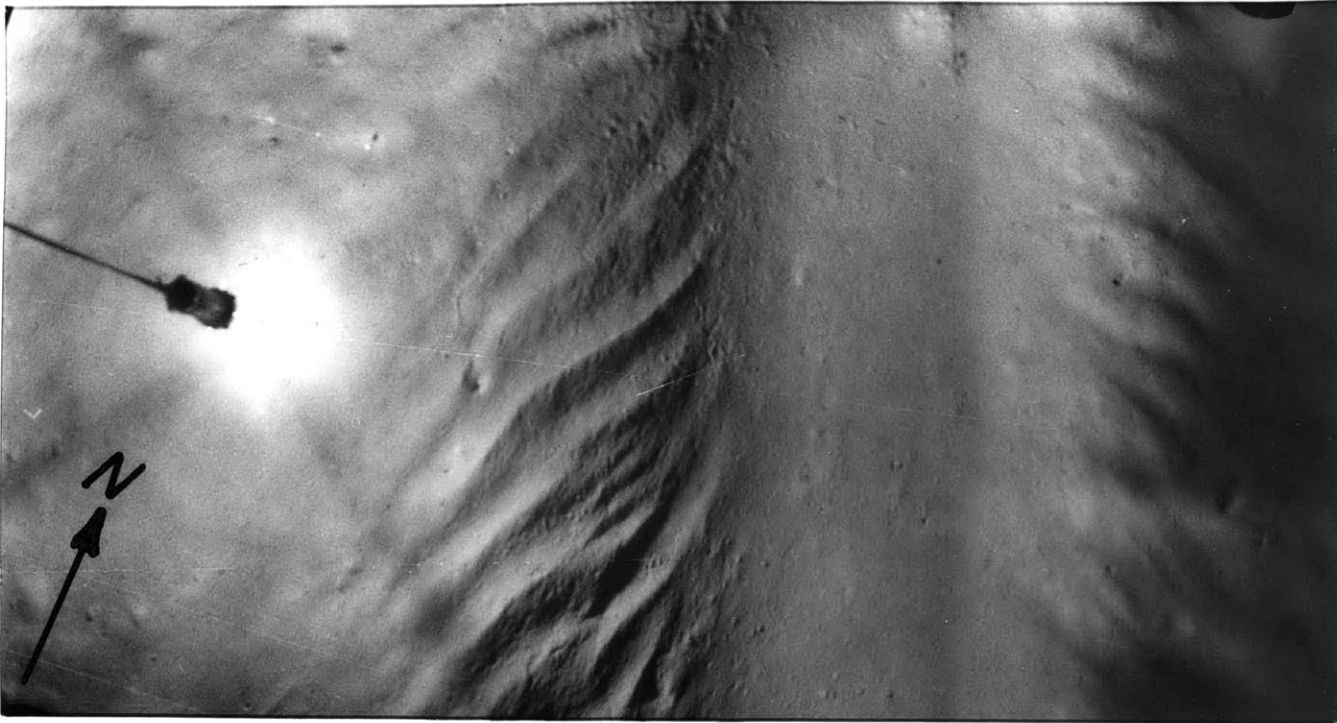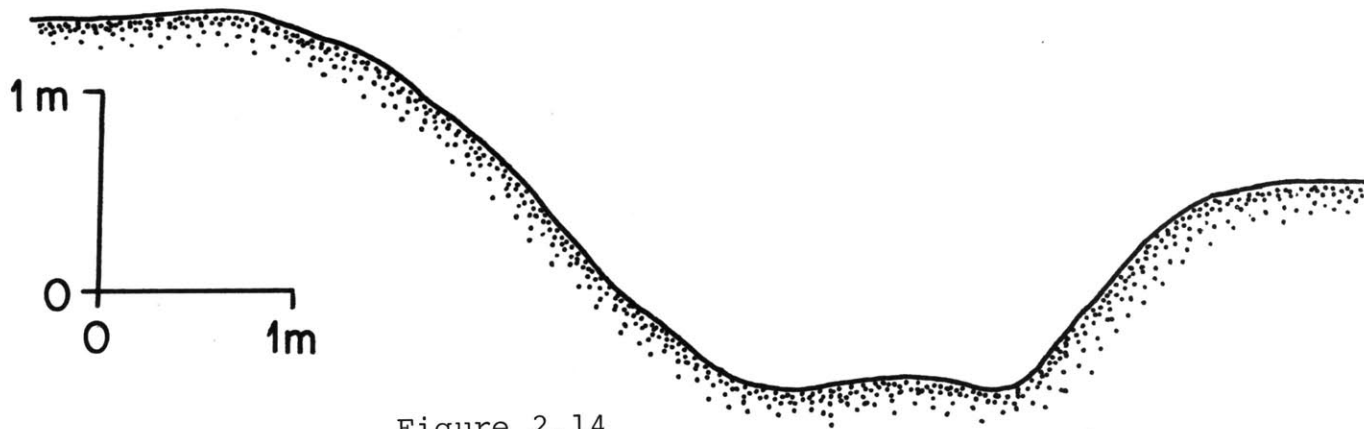
Figure 2.14

Figure 2.15. Oblique photograph of a furrow (Hdg. 134°) taken on TRIESTE II DIVE 16-77. Notice asymmetry (western wall is shorter and steeper than eastern wall). Flat furrow floor is about 1 m wide. Cores TII-12, 13, and 14 are from this furrow (see figure 2.45).

Figure 2.16.   Photographs of small furrows.

           a.   Camera run 3-1 (ID.071924)
           b.   Camera run 3-2 (ID.001022)
           c.   Camera run 3-3 (ID.074553)
           d.   Camera run 3-4 (ID.174227)
           e.   Camera run 3-5 (ID.121309)
           f.   Camera run 3-1 (ID.072527)

           Camera runs indexed on Figure 2.7.

           North is toward the top of the page, scale
           bar is approximately one meter.
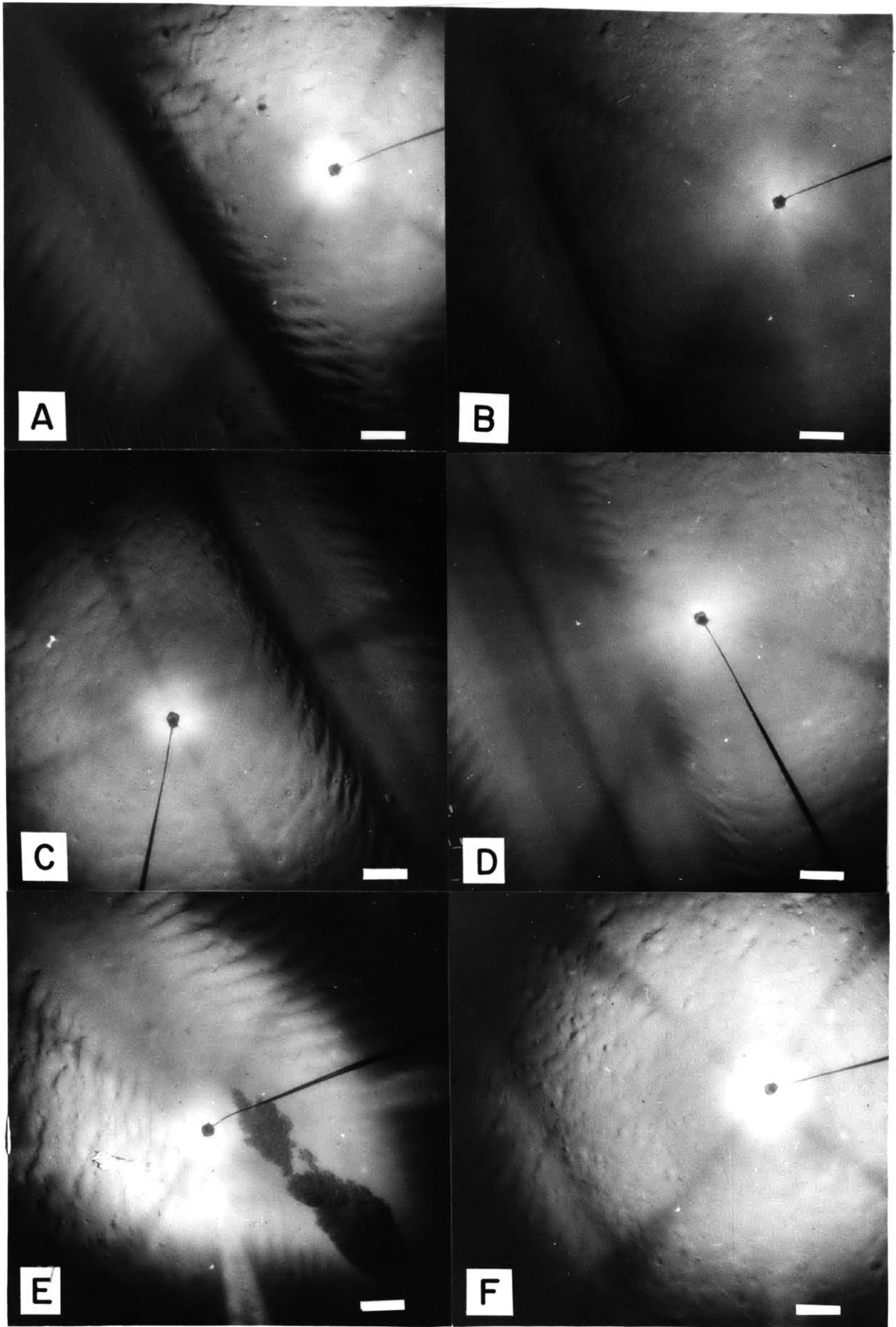
Figure 2.16
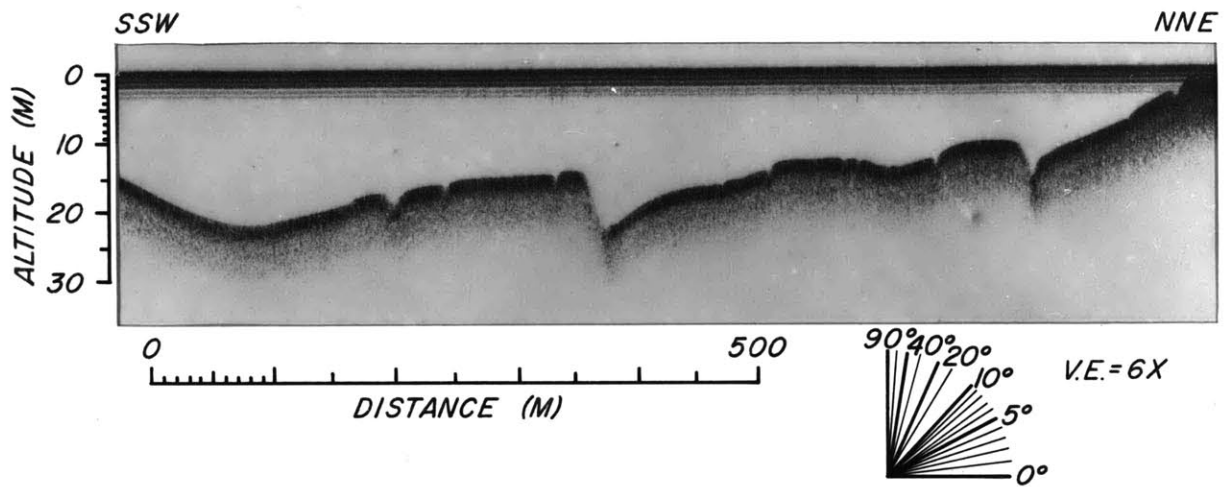
Figure 2.17. Narrow-beam altimeter profile of small furrows
(DSV TRIESTE II, Dive 12-77). V.E. = 6X.
Long-wavelength (ca. 100 m) smooth variations
in altitude are due to vertical motion of the
submersible.

situation thus appears similar to a smaller furrow at the base of a larger depression. Ripples are found decorating the walls of these large furrows.

While the larger furrows are asymmetrical with the higher and steeper wall on the southwestern side, the smaller furrows often have a higher wall on the northeastern side (Figure 2.17). There are exceptions to this rule, and some small furrows are symmetrical, but few have high southwestern walls.

The ripples developed on the steep portions of the furrow walls have wavelengths of about 20 cm and amplitudes of about 5 cm. The ripples are asymmetrical (Figure 2.18) with the steeper side of the ripple on the downstream side. The ripples appear to be developed only on the slopes associated with the walls of the furrows. In contrast to ripples developed in cohesionless sand and silt-sized material, (Allen, 1968b; Harms, 1969) these ripples which are developed in cohesive sediment have rounded upstream sides and often exhibit a slight overhand on the downstream side of the crest (Figure 2.18 b,d).

The ripples, found on both walls of the furrows, are orientated with their long axes at approximately 45° to the long axis of the furrow (Figure 2.14). The deeper end of the

Figure 2.18. Near-bottom photos of furrow walls, floors, and
              inter-furrow areas.

              (a) Inter-furrow area.
              (b) Furrow bottom and ripples on wall.
              (c) Ripples near base of furrow wall.
              (d) Ripples near top of furrow wall. Camera
                   is pointed to southwest. Sediment blocks
                   in furrow trough are due to disturbance of
                   the area by the submersicle.

              Photos a-c are from camera station KN31-C3
              (Figure 2.7). Photo d is from DSV TRIESTE II
              Dive 13-77 (Figure 2.6). Scale bar is 50 cm.
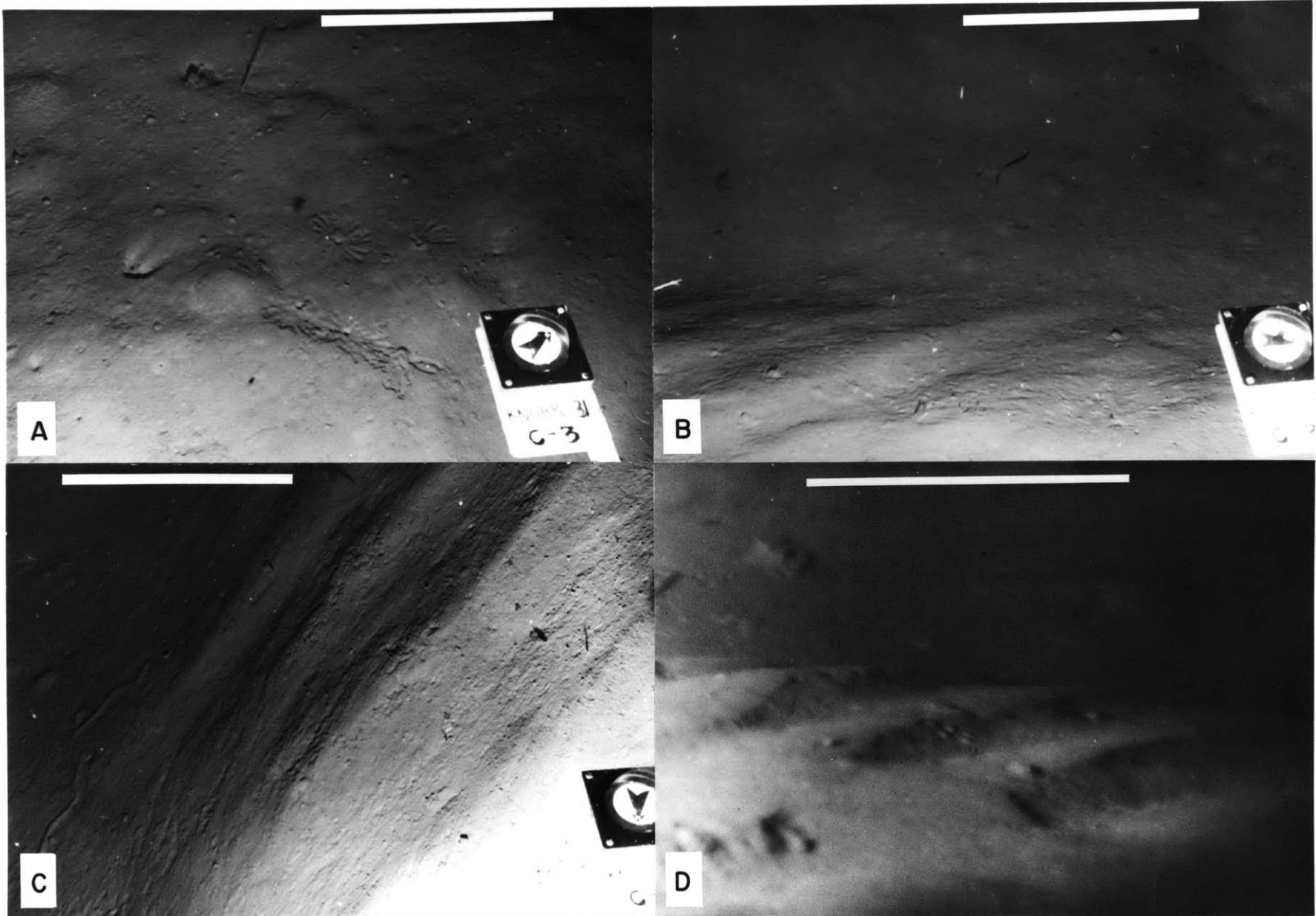
Figure 2.18

ripple points to the down-current direction.

The texture of the furrow floor is quite different from that of inter-furrow areas (Figure 2.16, 2.18). Few amimal tracks or burrows are found on the smooth furrow floors (Figure 2.18 b), while many are observed between them (Figure 2.18 a). In addition, large and small clumps of sea weed (possibly *Sargassum*) are found in the furrows (Figure 2.16 e), often partially buried by subsequent sedimentation. No sea-weed was observed in the inter-furrow areas.

Photographs from the area in between the furrows (Figure 2.18 a) are similar to those from other areas of the deep sea where deep currents are important geological agents (see Heezen and Hollister, 1971). Animal tracks and trails can be seen, but current activity has smoothed all but the most recent traces of animal activity. Moating is common around worm burrows, as are organisms bending in the current (Figure 2.18 a). These current indications are consistent with currents flowing towards N 25° W.

Few motile organisms were noted on the bottom photographs or observed from DSV TRIESTE II. Only two rat tail fish, one tripod fish, one vampire squid, and several jellyfish were observed from DSV TRIESTE II, and a possible holothurian and several vampire squids were noted on 750 deep-tow stereo photograph pairs.

Sessile organisms are abundant, particularly polychaetes. Many sponges and a few crinoids were also observed with both the deep tow and DSV TRIESTE II. Although organisms were common on the furrow walls and in the inter-furrow areas, they were rarely found on the floor of the furrow.

Near-bottom 4 kHz profiles (Figure 2.9) suggest that there is some sub-surface expression of the furrows. Although there are some side echoes because of the radiation pattern of the near-bottom transducer (Spiess and Tyce, 1973), many of the furrows, especially the larger ones, can be traced into the sediments indicating that these features have existed for a considerable period of time.

A short segment of side-scan sonar record recorded at 4370 m on the eastern side of the Bahama Outer Ridge crest (Figure 2.6, 2.19) shows that furrows are also developed in this area. The furrows trend roughly east-west, and tuning-fork junctions which open toward the east suggest that the furrows were formed by currents flowing to the west (in this case, flowing up the regional slope). Deep tow photos show that these furrows are quite similar to those on the west of the outer ridge, with relatively steep slopes and flat floors. (Figure 2.20 c,d), but no ripples are developed on the walls. The furrows here are spaced 40-80 m apart and have widths of 2 to 4 m, and depths of 1 to 2 m. These furrows are less deep

Figure 2.19.   Side-scan sonar record of furrows on east side
                of Bahama Outer Ridge crest. Record includes
                camera station 3-7 (Figure 2.6). Large curva-
                ture of furrows result from course changes,
                small wiggles from deep-tow vehicle yaw.

- 300

- 300

SLANT RANGE (m)

O

74

O ———————————————— I KM
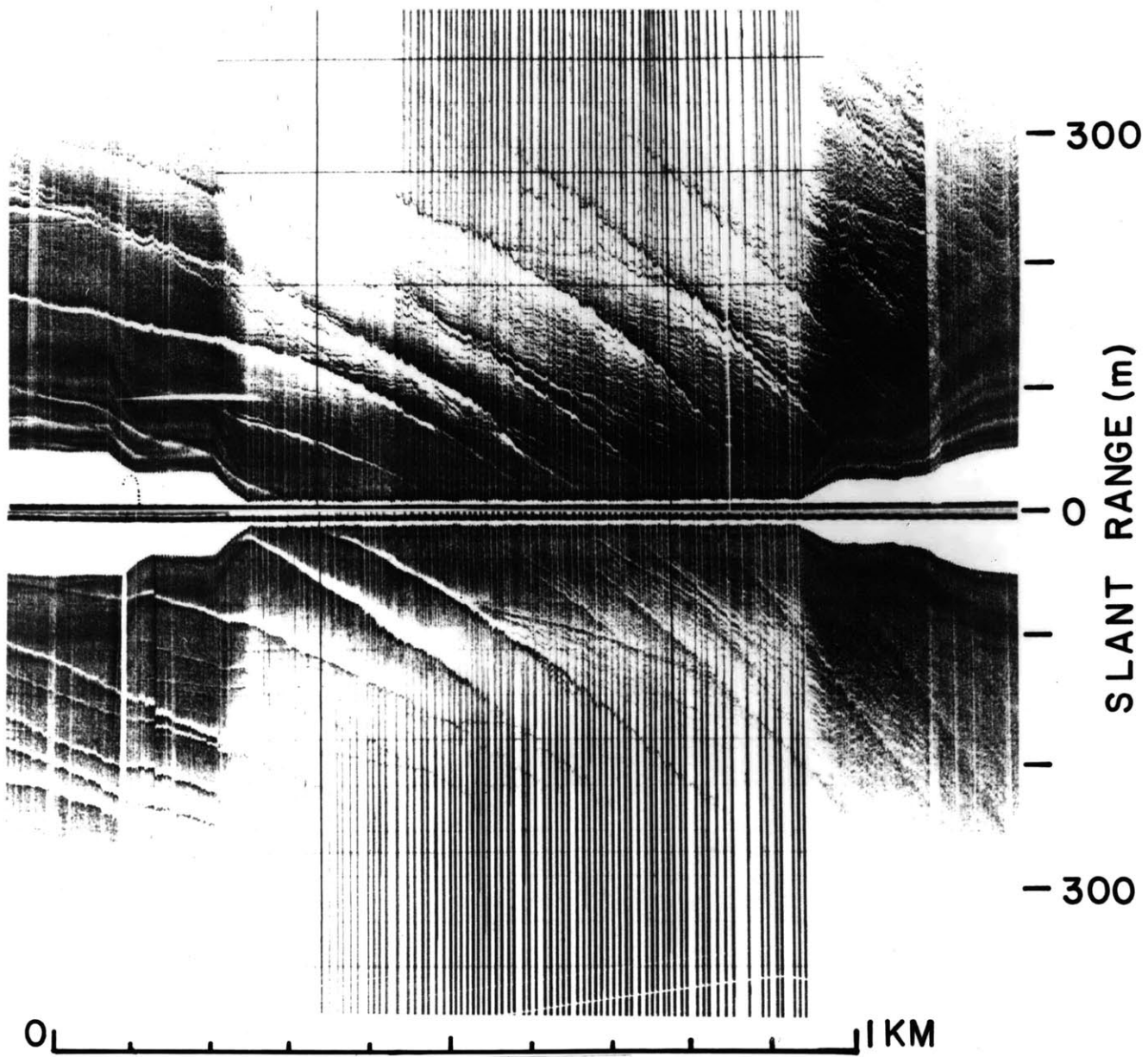
Figure 2.19

Figure 2.20.   Bottom photos of crest of Bahama Outer Ridge.

(a)   Smooth sea floor of camera station 3-5.
(b)   Inter-furrow area, camera station 3-7.
(c)   Furrow, camera station 3-7.
(d)   Furrow, camera station 3-7.

Camera stations indexed on Figure 2.6.   North towards the top of the page, scale bar is approximately one meter.
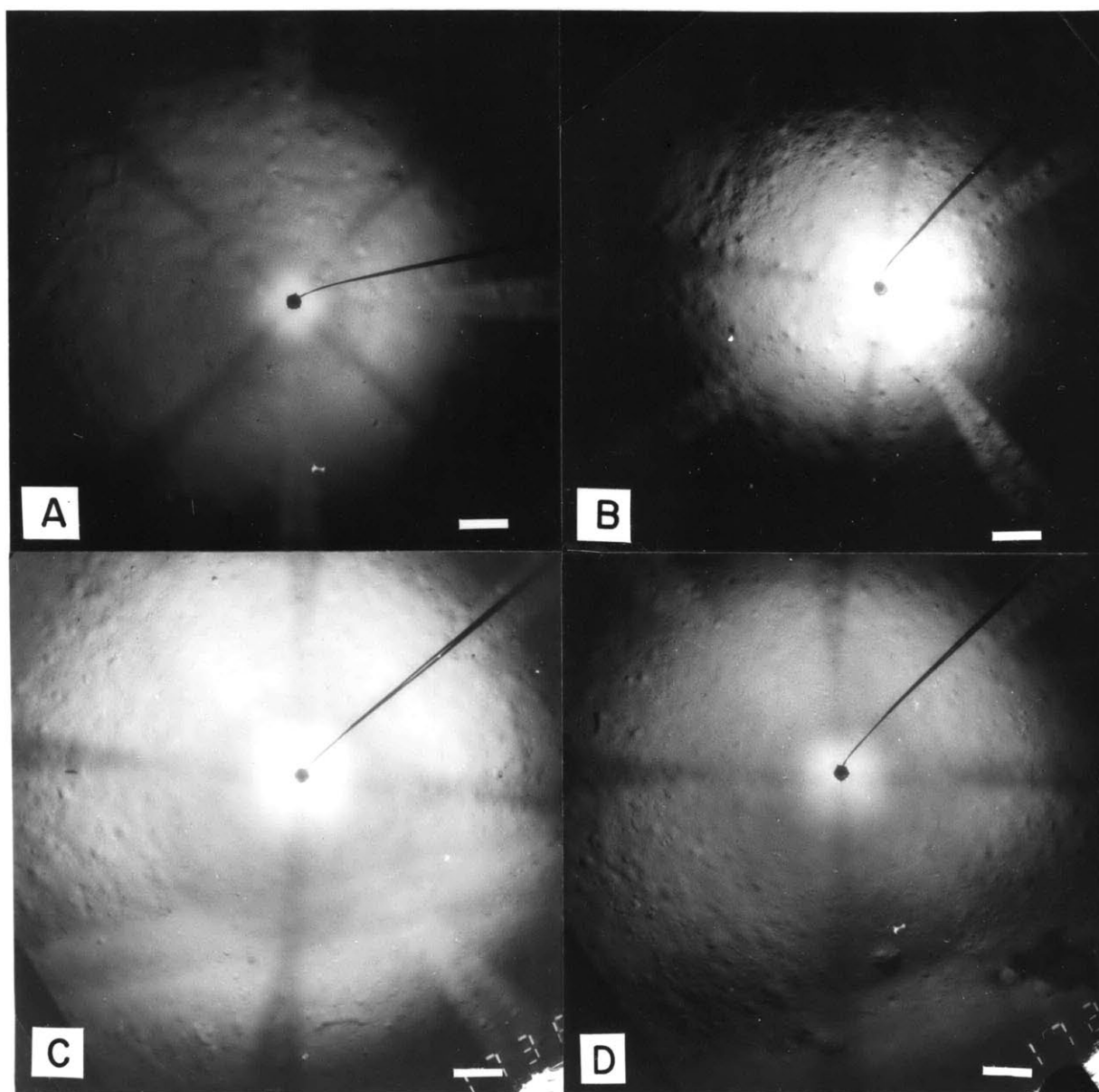
Figure 2.20

in the west than in the east. Bottom photographs (Figure 2.30b) show that the sea floor in the inter-furrow areas is smoothed less by bottom currents than is typical of the furrowed area on the western side of the ridge.

Superimposed on the furrow pattern on the side-scan sonar record is a pattern of smaller-scale features which trend northeast-southwest (Figure 2.19). They are spaced about 5 m apart and are 10 to 50 cm high. The features responsible for this pattern could not be identified in bottom photographs.

No hyperbolic echoes are observed on surface-ship echo sounding profiles in this area (Figure 2.10), although there is some suggestion of an interference pattern in the sub-bottom reflectors.

No current records were obtained from this site, but bottom photographs suggest that any current activity here is quite sluggish. These furrows are thought to be relict although not enough data are available for a definite statement.

Interactions between Furrows and Sediment Waves

Systematic relationships are observed between both the spacings of the furrows and the strike of the furrows and the position of the furrow on the large waves. The spacing between furrows is not constant over the entire area surveyed, but is related to the position of the furrow on the wave

topography. The furrows are most closely spaced on the northwest (downstream) side of a wave crest (Figure 2.21, 2.11). As they continue to the northwest, they join in tuning-fork junctions and become more widely spaced when the next wave crest is reached. At this point the furrows are the most widely separated. The pattern is repeated, as many furrows start on the northwest (downstream) side of the next wave crest, leading again to closely-spaced furrows.

The furrows are not straight over long distances, but they meander slowly as they pass over the large waves. They are displaced to the right as they go up a wave and to the left as they go down the other side (Figure 2.11). The deviation from perfect linearity is on the order of 100 m, well within the accuracy of the deep-tow navigation system (ca. 10 m).

The furrows strike in a more westerly direction on the southeast side of a wave and in a more northerly direction on the northwest side (Figure 2.21). A variation of 10 to 20° is observed between the strikes of furrows on different flanks of the same wave.

The furrows could be developed along places where planes of weakness (faults, etc.) crop out at the sediment surface. The meandering of the furrows over the sediment waves would
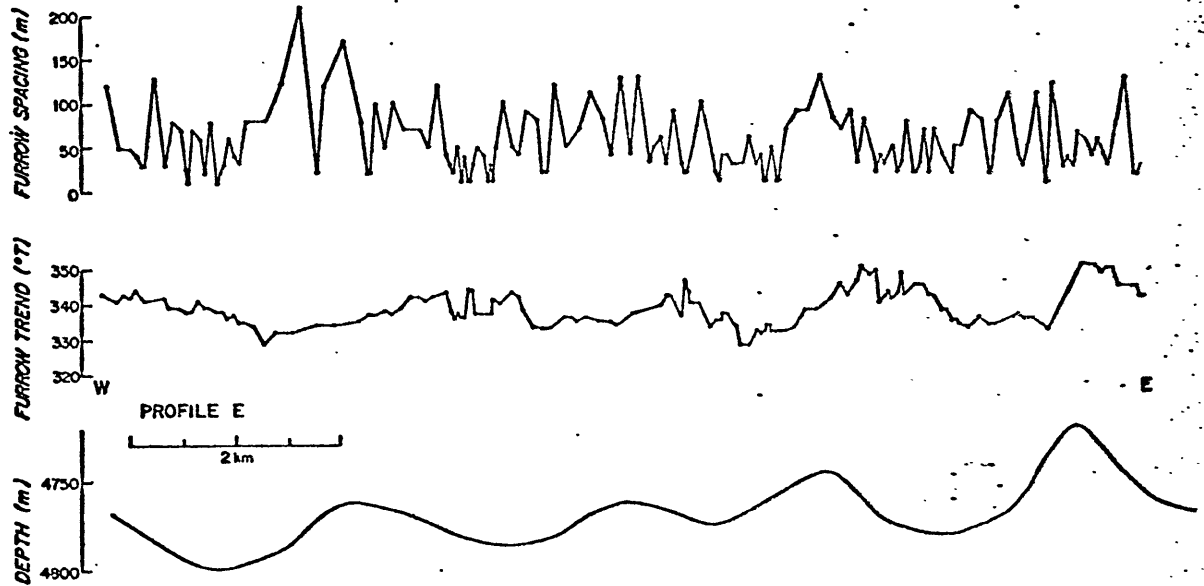
Figure 2.21. Variation of furrow spacing and orientation
over sediment waves. Variations are measured
along profile E (Figure 2.7).

then result from the intersection of a dipping plane with the wavy sediment surface (Lahee, 1952, p. 205-6). If this were the case, these planes would stike N 25° W and dip about 55° to th southwest. Two features of the furrow distribution argue against such an origin (Figure 2.11). First, the furrows join in a systematic manner with tuning-fork junctions opening to the southeast. Second, a large number of furrows begin on the northwest side of a wave crest. Neither of these patterns would be expected if the furrows were structurally controlled. In addition, where the furrows can be followed into the sediment (Figure 2.9), they suggest a dip of 90°, rather than the 55° needed for a structural origin.

Pockmarks

The extensive side-scan sonar coverage in this area has revealed another feature of the sea floor previously unidentified from the deep sea: pockmarks (Figure 2.22). The pockmarks are circular depressions in the sea floor which range from 30 to 40 m in diameter. Slant-range calculations suggest that the pockmarks may be 6 m deep. These are morphologically similar to the "pockmarks" which have been reported from continental shelves (King and MacLean, 1970; VanWeering et al., 1973).

Figure 2.22.   Pockmarks on the Bahama Outer Ridge. Circu-
                lar side-scan sonar targets are pockmarks,
                long targets are furrows. Large curvature of
                furrows results from a course change, small
                wiggles from yaw of deep-tow vehicle. Record
                indexed as "B" on Figure 2.7.
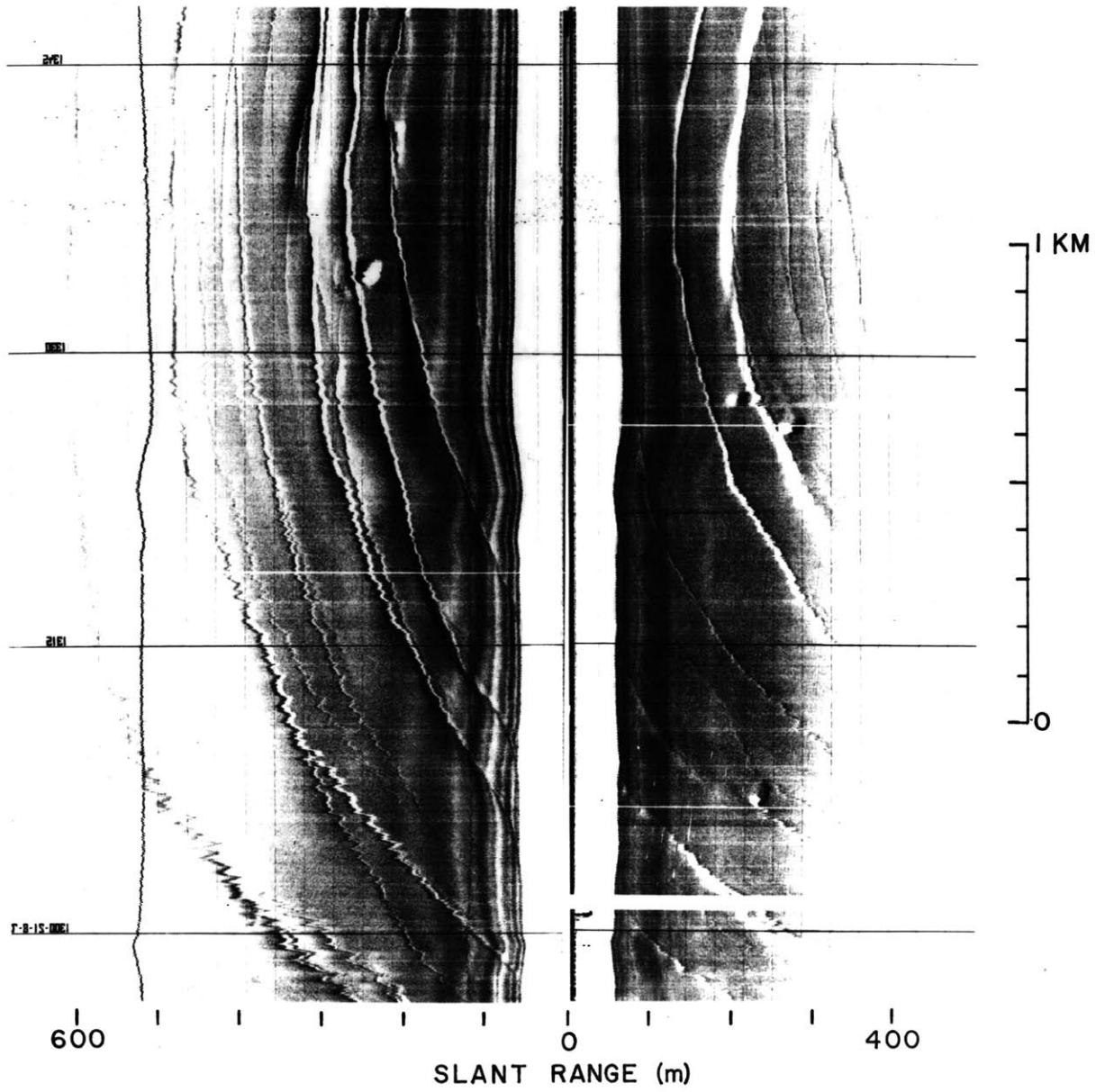
Figure 2.22

In all, 15 of these features were found in the trans-
ponder navigated survey area (the small circular targets on
Figure 2.11) and 25 were found during the tow to the ridge
crest. The pockmarks were not observed by any of the other
instrumentation systems used.

The pockmarks appear to be found in groups rather than as
uniformly distributed entities. Pockmarks are more commonly
observed upslope from the navigated survey area.

Two hypotheses have been put forward to explain the ori-
gin of these features where they are seen on the continental
shelves (King and MacLean, 1970). One is that the pockmarks
mark the site of gas seeps from underlying gas-rich sedi-
ments into the water column. The other is that they mark
sites where water from the sediments escapes into the water
column. In either case the upward motion of the gas or water
is thought to enhance erosion around the seep and cause the
formation of a conical depression. Studies of pockmarks on
the continental shelf have supported the idea that they are pri-
marily produced by the seepage of gas from the sea floor
(King and MacLean, 1970); however, the role of water seepage
cannot be ruled out.

At the depths at which the pockmarks are observed on the
Bahama Outer Ridge, (4400 to 4800 m) they are apparently form-
ed by water, rather than gas, seepage. At these depths, very

high partial pressure of gas (ca. 500 atm) would be required to form gas bubbles. At these high partial pressures and the low ambient temperatures (ca. 2.2°C) the gas (most likely methane) would tend to form solid clathrates rather than gas bubbles (Tucholke et al., 1977). The clathrates would remain in the sediments and not produce the features seen here. The sediments of the Bahama Outer Ridge have been deposited at high, and most likely variable, sedimentation rates. Average Neogene sedimentation rates are greater than 50m/my, since the ridge is thicker than 500 m and is generally younger than Middle Miocene (10 my) (Section II.A). This high (and probably variable) sedimentation rate may not have allowed interstitial waters to leave the sediments as fast as compaction occurred. This is especially true if the most recent sedimentation rates are lower than those at which the bulk of the ridge was deposited. The interstitial waters may seep out at localized vents. The pockmarks are the surface expression of these vests.

Bahama Ridge Crest

The furrows and occasional pockmarks extend upslope to the end of the hyperbolic echoes observed on the surface-ship echo sounder (Figure 2.1, 2.10, and 2.23). At this point the character of the bottom changes drastically. The furrows die

W C

FURROWS ◀

CAM RUN
3-5

CAM RUN
3-6

FURROWS

C' E
4200 m-

CAM RUN
3-7

BAHAMA OUTER RIDGE CREST
NEAR-BOTTOM 4 KHZ PROFILE

4600-

0   5
KILOMETERS
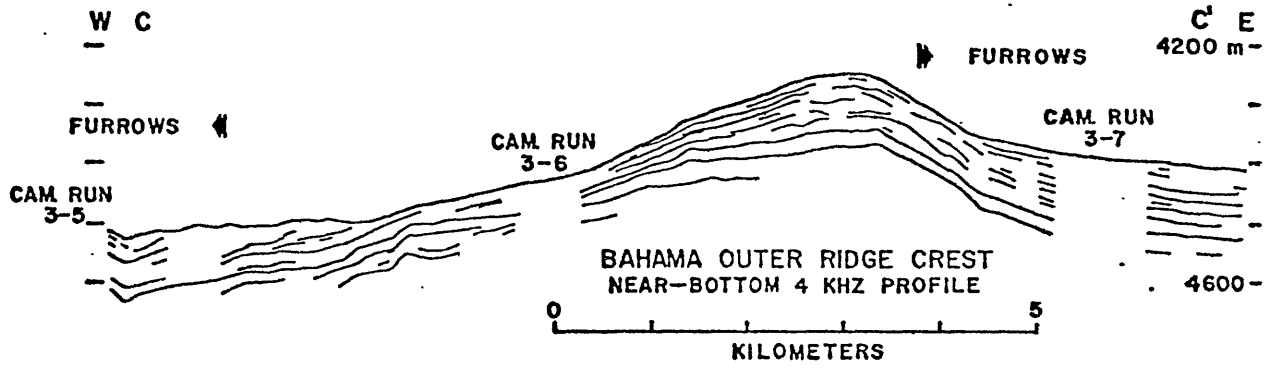
Figure 2.23.   Near-bottom 4 kHz profile of crest of Bahama
Outer Ridge. Profile indexed on Figure 2.6.
V.E. = 6X.

out and, at the same time, sub-bottom reflectors appear to crop out at the base of a small depression (Figure 2.23). reflectors also appear to crop out at other locations on the step slope, generally at breaks in slope. The slope is quite steep (up to 6°), and bottom photographs (Figure 2.20 a) and side-scan sonar show it to be generally feature-less. Animal tracks and trails appear to be quickly smooth-ed over indicating that strong currents are present. One possible pockmark provided the only side-scan sonar target.

As no material is seen piled up at the base of this erosional area, the erosion is assumed to be due to current activity rather than to some other process, like slumping.

AREA 2 (LARGE FURROWS, RIPPLES, TRIANGULAR RIPPLES, CONTACT WITH ABYSSAL PLAIN)

Area 2, at lat. 28°37'N, long. 75°21'W, average depth 4970 m, is characterized by the presence of pronounced hyper-bolic echoes and includes the transition between Bahama Outer Ridge (characterized by hyperbolic echoes) and an embayment of the Blake-Bahama Abyssal Plain (characterized by a coher-ent echo return; Figure 2.24, profile A). The objectives of surveying this area were (1) to determine the nature and origin of the features responsible for the hyperbolic echoes, (2) to study the nature of the abrupt transition between the Bahama Outer Ridge and the Blake-Bahama Abyssal Plain, and (3) to determine the surface morphology of the abyssal plain.

Figure 2.24.   Echo-sounding profiles of large furrows.

Profile A.   Surface-ship 3.5 kHz profile of
Bahama Outer Ridge-Abyssal Plain contact.

Profile B.   Near-bottom 4 kHz record of contact
shown in profile A. (Slight undulations in
record result from variations in fish eleva-
tions.)

Profile C.   Upper profile: Near-bottom narrow-
beam echo-sounding (40 kHz) record of furrows.

Lower profile: Near-bottom 4 kHz
taken simultaneously with bathymetric profile.
Note edge effects caused by wide beam angle.

PROFILE A

SW   0 ⊢———⊣ 1 KM   NE   ⌐ 4950 m

5000 m

5050 m

PROFILE B

W   E ⌐ 4950 m

5000 m

5050 m

PROFILE C - 40 KHZ

W   E ⌐ 4950 m

5000 m

PROFILE C - 4 KHZ

4950 m

5000 m

0 ⊢—————⊣ 1 KM   5050 m
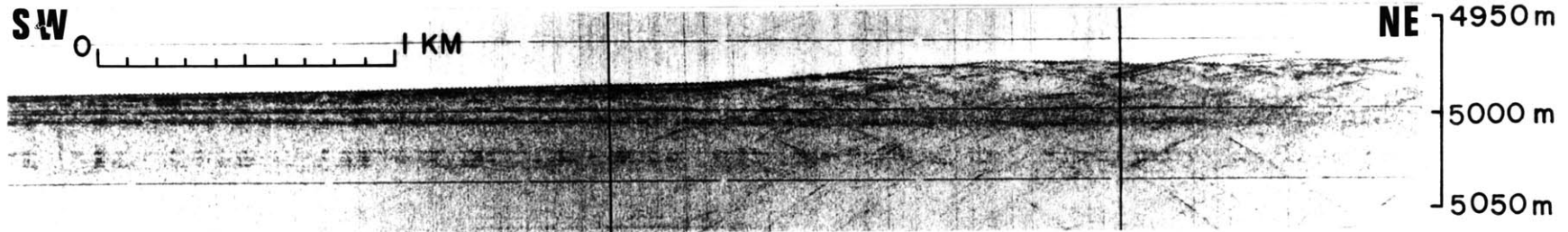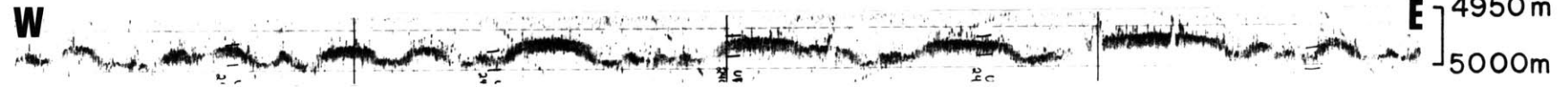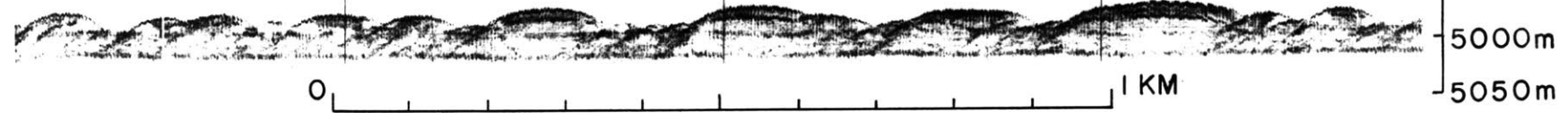
Figure 2.24

A total of three deep-tow lowerings were made in this
area (Figure 2.25). Lowerings 1 and 2 of R/V Knorr, Cruise
31, leg 5, were transponder-navigated surveys which studied
the outer ridge morphology and the contact of the outer
ridge with the abyssal plain. Deep-tow lowering 4, a satel-
lite-navigated tow, studied the surface morphology of the
abyssal plain. (Lowering 3 was in Area 1.) Three current
meters were deployed for the duration of lowerings 1 and 2.
Three photos from two bottom-camera lowerings also came from
this area. One dive was made with the Bathyscaphe TRIESTE II
at lat. 28°37.5'N, long. 75°26'W (Dive 15-77) to study these
features (Figure 2.25). Along with bottom photographs of
the entire region, one short core was recovered from a tri-
angular ripple. Subsequent sections will discuss the sedi-
ment studies and the near-bottom fluid motions.

Large Furrows

The most striking features of this area are the large,
linear grooves which are responsible for the hyperbolic
echoes (Figures 2.24, 2.26 and 2.27). These features have
some morphological similarities to the furrows described from
Area 1 and are therefore also termed furrows. They are long,
linear features which trend N 5° W, parallel to the direction
of the regional contours and to the currents measured at the
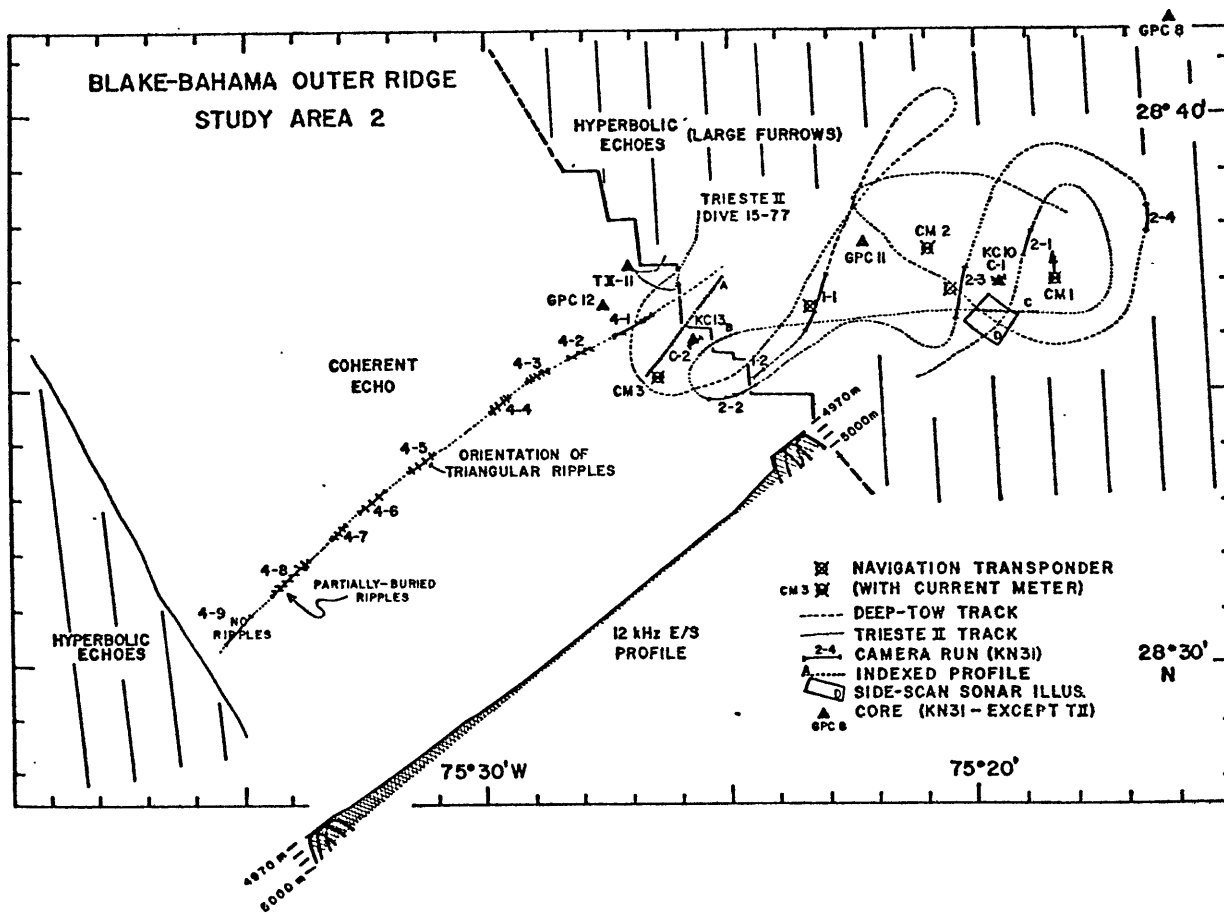
Figure 2.25.   Echo character and index map for Area 2.   Area
covered by map is shown on figure 2.1.

Figure 2.26. Side-scan sonar record of large furrows, Area
2. Wiggles due to yaw of deep tow. Record
indexed as D on Figure 2.25.
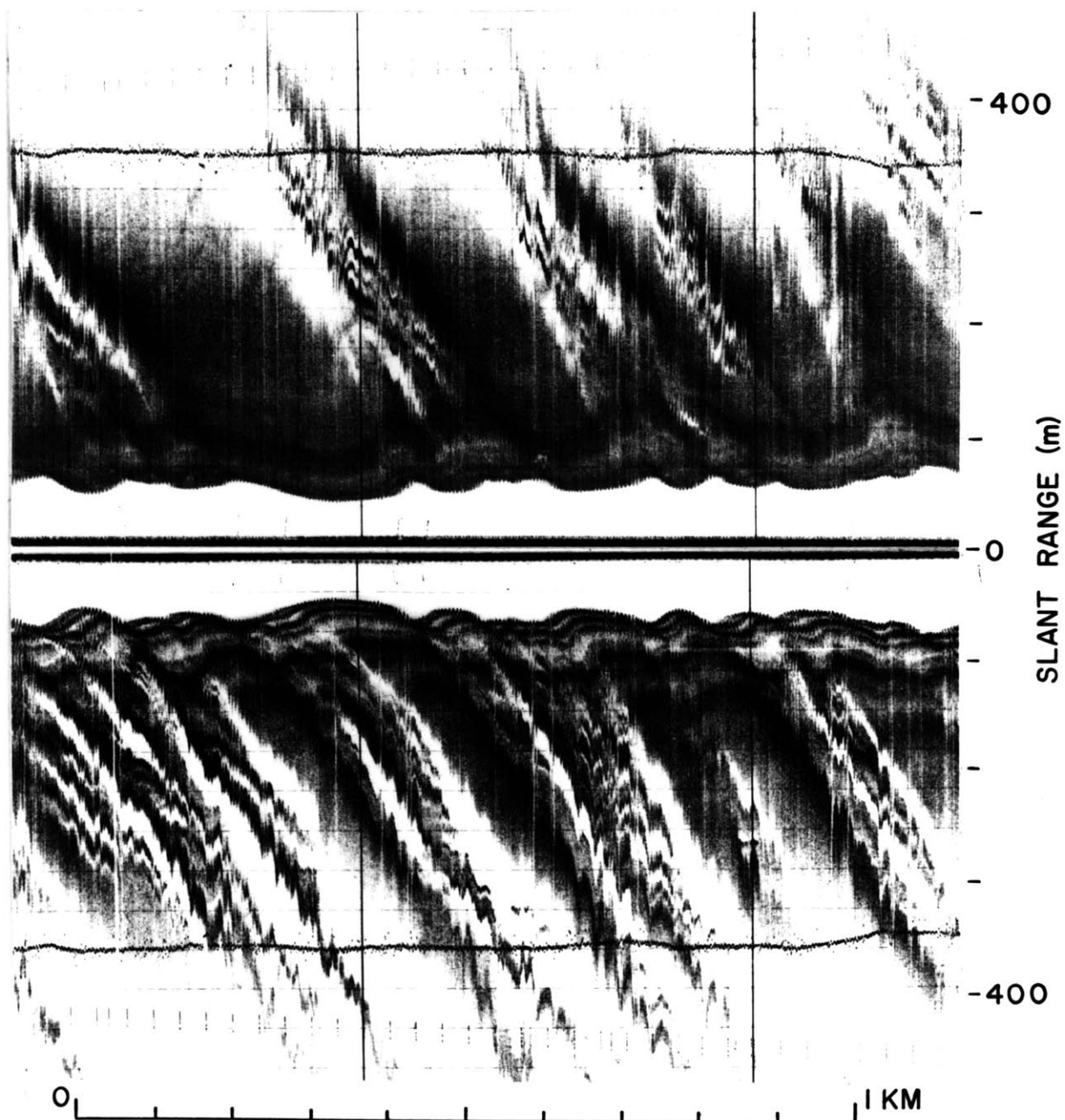
Figure 2.26

Figure 2.27. Side-scan sonar mosaic of furrows in Area 2.
Side-scan sonar records (not corrected for
slant range) are shown at the proper scale
along the deep-tow track.

SIDE-SCAN SONAR MOSAIC — LARGE FURROWS
BLAKE-BAHAMA OUTER RIDGE (AREA 2)
NAVIGATION TRANSPONDER
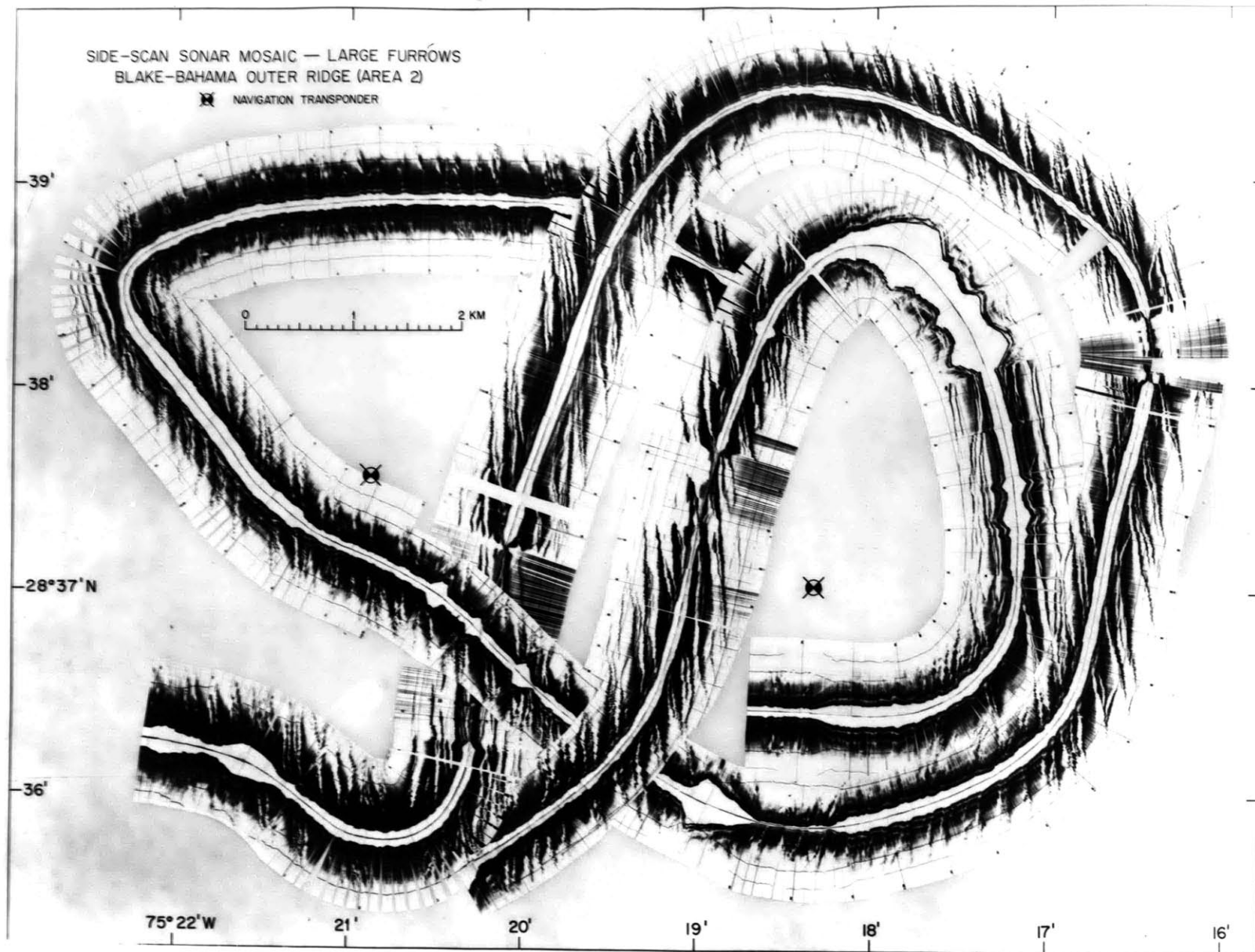
Figure 2.27

time of the survey (Section II.B.2), and tuning-fork junctions

opening to the south (into the current direction) are often

observed (Figure 2.27). However, these furrows are much

larger than those mapped in Area 1. They are from 50 to

150 m wide, 4 to 27 m deep, and are spaced 50 to 350 m apart

with an average spacing of 190 m (Figure 2.28). Near-bottom,

narrow-beam echo-sounding profiles taken with the deep-tow

indicate that these features have steep sides (slopes of up

to 45° common) (Figure 2.25, profile C).

Deep-tow 4 kHz sub-bottom records clearly show that the

furrows are erosional, since shallow sub-bottom reflectors

are observed to crop out on their walls and deep reflectors

continue undisturbed beneath the furrows. The surface of

one inter-furrow area often corresponds to a sub-bottom

reflector of some nearby inter-furrow area (Figure 2.24,

profiles B,C) implying that material has been eroded from

these areas. Sub-bottom profile (Figure 2.24, profiles A,

B, and C) show that deep reflectors continue undisturbed

beneath the furrows (hyperbolic echoes) and the abyssal

plain suggesting that furrow development has not been

structurally controlled. Sediments recovered from this area

also show the erosional origin of this topography (Section

II.B.2).
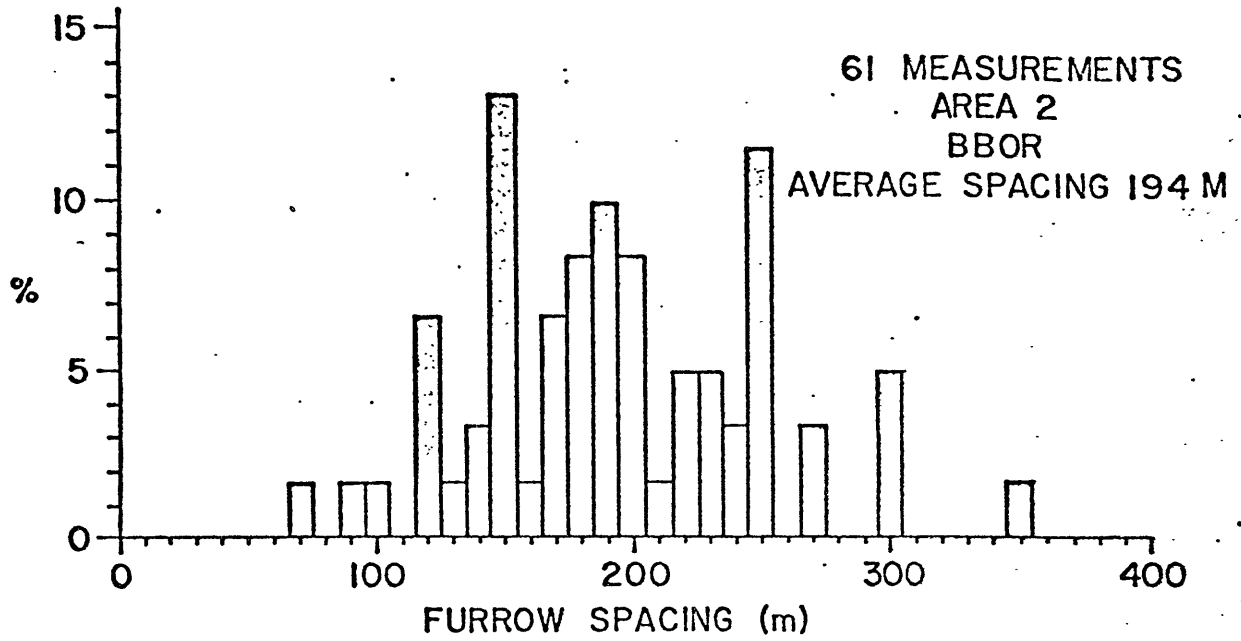
Figure 2.28.   Spacings between furrows in Area 2.

Photographs and visual observations indicate that the areas between the furrows are generally flat and quite featureless, with few animals or their tracks present. The walls of the furrows are quite steep. Measurements of stereo photographs indicate that the steepest slope photographed was 45° with slopes as steep as 30° common. Visual observations indicate that near-vertical cliffs are common (Figure 2.29 a), but often extend vertically for only a few meters. The walls are sites of active erosion, as sedimentary layers are seen outcropping on them. The outcropping layers appear to be hard and thin. The origin of these layers is not known, but they may be formed by the lithification of silt laminae as they are exposed to oxygen-rich sea water by erosion of the furrow. This is in contrast to the furrows mapped in Area 1, where a well-developed ripple pattern was observed.

The bases of the walls are often the site of accumulations of large lumps of sediments forming prominent talus slopes resulting from sediment removed from the walls (Figure 2.29 b and c). The floors of the furrows are quite active areas with ripples, sediment tails, and even small furrows often found there (Figure 2.29 b-f). The continuing input of sediment from the walls has made the furrow floors depositional areas and the walls erosional ones. The continuing

Figure 2.29. Photographs of large furrows.

    (a) Steep furrow wall. DSV TRIESTE II Dive
          15-77.

    (b) Base of furrow wall and talus. (2-3, ID.
          222031.)

    (c) Talus at base of furrow wall. (2-2, ID.
          175714.)

    (d) Furrow floor.(2-1, ID.043040.)

    (e) Furrow floor.(2-1, ID.730817.)

    (f) Furrow floor showing small furrow in
          large one .(2-4, ID.044717.)

    a: Camera pointed towards 238°, b-f: North
       is toward the top of the page. Scale bar
       is approximately one meter.
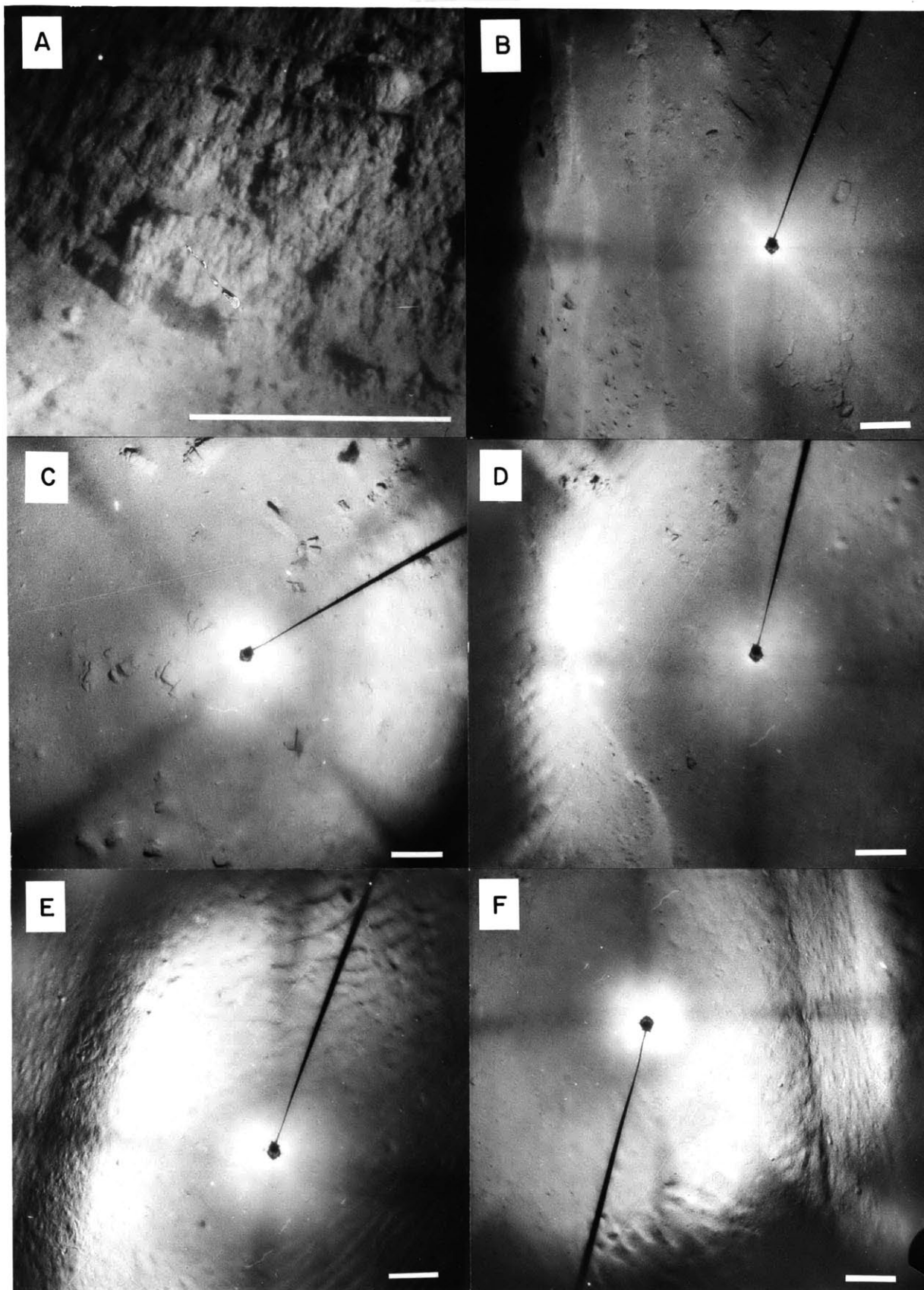
Figure 2.29

supply of sediments to the furrow floors provides abundant sediment for sculpting by currents. The furrows also act as traps, catching material moved along the sea floor by currents, such as bundles of seaweed and coarse sedimentary material (Section II.B.2).

The manner in which the furrow walls are eroding, and the relative importances of biological and current activity in causing such erosion can be estimated from bottom photographs. Animals can often be seen living in areas of the furrows where outcropping sediments are observed. Either these animals may be taking advantage of possible organic-rich sediments exposed by erosion, or they may have found a suitable substrate for attachment. As the organisms either feed on or attach themselves to the sediments, they loosen them and make the sediments more readily removed by currents or gravity. The feeding of pelagic animals on the infauna of the sediments of the walls also will enhance erosion. The rate at which these biological processes act is not known. Although their rates may be quite small, these processes may be significant over long periods of time. The gradual nature of this erosion is indicated by the presence of delicate(?) sedimentary layers only a few centimeters thick cropping out several centimeters as they are undercut by the action of the currents and/or organisms. The undercutting continues until

such time as the overlying layer is no longer capable of supporting its own weight; then it breaks off, falls down slope, and becomes part of the talus slope at the base of the furrow wall.

As the walls of the furrows appear to be sites of active erosion, the features should be termed active. The role of currents in maintaining these features is not clear. Bottom currents were steady and flowing to the north, parallel to the furrows, at the time the deep-tow investigations in August 1973 (Section III.B.3). However, during the DSV TRIESTE II dive in September, 1977, the bottom current was flowing toward 260°, nearly perpendicular to the furrow trend.

Triangular Ripples

A tongue of coherent echo return, a portion of the Blake-Bahama Abyssal Plain, intrudes into the area characterized by hyperbolic echoes (Figure 2.2 and 2.25). The most pronounced topographic feature of the embayment is the "triangular ripple" (Figure 2.30). These features are a series of 2 m to 10 m long parallel ridges of triangular cross section spaced 1 m to 5 m apart. The ripples appear to be 10 to 20 cm high and about 75 cm wide at the base. Similar features have been reported from other areas of the deep-sea where deep currents are thought to be active (Zimmerman, 1971; Heezen and

Figure 2.30. Photographs of triangular ripples. Note
change in orientation of ripples (North is
towards the top of the page).

(a) Camera station 4-1 (ID.073936)
(b) Camera station 4-2 (ID.090521)
(c) Camera station 4-4 (ID.105411)
(d) Camera station 4-6 (ID.135919)
(e) Camera station 4-8 (ID.163322)
     Note: triangular ripples are partially
            buried.
(f) Camera station 4-8 (ID.163815)
     Note: Triangular ripples almost com-
            pletely buried.

Camera stations located on Figure 2.25.
Scale bar is approximately one meter.
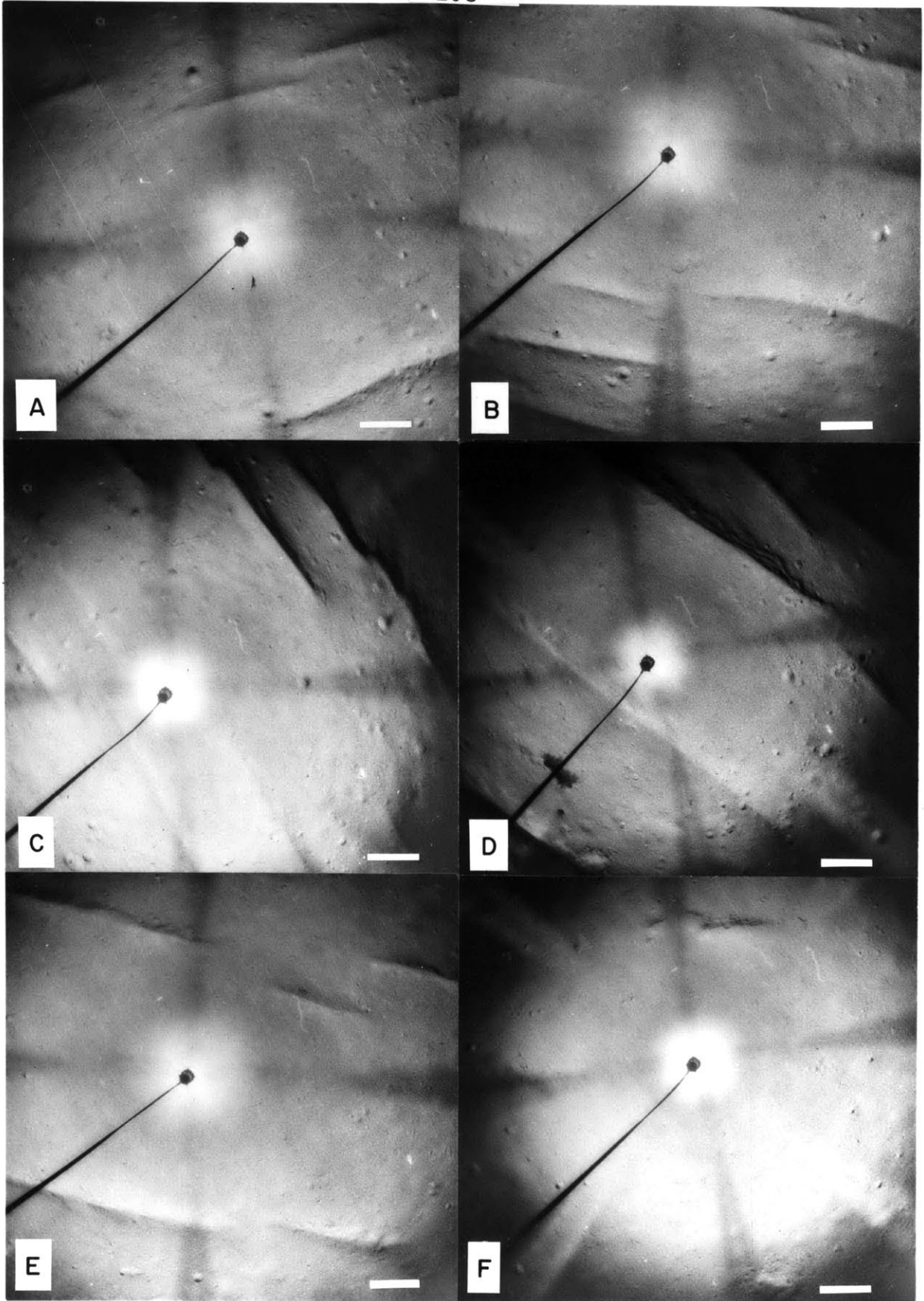
Figure 2.30

Hollister, 1971) and have been described as paralleling the currents. In this area, they do not have a constant orientation; the long axis of the ripples rotates through an angle of 45° (from 070° to 125°) over a distance of 5 km from the contact with the outer ridge (Figures 2.25 and 2.30 a,c). The triangular ripples rotate back to 070° as the other side of the embayment is approached (Figure 2.25 and 2.30 e,f). At both the southwestern and northeastern margins of the embayment, the ripples are gradually buried by more recent sediments. The zone of burial is 3 km wide on the SW side and only about 100 m wide on the NE side. No trace of the ripples can be seen in the last camera run of the transect (Camera station 4-9; Figure 2.25).

The true abyssal plain (slopes less than 1:1000; Heezen et al., 1959) is only present over the middle portion of the embayment (Figure 2.25). As either side is approached, a small sedimentary wedge (slopes of 1:250 to 1:550) is observed prograding onto the abyssal plain. The surface of such wedges have been termed periplains by Heezen and Tharp (personal communication). These sediment wedges appear to be built from sediments eroded from the furrowed areas. The presence of a larger sediment wedge on the south side suggests that northward-flowing currents have been more important geologically.

The burial of the triangular ripples on these periplains sugguests one of two things. First, the triangular ripples may have been formed in a period when current speeds were higher. Second, these ripples may only be out of equilibrium with the present regime near the margins of the embayment. This may result from a higher sedimentation rate along the margins. Available data do not allow us to choose between these two alternatives.

The presence of triangular ripples in this area also was noted by Bryan and Markl (1966). They related these features to the fuzzy and hyperbolic echoes of the outer ridge rather to the coherent echo return of the abyssal plain.

Abyssal Plain - Outer Ridge Transition

The transition between the abyssal plain (periplain) and
(hyperbolic echoes)
the outer ridge∧is quite abrupt. Surface-ship 3.5 kHz echo-sounding records and airgun records indicate that the contact is on the order of a few hundred meters wide (Figure 2.24, profile A). Deep-tow 4 kHz and narrow-beam echo-sounding records, on the other hand, indicate that this contact may be much sharper (Figure 2.24, profile B), perhaps on the order of 10 m. Side-scan sonar records also indicate that the contact (end of furrowed topography) is quite sharp, on the order of 50 m wide. Side-scan sonar records and transponder navigated

surface-ship profiles indicate that the contact is not a
linear one, but consists of a series of short, straight seg-
ments about 1 km long which intersect at 90° (Figure 2.25,
2.31). Outliers of the outer ridge sediments, seen on side-
scan sonar records (Figure 2.31) indicate that the contact
may be migrating with time.

These observations show that the contact between the
outer ridge and abyssal plain in this area is a dynamic one.
Sub-bottom reflectors are observed to pass under the contact
between the outer ridge and the abyssal plain (Figure 2.24,
profile A), and giant piston cores from this region reveal
turbidites interbedded with hemipelagic sediments (Section
II.B.2). Sedimentary wedges of fine-grained material are
presently covering the abyssal plain.

AREA 3 (SEDIMENT WAVES)

Area 3 extends from 29°25' to 30°00' N and from 75°05'
to 75°50'W (Figure 2.32), from slightly east of the crest of
the Bahama Outer Ridge to the Blake-Bahama Basin. The ob-
jectives of the study in this region were (1) to determine
the distribution of a large group of sediment waves and (2)
to make profiles with an STD over the sediment waves to
obtain the temperature distribution within the lower portion
of the water column and to observe how it varied over a wave.

Figure 2.31. Side-scan sonar mosaic of transition between
              outer ridge (furrowed topography) and abyssal
              plain. (Side-scan sonar records not corrected
              for slant range.)

FURROWS

PERI-PLAIN

28°36'N

FURROW OUTLIER

SIDE—SCAN SONAR MOSAIC
TRANSITION BETWEEN
OUTER RIDGE AND ABYSSAL PLAIN
BLAKE—BAHAMA OUTER RIDGE
(AREA 2)

✖ NAVIGATION TRANSPONDER

0   1   2 KM

35'

26'   25'   24'   75°23'W   22'

Figure 2.31

109
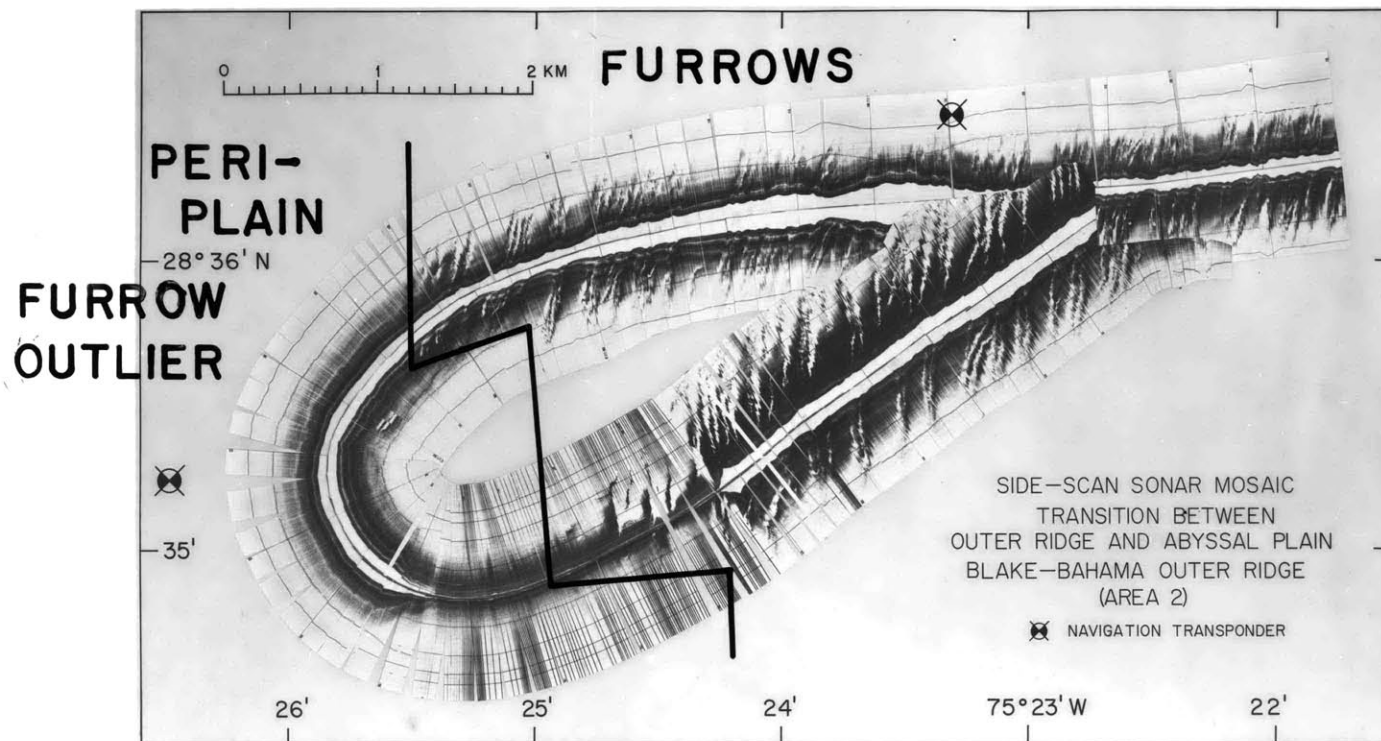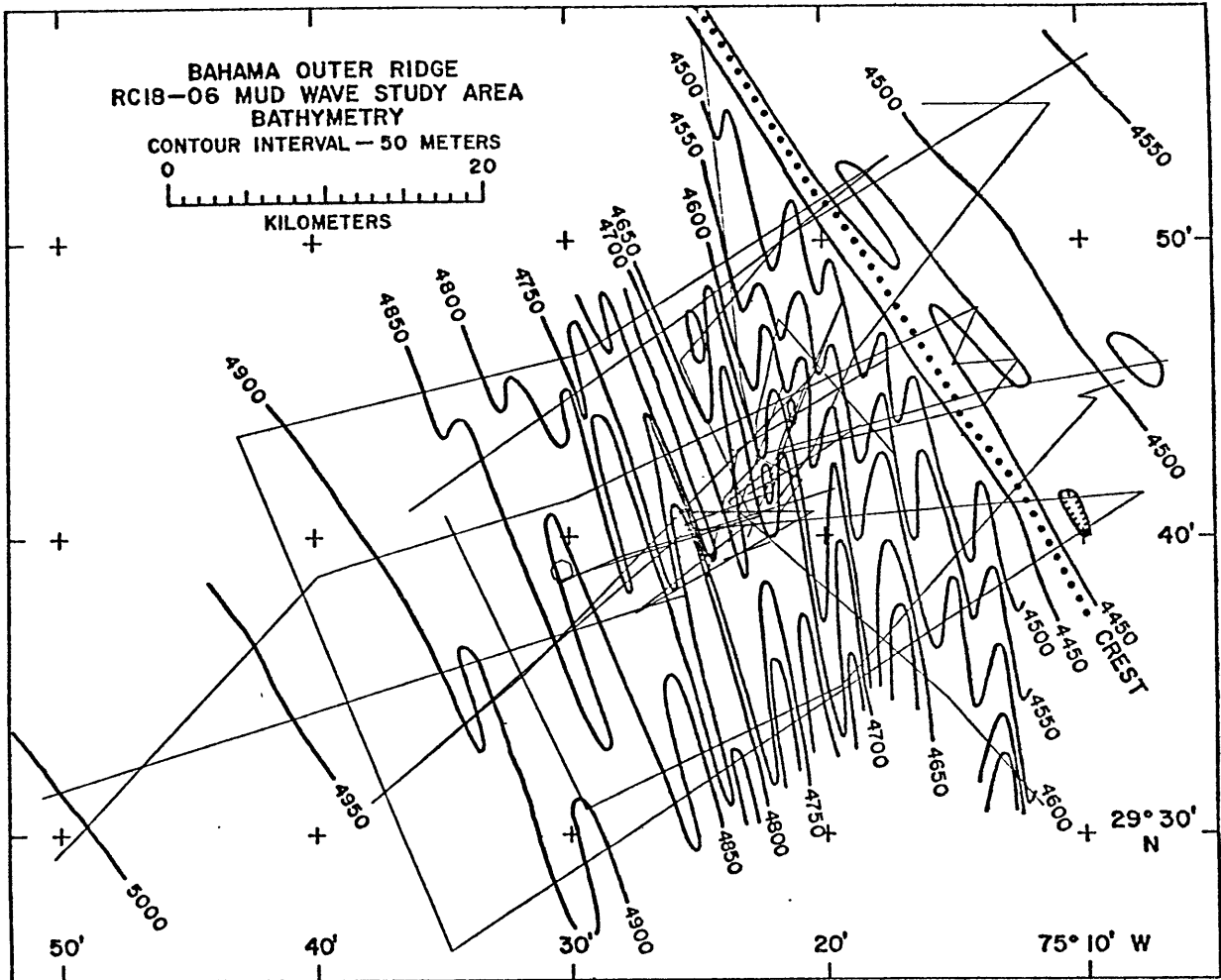
Figure 2.32. Bathymetric map of Area 3 (RC18-06 study area)
             contour interval 50 m. The area covered by
             this map is shown on Figure 2.1.

Ten days were spent in this area in July, 1975, on the R/V

Robert D. Conrad, Cruise 18, Leg 6. During that time a

detailed 3.5 kHz echo-sounding survey was made. Also ten STD

stations to the bottom (eight of which consisted of two or

more hits on the bottom; yo-yo's), 11 camera stations, and

ten nephelometer stations were occupied. Five cores and one

ten-day current meter time-series nephelometer array (moored

10 and 15 m above the bottom at 29°42' N;75°22' W in a water

depth of 4638 m) were also recovered. Subsequent sections

will describe the results of the sediment studies and the

near-bottom STD and current measurements.

Sediment waves

A total of 19 large sediment waves were mapped on the

eastern flank of the Bahama Outer Ridge (Figure 2.33) on the

basis of the extensive coverage of satellite-navigated bathy-

metric profiles. All profiles were collected at speeds less

than 6 knots. Profiles were adjusted as necessary to give a

consistent picture of the bathymetry. These adjustments were

rare and generally less than 1 km.

Fourteen of the large mud waves have a lateral extent

greater than 10 km, and a few waves can be followed for 30 km

(Figure 3.33). The remaining five waves are considerably

more limited in extent, often extending for less than 5 km.

The sediment waves are oriented at an angle to the regional

contours. This orientation is in the same sense as that

BAHAMA OUTER RIDGE
RCI8—06 MUD WAVE STUDY AREA
——— WAVE CREST
------- WAVE TROUGH

▲ CURRENT METER
——— STD YO YO
● CORE (RCI8)
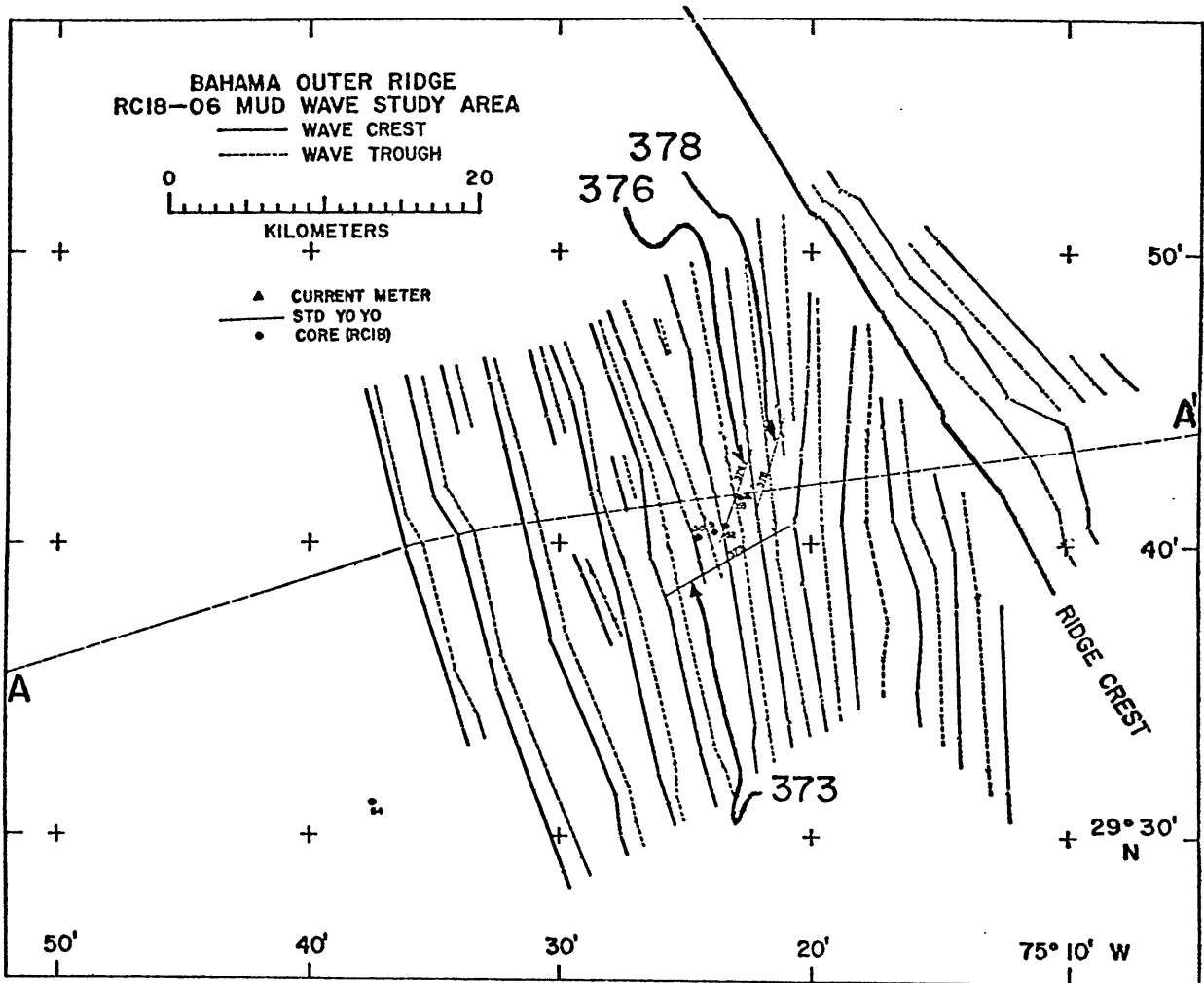
Figure 2.33. Locations of sediment wave crests and troughs, Area 3. The positions of the current meter/ nephelometer array, three STD yo-yo's, sediment cores, and profile AA' are shown.

observed in Area 1 (i.e., the southern end of the wave is deeper than the northern end). The waves are oriented at the largest angle to the regional contours (40°) near the ridge crest, where the regional gradient is the steepest (1:40), and at the shallowest angle (20°) where the regional gradient is less (1:160). The waves do not appear to extend all the way to the ridge crest, but end as small-amplitude waves two or three kilometers from the crest (Figure 2.34). Two of the major sediment waves start within the survey area. These waves mark places where the orientation between the sediment waves and the contours changes abruptly. It was not possible to determine a more detailed bathymetry for these critical locations, as the navigational uncertainties become limiting.

All sediment waves developed on the western side of the outer ridge crest do not have the same shape (Figure 2.34). Waves shallower than 4850 m have a regular, nearly sinusoidal shape similar to the regular sediment waves described from Area 1. Waves deeper than 4850 m are more asymmetrical, with the downslope flanks being three to four times longer than the upslope flanks. The waves have maximum heights of about 100 m in a depth range of 4650 to 4850 m (spacing between crests 2 to 3 km). Those deeper than 4850 m average 30 m in height (spacing 2 to 4 km), while waves shallower than 4650 m average 50 m in height (spacing 2 to 4 km).
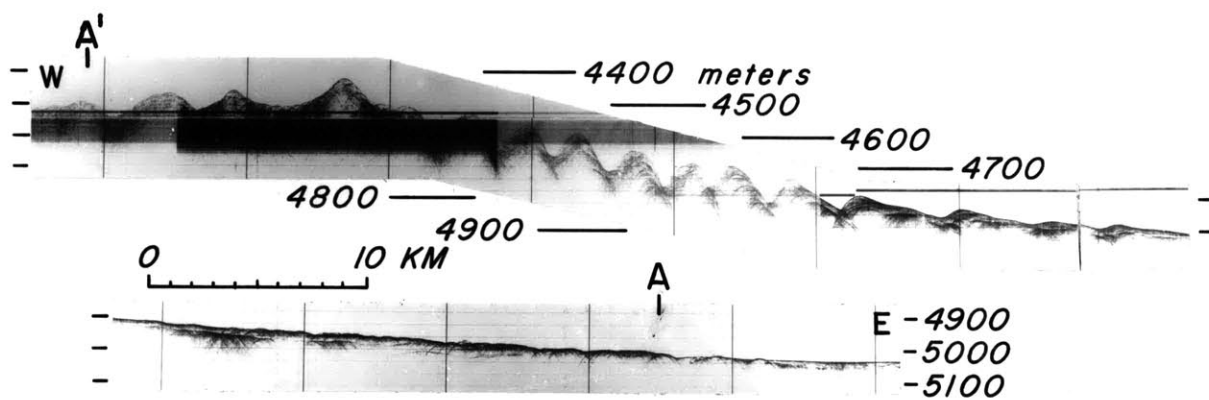
Figure 2.34.   Surface-ship 3.5 kHz record of sediment waves
(Area 3).   Profile indexed on Figure 2.33.

Some sediment waves were also observed on the eastern
side of the crest of the Bahama Outer Ridge. They are
symmetrical, parallel to the ridge crest, and are best
developed on a slight bathymetric high near the crest. The
amplitudes of these waves are less than 50 m.

The internal structure of the sediment waves is similar
to that reported for the waves in Area 1. Although intense
hyperbolic echoes often obscure the sub-bottom reflectors,
3.5 kHz records indicate that the sediment waves on both
sides of the ridge crest have migrated upslope (towards the
crest). Many of them have hyperbolic echoes developed on
internal reflectors as well as on the sediment surface
(Figure 2.34). Records of shallow-sediment structure ob-
served with a 12 kHz pinger attached to near-bottom instru-
ments (Ewing et al., 1973) show that, in some parts of the
survey area, sedimentary layers crop out on the sediment
surface.

Hyperbolic Echoes (furrows)

Hyperbolic echoes are present over much of the area sur-
veyed, occurring on most of the sediment waves on the western
side of the Bahama Outer Ridge, on the crest of the outer
ridge, and on the sediment waves to the east of the ridge.
The topographic features responsible for the hyperbolic
echoes were not directly observed, but they appear to be

similar to the large furrows described from Area 2. The
hyperbolic echoes are caused by sea-floor lineations trend-
ing 322° (parallel to the regional contours). The orientation
of the linear features was determined by turning the ship in
a tight circle (ca. 100 m diamter) and noting the headings
which corresponded to times when the ship was running paral-
lel to the lineations. A similar approach was used by
Embley (1975) to determine the orientation of hyperbolic
echoes on the continental margin of NW Africa.

Possible linear features were also observed on the sea
floor by careful examination of echo returns from pingers
attached to oceanographic instruments (Figure 2.35). In
several instances, sound originating from a pinger about 30
m above the sea floor was observed to reflect from topograph-
ic features on the sea floor and to return to the surface.
The resulting picure of the sea-floor is, in some ways,
similar to that produced by a side-scan sonar system. The
variable geometry associated with this arrangement of sound
source, target, and receiver preclude reliable determination
of the orientations of the features. With some assumptions,
their spacing can be reliably determined. Spacings for ten
of these features range from 17 to 105 m averaging approxi-
mately 60 m. These spacings are similar to those observed
for the furrows mapped in Area 1.
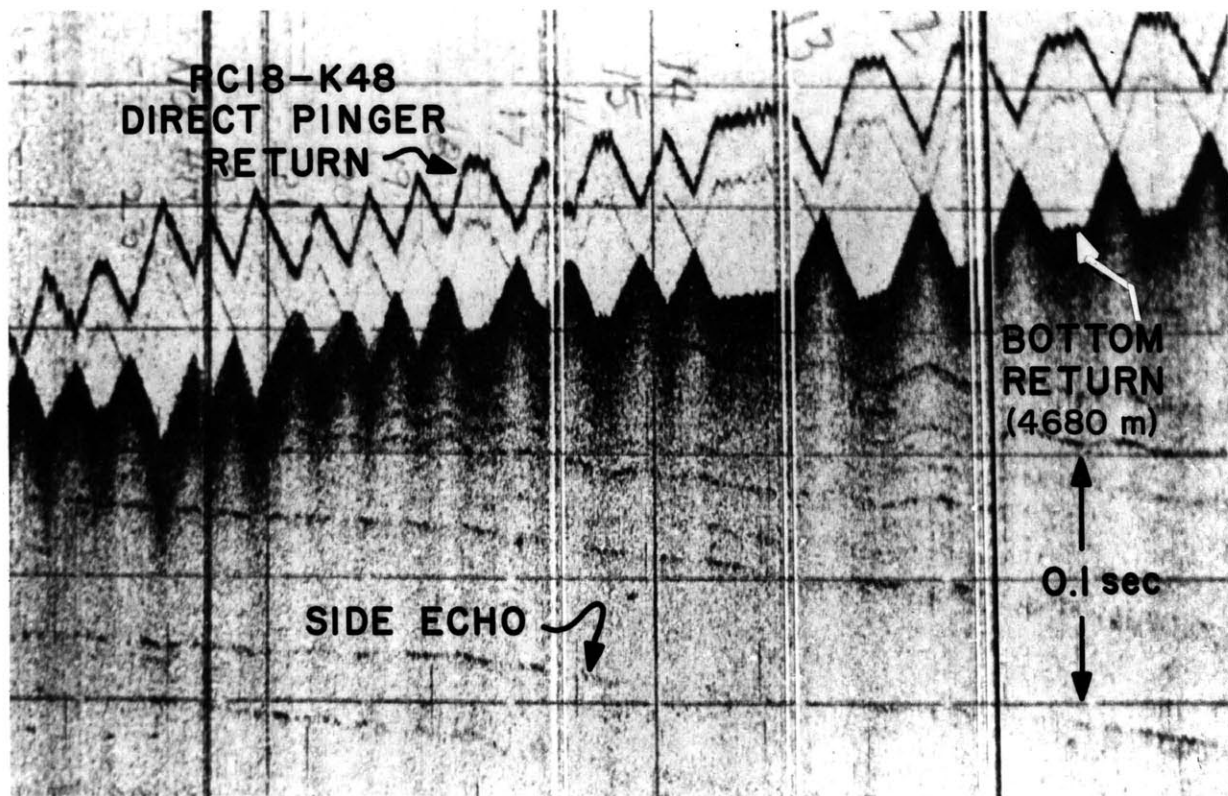
Figure 2.35. Side echoes from near-bottom pinger. These echoes indicate the presence of prominent topographic features (furrows?) on the sea floor.

No bottom photographs were obtained which show furrows, but several patches of ripples were photographed. These ripples may be associated with furrows. Photographic evidence of bottom currents, such as smoothing of the sea floor and bending of organisms, was often observed in the bottom photos.

2. Sediments of Study Areas

In order to describe the sediments in which these sedimentary features are found, to discern the timing of events important in their formation, and to delineate the history of sedimentation in these areas, studies were carried out on sediment samples recovered from the detailed study areas. A total of 20 cores or surface sediment samples were recovered from these survey areas (Table 2.1). Only samples collected during these surveys were studied, as the knowledge of the location of the sediment sample with respect to the feature under discussion was often critical.

Bio and lithostratigraphic studies were undertaken on all of the cores. Bulk mineralogy was determined (by X-ray techniques) on six cores. Grain size analyses were performed as required. Geotechnical properties of Giant Piston Cores (GPC's, Hollister et al., 1973) KN31-GPC 7,8,9, and 11 are discussed by Silva and Hollister (in press). Figures 2.36 through 2.40 summarize these investigations for cores

TABLE 2.1

CORES IN BBOR STUDY AREAS

Core designation	Latitude (N)	Longitude (W)	Depth (m)	Length (cm)	Location
KN31-GPC 7	28°17.9'	72°17.8'	4935	3058	Nose of Blake Outer Ridge
GPC 8	28°41.7'	75°16.0'	4962	2898	Area 2, large furrows
GPC 9	28°14.7'	74°26.4'	4758	2461	Area 1, sediment waves
KC 10*	28°36.8'	75°19.5'	4967	99†	Area 2, large furrows
GPC 11	28°38.0'	75°21.5'	4967	1710	Area 2, large furrows
GPC 12	28°35.6'	75°27.3'	4980	650	Area 2, abyssal plain
KC 13	28°35.7'	75°25.5'	4982	106†	Area 2, triangular ripples
KC 14	28°15.0'	74°24.5'	4765	110†	Area 1, sediment waves
FF 16	28°16.2'	74°25.4'	4788	96	Area 1, sediment waves
FF 18	28°16.5'	74°25.2'	4780	76	Area 1, sediment waves
FF 19	28°16.5'	74°25.1'	4773	96	Area 1, sediment waves
RC18-50	29°40.2'	75°24.4'	4710	1140	Area 3, sediment waves
51	29°40.3'	75°23.7'	4706	1117	Area 3, sediment waves
52	29°40.5'	75°23.3'	4671	1045	Area 3, sediment waves
53	29°42.0'	75°22.8'	4699	972	Area 3, sediment waves
54*	29°31.2'	75°37.2'	4940	792	Area 3, buried hyperbolae
TII-11	28°37.2'	75°26.9'	4984	37†	Area 2, triangular ripple crest
12	28°22.0'	74°12.2'	4596	39	Area 1, furrow floor
13	28°22.0'	74°12.2'	4595	20	Area 1, furrow wall
14	28°22.0'	74°12.2'	4594	30	Area 1, between furrows

* Core not discussed in this study

† Multiple-penetration core sample

Figure 2.36.   KN31-GPC 7 core summary. Lithology, carbonate
content (with estimated ages), C-14 dates
(corrected), *Globorotalia menardii* abundances
(>177 μ; arrow indicates last appearance of
G. menardii flexuosa), and bulk X-ray
mineralogy.

Figure 2.36

KN31—GPC 7

28°17.9'N   72°17.8'W   4935 m
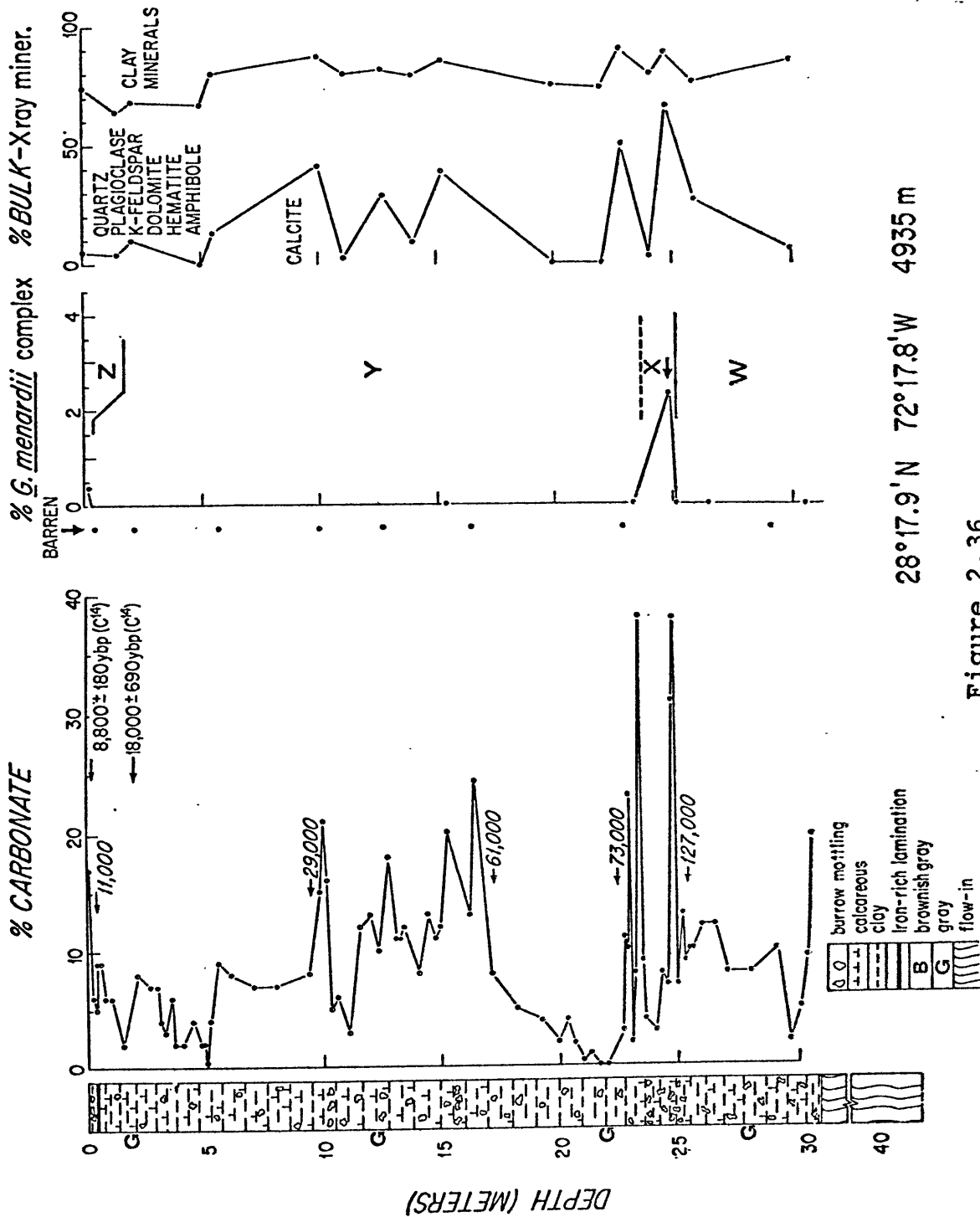
Figure 2.37.   KN31-GPC 8 core summary. Lithology, carbonate
content (with estimated ages), C-14 ages
(corrected), *Globorotalia menardii* abundances
(>177 µ; arrow indicates last appearance of
G. menardii flexuosa), and bulk X-ray
mineralogy.
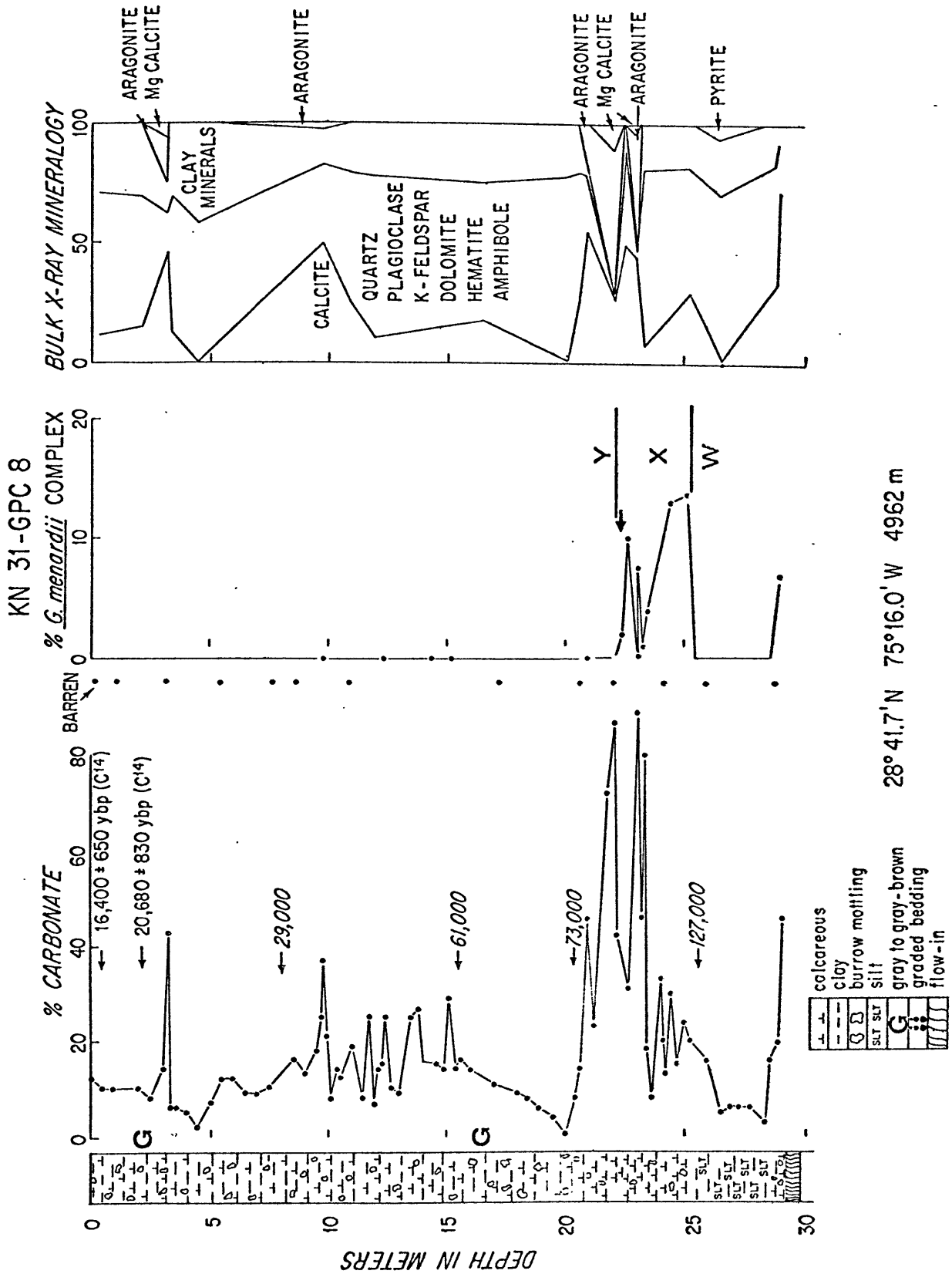
Figure 2.37

Figure 2.38. KN31-GPC 9 core summary. Lithology, carbonate content (with estimated ages), C-14 dates (corrected), *Globorotalia menardii* abundances (>177 μ; arrow indicates last appearance of *G. menardii flexuosa*), and bulk X-ray mineralogy.
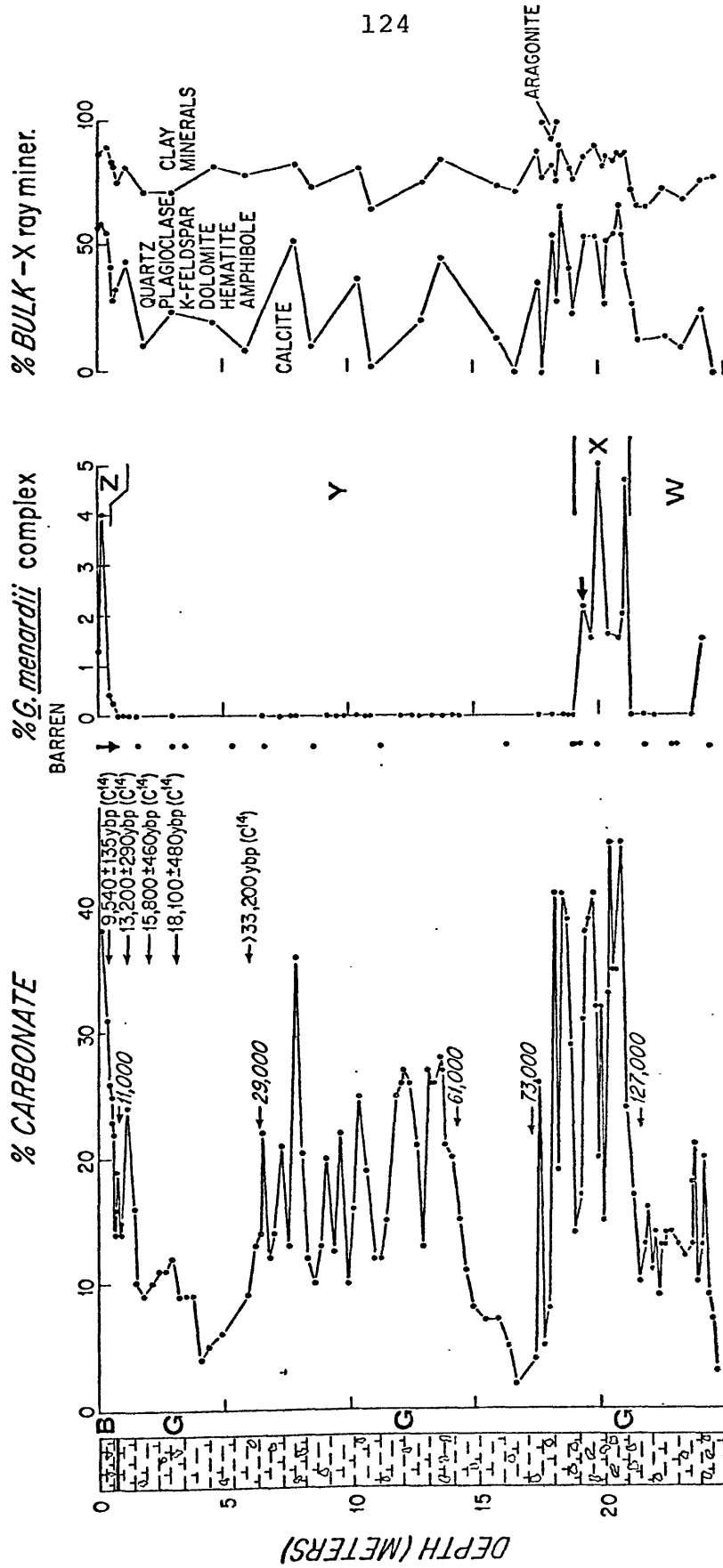
Figure 2.38

Figure 2.39. KN31-GPC 11 core summary. Lithology, carbonate
content, C-14 date (corrected), grain size,
Globorotalia menardii abundances (>177 µ;
arrow indicates last appearance of *G. menardii
flexuosa*), and bulk X-ray mineralogy.

KN 31-GPC 11

% BULK MINERALOGY

% G. MENARDII

% SIZE

% CARBONATE

28°38.0'N 75°21.5'W   4967 m
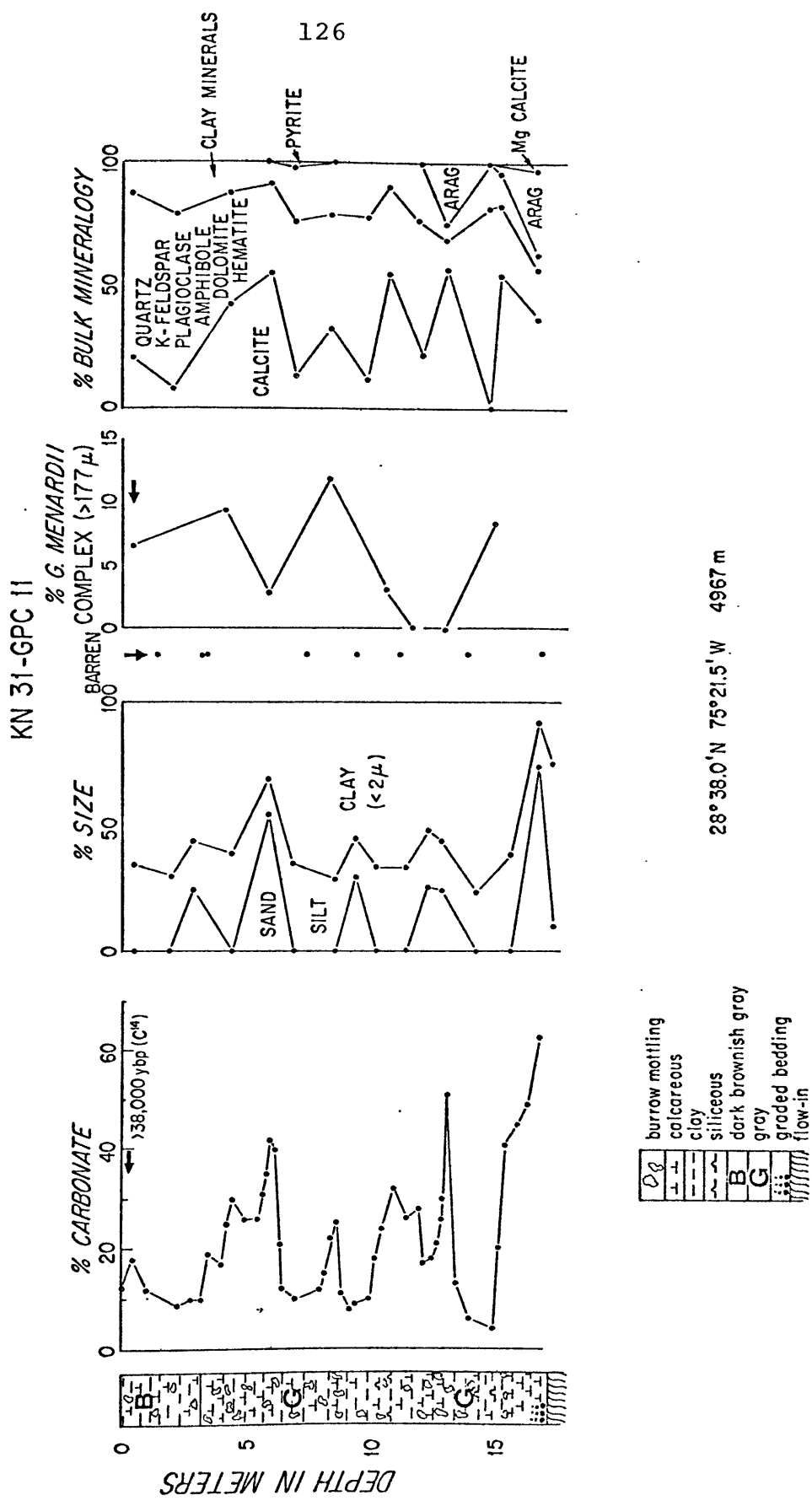
Figure 2.39

Figure 2.40.   KN31-GPC 12 core summary.   Lithology, carbonate
content, *G. menardii* abundances (>177 μ; arrow
gives last appearance of *G. menardii flexuosa*),
and bulk X-ray mineralogy.
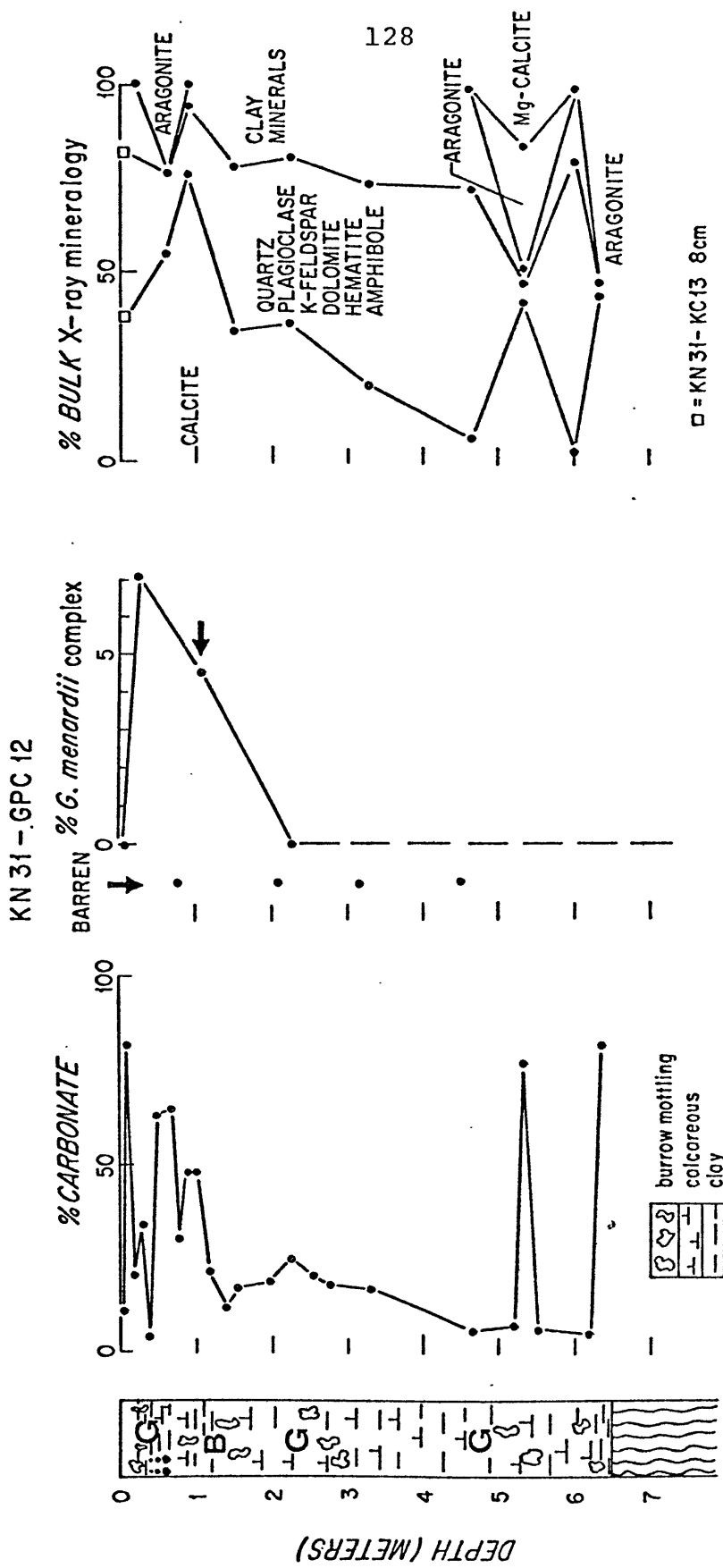
Figure 2.40

KN31-GPC 7, 8, 9, 11, and 12. Sediments recovered by the GPC's are all normally magnetized (C. Denham, personal communication).

LITHOLOGY

As these cores were collected from a relatively narrow depth range (4580 to 4982 m) and from a restricted area (the Bahama Outer Ridge), most of the sediments recovered are quite similar. These sediments are brown to gray-brown hemipelagic muds (deflocculated size: 0-5% sand, 10-30% silt, and 65-80% clay (less than 2μ)). The sand and coarse silt fraction is mainly made of the remains of planktonic organisms (primarily foraminifera), while the finest silt and clay-sized material is predominantly terrigenous, al-though biogenic constituents, such as coccolith plates, are also present. Thin laminations of terrigenous silt are commonly found in these cores. They may be produced by bot-tom current activity (contourites of Hollister and Heezen, 1972). In addition, cores KN31-GPC 8, 11, and 12 contain calcareous turbidites, cores KN31-13 KC and TII-11 contain large amounts (up to 30%) of calcareous sand (planktonic foraminifera), and core KN31-GP 11 contains some intervals with high percentages (up to 60%) of terrigenous sand. Cores KN31-GPC 7 and 9 and FF 16, 18, and 19 cored a pronounced partially-to-strongly lithified layer at a depth of 10 to

67 cm separating the uppermost brown hemipelagic sediments from the underlying dark gray hemipelagic sediments. This layer is similar to the widespread iron-manganese lithified layers described by McGeary and Damuth (1973).

Stratigraphy

The ages of the cored sediments were determined by the use of a number of stratigraphic techniques. These techniques include: variations in the abundance of the planktonic foraminiferal complex *Globorotalia menardii, G. tumida* and *G. menardii flexuosa;* a stratigraphy based on the amount of carbonate in the sediments; and radiocarbon dates on the inorganic carbon fraction of the sediments.

Variations of the *G. menardii* complex in deep sea cores have been used extensively to determine the age of deep-sea sediments in the tropical-subtropical Atlantic (e.g., Ericson and Wollin, 1968; Kennett and Huddlestun, 1972; Tucholke, 1975). The presence or absence of this complex has been related to glacial/interglacial climatic cycles with the *G. menardii* complex generally present during interglacial periods and absent during glacial periods (Ericson and Wollin, 1968). Dates used in this study have been assigned by Broeker and Van Donk (1970); however, a comparison between *G. menardii* variations and the carbonate strati-

graphy for cores KN31-GPC 7 and KN31-GPC 9 suggests an age
of 95,000 years before present for the X-Y Boundary in this
area (Figure 2.36 and 2.38).

One member of the *G. menardii* complex, *G. menardii*
flexuosa, is consistently found only when the *G. menardii*
complex is present in X-zone and older sediments in the
typical subtropical Atlantic, the Gulf of Mexico, and the
Greater Antilles Outer Ridge (Ericson and Wollin, 1968;
Kennett and Huddlestun, 1972; Tucholke, 1975). A similar
abundance pattern is present in cores KN31-GPC 7, 8, and 9
from the BBOR (Figure 2.36, 2.37, and 2.38).

Counts of the *G. menardii* complex were made on splits
containing more than 300 specimens of the greater than 250μ
(T-IIcores) or 177μ (all other cores) size fraction. If
less than 50 forams were present (original sample size ca.
10 grams), the sample was described as barren.

Previous investigators have established that variations
in the carbonate curve follow closely variations in the
oxygen isotope curve (Prell and Hays, 1977; McIntyre et al.,
1972; Damuth, 1975b; Laine, 1977). Dates determined for
oxygen isotope variations have been applied to the carbonate
curves (Hays et al., 1976). The weight percent of carbonate
minerals was determined for these cores by the gasometric

method of Lohmann (1974). The depths and ages assigned by
this method are shown in figures 2.36 to 2.38.

Ten carbon-14 dates were determined on the inorganic
carbon fraction of the sediments (Table 2.2). As dating
materials by this technique assumes that all the carbon in
the sample was freely exchanged with carbon in the atmos-
phere until death and burial of the sample, a correction
must be made to the reported age if any "older" carbon is
present (Olsson, 1968). In some of the samples dated, dis-
coasters (calcareous remains of organisms extinct for the
last 1.6 million years) were present, although only in trace
amounts. X-ray studies (discussed below) showed that
dolomite was present in the intervals dated. Milliman
(1974) suggests that much of the dolomite found in deep sea
sediments is detrital; consequently, this dolomite may be
quite old. The reported C-14 ages were therefore corrected
assuming that all of the dolomite was infinitely old and all
the calcite was contemporary when deposited (Olsson, 1968,
and references therein) (Table 2.2). In most instances, the
calculated corrections to the total inorganic carbon C-14
ages are about the same as the reported errors. In several
cases, notably those with low carbonate concentration, the
corrections are substantial. Where these corrections were
large, the revised age fits better with the stratigraphy

TABLE 2.2

CARBON-14 DATES (KN31 CORES)

ID.	Core (GPC)	Depth	$(C^{14}$ age (reported ybp)	X-RAY SAMPLE Depth	$\dfrac{C_{dolo}}{C_{total}}$	Correct. to age (years)	C^{14} age[2] (Corrected) ybp
I-8587	7	10- 20	12,090±180	10	0.34	-3340	8,800
I-8588		200-217	19,900±690	210	0.21	-1900	18,000
I-8589	8	19-28	18,420±650	35	0.22	-2000	16,400
I-8607		202-217	21,360±830	215	0.08	- 670	20,680
I-8608	9	38-46	9,700±135	34	0.02	- 160	9,450
I-8609		110-118	13,600±290	115	0.05	- 410	13,200
I-8610		197-213	18,420±460	185	0.28	-2640	15,800
I-8611		302-315	18,660±480	300	0.07	- 580	18,100
I-9224		593-613	>38,000	595	0.50	-5570	>33,200
I-8612	11	8-20	>40,000	40	0.18	-1600	>38,000

[1]Determined on total inorganic carbon

[2]Calculated assuming all dolomite infinitely old (dead)

$$\text{Correction} = \frac{T_{\frac{1}{2}}}{\ln 2} \ln \left(1 - \frac{C_{dead}}{C_{total}} \right)$$

determined by other methods than did the reported age. Only the corrected ages will be used in this study.

Sediment smear slides were examined for the presence of the coccolith *Emiliania huxleyi*. The coccolith, identified mainly by its small size, was present through all cores examined, indicating that these sediments are less than 268,000 years old (Thierstein et al., 1977).

Three cores recovered sufficient sediment to provide details of variations in sedimentation rate during the last 127,000 years. These cores also provide stratigraphic framework for the more localized studies which follow.

Cores KN31-GPC 7, 8 and 9 show significant down-core variations in sedimentation rates (Figure 2.41). Cores GPC 7 and 8 have high sedimentation rates during glacial time from 20 to 30 kybp (1 ky = 1000 years) (70 cm/ky) and during the glacial period from 60 to 73 kybp (45 to 50 cm/ky). Lower rates are found during glacial time from 11 to 20 kybp (25 to 45 cm/ky) and in the minor interglacial period from 29 to 61 kybp (22 cm/ky). The lowest sedimentation rates for these cores are found in the interglacial periods from 0 to 9 kybp (2 cm/ky, GPC 7 only) and from 73 to 127 kybp (5 to 10 cm/ky). As several turbidites are found in the interval from 73 to 127 kybp in core GPC 8 (Figure 2.38), the sedimentation rate for this interval can only be an average rate.
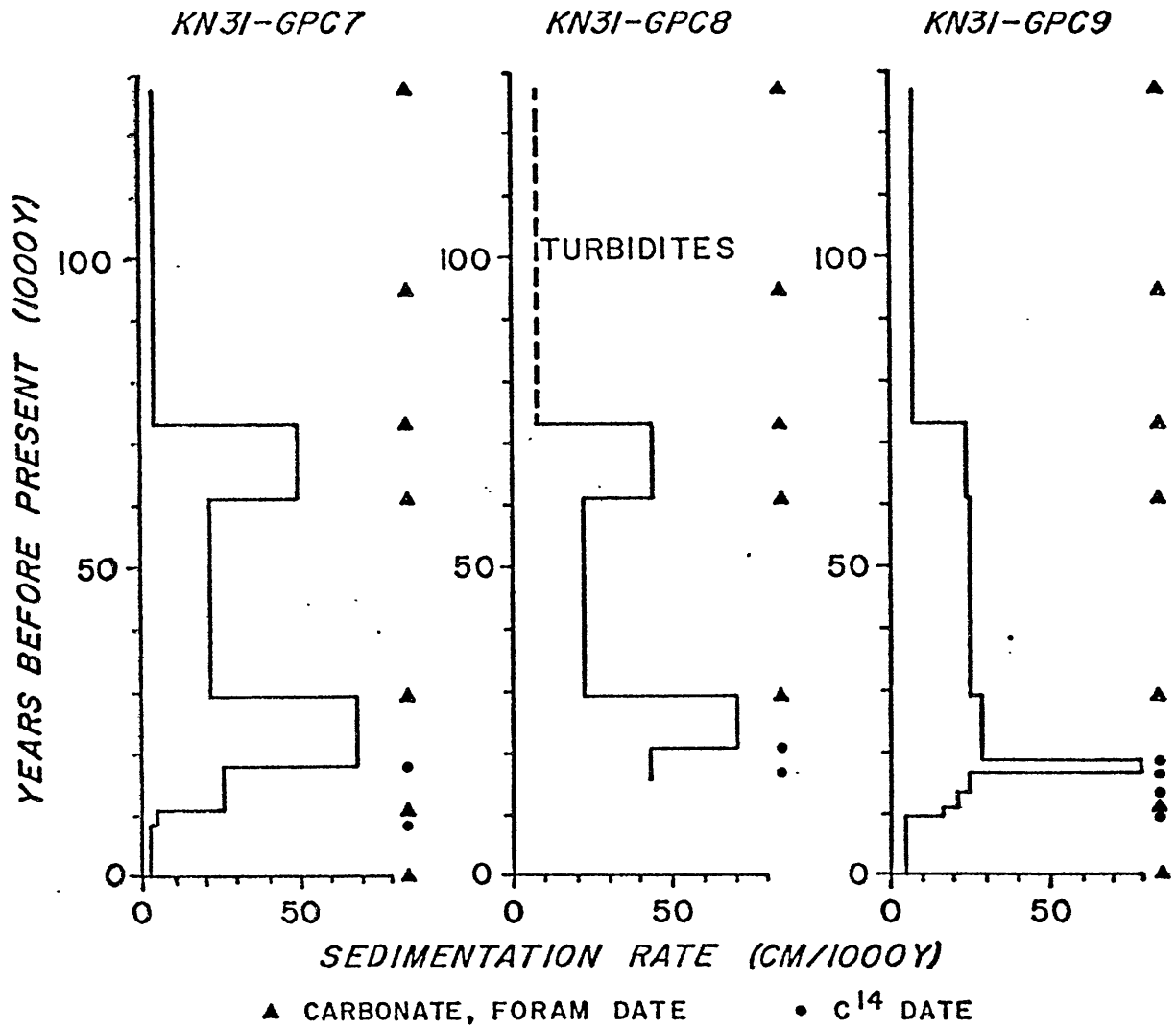
Figure 2.41.   Sedimentation rate variations, KN31-GPC 7, 8, and 9.

Core GPC 9 shows a somewhat different pattern: the
highest sedimentation rates are found from 16 to 18 kybp
(80 cm/ky), while the rest of the interval from 9 to 73
kybp has an almost constant, but high, sedimentation rate
(22 to 30 cm/ky). Again, the lowest sedimentation rates are
found from 0 to 9 kybp (4 cm/ky) and from 73 to 127 kybp
(7 cm/ky).

While variations in sedimentation rate in these cores
are generally similar to those determined by Laine (1977), for a
core collected from the northern Bermude Rise (high sedi-
mentation rates during glacials and low rates during inter-
glacials), the details of sedimentation appear to be
different. Laine (1977) reported a major pulse of sedi-
mentation around 13 kybp, while in this study the major pulse in
sedimentation is earlier at 18 to 30 kybp.

Decreased sedimentation rates during interglacial
periods, and especially during the last 9 ky, may result
from decreased continental erosion and the trapping of flu-
vial loads in estuaries during high stands of sea level
(Milliman, 1976).

The sedimentation pattern found in GPC 9 appears to be
significantly different during the period 11 to 73 kybp.
Either the pattern may be due to local
sedimentation-rate variations associated with the sediment

waves in which this core was taken, or it may result from faulty assumptions in determining the ages of the various horizons in these cores. The latter possibility is unlikely, since these horizons were chosen in a consistant manner.

X-RAY MINERALOGY

Bulk X-ray mineralogy of sediments in cores KN31-GPC 7, 8, 9, 11, and 12 and KC 13 was determined to show the nature and origin of the sediments in the study areas. Samples were X-rayed as random powders following the method used by Flood (in press), a modification of the methods developed by Cook et al. (1975). A brief description of the method used, its success at measuring the actual mineral concentrations, and the tabulated results are in Appendix III. Down core plots of the mineral abundances are shown in Figures 2.36 to 2.40.

No peaks for montmorillonite were observed in the bulk samples analyzed for this study, although X-ray analysis on the clay sized fraction showed that it was present. This discrepancy may result from the small size of the montmorillonite particles and their low concentration in the total sample. Many individual montmorillonite particles must be superimposed in order to see a strong reflection from the basal plane (Tucholke, 1974).

Most of the compositional variation in these cores is
due to changes in the relative proportions of four end mem-
bers. These end members are the pelagic input (tests of
pelagic organisms), the detrital input (sediments carried
from upstream by deep currents), the turbidity current in-
put (sediments derived from the Bahama Banks and the Blake
Plateau) and the authigenic component (mineral phases form-
ed after deposition). In addition to these crystalline
components, about 40% of the sediment is amorphous (e.g.,
siliceous tests; Appendix III).

The pelagic input is low-magnesian calcite. The detri-
tal input consists of (in decreasing abundance) quartz,
plagioclase, mica, kaolinite, K-feldspar, chlorite, dolo-
mite, hematite, and amphibole. The turbidity-current input
consists of aragonite, low-magnesian calcite, and high-
magnesian calcite, and the authigenic fraction is pyrite.
The turbidity-current component is similar to that found by
Bornhold and Pilkey (1971) for carbonate turbidites from
Great Bahama Bank.

When the mineral abundances are recalculated on a low-
magnesian calcite-free basis (e.g., Figure 2.42), the rela-
tive abundances of the remaining minerals, is quite constant,
except when an aragonite/high-magnesian calcite-rich turbidite
is sampled. The average composition of the detrital frac-

KN 31 – GPC 8

BULK X-RAY MINERALOGY (CALCITE-FREE)
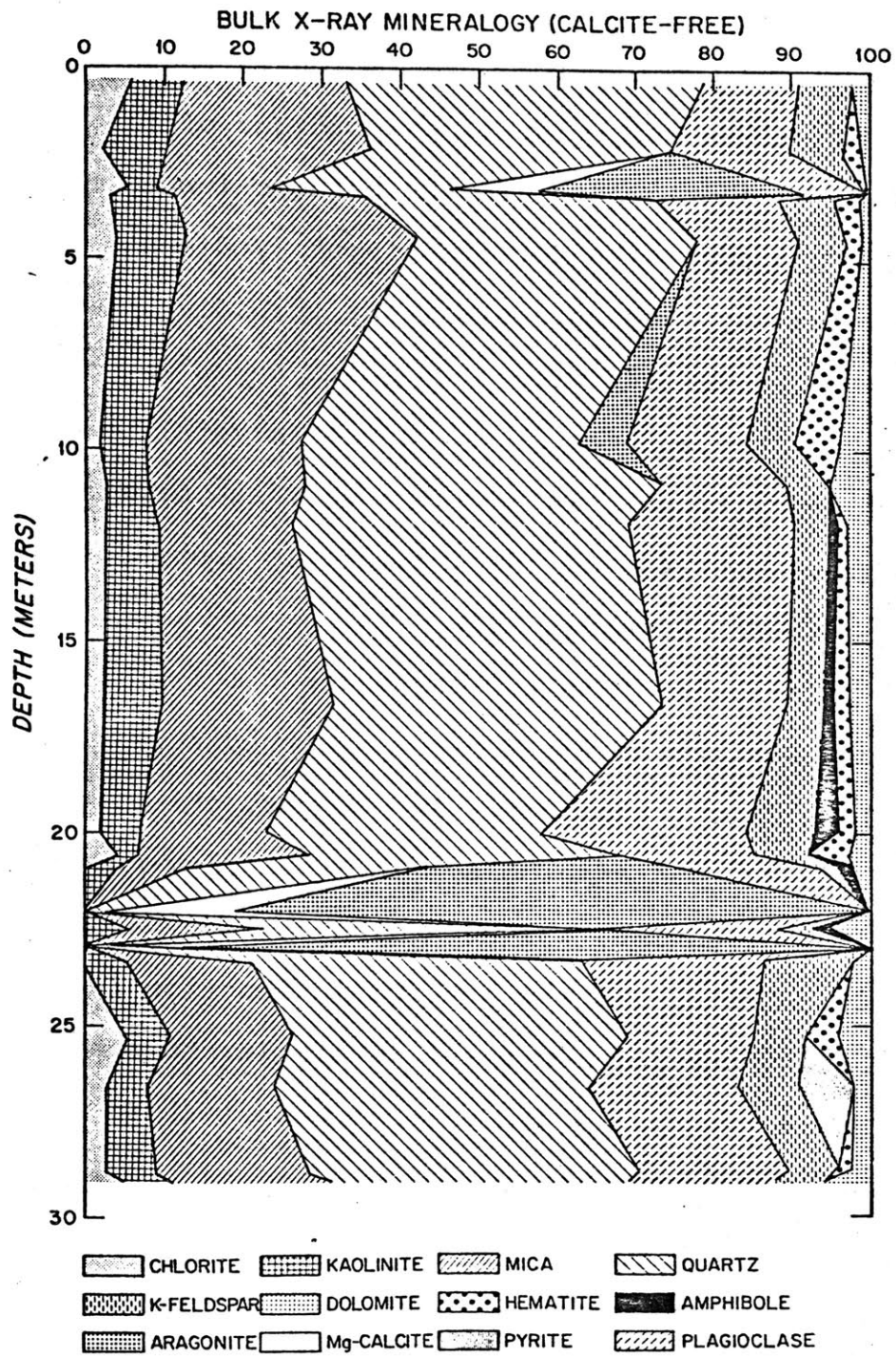
Figure 2.42.   KN31-GPC 8 X-ray composition (low-magnesian
calcite-free).

tion (determined by recalculating the mineral abundances on a low-magnesian calcite/pyrite-free basis for samples with no aragonite or high-magnesian calcite) is given in Table 2.3.

The turbidity current fraction, especially aragonite, was always present in sediments which exhibited graded bedding and in which smear slides showed the presence of carbonate rhombs. These minerals were also found in other intervals of the sediments which contained no turbidity current structures or carbonate rhombs. Such occurrences were at the pronounced gasometric carbonate peaks at 320 and 977 cm in KN31-GPC 8 and at 1820 cm in KN31-GPC 9 (Figure 2.37 and 2.38).

The aragonite zone in GPC 9 appears to be the same age as a series of major turbidites at around 2200 cm in core GPC 8, 110 km away and 250 m deeper. The aragonite present in GPC 9 may represent the fine fraction of the carbonate turbidites deposited at the site of GPC 8. As GPC 9 is 250 m shallower than GPC 8, this fine-grained fraction must have been carried to the site by deep currents after those currents picked up the fine fraction from the turbidite as it flowed along the basin floor. GPC 7, on the eastern flank of the Bahama Outer Ridge, does not contain any aragonite at this or any other level, suggesting that the turbidity

TABLE 2.3

BULK MINERALOGY OF DETRITAL FRACTION (KN31 CORES)

% Composition[1]

core	# Samples	Quartz	Plagioclase	Mica	Kaolinite	K-Feldspar	Chlorite	Dolomite	Hematite	Amphibole
GPC 7	17	41+5[2]	23±7	17±5	7±2	4±4	1±2	2±2	2±2	0.5±1
GPC 8	15	40±3	18±4	20±4	6±2	7±2	3±2	3±2	2±2	0.5±1
GPC 9	40	38±4	18±3	20±4	7±2	9±2	3±2	2±2	2±1	0.5±1
GPC 11	10	40±5	22±5	16±3	5±1	9±4	3±2	3±3	2±1	1±1
GPC 12 and GPC 13	8	40±4	20±6	19±3	7±2	7±4	3±2	3±1	2±1	0.5±1
All Samples	90	40±4	19±5	19±4	7±2	8±4	3±2	3±2	2±1	0.5±1

[1]Detrital composition calculated on a low-magnesium calcite/ pyrite-free basis in samples with no aragonite or high-magnesan calcite.

[2]Mean ± standard deviation.

current fines were restricted to the Blake-Bahama Basin.

The non-graded(?) aragonitic zones at 320 and 977 cm in GPC 8 may be examples of the same process occurring with smaller turbidity currents although these sediments may also represent the distal sequences of small turbidity currents. No aragonite was found at these levels in GPC 9.

The mineralogy of the clay fraction has been determined at scattered locations in these cores by Beverly (1975) (see also Silva and Hollister, in press) (Table 2.4) following the method of Hathaway (1972). Illite (mica) is present as the predominant clay mineral in all but one of these samples, and chlorite is always present. This clay mineral assemblage, along with the common occurrence of amphibole, suggests that these sediments have a northern origin (Hathaway, 1972; Tucholke, 1975; Hollister, 1967). One clay mineralogy sample (GPC 8, 2025-2030 cm) has montmorillonite as its principal clay mineral. This sample is from just above the turbidity current deposits and may reflect southern fine-grained sediment source (Hathaway, 1972), possibly as a result of the turbidity current activity. In spite of the presence of the aragonite and montmorillonite-tagged turbidity current fines, the non-biogenic component of these sediments is derived mainly from northern sources.

TABLE 2.4

CLAY MINERALOGY (KN31 CORES)[1,2]

Core (GPC)	Depth	Mont.	Illite	Chlorite	Kaol.
7	297-301	25	49	13	13
	923-030	24	52	12	12
	2547-2555	15	37	15	16
8	1029-1039	13	55	16	16
	2025=2030	56	25	10	10
	2180-2184	25	52	11	13
	2783-2787	4	48	24	24
9	867-872	15	64	10	11
	1474-1478	33	51	8	8
	2360-2365	17	57	15	11
11	225-232	7	67	15	11
	1690-1696	18	54	14	15

[1]from Beverly (1975).

[2]% Based on calculation method of Hathaway, 1972.

The bulk mineralogy of one sample from core KN31-KC 13 was determined. This core sampled the uppermost sediment of the Blake-Bahama Abyssal Plain embayment and was free of aragonite. Thus, the sediment in which the longitudinal ripples are formed is not of turbidity current origin. This sample from KN31-KC 13 is also used as a surface sample for GPC 12, the upper protion of which was lost on recovery.

SEDIMENTS ASSOCIATED WITH BED FORMS

Sediment waves

Core profiles were taken over sediment waves in both Areas 1 and 3. In Area 1, the profile consists of cores KN31-GPC 9, FF 16, FF 18, FF 19, and KC 14 (Figure 2.43). Core GPC 9 is a 25 m long Giant Core; FF 16, 18, and 19 are 1 m long free-fall gravity cores, and KC 14 is a 20 cm long gravity core taken with a coring tube attached to a bottom camera. The core profile in Area 3 (Figure 2.44) consists of cores RC18-50 to 53. These cores are 10 m long standard piston cores.

Variations in sedimentation rate are observed over the sediment waves in Area 1. The four longer cores cored the iron-manganese crust, dated by interpolation between C-14 dates at 11 kybp, and three reached a prominent olive-colored lamina, similarly dated at 14.5 kybp. The sediment

CORE PROFILE OVER LARGE MUD WAVES
SAND·SILT·CLAY
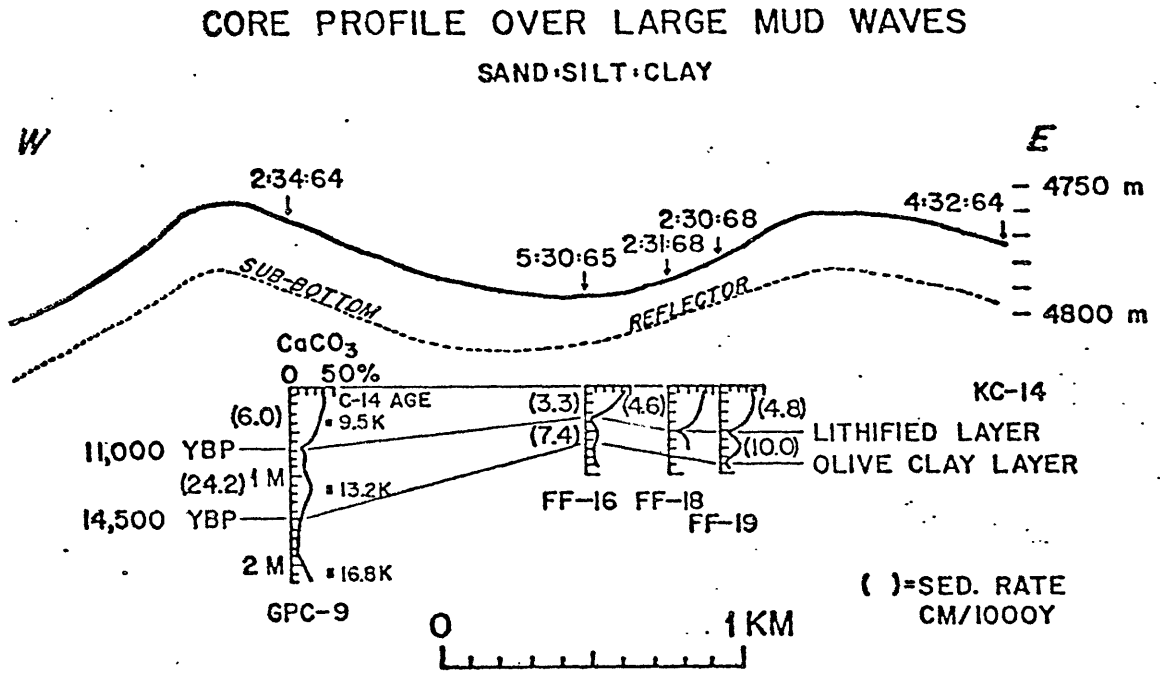
Figure 2.43.   Core profile over sediment waves, Area 1.
Cores are located in Figure 2.7.
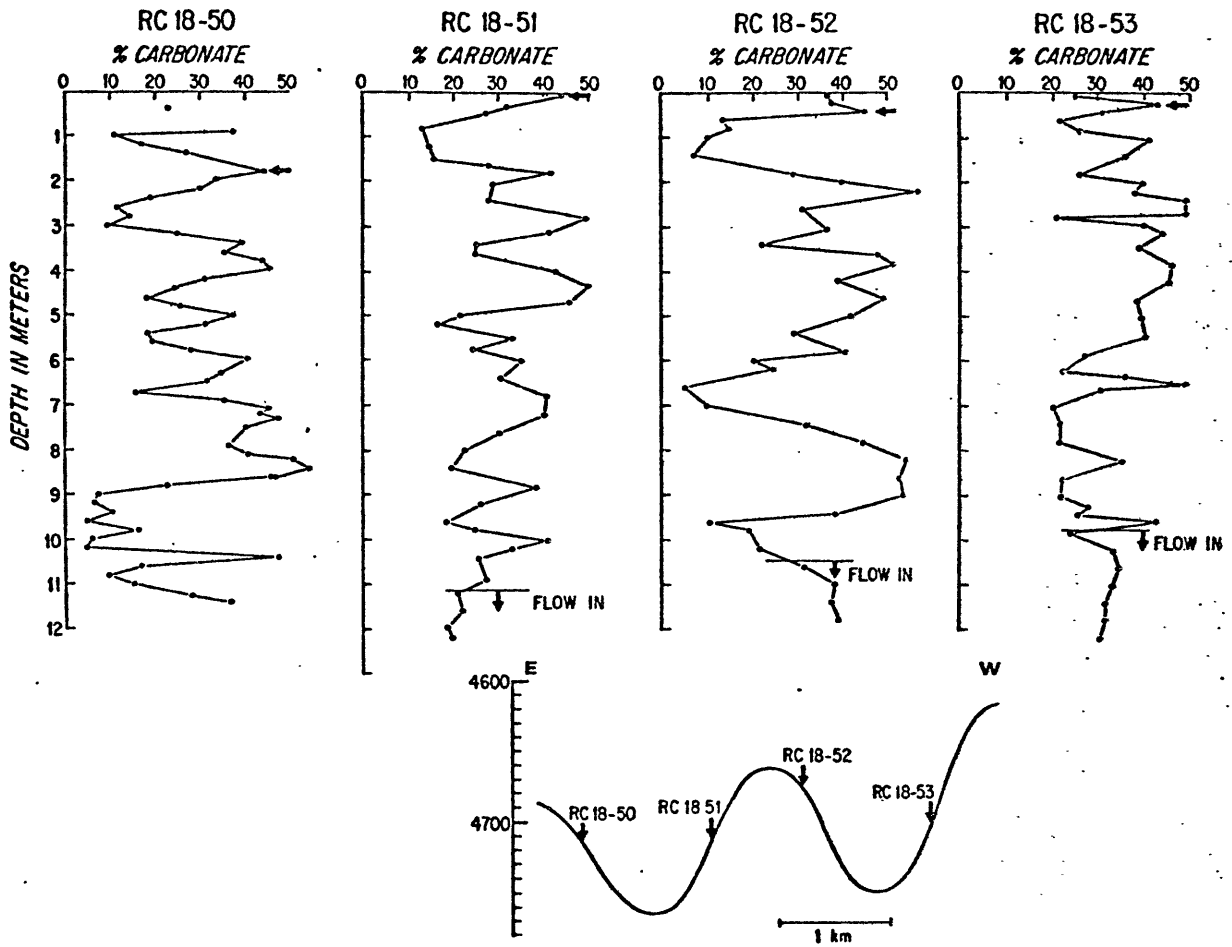
Figure 2.44. Core profile over sediment waves, Area 3.
Arrows indicate last appearance of *G. menardii*
flexuosa. Cores located Figure 2.33.

surface is taken as 0 years, consistent with the high
carbonate content of the surface sediments.

The highest sedimentation rates are in GPC 9, on the
upslope, upstream side of the wave. The lowest rates are in
FF 16, in the wave trough. Cores FF 18 and FF 19, on the
downslope, downcurrent side of the wave have intermediate
values. This pattern is consistent with that observed on
acoustic sub-bottom profilers (Figures 2.8 and 2.9).

Relatively more sediment is deposited on the upstream,
upslope side of the wave from 11 to 14.5 kybp than from 0
to 11 kybp (Figure 2.43). The ratio of upstream sedimen-
tation rate to downstream sedimentation rate (GPC 9:FF 19)
is 2.4 for the interval 11 to 14.5 kybp, while only half
as large (1.2) for 0 to 11 kybp.

These results show that preferential deposition has
occurred during the last 11 ky (during the present inter-
glacial period). Stratigraphic resolution is not good
enough to determine whether or not these depositional trends
continue today. Since preferential deposition was more pro-
nounced during the end of the last glacial period (11 to
14.5 kybp), the sediment waves may have been more active in
the past than they are at present. This may reflect either
variation in the input of sediments into the ocean basins or
changes in the flow regime.

The thickness of the iron-manganese layer also varied along this transect. The layer was a thin (5 mm), hard crust in FF 16, where the lowest sedimentation rates were recorded, and a thick (15 mm), stiff layer in GPC 9, where the highest sedimentation rates were present.

Grain size analyses were made on surface and near-surface sediments along this profile using the pipette method described by Folk (1974). The median size of all deflocculated samples was 1μ. No systematic variations in the size distribution of these sediments were observed (Figure 2.43), but any trend might be overshadowed by the grain size changes associated with the furrows (described below).

The core profile of a sediment wave in Area 3 (Figure 2.44) proved more difficult to interpret. In none of these cores could the carbonate variations be related to the regional pattern typified by core KN31-GPC 9. In addition, the planktonic foraminifer *G. menardii flexuosa* was found near the top of all cores, suggesting that some component of the sediment may be reworked. Comparisons between piston cores and pilot cores indicate that no more than five to ten centimeters are missing from the piston core tops. These waves therefore appear to be somewhat eroded at the present time. As discussed in section II.B.1, a near-bottom profile

resolved small erosional scarps, similar to the walls of the large furrows in Area 2, and other evidence also showed the presence of furrows.

Differences between the surface sediments of the waves in Areas 1 and 3 are probably due to the nature of the super-imposed furrows rather than to differences in origin for the waves. This demonstrates the importance of local conditions in determining the present-day expression of any bed form.

Small Furrows and Associated Current Ripples

Three cores, recovered by TRIESTE II, form a partial transect of a small furrow in Area 1. Core TII-12 is from a 1.5 m wide flat furrow floor, TII-13 is from the 1.5 m high eastern wall of the same furrow and, at the same time, from the trough of a current ripple, and TII-14 is from an inter-furrow region near that furrow (Figure 2.45a). Grain size, carbonate content, and the abundance of the *G. menardii* complex in the >250μ size fraction were determined for these cores.

The sediments recovered were cohesive, brown hemipelagic muds with 2-11% sand, 31-36% silt and 58-63% clay sized material. Carbonate curves (Figure 2.45 b), when compared to that determined for KN31-GPC 9 (Figures 2.38 and 2.43), suggests that the surface sediments are quite recent. They have high

Figure 2.45.   Core profile over a small furrow (Area 1).

(a)   Location of cores and grain size of surface sediments.

(b)   Downcore plots of carbonate content, sand fraction, and *G. menardii* variations (>250μ size fraction).

Furrow studied is shown in Figure 2.15.

DSV TRIESTE II − DIVE 16-77
FURROW TRANSECT (4594 M)

a.

Figure 2.45

% CARBONATE % SAND %G.menardii

b. TII-12
FURROW
TROUGH

TII-13
FURROW
WALL

TII-14
INTER-
FURROW

DEPTH (CM)
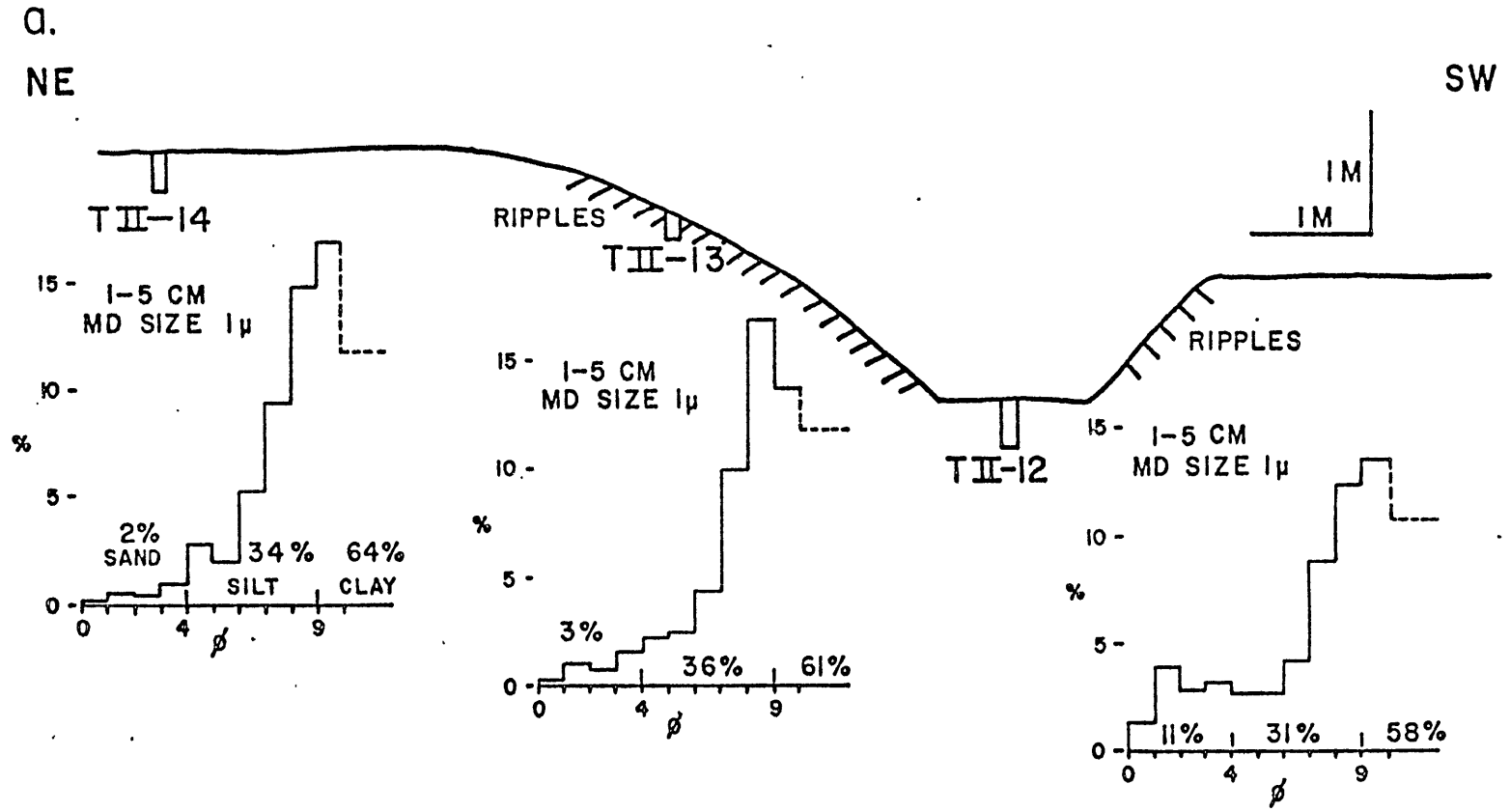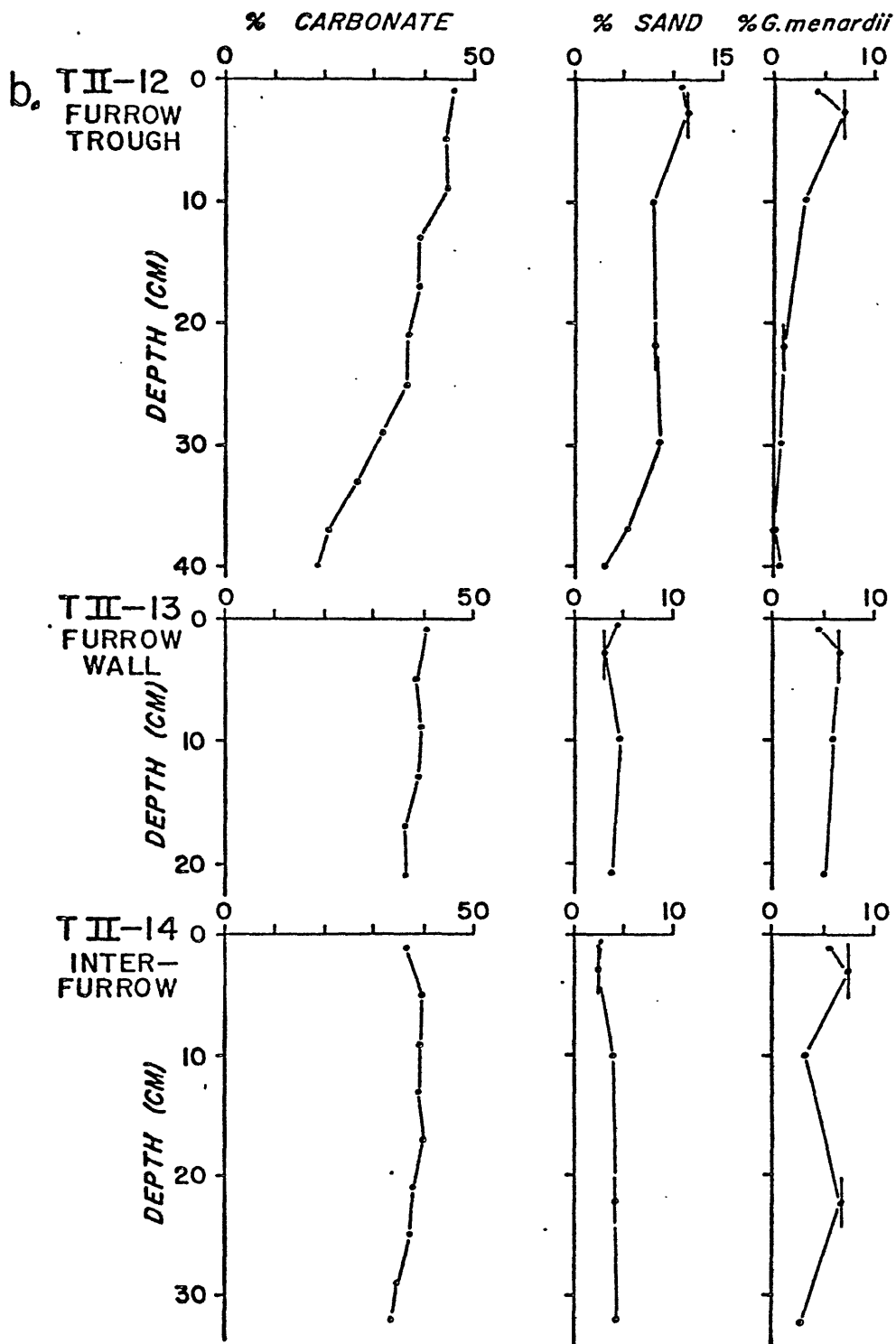
Figure 2.45

carbonate contents (38 to 45%) and are thought to be con-
temporary. The smooth carbonate curves suggest few long
(greater than 1000y long) erosional or non-depositional
events. The current ripples developed on the furrow wall
are clearly composed of these cohesive sediments.

Salt-corrected water contents for the top centimeter of
each core were determined when these cores returned to the
laboratory. Surface water contents (percent dry weight)
were 110%, 142% and 133% for cores TII-12, 13 and 14. Ex-
pressed as percent wet weight, the water contents are 52%,
58%, and 56%. Actual surface water contents may have been
higher. The soupiest sediments were those of the rippled
wall, while the firmestwere those of the furrow trough.

There are significant grain-size variations from core to
core. Surface sediments in the furrow trough (TII-12; 11%
sand) are coarser than those found either on the furrow wall
(TII-13; 3% sand) or in the inter-furrow area (TII-14; 2%
sand). The trend for higher sand content in the furrow
floor sediment continues down core (Figure 2.45 b). The
slightly higher surface carbonate content of the furrow
trough sediment (45% vs. 38 or 40%) results from the large
percentage of coarse calcareous material in the trough sedi-
ments.

Cores on the wall and between furrows have high, nearly constant abundances for the *G. menardii* complex down core, implying that the bases of these cores are younger than 11 ky (sedimentation rates greater than 2 cm/ky and greater than 2.9 cm/ky respectively). The core from the furrow trough (TII-12) is not easy to interpret. There is a significant trend from high abundances of the *G. menardii* complex at the surface to lower abundances at depth, perhaps indicating the Y-Z boundary at 20 cm (sed. rate 1.8 cm/ky). But other factors suggest that this core did not penetrate the Y-Z boundary (sed. rate greater than 3.6 cm/ky). Carbonate contents decrease to the bottom of the core, and the deepest sediments are brown rather than the gray-brown expected for the glacial age sediments (compare with KN31-GPC 9). Also, no iron-manganese layer, expected to mark this boundary, was recovered.

A more detailed comparison between trough (TII-12) and inter-furrow (TII-14) cores suggests that the furrow trough has a lower sedimentation rate. This is reflected in the higher abundance of the *G. menardii* complex at depth in TII-14, and by the lower carbonate content of TII-12 at 31 cm (28% vs. 34%). The carbonate variation occurs despite the higher calcareous sand fraction of TII-12 at this depth (approx. 8% vs. 4%). Cores TII-13 and TII-14 are not long

enough to be usefully compared in this manner, but the sedimentation rates appear comparable.

The concentration of coarse material on the furrow floor can result from (1) the addition of coarse material to those sediments, or (2) the removal of some fine material. If the increased coarse material in the trough were solely due to the addition of extra coarse material, one would expect to see a higher sedimentation rate there. As that sedimentation rate appears to be lower, the fine component of the suspended sediments is either not deposited in this area or is removed after deposition. However, some additional coarse material may still be reaching the trough.

Since a higher sand fraction in the furrow trough can be documented to a depth of 40 cm (almost 11 kybp), it has existed since that time. During this time interval, the furrow has grown as a result of cross-furrow variation in deposition rates. The cores do not extend deep enough to provide any information on the deeper structure of the furrow or any estimate for a time of formation, except that these must be at least 11,000 years old. Some of the larger furrows have probably existed for a much longer period of time.

Large Furrows

Two cores (KN31-GPC 8 and GPC 11) were collected in the large furrows of Area 2. As these samples were collected by surface-ship samplers, their positions with respect to the furrows is not known.

Core KN31-GPC 8 has, at a depth of 19-28 cm, a corrected Carbon-14 age of 16,450 years before present (Table 2.2). By extrapolation of near-surface sedimentation rates (Figure 2.41), an age of 15,900 years is obtained for the top of the core. The surface sediments at this site are thus younger than 15,900 years. Although no pilot core was obtained in conjunction with GPC 8, 15,900 years will be assumed to represent the age of the sediment surface as the erosional nature of this region is well established (Section II.B.1). If GPC 8 is from the sequence of partially eroded, laminated sediments found between furrows (Figure 2.24, profiles B and C), the date of less than 15,900 years for the sediment surface provides a lower limit for the time of furrow formation. The stratigraphy of the remainder of GPC 8 fits quite well with the regional sedimentation pattern.

Core KN31-GPC 11 has a much different sedimentation history. Down-core variations of carbonate and the *G. menardii* complex (Figure 2.39) do not resemble the

regional patterns (e.g., KN31-GPC 9, Figure 2.38). The

G. menardii complex, except in barren intervals, is present

through the core, and *G. menardii fluxosa* is present near

the top of the core. A carbon-14 date on inorganic carbon

at a depth of 20 *cm* gives an age of greater than 38,000 years

(Table 2.2).

The sediments of the upper 12 m of GPC 11 are similar to

those recovered by GPC 8, except that sand-sized material

(primarily quartz) is common. Although the sandy zones do

not occur as distinct layers, sand-sized material can

account for up to one half of the sediments (Figure 2.39).

This sand-sized material is not all carbonate, since the

coarser intervals do not always have a high carbonate con-

tent. Below 12 m, a series of calcareous turbidites are

present. These turbidites are tentatively correlated with

the turbidites found from 20 to 24 m in GPC 8.

On the basis of a geotechnical analysis of the sediments

in GPC-11, Silva and Hollister (in press) suggest that as

much as 10 m of sediment overburden has been removed from the

area in which this core was taken. They suggest that the

core was recovered from the trough of one of the large fur-

rows. If only erosion of overlying sediments were involved,

one would expect better correlations between GPC 11 and

portions of GPC 8.

The high concentration of terrigenous sand and the difficulty of correlating this core with the regional stratigraphic pattern leads to the speculation that the sediments of GPC 11 are filling a furrow trough. In this scenario, the floor of the furrow was originally eroded to approximately the layer of the turbidites, and about 10 m of sediment has been deposited since that erosion. The fill is derived from both erosion of the surrounding furrow walls and transport from upstream sources by deep currents. The carbonate present in these sediments is a combination of both old material derived locally and new material from the surface of the ocean, leading to an artificially old C-14 date of >38,000 years. These cores from the large furrow, indicate that they were eroded to a depth of about 20 m sometime in the last 15,900 years. Erosion was halted at 20 m by a series of coarser carbonate turbidites. Following this erosion, the troughs of the furrows have been filling in at an extremely high rate (ca. 90 cm/ky). The sediment has come from the erosion of the furrow walls, upstream sources, and the ocean surface.

Triangular Ripples

Two samples of the sediments which make up the triangular ripples on the embayment of the Blake-Bahama Abyssal Plain in Area 2 have been recovered: Core KN31-KC 13, a surface sample obtained with a core tube attached to a bottom camera, and core TII-11, obtained from a ripple crest by DSV TRIESTE II.

Grain-size analysis shows that these sediments have a large percentage of sand-sized material (8 to 30%), primarily planktonic foraminifera. X-ray study of one sample showed no aragonite, suggesting that turbidity currents from the Bahama Banks have not provided this sediment. Not enough samples were collected to discern any variation between the sediments of the ripple crest and those of the inter-ripple area, but a deflocculated sample from a ripple crest (TII-11) consists of 18% sand, 34% silt and 48% clay-sized material (Figure 2.46).

The coarse sediments are assumed to be derived from the erosional large furrows which surround the area.

3. Near-Bottom Current Velocity and Water Temperature Structure

Local near-bottom water circulation patterns were studied to provide a link between the morphology of the sediment surface and the water flow over that surface. These
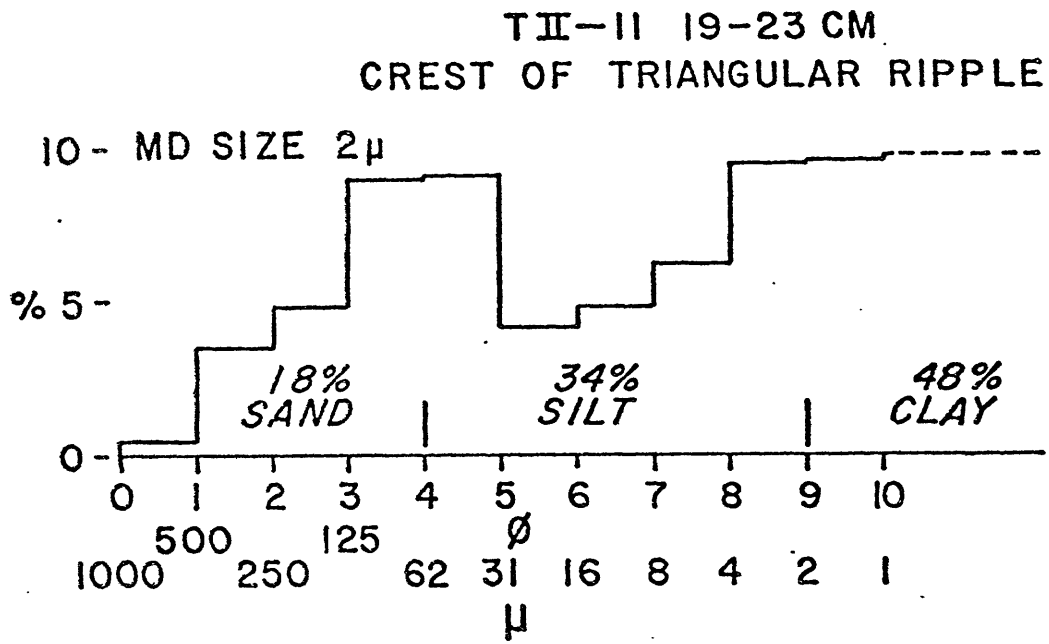
Figure 2.46.   Grain size distribution (crest of longitudinal triangular ripple).

circulation patterns may allow one to speculate on the origin of the bed form in question. The current speeds and directions measured are consistent with the general circulation pattern around the BBOR system as described in section II.A.

METHODS

Four MPL current meters (Schick et al, 1968) and one Geodyne current meter (Model 102) were utilized for a total of eight current meter deployments during these investigations (Table 2.5). The MPL current meters, used for seven deployments, were mounted on navigational transponders at a height of 20 m above the bottom, except for meter CM 5 at 60 m above the bottom. Current directions and speeds are averaged over 15 minute intervals with the direction reported to the nearest 5°. Current meter records KN31-CM 1,.CM 2, and CM 3 were obtained from Area 2 (Figure 2.25) and records KN31-CM 4, CM 5, CM 6, and CM 7 were obtained from the detailed survey in Area 1 (Figure 2.7). The Geodyne current meter (record RC18-CM03) was moored 10 m above the bottom in Area 3 (Figure 2.33). Current velocities and directions are averaged over 20 minute intervals. All current meters worked correctly with the exception of KN31-CM 5, which recorded direction only.

TABLE 2.5

BAHAMA OUTER RIDGE

CURRENT METER SUMMARY

METER	LAT (N)	LONG (W)	WATER DEPTH (M)	HEIGHT OFF BOTTOM (M)	DURATION (h)	MEAN SPEED cm/sec	MEAN DIRECT. °T	MAX. SPEED @ DIRECT.	ESTIMATED TIDAL COMP.	COMMENTS
KN31-CM 1	28°36.7'	75°18.2'	4965-4980*	20	153	4.8	348	8.7 @ 355°	1	Area 2 Furrows*
CM 2	28°37.2'	75°20.6'	4965-4977*	20	82	3.4	001	6.6 @ 325°	1.2	Area 2 Furrows*
CM 3	28°35.0'	75°26.0'	4986	20	144	2.5	348	4.4 @ 355°	1.1	Area 2 Abyssal Plain
CM 4	28°16.0'	74°24.3'	4771	20	108	3.7	342	8.9 @ 330°	1.2	Area 1 Wave Trough
CM 5	28°18.3'	74°25.8'	4776	60	107	---	---	----	---	Area 1 Wave Crest (Direction Only)
CM 6	28°17.3'	74°25.1'	4788	20	106	3.7	344	10.8@ 325°	1.6	Area 1 Wave Trough
CM 7	28°17.9'	74°23.0'	4750	20	102	5.0	326	10.8@ 335°	1.6	Area 1 Wave Crest
RC18-CM 3	29°41.7'	75°22.4'	4638	10	192	4.4	301	7.6 @ 285°	2	Area 3 Wave Crest

* Meter may be in or between furrows, thus uncertainty in depth.

Near-bottom temperature measurements were made in all three survey areas. Data from Areas 1 and 2 were collected by a thermometer mounted on the deep tow, from Area 3 with an STD.

At the time of the surveys of Area 1 and 2, the deep tow was equipped with a quartz-crystal thermometer for precise measurement of water temperature (Spiess and Tyce, 1973). Water temperature was recorded every ten seconds as the deep tow was towed through the water at a speed of approximately 1.2 knots (60 cm/sec). The thermometer, mounted on the deep tow, was usually 40-80 m above the sea floor, but occasional "vertical" temperature profiles were made extending up from approximately 10 m off the bottom. The resonant frequency of the quartz crystal (3 second time constant) is temperature dependent and is determined by counting the crystal oscillations for a period of about one-half second. The temperature is determined to a precision of $\pm0.002°C$. Depth control for the temperature measurement is provided by an upward-looking echo sounder mounted on the instrument. The probe was calibrated by comparison with standard hydrocast data collected on the same cruise. Potential temperatures were calculated in the near-bottom region (within 300 m of the bottom) from the *in-situ* temperature, depth and salinity (assumed constant for each area: 34.89‰ for Area 1 and 34.88‰ for Area 2).

Errors in calculation of potential temperature can result form errors in the *in-situ* temperature, depth, or salinity. The manufacturer of the temperature probe specifies the long-term drift of the quartz-crystal thermometer as less than $\pm 0.01°C$ per month and short-term jitter less than $5 \times 10^{-5°}$ C. As all measurements reported in this section were collected over a time span of one week, significant temperature variations should not be due to instrument drift. Depths were read from a 19 inch (48 cm) wide 400 fm/sweep echo sounder to ± 1 fm (± 1.83 m) and corrected for variations in sound speed (Matthews, 1939). An error of ± 10 m in depth, larger than the maximum error expected, will lead to an error of $-0.0013°C$ in potential temperature at these depths (4500 to 5000 m). Variations in salinity in the bottom 300 m of the Blake-Bahama Outer Ridge are less than 0.02‰ (e.g., Amos et al., 1971). An error in salinity of +0.02‰ will lead to an error of $-0.0016°C$ in potential temperature. The precision of the potential temperature measurements is therefore assumed to be $\pm 0.005°C$, with an absolute accuracy of $\pm 0.02°C$

The near-bottom temperature data in Area 3 were collected with a Plessey Model 9040 Salinity/Temperature/Depth (STD) system with a 6000 m full-scale depth sensor. In order to assure a close approach to the sea floor, a bottom-finding pinger was used on the first four stations. Following the loss of the pinger, a bottom contact switch (Knox and Millard,

1973) was installed which alerted the winch operator when the STD was 5 m above the bottom. The temperature, salinity, and depth information was recorded digitally on magnetic tape and on an analog record. In order to calibrate the STD, a 12 bottle Niskin rosette sampler was attached to the STD. Temperature, depth and salinity correction factors were determined by comparing bottle samples with STD values (Amos et al., 1971). Potential temperatures were calculated for the bottom 400 m of each station.

SEDIMENT WAVES (AREAS 1 AND 3)

Data on the circulation patterns over the large sediment waves are available from Area 1 and 3.

Current Velocity

Four current meters (KN31-CM 4, 5, 6 and 7; no speed record from CM 5) were deployed in Area 1 (Figure 2.47). The current meters all showed a general northwesterly current flow with average velocities of 3 to 5 cm/sec toward 326 to 344°. Maximum speeds were 9-11 cm/sec toward 325-335°.

Only one current meter record (RC18-CM03, 10 m above the bottom, Table 2.5) was obtained from Area 3 (Figure 2.48). This meter was on the downstream, down-current side

CURRENT SPEED AND DIRECTION
BLAKE—BAHAMA OUTER RIDGE—AREA 1
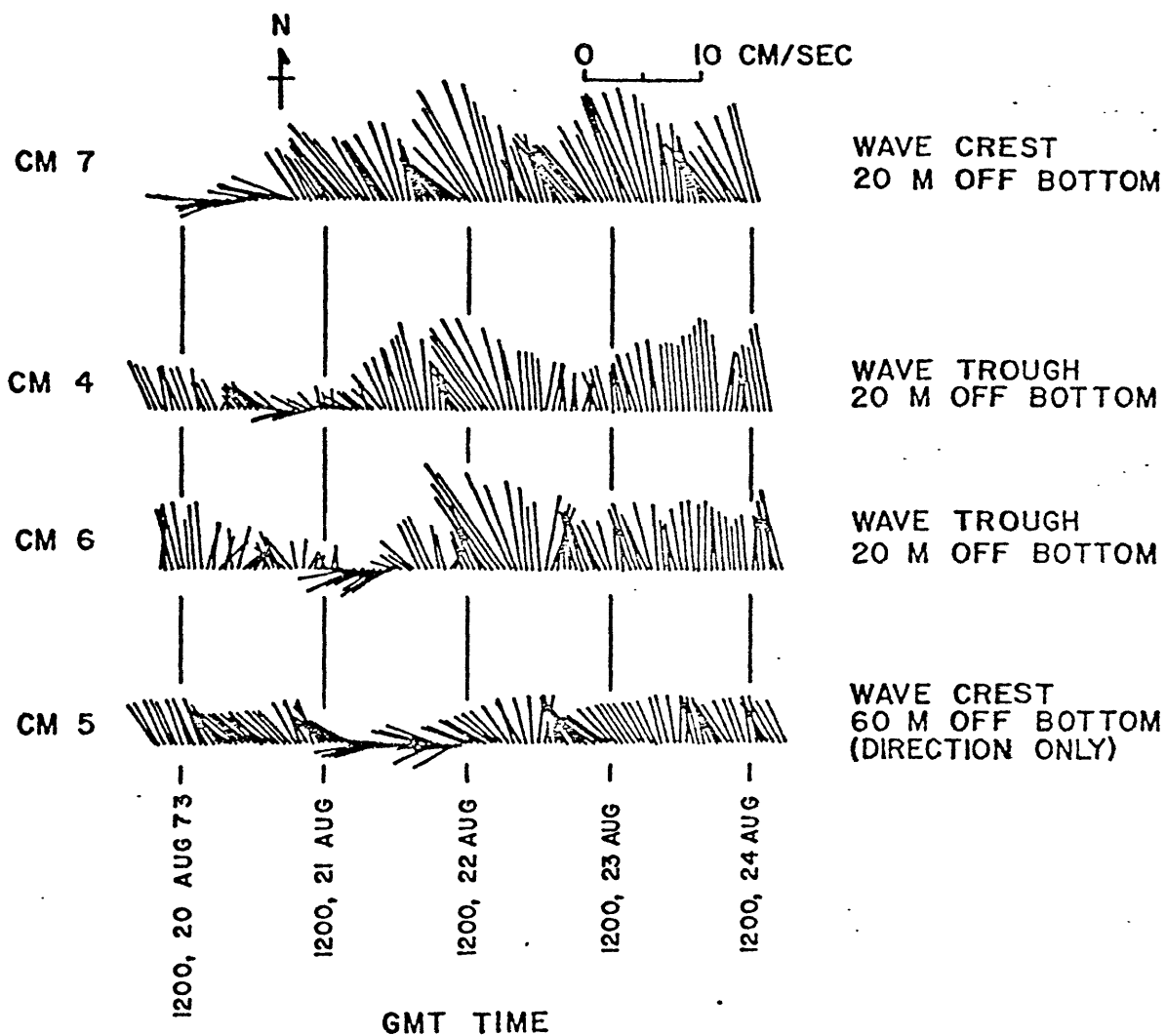
Figure 2.47. Current meter results (Area 1). Orientation
of stick gives direction, length gives speed.
One-hour averages are plotted.

Figure 2.48.   Current meter results, Area 3. See caption
               to Figure 2.47 for an explanation of the
               figure. Velocities averaged over four hours.

STD
373

STD
376

STD
378

3   4   5   6   7   8   9   10   11

0000 Q
JULY 1975

RC18   CM-03   SEDIMENT WAVES
(AREA 3)
4 HR. AVERAGE

0   5   10
cm/sec

N

168
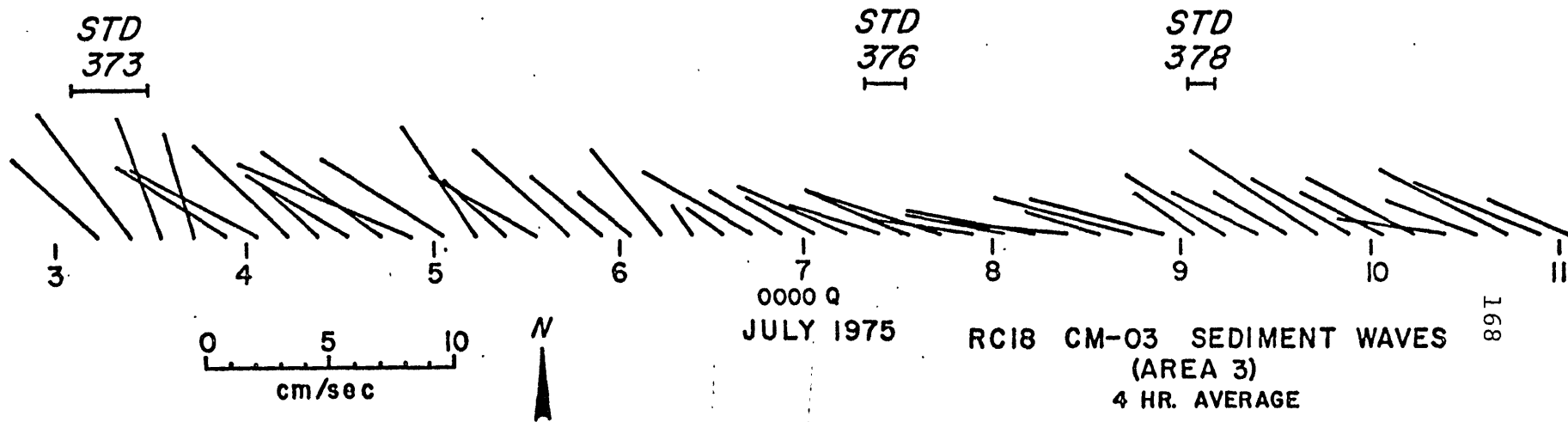
Figure 2.48

of a sediment wave (Figure 2.33). The current meter
recorded a northwest flow with an average velocity over the
eight-day record of 4.4 cm/sec toward 301°. Maximum velo-
city averaged over 20 minutes was 7.6 cm/sec toward 285°.
The average current is roughly parallel to the regional con-
tours and the assumed furrow trend (toward 320°, Section
II.B.1).

An ocean-bottom nephelometer (RC18-OBN1) was deployed
on the current meter mooring at 15 m above the bottom
(record in Eittreim et al., 1976). Light scattering (log
E/E_D, Eittreim et al., 1976) varied from 0.96 to 1.19 over
the 11 day deployment, corresponding to a variation in
suspended matter concentration from ~16 to ~32 µg/l (Biscaye
and Eittreim, 1974). These concentrations are in agreement
with those determined by water filtering (P. Biscaye, per-
sonal communication).

Apart from the unidirectional nature of this flow, one
of the most striking aspects of these current meter records
is the apparent passage of an "event" across Area 1 (Figure
2.47) from 1200 Z, 20 August to 1200 Z, 22 August, 1973.
During the 12-24 hours it takes this event to pass a current
meter, speeds drop to less than 4 cm/sec and current direc-
tions turn to the west and southwest. The current then
swings back to the NNW and the speeds pick up to 6-8 cm/sec.

From the well known geometry of the current meter array one can determine that this event moves across the survey area from east to west with a velocity, normal to its trend, of 5 cm/sec. Temperature measurements, made by the quartz-crystal thermometer attached to the deep-tow vehicle, suggest that the water on the western side of this current event was approximately 0.03°C colder than that on the eastern side. The event corresponds roughly to the 1.765°C potential temperature isotherm 50 m above the bottom. This isotherm moved across Area 1 at the same time as the current event.

Systematic differences between current speeds and directions recorded for the same time at the various meters may be related to the positions the current meters on the waves. Two of the current meters (KN31-CM 4 and CM 6) were located near the centers of the wave troughs, and two meters (KN31-CM 5 and CM 7) were located slightly east of the crests (Figure 2.7). Curent meter CM 7 (wave crest) records a generally higher speed (Figure 2.47) and has an average speed about 1 cm/sec higher than current meters CM 4 and CM 6 (wave troughs) (Table 2.5).

Differences in current direction between wave crests and troughs are also evident. During periods of high current speeds (greater than about 8 cm/sec at CM 7) the directions recorded on wave crests (CM 5 and CM 7) are aligned with those recorded in the wave troughs (CM 4 and CM 6) (Figure

2.49 a). The currents at these times closely parallel the furrows. At lower velocities (less than 6 cm/sec at CM 7) the currents in the wave troughs are northerly, at times almost parallel to the wave trend. At the same time, the currents on the wave crests are more westerly (Figure 2.49 b). These currents do not follow the furrow patterns observed, but when visually averaged over one wave, they are still parallel to the regional contours (NNW). Changes in current direction (marking the shift from one flow regime to another) lag changes in speed (which result from tidal current fluctuations) by 2-4 hours. This may be the time required for the flow pattern to shift from one mode to the other.

These results suggest that the currents are interacting with the wave topography and that the form of this interaction changes with changes in the speed of the current.

Temperature Structure

One complete temperature profile over a sediment wave in Area 1 was obtained with the deep-tow temperature sensor (Figure 2.50). At the time of this profile, currents measured at KN31-CM 7 were 6 cm/sec and were flowing toward 325° slightly to the west of the furrows. Temperature surfaces within the water correspond quite well to the surface

a. "HIGH-SPEED" CURRENT PATTERN

CM 5
(DIRECTION
ONLY)

CM 7

CM 6

WAVE CREST

WAVE TROUGH

CM 4

1600 22 AUG 1973

b. "LOW-SPEED" CURRENT PATTERN

28° 17'
N

74° 25'
W

0300 23 AUG 1973

0   10 CM/SEC   0   2 KM
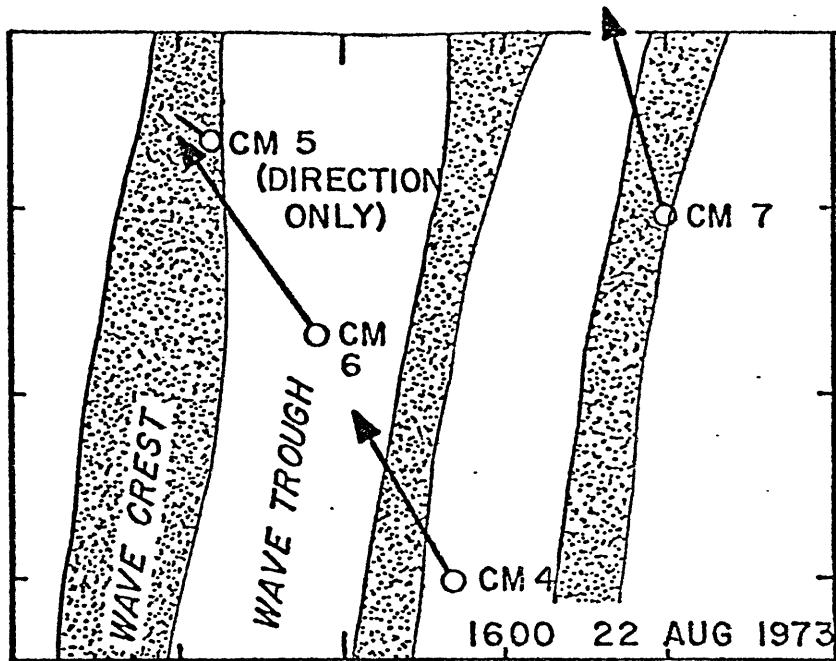
Figure 2.49.   Bottom current-sediment wave interactions, Area 1.
                (a)   "High-speed" current pattern.
                (b)   "Low-speed" current pattern.

Figure 2.50.   Temperature section over a sediment wave, Area 1.
(a)   Temperature contoured over wave.
(b)   Temperature measured by the deep tow. Temperature profile indexed on Figure 2.7 as profile F.

DEEP—TOW TEMPERATURE SECTION OVER LARGE MUD WAVES
BLAKE—BAHAMA OUTER RIDGE—(AREA 1)
(PROFILE F)
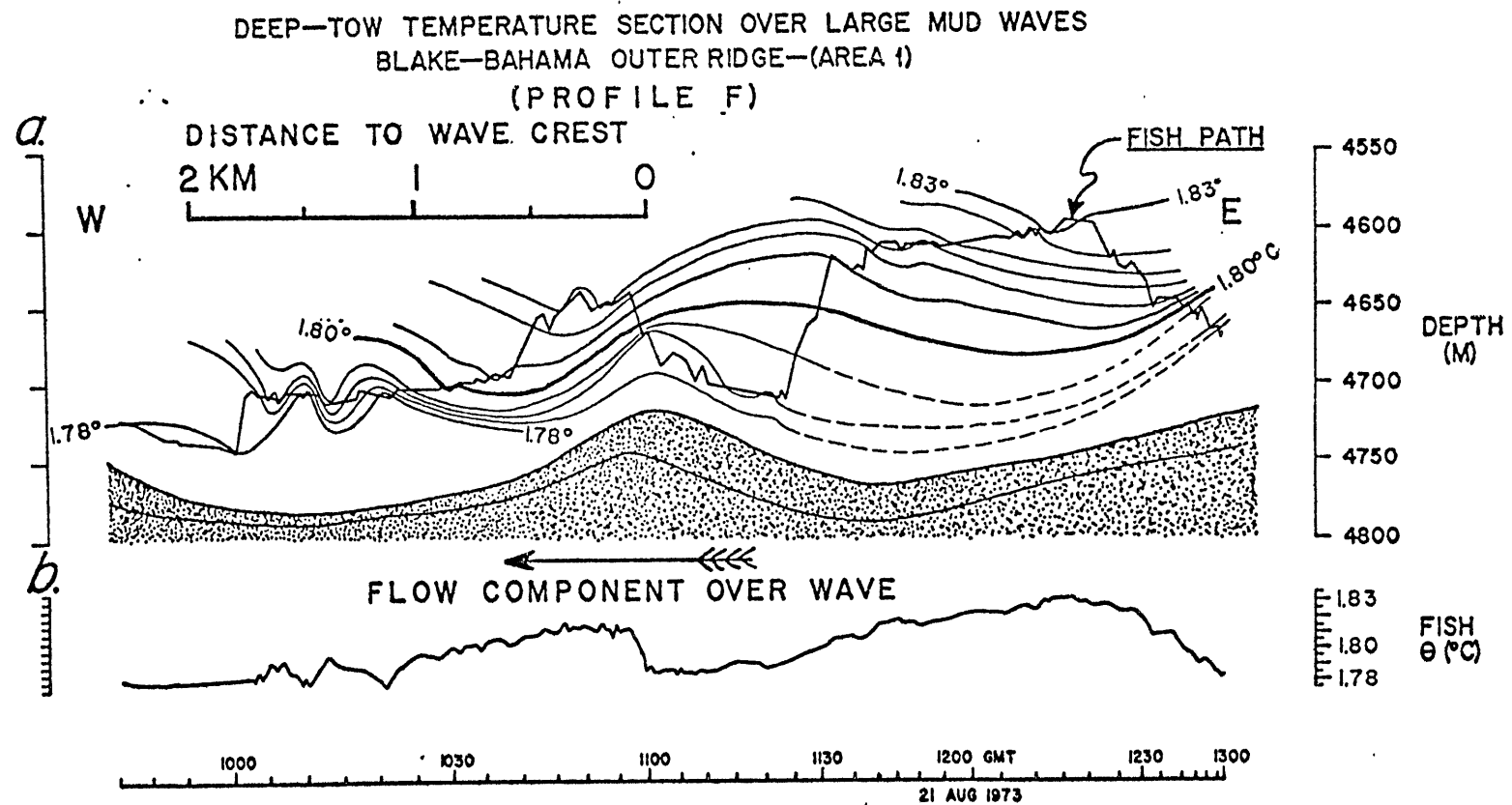
Figure 2.49

of the sediment wave, but they have slightly larger ampli-
tudes and are phase-shifted upstream. The 1.81° isotherm
(at about 125 m above the bottom) is shifted upstream about
one quarter of a wavelength (phase shift of 90°). The
The phase shift increases with height, producing larger
vertical temperature gradients on the downstream side of a
wave. The pattern appears to continue over the adjacent
waves to the east and to the west, and may reflect the
presence of internal waves positioned over the sediment
wave.

Near-bottom densities, referred to a depth of 4650 m
(σ_{4650}), were calculated for one-minute samples of
temperature along this profile. A potential temperature-
salinity relationship, based on a least-squares fit of his-
torical hydrographic data potential temperature (less than
1.9°C) collected in this region, was used to obtain a
salinity value for each previously determined potential
temperature. The *in-situ* temperature, salinity, and depth
were used to calculate the potential temperature the water
would have if it moved adiabatically to 4650 m (Fofonoff,
1977). The specific volume at 4650 m, and thus the density,
were then determined (Ekman, 1908).

The density profile over the wave (not shown) closely
followed the temperature profile. The overall near-bottom
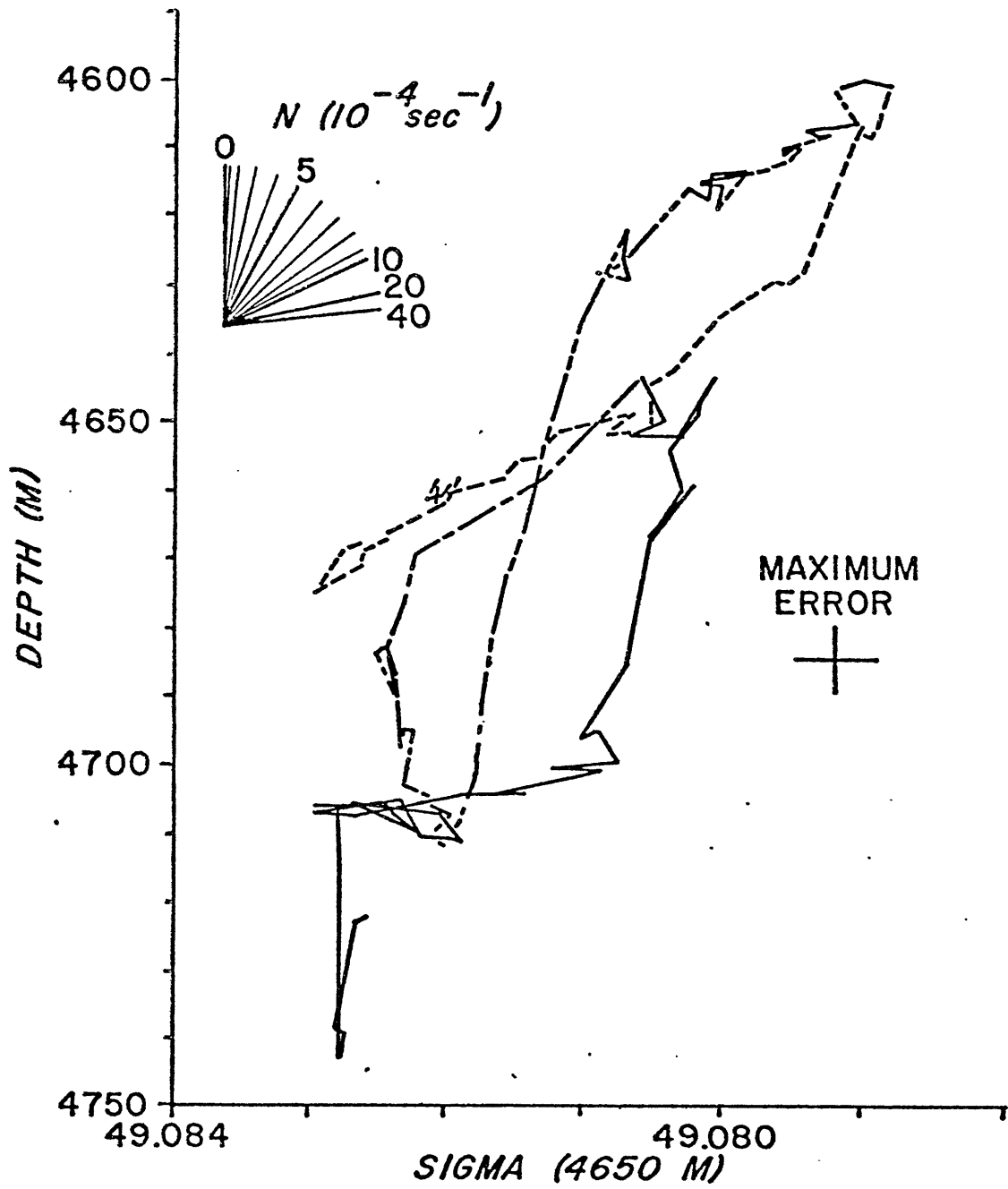
Figure 2.51.   Density (σ_{4650}) vs. depth for temperature
section in Figure 2.50.

density gradient, expressed as a buoyancy frequency or

Väisälä frequency (N)*, is $5 \times 10^{-4} \sec^{-1}$ (Figure 2.51). N

ranges from 10 to $40 \times 10^{-4} \sec^{-1}$ in deep thermoclines to 2 to

$6 \times 10^{-4} \sec^{-1}$ in less stratified portions of this transect.

Several temperature sections over sediment waves in Area 3 were made by repeatedly profiling (yo-yoing) the lowest 400 to 1000 meters of the water column with the STD as the ship drifted over the bottom. Of the seven yo-yo profiles made, three (stations 373, 376 and 378; located on Figure 2.34) proved adequate for delineating the structure of the water column over the sediment waves. The remainder of the profiles either were incomplete due to data loss or did not traverse an entire wave.

Time-temperature sections (Figures 2.52 a,b,and c; constructed by plotting temperatures, at the appropriate depths, along the track of the STD) were converted to distance temperature sections by assuming a constant drift velocity (0.9

---

*The buoyancy frequency (N) is the angular frequency at which a parcel of water will oscillate if it is displaced vertically a small distance from its equilibrium in a stable density gradient.

$$N(\sec^{-1}) = \left(- \frac{g}{\rho} \frac{\partial \rho o}{\partial z}\right)^{\frac{1}{2}}$$

Where: g = gravitational acceleration
  $(cm/\sec^2)$
  ρ = average density (gm/cm^3)
  ρo = potential density (gm/cm^3)
  z = depth, positive upwards (cm)

Figure 2.52. Temperature sections   over sediment waves, Area 3.

    (a)   RC18 STD station 376. Flow component over waves is from NE to SW.

    (b)   RC18 STD station 378. Flow component over waves is from NE to SW.

    (c)   RC18 STD station 373. Flow component over waves is from E to W.

Profiles indexed on Figure 2.33.

a. SW

DISTANCE FROM WAVE CREST (KM)

2

o

NE

4400

θ

1.88

1.87

1.86

1.85

1.84

1.83

1.82

DEPTH (M)

4600

1.81

376

ONE KILOMETER

06 07 08 09 10 11

7 JULY 1975

TIME (HOURS)

b. SW

DISTANCE FROM WAVE CREST (KM)

2

o NE

4300

θ

1.88

1.87

1.86

1.85

1.84

1.83

DEPTH (M)

4500

1.82

1.81

378

ONE KILOMETER

4700

23 00 01 02 03

9 JULY 1975

TIME (HOURS)
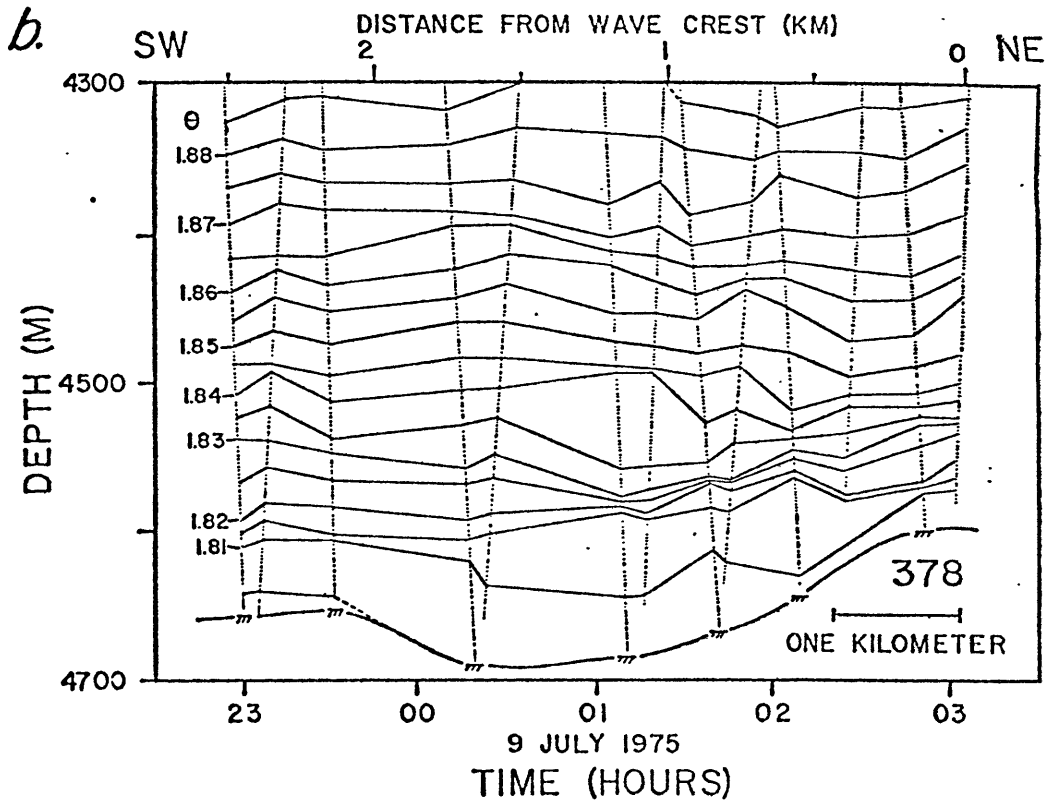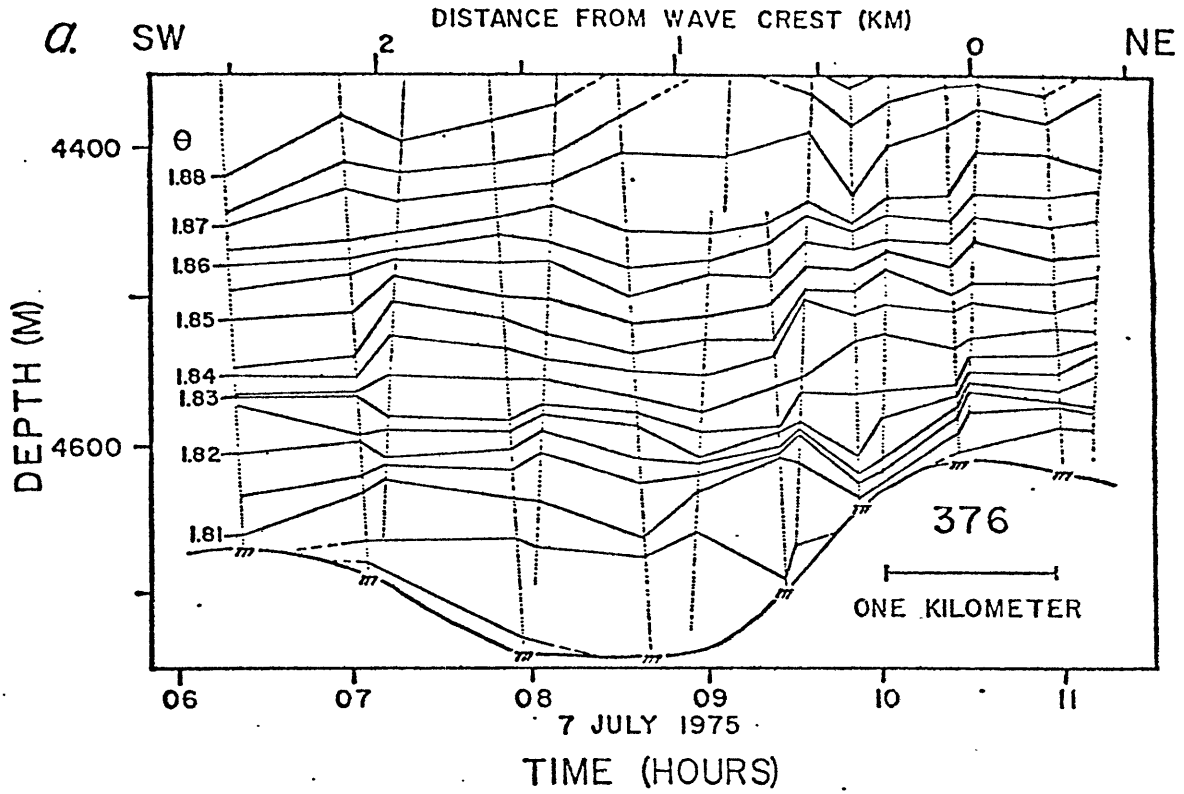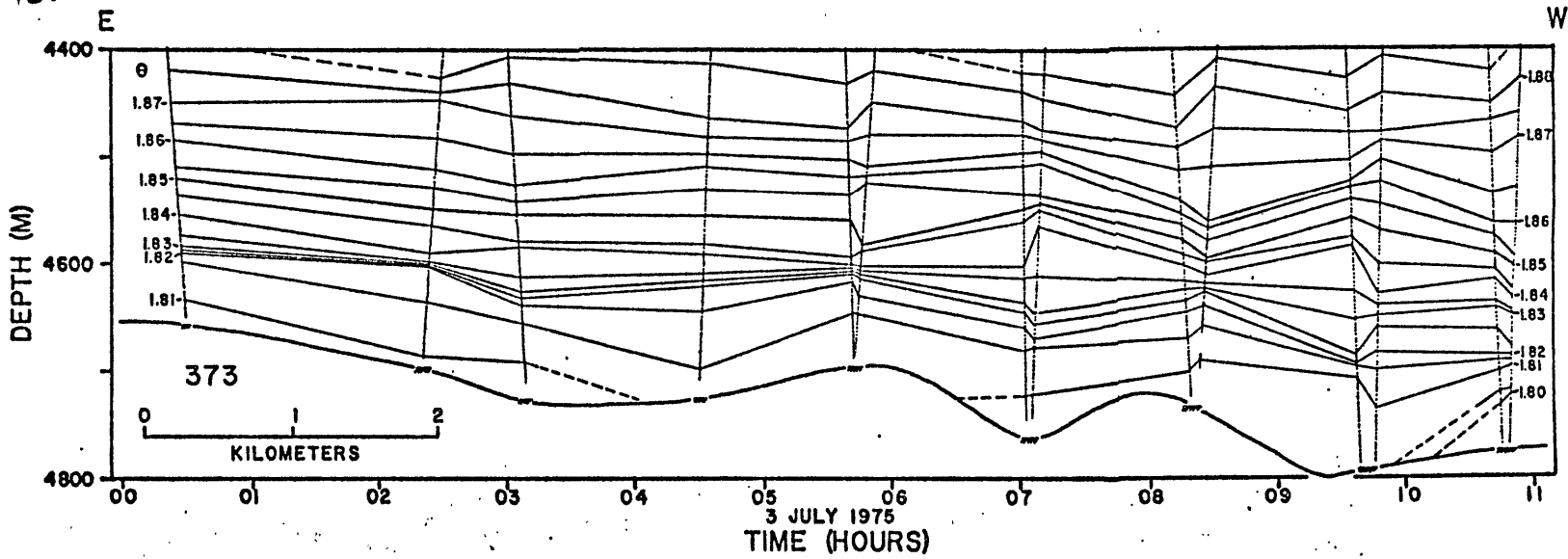
Figure 2.52

Figure 2.52

to 1.4 km/hr). Satellite fixes indicate that this is a
reasonable assumption. For profiles 376 and 378, which were
not perpendicular to the sediment waves, the distance to the
wave crest also is given. Sediment wave shape is based on
the depth below the STD at its deepest point and on the sur-
face-ship echo-sounding trace. The ship was as much as 3 km
ahead of the STD when these profiles were made. Current
speeds at RC18-CM03 ranged from 3 to 5 cm/sec while these
profiles were made (Table 2.6, Figure 2.52).

The temperature sections show a systematic interaction
between the sediment waves and the isotherm displacement
similar to that observed in Area 1. Internal waves with the
same wavelength as the sea floor topography are present
throughout the water column. These waves are phase-shifted
upstream (east) with increasing height above the bottom.
The pattern can be quantified by calculating correlation co-
efficients (c_i's)* between the sea floor and the depth of
isotherm i (Figure 2.53). Regional bathymetric trends were

---

*

$$c_i = \frac{\sum_j (x_j - \bar{x}_j)(y_{i,j} - \bar{y}_i)}{[\sum_j (x_j - \bar{x}_j)^2 \sum_j (y_{i,j} - \bar{y}_i)^2]^{\frac{1}{2}}}$$

In this case, x is sea-floor depth, y_i is the depth of
isotherm i, and $\bar{x}$ and $\bar{y}_i$ are the average seafloor and iso-
therm depth (regional sea-floor trend removed).

TABLE 2.6

SEDIMENT WAVE TEMPERATURE PROFILES: DATA AND RESULTS[1]

Temperature profile	Sediment wave wavelength (m)	Vertical wave wavelength[2] (m)	Sediment wave height (m)	Observed current V_o (cm/sec)	$V_o \sin \theta$[3] (cm/sec)	Calculated wave parameters[4] c (cm/sec)	ω(sec^{-1})	κ $\dfrac{N\,h}{V_o \sin \theta}$
Deep tow profile	2500	500	30	5.0	3.5	3.9	1.0×10^{-4}	0.4
373	2000	460	50	5.3	2.7	3.6	1.1×10^{-4}	0.9
376	2600	1060	100	3.6	3.3	7.8	1.9×10^{-4}	1.5
378	2250	520	60	3.3	2.4	4.1	1.0×10^{-4}	1.3

[1] $N = 5 \times 10^{-4}$ sec^{-1}, $f = 6.8 \times 10^{-4}$ sec^{-1}

[2] Four times height of 90° phase shift

[3] Flow component perpendicular to wave

[4] $c^2 k^2 = \omega^2 = \dfrac{N^2 k^2}{k^2 + 1^2}$
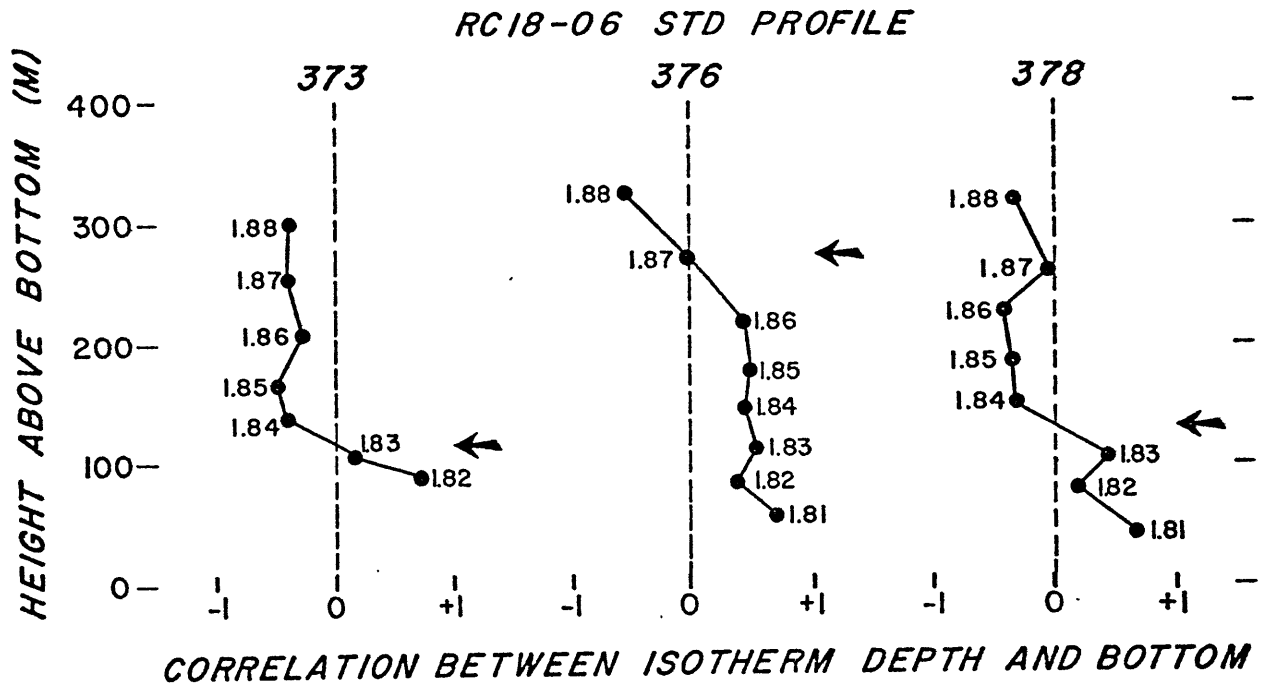
Figure 2.53.   Correlations between sediment surface and
isotherm depth, Area 3. Arrow indicates
height where correlation is zero. Temp-
erature sections were digitized at 23 points
for 373, 14 for 376, and 13 for 378.

removed from the data before the correlations were calcula-
ted.

Near-bottom isotherms are positively correlated with the
sea floor ($c_i>0$), while higher isotherms are negatively cor-
related (Figure 2.53). The height where $c_i=0$ (115 to 280 m),
corresponds to a phase shift of 90° between the internal
wave and the sea floor.

Flow Pattern over Sediment Waves

As internal waves showing the same relationships to the
sediment waves were present over those waves on several
occasions, they may be fixed in position. Internal waves
can be stationary if their phase velocity is equal to the
velocity at which water flows over the wave. The phase velo-
city (c) of an internal wave is $c=\omega/k$. In a non-rotating,
constant density-gradient fluid,

$$\omega^2 = \frac{N^2k^2}{k^2 + l^2}$$

gives the frequency of the internal wave (ω) where $k=2\pi/L$ is
horizontal wavenumber and $l=2\pi/M$ is the vertical wavenumber
(Turner, 1973). In this instance, the horizontal wavelength
(L) is that of the sediment wave and the vertical wavelength
(M) is four times the height at which a 90° phase shift
occurs between the internal wave and the sea floor.

For typical values of L = 2000 m, M = 650 m, and N = 5×10^{-4} sec^{-1} , c = 4.9 cm/sec and ω = 1.5×10^{-4} sec^{-1} . This corresponds to a fluid speed of 8 cm/sec flowing at an angle of 35° to the long axis of the sediment wave. This velocity is quite close to that measured for the flow. The frequency of the wave is between the buoyancy frequency (N = 5×10^{-4} sec^{-1}) and the inertial frequency (f = 6.8×10^{-4} sec^{-1}), as it must be for the wave to exist. The frequency is close to N, indicating that the non-rotating approximation used is not a bad one; although, rotatinal effects may be important for lower velocities (lower ω). Values of c and ω, calculated for the actual temperature profiles, are compared to the measured current component perpendicular to the sediment wave in Table 2.6. The agreement between the measured and calculated velocities is quite good, suggesting that internal waves are stationary over these sediment waves.

Stationary patterns of internal waves such as the ones described here form when a stratified fluid flows over an obstacle (e.g., atmospheric flow over a mountain range). The pattern of these lee waves is related to κ, where $\kappa = Nh/v_y$ (v_y is the flow velocity perpendicular to the crest and h is the height of the obstacle). For a barrier of a given height, lee waves will be more pronounced for low velocities and high stratification (larger κ; Turner, 1973, Figure 2.54). Values of κ associated with the temperature profiles, range from 0.4

a. $K=0.5$

b. $K=1.0$

FLOW ⟶

c. $K=1.27$

d. $K=1.5$
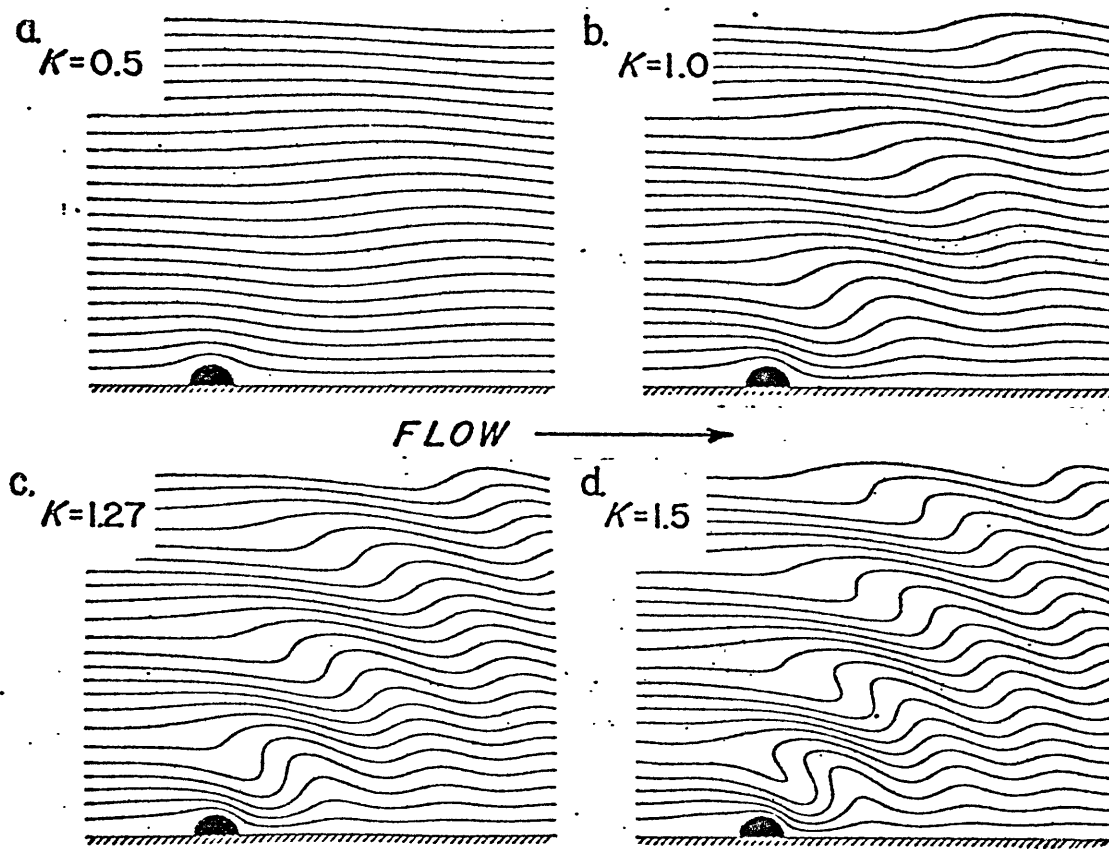
Figure 2.54.　Lee waves formed by a semicircular ridge.
(After Huppert, 1968.)

$$K = \frac{N\ h}{V}$$

to 1.5 (Table 2.6). Strong lee wave patterns can be
generated for these conditions.

For cases when the flow is perpendicular to the obstacle,
the associated flow pattern has higher velocities on the
downstream side of the (streamlines closer together) wave
and lower velocities on the upstream side (streamlines
farther apart, Figure 2.54). In this instance the flow
direction is at an angle to the obstacle (sediment wave).
Since current meter measurements in Area 1 show that the
flow directions are comparable in the wave troughs and
on the crests for velocities greater than 8 cm/sec (Figure
2.49a), the resulting current pattern appears to have simi-
larities to a ridge perpendicular to the flow. At low velo-
cities (less than 6 cm/sec), the observed current patterns are
quite different (Figure 2.49 b). At low velocities κ becomes
large, and blocking of the flow, or stagnation, can occur up-
stream of the wave crest, also leading to higher current velo-
cities of the flow on the downstream side.

Vertical temperature profiles (Figure 2.55 a,b) show the
presence of near-bottom constant-temperature layers only on
the downstream (west) side of the sediment wave. This well-
mixed region may result from increased turbulent activity in a
region of higher flow velocity.

Figure 2.55.   Vertical STD potential temperature profiles
over sediment waves, Area 3.

(a) "Down" potential temperature traces of
RC18-376.

(b) "Down" potential temperature traces of
RC18-378.

a.

DISTANCE FROM WAVE CREST (KM)

SW · · · 2 · · · 1 · · · 0 · · · NE

376 STD (DOWN)

DEPTH (M)

4400

4600

1825°

1 KM

180 · · · POTENTIAL TEMPERATURE (°C) · · · 190

06 · · · 07 · · · 08 · · · 09 · · · 10 · · · 11

7 JULY 1975

TIME (HOURS)

b.

DISTANCE FROM WAVE CREST (KM)

SW · · · 2 · · · 1 · · · 0 · · · NE

4300

378 STD (DOWN)

DEPTH (M)

4500

1825°

1 KM

180 · · · POTENTIAL TEMPERATURE (°C) · · · 190

4700

23 · · · 00 · · · 01 · · · 02 · · · 03

9 JULY 1975

TIME (HOURS)
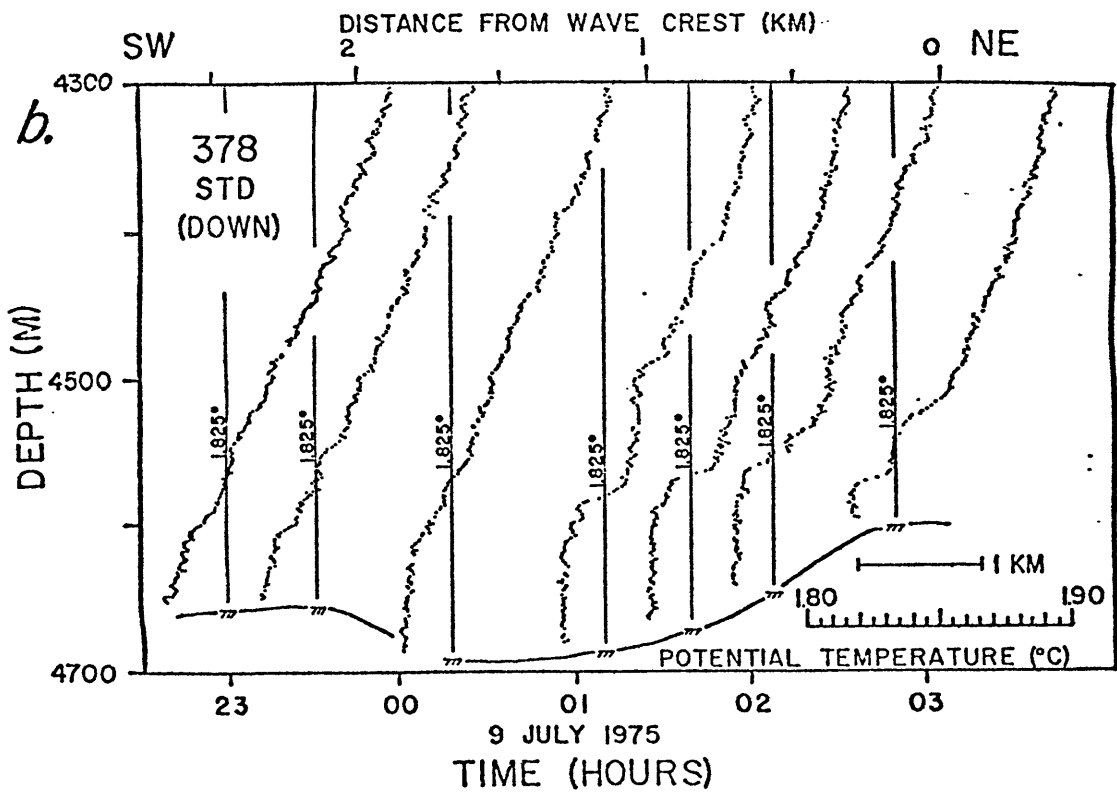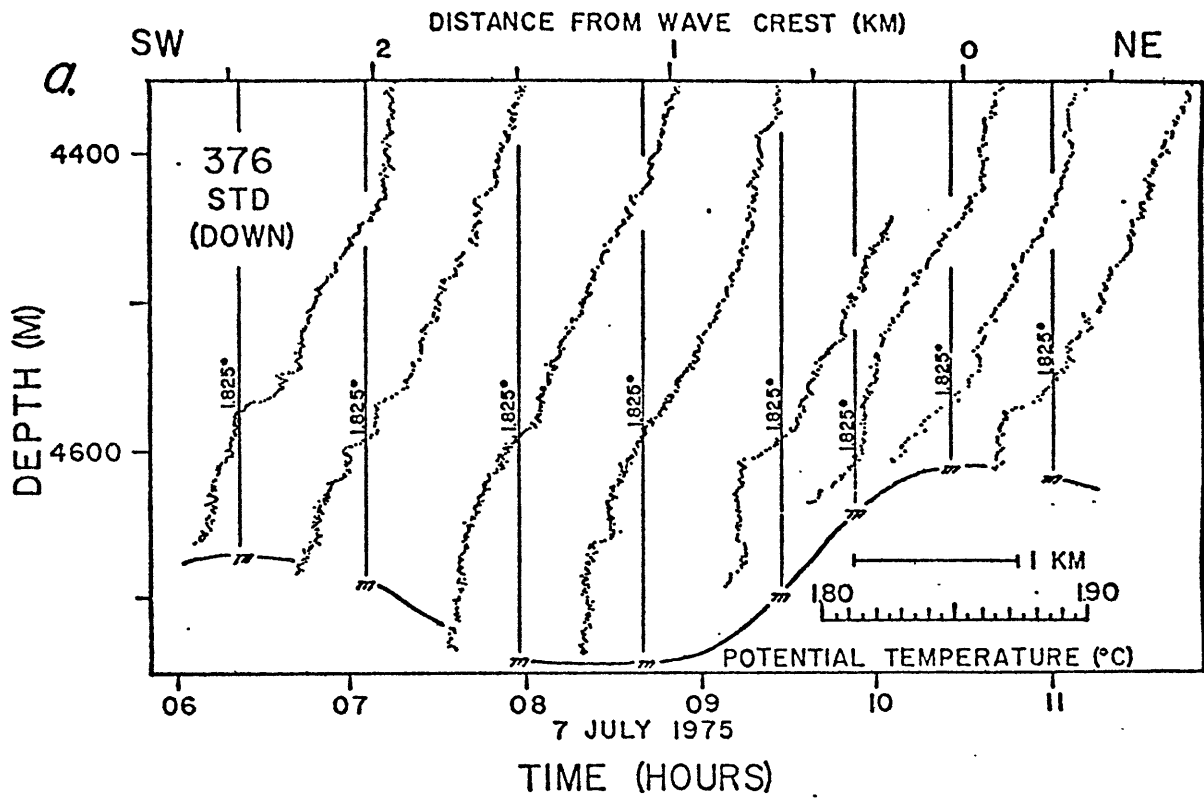
Figure 2.55

The variations in the furrow trends over the sediment waves (Figure 2.21) can be explained by the flow pattern over the sediment wave. At higher flow velocities (about 8 cm/sec), the flow pattern can be resolved into a flow component parallel to the wave crest (constant over the sediment wave) and a one perpendicular (varying over the sediment wave). As the perpendicular flow component is higher on the donwstream side of the wave, the velocity vector will be at a larger angle to the sediment wave crest than that on the up-stream side. The furrows develop parallel to that velocity vector and follow the same trends.

Preferential sediment deposition on the upstream side of the sediment wave can also be explained by such a flow pattern (Section IV.E).

SMALL FURROWS (AREA 1)

As described above, there is an interaction of the water flow over the waves with the sea floor. For the higher current velocities (greater than 8 cm/sec at 20 m above the bottom), the water flow is parallel to the furrows, suggesting that the furrows were formed by currents stronger than 8 cm/sec. The highest currents measured in Area 1 were 11 cm/sec (Table 2.5).

Visual observations from DSV TRIESTE II in Area 1 indi-
cated currents flowing at 15-20 cm/sec toward 320° to 330°,
parallel to the furrow trend at the dive site. No variations
in either the strength or direction of the currents were
detected across the furrowed topography.

Any array of ten speed rotors, extending to a height of
30 m above the bottom was deployed at the time of these
dives. The speed array, observed from DSV TRIESTE II, was
located in the center of a small furrow (about 1 m deep, 5
m wide at the surface, flat furrow floor 0.5 m wide). Very
preliminary results (Georges Weatherly, personal communica-
tion) indicate currents flowing at 20 cm/sec 30 m above the
bottom and decreasing to 8 cm/sec 15 cm above the bottom. A
logarithmic velocity profile, observed for the bottom 4-5 m,
suggests a bottom shear stress of about 0.9-1.0 dyne/cm^2.

The *in-situ* and laboratory experiments of Young (1975,
1977) on cohesive Buzzards Bay sediments suggest that such
bottom shear stresses may be capable of eroding bioturbated
cohesive sediments.

Also deployed in conjunction with the DSV TRIESTE II
studies in Area 1 was a bottom camera/current meter array.
This array was positioned by the submersible to photograph
the ripples on the sides of the furrow. Some current-induced

movement of sea-floor sediments can be observed on the
bottom photographs (Mark Wimbush, personal communication).
Much of this activity is concentrated where the sea floor was
disturbed when DSV TRIESTE II maneuvered the array into
position. The associated current meter record has not been
processed at this time (December, 1977; M. Wimbush, personal
communication).

The asymmetrical distribution of the temperature surfaces
over the sediment waves may lead to the observed distribution
of furrows over the sediment waves (Figure 2.21). Many
furrows start in the region where the isotherms are most
closely grouped, the downstream side of the wave. The nature
of the interaction between the isotherm and the furrows is
not known. One suggestion is that a thinner well-mixed,
constant-temperature layer in the water column on the down-
stream side of the wave may lead to more closely spaced fur-
rows. The temperature studies in Area 2 show that the furrow
spacing is three to four times the thickness of the well-
mixed bottom layer in that region. Such well-mixed layers
tend to be thinner, or at least more common, on the down-
stream side of a sediment wave (Figure 2.55 a,b).

LARGE FURROWS (AREA 2)

Current meters KN31-CM 1, located 20 m above the bottom in the furrowed area, and CM 3, located 20 m above the abyssal plain, show remarkably steady currents with average directions of 348° (Figure 2.56, Table 2.5). CM 3, on the abyssal plain, is not near any large topographic features and therefore records the actual flow direction. This flow direction agrees quite closely with the orientation of the furrows in this study area (355°, Figure 2.26). Current meter CM 2, also from the zone of furrowed topography, has an average direction of 001°, which does not correspond well to either the directions measured by the other current meters or the furrow trend. This discrepancy may result from the placement of this meter (20 m off the bottom) in a furrow, possibly near the wall (ca. 20 m high). The actual locations of CM 1 or CM 2 with respect to the furrows (50-100 m wide) were not determined. Current meter CM 3, on the abyssal plain, recorded velocities lower than those recorded in the furrowed area by CM 1 or CM 2 (2.5 cm/sec vs. 4.8 for CM 1). Maximum velocities recorded, averaged over 15 minutes, were 4.4 cm/sec toward 355° at CM 3 on the abyssal plain and 9 cm/sec toward 355° at CM 1.

Figure 2.56.   Current meter results (Area 2).   See caption
                to Figure 2.47 for an explination of the
                figure.

CURRENT SPEED AND DIRECTION
BLAKE—BAHAMA OUTER RIDGE—AREA 2

N

0   10 CM/SEC

CM 1   FURROWS, 20 M OFF

CM 2   FURROWS, 20 M OFF

CM 3   ABYSSAL PLAIN, 20 M OFF

1200, 13 AUG 73   1200, 14 AUG   1200, 15 AUG   1200, 16 AUG   1200, 17 AUG   1200, 18 AUG   1200, 19 AUG

GMT TIME
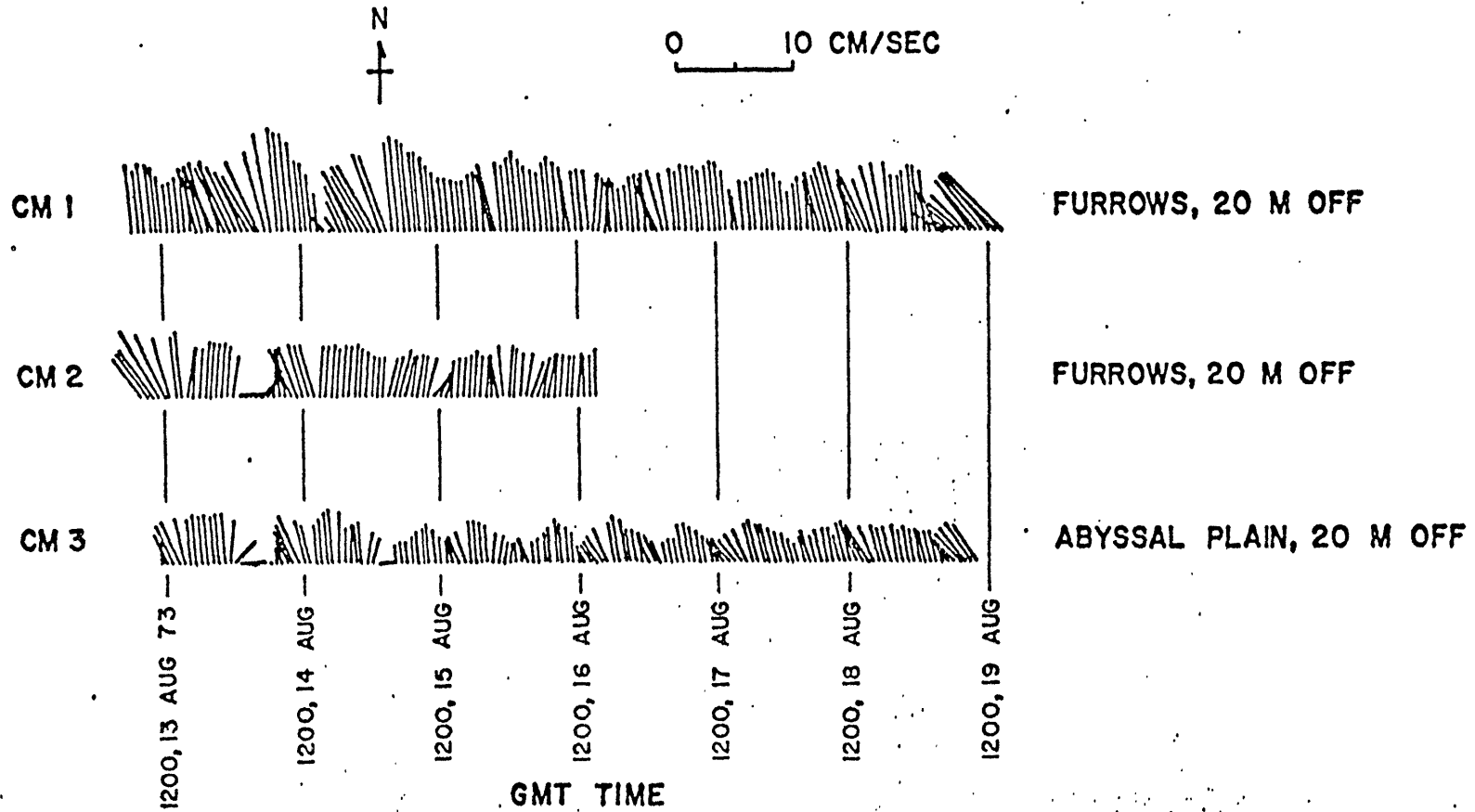
Figure 2.56

Temperature was measured every 10 sec for the duration
of deep-tow lowering 2 (Area 2). At any given depth, the
temperature changes markedly throughout the 40-hour duration
of the survey (Figure 2.57). These variations could be the
result of either temporal of horizontal variations in the
temperature field. To study the distribution of a parameter
such as temperature with a moving sensor it is necessary to
resolve these temporal and spatial variations, ideally by the
simultaneous measurement of the parameter at several fixed
points as well as by the moving sensor. No such measurements
were made during this survey. As a result, certain assump-
tions, supported by the observations, will be made to resolve
the temperature distribution.

Temporal variations may result from the advection of
waters of different temperatures across the survey area, from
changes in vertical temperature structure resulting from
events such as internal waves, or from the effects of turbu-
lence in the temperature structure of the benthic boundary
layer. Steady horizontal variations in temperature could
result from the interaction of the flow with bottom topo-
graphy or by density gradients in the fluid which balance the
geostrophic shear.

Periods associated with internal waves range from the inertial period (25 hours at 28°30'N) to the buoyancy period (approximately 4 hours). The 40-hour record obtained in this survey area is not long enough to adequately resolve the internal wave field present in this region. Significant temperature variations are present with periodicities between 4 and 25 hours. These variations could be related to the internal wave field.

Some of the temperature variation appears to be due to the advection of generally warmer water into the study area. Some estimate of the importance of advection can be obtained by determining the track of the fish through the water which has been advected across the study area. For the purposed of this estimate, it was assumed that water was advected through the area at an average velocity of 3.5 cm/sec toward 348°. This is quite close to the actual situation (Figure 2.56, Table 2.5). The track of the fish through the water was calculated by moving the fish position 167 m toward 168° for every hour after 0000-17 August. The resulting fish path is the one the fish would have taken if towed through a stationary water column. Temperature values were plotted along this track and contoured for various depths. The most data were available for a depth of 4912 m (Figure 2.58). Plots of temperatures at other depths are not shown, but give similar results.
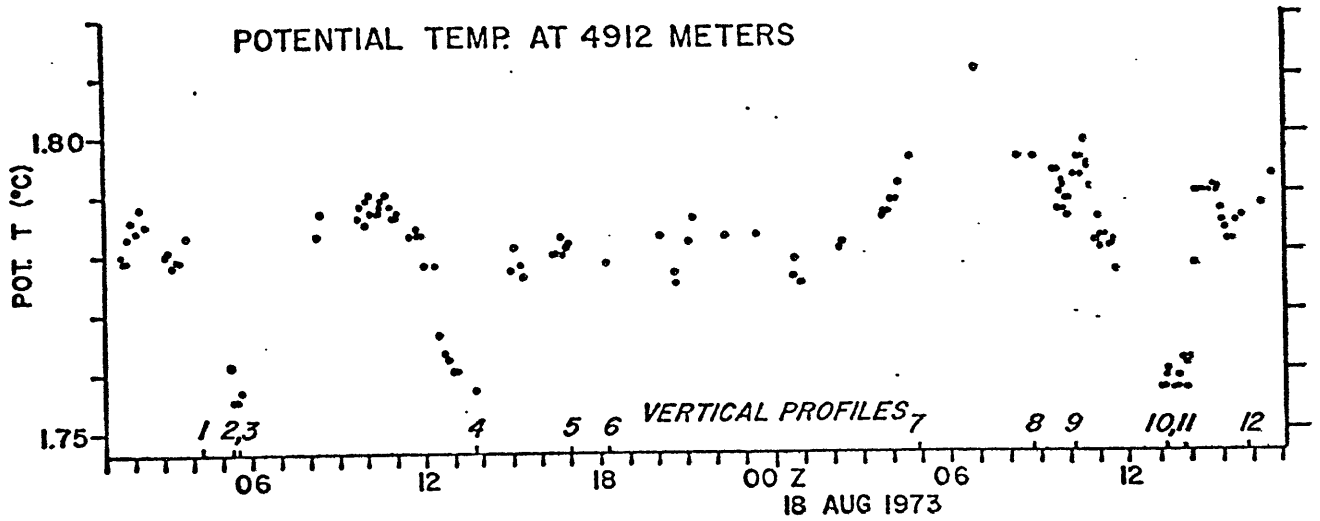
Figure 2.57. Potential temperature at 4912 m for lowering 2, Area 2. Numbers indicate times of vertical temperature profiles shown in Figure 2.59.

199

BBOR—AREA 2

5 KM

CM 2

1.78°C

DEEP-TOW TRACK

CM 3

VERTICAL PROFILE

E

1.79

1.80

1.81

5

6

10

11

12

7

8

9

POTENTIAL TEMP.
AT 4912±1 M
(WATER "FIXED" AT
0000Z 17 AUG '73)

1.78
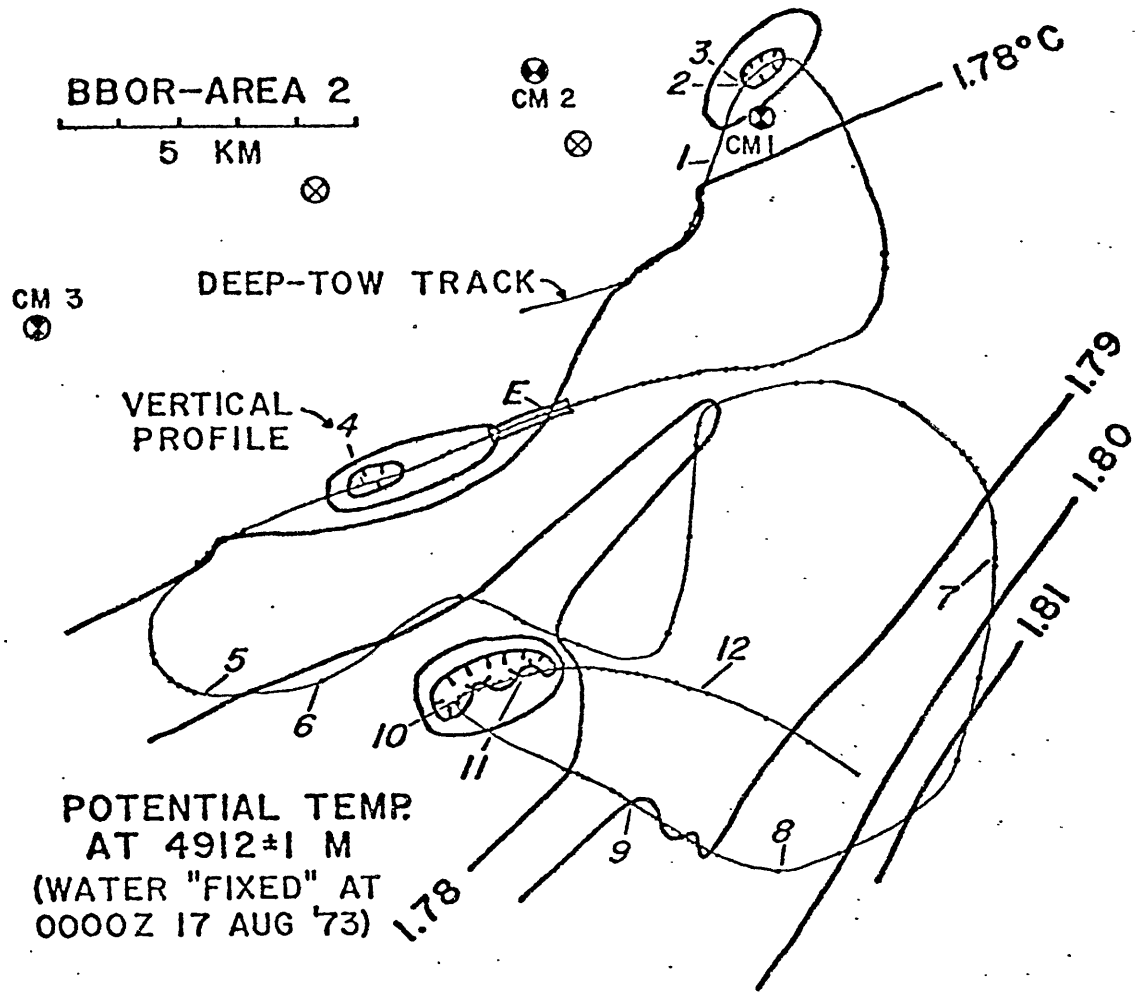
Figure 2.58.   Temperature contoured along track, Area 2.
Track is shifted as described in text to
compensate for the northward flow of water
across the area.   Circled numbers refer to
vertical temperature profiles (Figure 2.59).
Temperature profile at E is in Figure 2.61.

The pattern which results may be indicative of warmer water advecting across the area from the south. The horizontal temperature gradient is 0.003°C/km.

During the course of this survey a number of nearly-vertical temperature profiles were made. Twelve of these profiles showed a constant-temperature, well-mixed region at the base of the water column (Figure 2.59). The remaining profiles did not extend deep enough to show this layer. The well-mixed layers are bounded by sharp temperature gradients. The structure of the boundary layer remains the same, but with an overall temperature increase due to the regional warming trend. Benthic thermoclines occur at depths ranging from 4930 to 4890 m over the furrows, the tops of which range in depth from 4965 to 4970 m. The well-mixed layers range in height from 30 to 75 m with an average thickness of 50 m.

The coldest potential temperature of the survey (1.747°C) was recorded in a 30 m thick, well-mixed layer over the abyssal plain (Profile 5, Figure 2.59). Profile 6, taken one hour later and two kilometers away, shows a shallower, thicker, and warmer well-mixed layer (layer thickness 40 m, temp. 1.753°C). Profile 6, over the large furrows, may result from mixing profile 5 to a greater height. The thickness or

Figure 2.59.   Vertical deep-tow temperature profiles, Area 2.
               They are arranged with profiles from warmer
               water on the right (see Figure 2.58).

VERTICAL DEEP—TOW TEMPERATURE PROFILES
BLAKE—BAHAMA OUTER RIDGE (AREA 2)
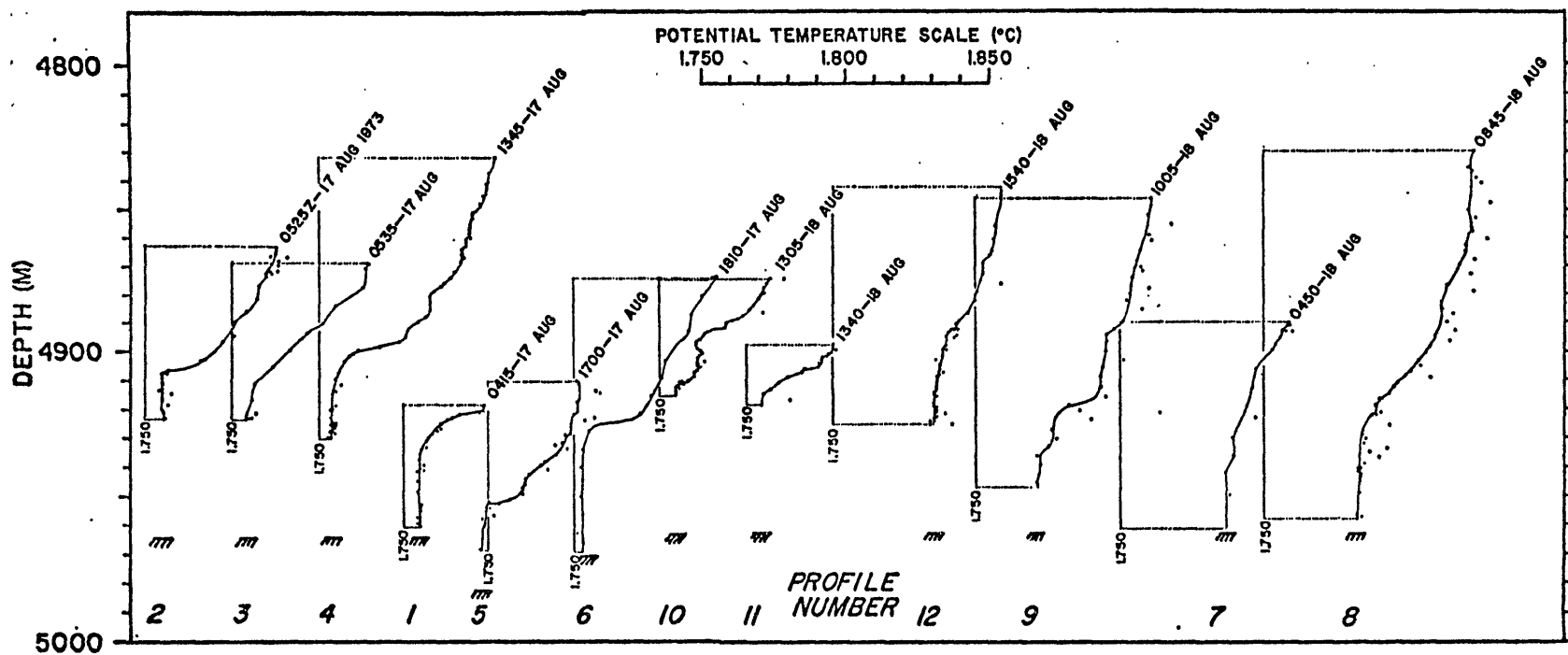
Figure 2.59

temperature of the well-mixed layer does not bear any simple relationship to the distance water has travelled over the furrows.

These profiles are similar in structure to those described by Armi and Millard (1976) and Armi (1977). The average layer thicknesses and current velocities over the furrows (50 m @ 4.5 cm/sec) and over the abyssal plain (30 m @ 2.5 cm/sec) are in agreement with well-mixed layers over smooth topography in the MODE region.

The thickness of the well-mixed benthic boundary layer in the furrowed region (50 m to top of furrows, 65 m to base of furrows) is roughly one-quarter of the average spacing between the furrows (200 m; Figure 2.28, 2.60). This is the relationship that would be expected if the furrows were related to large-scale secondary circulations within the well-mixed constant temperature bottom layer (Section IV.D).

The temperature data collected at ten-second intervals as the fish is flown at a nearly constant height also shows some interesting features. A 35-minute temperature record centered around 1200, 17 August shows large temperature variations (0.02°C) with a period of 5-10 minutes and a wavelength of 150 to 350 meters (Figure 2.61 a). During this time the fish was towed perpendicular to both the currents and furrows (Figure 2.58). In order to remove any changes in

POTENTIAL TEMPERATURE
°C

4850 —

1.750   1.850

DEPTH (m)

4900 —

4950 —

5000 —

0   100   200 m
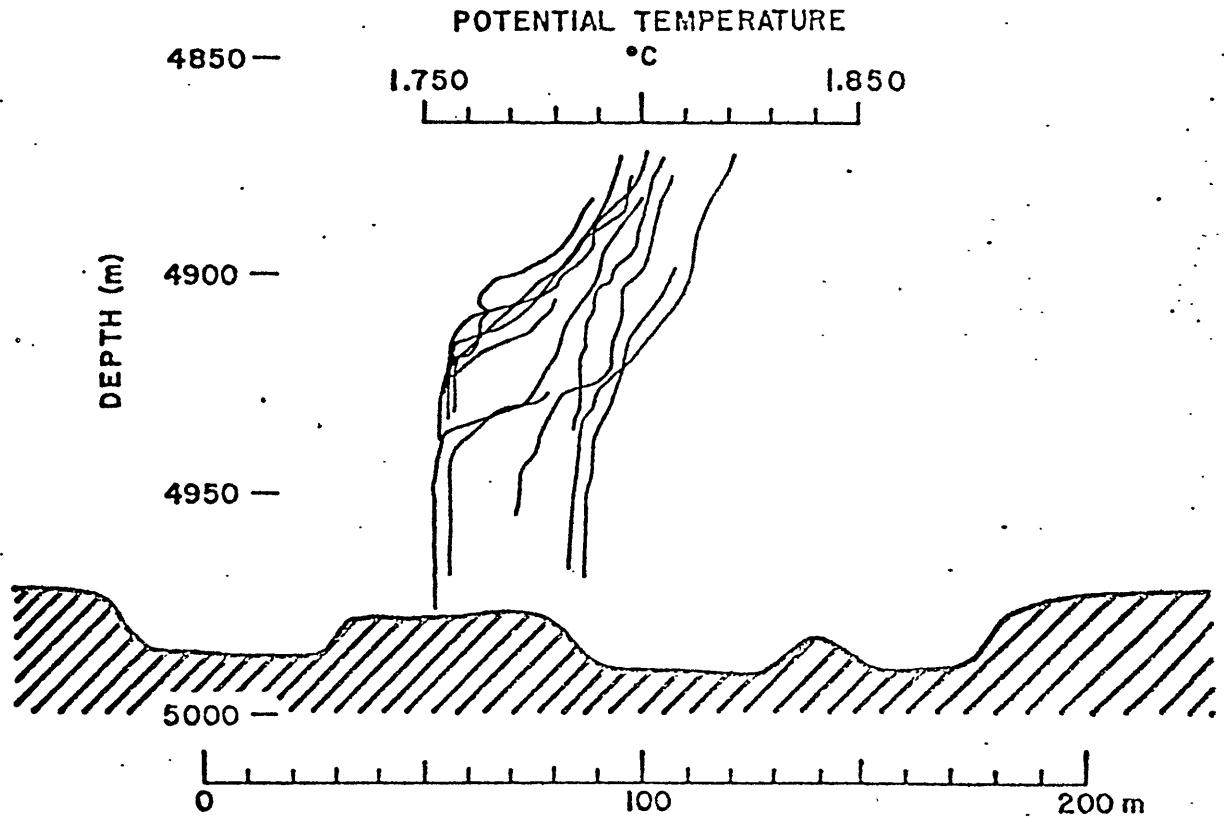
Figure 2.60.   Vertical temperature profiles and large furrow
topography.   Thickness of well-mixed layer is
about half of furrow spacing.   All temperature
profiles are plotted above a representative
section of furrow topography.

DEEP—TOW TEMPERATURE OVER LARGE FURROWS
BLAKE—BAHAMA OUTER RIDGE — AREA 2
PROFILE AT 90° TO CURRENTS (FROM S AT 6 CM/SEC) AND TO FURROW TREND
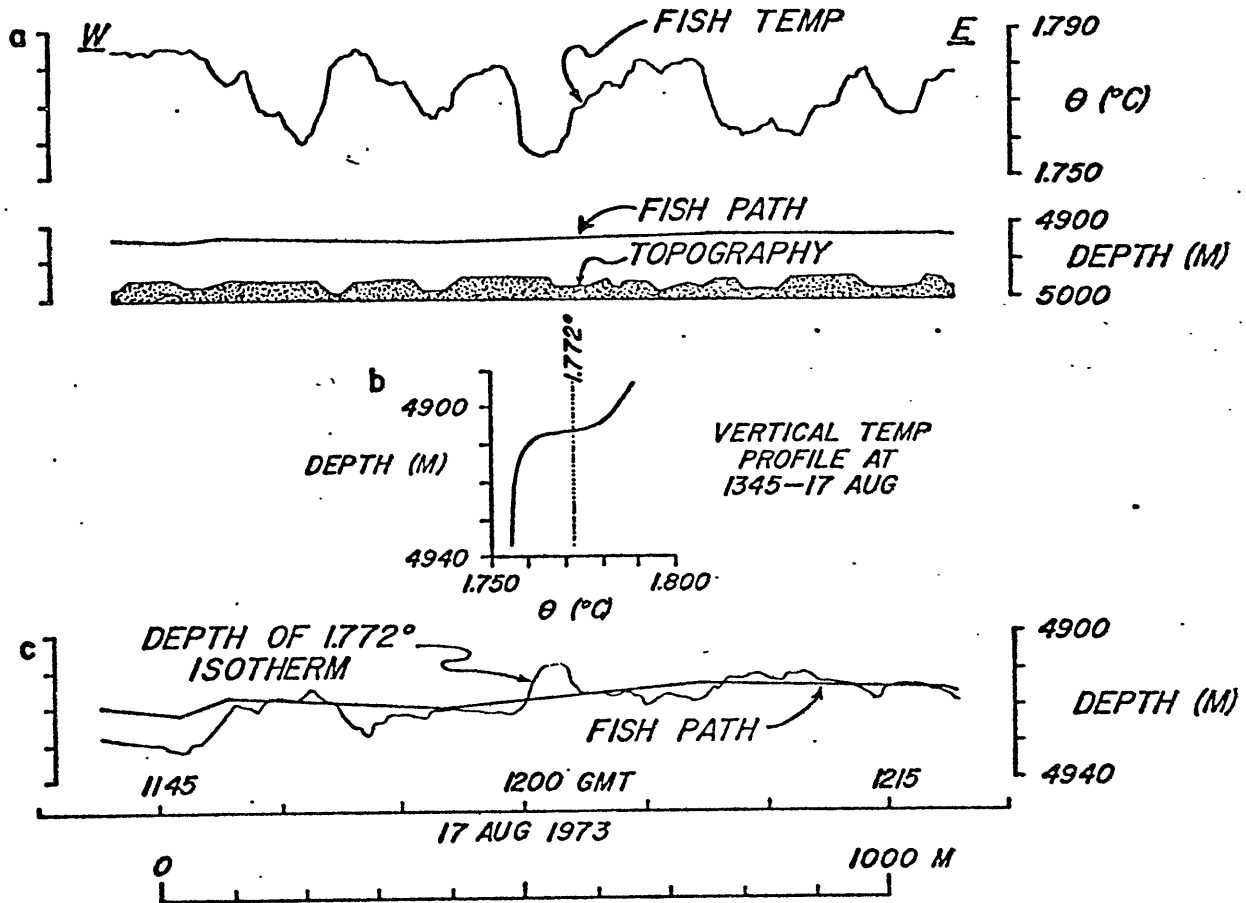
Figure 2.61. Horizontal temperature profile over large furrows. Profile indexed on Figure 2.59.

(a) Temperature along track, fish elevation, and bathymetry.

(b) Vertical temperature profile

(c) Computed depth of $1.772°$ C isotherm (inflection point of vertical profile).

fish height from the temperature record, the depth of the
1.772°C isotherm was computed (Figure 2.61 c) from a "verti-
cal" profile at 1345, 17 Aug. (Figure 2.61 b). During this
35-minute period (a distance of 1200 m) the average position
of the 1.772°C isotherm (the inflection point of the benthic
thermocline) climbed from 4930 m to 4915 m. The displacement
of the isotherm from the mean depth continues to show the
150-350 m wavelength with an amplitude of 3-7 m.

This wavelength corresponds with the spacing of the fur-
rows crossed by this profile (Figure 2.61 a), and the colder
water is often found over the furrow troughs. These tempera-
ture variations may be due to strong interactions between the
furrow topography and the water flow.

Visual observations of current speed and direction made
during DSV TRIESTE II Dive 15-77 gave a velo-
city of 10-15 cm/sec toward 260°, nearly 90° to the furrow
trend. This current, possibly due to an "event" similar to
that described in Area 1 (Figure 2.47) persisted long enough
for drag marks to be formed by bending organisms. Nothing
more is known about the long-term variability of the currents
in this area.

Triangular Ripples (Area 2)

Two current measurements have been made in the area of triangular ripples. Current meter KN31-CM 3 recorded a very steady current with a six-day average velocity of 2.5 cm/sec towards 348° in August, 1973 (Figure 2.56, Table 2.5). DSV TRIESTE II observations on 27-28 Sept., 1977, (Dive 15-77) indicated a current of 5 cm/sec flowing toward 260°, roughly parallel to the strike of the triangular ripples (N 70°E, Figure 2.25). Temperature profile 5, from the triangular ripple area (Figure 2.60), had a well-mixed layer 30 m thick.

Little can be said of the relationship between the triangular ripples and the currents which formed them as those currents were probably not sampled during this study. The longitudinal ripples may have been formed parallel to stronger currents (Heezen and Hollister, 1964; Zimmerman, 1971).

C. CONCLUSIONS

Many of the topographic features on the Blake-Bahama Outer Ridge can be understood as bed forms developed by a persistent bottom current circulation pattern. The bed forms range in size from a few centimeters to several kilometers and have been studied by a variety of techniques (Table 2.7).

Current ripples (Figure 2.62 c) developed in cohesive sediments, appear to be formed by the deposition of those sediments at speeds of 5 to 15 cm/sec. The ripples are often at an angle to the flow and appear to be always developed on slopes. Many of them appear to be forming at the present time, especially many of those observed visually from DSV TRIESTE II. Although ripples have evidently been present on the small furrow walls for some period of time, no distinctive sedimentary structures were identified in the core recovered from them.

Furrows (and associated hyperbolic echoes) are observed over wide areas of the outer ridge. Although the morphology of the furrow changes slightly from place to place (Figure 2.62 a,b, and d), all of the furrows studied show pronounced similarities. These similarities include a depression marking the bed form, a regular spacing, and junctions between the furrows which open consistently in one direction

TABLE 2.7

BED FORMS— BLAKE—BAHAMA OUTER RIDGE
SEDIMENT — HEMIPELAGIC MUD (0—5% SAND, 15—30% SILT, 65—85% CLAY)

BED FORM	DIMENSIONS	ORIENTATION TO CURRENTS	SURVEY AREA	HOW OBSERVED AND STUDIED
CURRENT RIPPLES	CM'S	TRANSVERSE	1,2,3	BOTTOM CAMERAS
LONGITUDINAL TRIANGULAR RIPPLES	CM'S HIGH M'S LONG M'S SPACING	PARALLEL	2	BOTTOM CAMERAS DEEP—TOW SIDE—SCAN SONAR
FURROWS	1'S—10'S M DEEP 1'S—100'S M WIDE 10'S—100'S M SPACING	PARALLEL	1,2,3	BOTTOM CAMERAS DEEP—TOW ECHO SOUNDER, 4 KHZ DEEP—TOW SIDE—SCAN SONAR SURFACE ECHO SOUNDER (HYPERBOLIC ECHOES)
LARGE MUD WAVES	10'S M HIGH KM'S SPACING 10'S KM LONG	OBLIQUE	1,3	DEEP—TOW ECHO SOUNDER, 4 KHZ SURFACE ACOUSTIC PROFILES PRECISELY NAVIGATED BATHYMETRY
OUTER RIDGE	100'S M HIGH 100'S KM WIDE 100'S KM LONG	PARALLEL	1,2,3	SURFACE ACOUSTIC PROFILES

Figure 2.62. Photos of different furrows investigated,
Bahama Outer Ridge.

(a) Steep, erosional wall of large furrow in
Area 2.

(b) Small furrow in Area 1 or west side of
Bahama Outer Ridge

(c) Rippled wall of small furrow in Area 1.

(d) Smooth-wall of furrow on east side of
Bahama Outer Ridge.

Scale bar = 1 m.
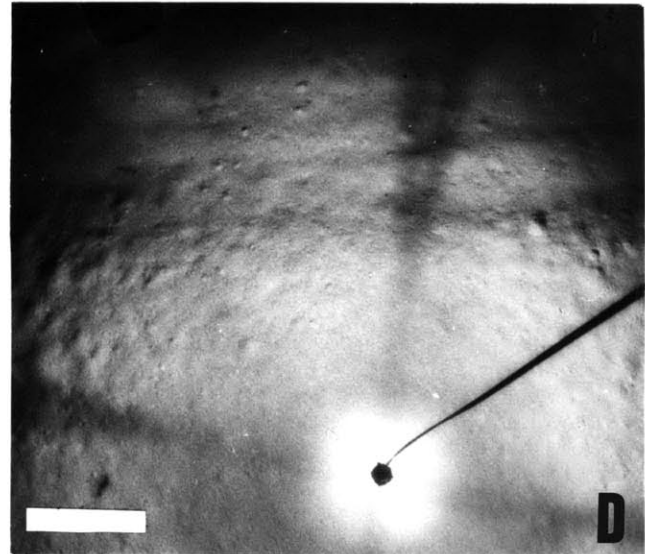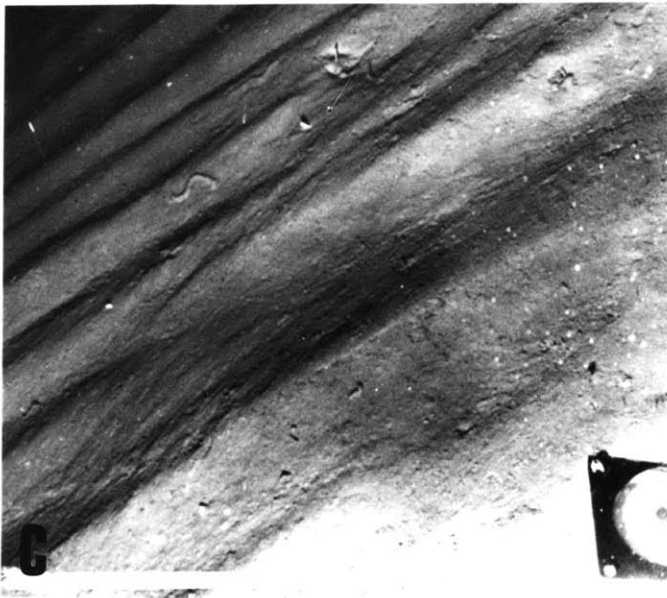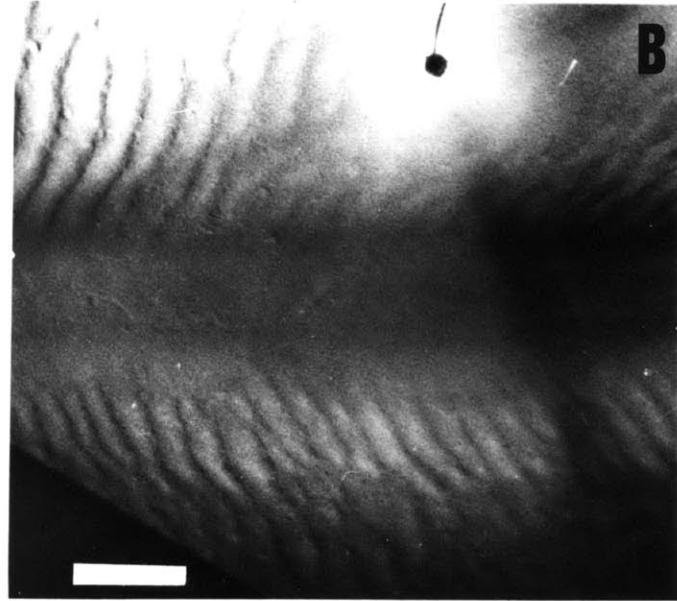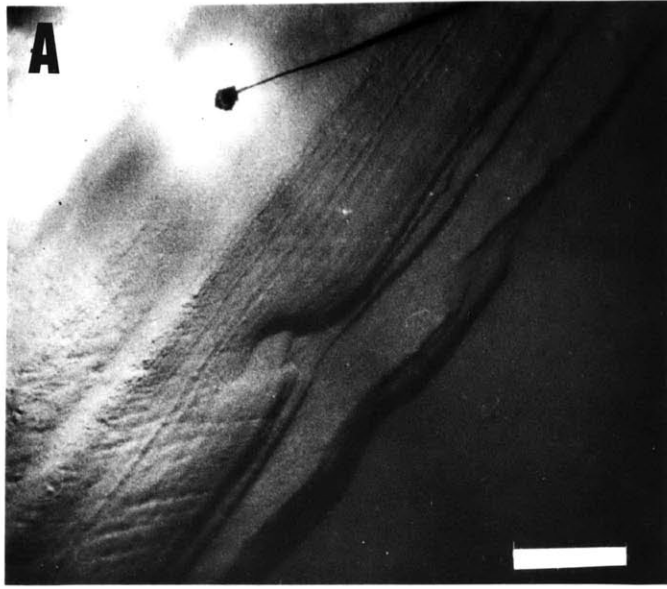
Figure 2.62

(into the flow). In any one area, the widths, depths, and spacings are quite uniform, and the furrows are parallel to the strongest flows. Because of their similar character-istics, these features are all termed furrows. These furrows are all developed in fine-grained cohesive sediments. The furrows (possibly of two or more types) can be erosional features (large furrows) or they can be depositional fea-tures (small furrows). It is not known if these furrows were formed in different ways or if they developed different-ly after being formed in the same manner.

Many of the small furrows of Area 1 have been depositional features for at least 11,000 years. The small furrows on the eastern side of the Bahama Outer Ridge crest do not appear to be active at this time. The large furrows of Area 2 were apparently eroded within the last 16,000 years, possibly at the time (11,000 years ago) an iron-manganese crust was formed in cores higher on the ridge. This possible erosional event was particularly intense, and may be related to changes in bottom water circulation patterns at the end of the last glacial period (Lohmann, 1977). Some of the smaller furrows may have been formed at that time, also as erosional features. Since their formation, these furrows would have developed as depositional features. The larger "small furrows" may have formed as erosional features during earlier high-velocity events.

Furrows have also been observed in other areas of the outer ridge. Several large "channels" have been observed in the northern Blake-Bahama Basin in large-area (100 m^2) LIBEC bottom photographs (76°00'N, 29°20'W, depth approx. 5000 m; Walter Brundage, personal communication). These features appear identical with the large furrows mapped in nearby Area 2. The furrows are oriented north-south and a nearby current meter indicated a flow of less than 5 cm/sec to the westsouthwest.

Small furrows have been observed near the crest of the Blake Outer Ridge (28°N, 73°30'W, depth 4000 m) with a towed camera sled (Brian Tucholke, personal communication). These furrows trend north-south (parallel to the contours), but have no ripples developed on their walls. They appear similar to the furrows seen on the eastern side of the Bahama Outer Ridge crest. No surface-ship hyperbolic echoes were recorded at this location, but some inter-ference patterns were observed.

A pinger attached to the camera sled revealed that a sub-bottom reflector apparently follows the form of the furrow, suggesting that these furrows have been deposi-tional features for some period of time. (Tucholke, personal communication).

There is a distinct boundary between the small hyper-
bolic echoes (returned from the small furrows) and the
pronounced hyperbolic echoes (returned from the large
furrows) at a depth of 4920 m on a profile which goes from
                  Area 2
Area 1 to∧(Profile 2, Figure 2.3). Many shallow sub-bottom
reflectors cannot be followed through the boundary but one
prominent deep reflector continues across apparently un-
disturbed. It is not clear why there should be such an
abrupt contact. One possible explanation is that, since
the Blake-Bahama Basin is a closed basin at depths greater
than 4800 m, little sediment is brought into the basin
from upstream. As a result, bottom currents have been
more erosive and erosional furrows have developed. At
depths less than 4900 m, there has been adequate sediment
supply and depositional furrows are present.

Measurements of the thickness of the well-mixed bottom
boundary layer suggest that the furrow spacing is at pre-
sent three to four times the mixed-layer depth. The
furrows may be in equilibrium with large-scale secondary
circulations within this layer. Although no long-term
current meter measurements are available, the small fur-
rows, and associated ripples, are evidently in equilibrium
with currents of 10 to 15 cm/sec. Currents of up to 8 cm/
sec are associated with the large furrows.

Regular sediment waves cover a large region of the Bahama Outer Ridge. The waves, oblique to the currents and migrating upcurrent as well as upslope, have possibly existed for approximately the last 10 million years. The angle between the sediment waves and the regional contours appears to depend on the regional slope.

Sediment cores indicate that some of these waves have been active features (have migrated) during the last 11,000 years, while others have been recently dominated by possible erosional events.

The flow over the sediment wave can be understood in terms of lee waves generated by a ridge perpendicular to the flow of a stratified fluid. Although the sediment waves are at an angle to the flow, current meter measurements indicate that such a flow pattern is feasible. Currents of greater than about 6 cm/sec are required for the formation of such lee waves. Such a flow pattern can explain variations of furrow trend and spacing over the waves as well as their upstream migration (Section IV.E.).

Longitudinal triangular ripples are found in a sandy mud. Some of these features, formed after the erosion of the furrows, are presently being covered over.

Distribution patterns of these four bed forms and their origins are discussed in Chapter IV.

Chapter III

SEDIMENT WAVES AND DEBRIS FLOWS IN THE ROCKALL TROUGH

A. INTRODUCTION

The detailed investigations of the morphology of the Bahama Outer Ridge (Chapter II) indicated the presence of a variety of current-produced sedimentary features, many of which could be detected, but not sufficiently resolved on surface-ship echo-sounding profiles. The broad correlations which could be made between echo type and surface morphology in that area need to be tested in other areas of the deep sea in order to demonstrate both the applicability and the limitations of these correlations. The Rockall Trough was chosen as the site of this test.

Near-bottom investigations were made with the Scripps deep-tow package at four sites in the Rockall Trough to study the morphology of the sea floor in those regions (Figure 3.1). These data were collected on R/V Knorr, Cruise 51, Leg 3, in August, 1975. In conjunction with the deep-tow studies, several cores were recovered in these study areas. Studies undertaken in Areas A and B will be reported by Lonsdale and Hollister (in press). This report concentrates on the surveys in Areas 1 and 2.

Rockall Trough (Figure 3.1), a 250 km wide ocean basin created by Mesozoic sea-floor spreading (Laughton, 1975), has been partially filled in with sediment to an

Figure 3.1   Bathymetric map and echo character
              Rockall Trough. Bathymetric profiles
              courtesy of the Woods Hole Oceanographic
              Institution, Lamont-Doherty Geological
              Observatory and U. S. NAVOCEANO. Deep
              tow study areas 1 and 2 are discussed in
              this report while study areas A and B are
              discussed by Lonsdale and Hollister (in
              press). Contours in meters after Roberts
              (1975). Arrows associated with survey
              areas indicate direction of measured or
              inferred currents.

Figure 3.1

218
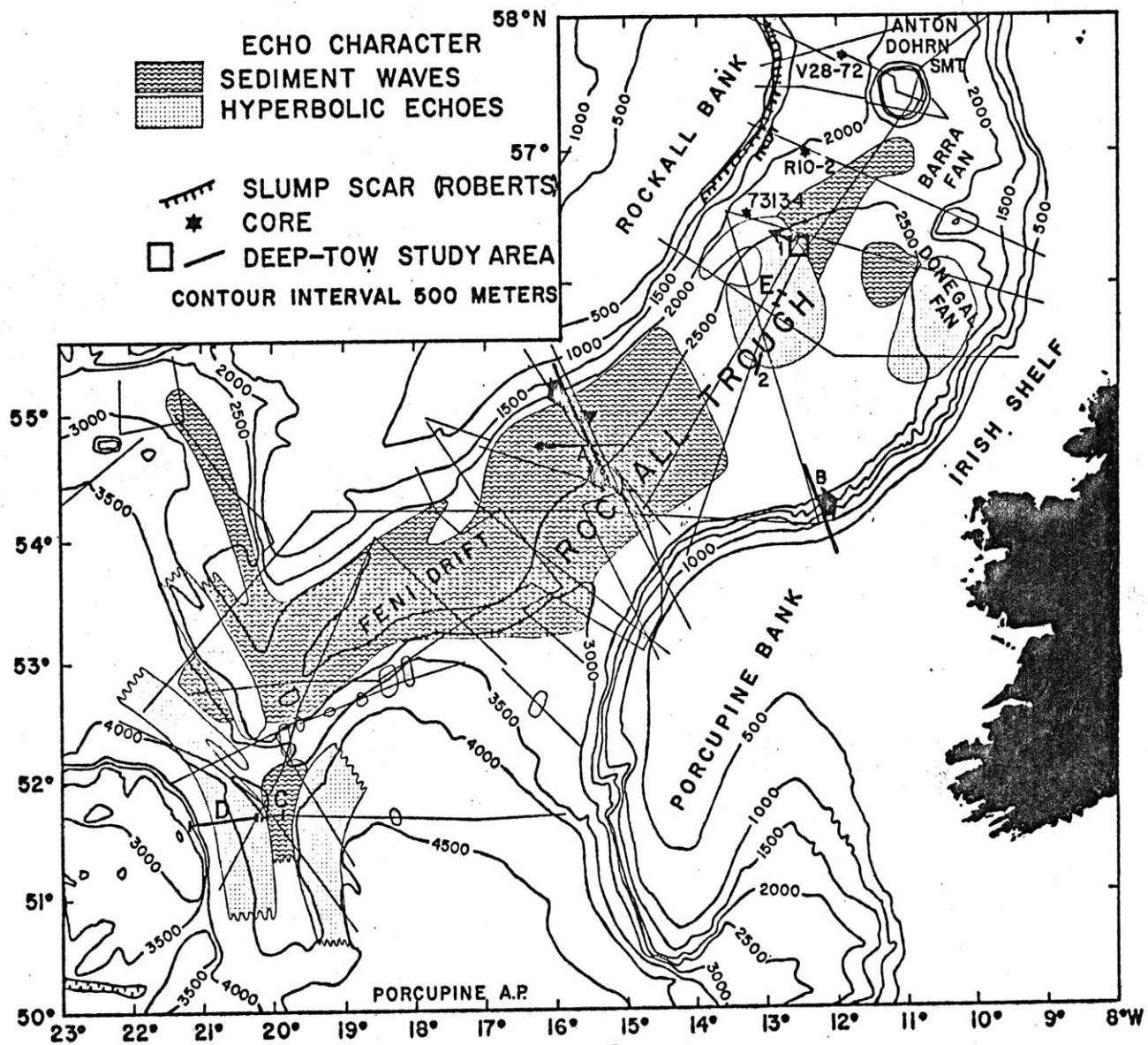
average thickness of several kilometers (Roberts, 1975).
The Upper Tertiary sediment fill is partitioned about
evenly between large deep-sea fans (e.g., Barra and Donegal
Fans) that are presumably built of turbidites and cover the
eastern side of the trough, and giant sediment drifts
(Feni Drift and associated·smaller drifts) on the western
side (Roberts, 1975).

Lonsdale and Hollister (in press) have emphasized the
geological importance of a cyclonic loop of Northeast
Atlantic Deep Water that has built the drifts on the western
side of the trough from the fine fraction of sediment that
it brought in suspension from canyon mouths on the Irish and
Hebridean margins. This cyclonic circulation pattern also
appears to control the distribution of large sedimentary
bed forms such as sediment waves (Figure 3.1).

Deep circulation patterns

Lonsdale and Hollister (in press) cite geological evi-
dence for the presence of an intense but thin (500 m) and
narrow (10 km) northward-flowing current entering the
western portion of the trough at a depth of 2500 m to 3000 m,
(along the base of Porcupine Bank). This high-silicate, low-
oxygen water is Northeast Atlantic Deep Water (NEADW) which
enters the trough from the West European Basin and has its
ultimate source in the Antarctic Bottom Water. This north-
eastward flow is thought to continue north along the south-

east margin and to cross the trough south of Anton Dohrn

Seamount in a broad, diffuse flow. Once across the trough,

the NEADW joins with the southward-flowing Norwegian Sea

Overflow Water (NSOW). The NSOW has entered the trough over

the Wyville-Thompson Ridge to the north (Ellett and Roberts,

1973) and has been an important geological agent north of

Anton-Dohrn Seamount (Roberts et al, 1974). The combined

southward flow is broad, covering most of the Feni Drift, with

a narrow, high-velocity core hugging the base of the slope.

A complicated flow pattern is observed on the Feni Drift. The

sinuous currents described here may be similar to those

described from the Blake-Bahama Outer Ridge (section II.A).

The current flows southwest along The Rockall Slope until

the southern extent of the Rockall Plateau is reached. The

current then turns to the west and flows along the southern

margin of Rockall Plateau. This circulation pattern is

similar to that determined for this area by Ivers (1975).

On the basis of bottom photography, Lonsdale and Hollister

(in press) suggest that the highest velocities associated

with this circulation pattern are 20 cm/sec with average

speeds of 12-15 cm/sec common. Current meters located in

the slow, cross-trough flow (Area 1) measured average

velocities of 3.7 and 3.3 cm/sec towards the west-northwest
(Figure 3.2)
over a 4½ day period. The maximum speed (averaged over 15

min) was 13.5 cm/sec. In contrast to the Blake-Bahama Outer

Ridge, tidal-current fluctuations are quite strong here

CURRENT METER RECORDS
ROCKALL TROUGH – STUDY AREA 1
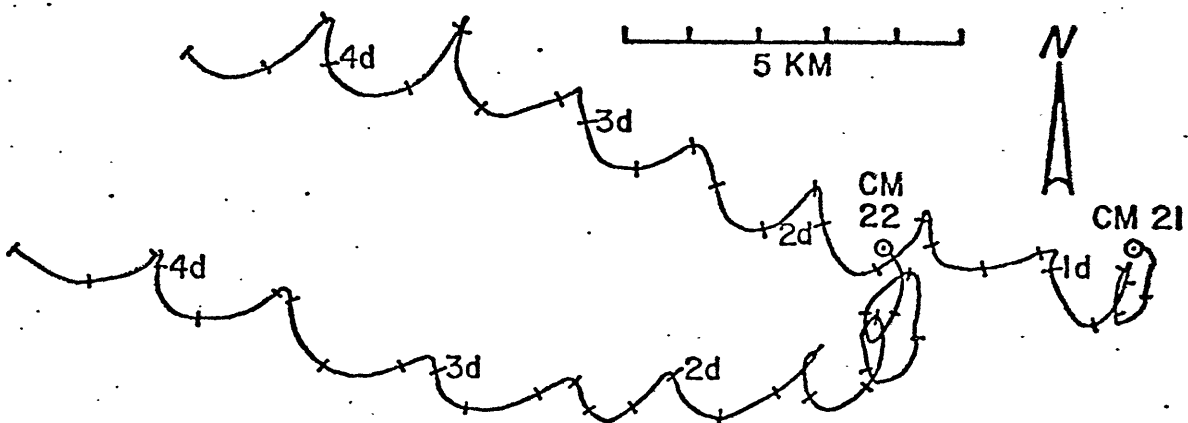
Figure 3.2   Progressive vector diagrams KN51-CM21
and CM22. Current meters are located
in Figure 3.6.

(tidal component about 6 cm/sec) in agreement with the pre-
diction of Pekeris and Accad (1969).

Echo character

Previous studies of the Rockall Trough have often in-
cluded a discussion of the surface echo character, or micro-
topography, of the region. These discussions have generally
included a few paragraphs describing the various types of
echo returns observed, but included little information about
their areal distribution. Jones et al., (1970), who first
described and named the Feni Drift, reported that the drift has
areas of well-developed sediment waves and areas of abundant
hyperbolic echoes. They suggested that the presence of
hyperbolic echoes and sediment waves were evidence for south-
ward-flowing bottom currents that may have played a role in
the development of the Feni Drift. Ellett and Roberts (1973)
cited the presence of hyperbolic echoes and sediment waves
as partial evidence for the role that southward-flowing
Norwegian Sea Overflow Water has had in the construction of
the Feni Drift, and Roberts (1975) presented a generalized
map of the areas of the trough characterized by various
sedimentary processes based on the microtopography of the
sediments.

In order to make detailed studies of the microtopographic
elements of Rockall Trough, the distribution of these micro-
topographic elements must be understood. As a part of this

study, all available 3.5 and 12 kHz echo-sounding records

of the Woods Hole Oceanographic Institution, Lamont-Doherty

Geological Observatory and the U. S. Naval Oceanographic

Office were studied in order to map the distribution of

sediment waves and hyperbolic echoes in the trough. The

track coverage, densest south of 58°N, was dense enough to

permit the mapping of areas characterized by various echo

returns (Figure 3.1).

B. SEDIMENT WAVES

Distribution

Sediment waves are found in at least five areas of

Rockall Trough (Figure 3.1). Side echoes resulting from the

wide beam angle of the 3.5 kHz echo sounder are common on

many of the echo-sounding records (Appendix I). The largest

grouping of sediment waves is on the Feni Drift south of

56°N, where the drift begins to have a pronounded topographic

expression (Roberts, 1975), and continues around the southern

end of Rockall Bank. These waves, found in a depth range of

2430 m to 2800 m, often have migrated toward the crest of

the drift. They have wavelengths of from 0.5 km to 1.5 km

and heights of 3 m to 20 m (Figure 3.3). Sediment waves are

found in a smaller area 200 km farther north (56°30'N,12°W),

a region where there is no topographic expression of the Feni

Drift. These waves are separated from the waves to the south

by a region of generally smooth, coherent echo return and by

a zone of hyperbolic echoes. The northern sediment waves are

Figure 3.3   Sub-bottom profiles of sediment waves (Area A).

a.   Surface-ship 3.5 kHz profile. Note strong
     echo return in trough of sediment wave.
     V.E = 2.4X

b.   Surface-ship 3.5 kHz profile. Detail of
     wave trough. V.E = 1X

c.   Near-bottom 4 kHz profile. Compare with
     profiles a, b. V.E. - 2X

d.   Near-bottom 4 kHz profile, not corrected
     for fish elevation for the same segment
     shown in profile c. Note regular thick-
     ening and thinning of layers over waves.

Scale bar is one kilometer. All profiles
from near 54°30'W, 15°15'N.
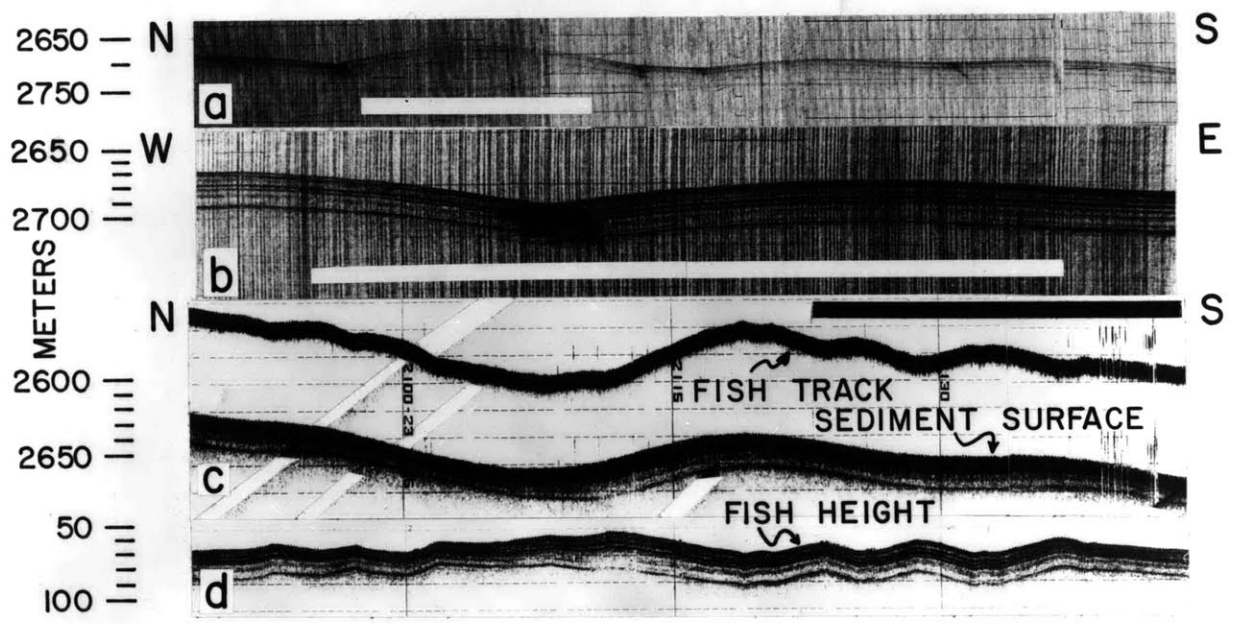
Figure 3.3

found in a patch extending in depth from 2200 m to 2400 m
at the northern end from 2400 m to 2600 m at the southern
end. These waves have wavelengths of about two kilometers
and heights of 5m to 30 m, and appear to have migrated to-
ward the north (Figure 3.4a).

In addition to these two large areas, several smaller
patches of waves were noted. An area of sediment waves
(56°N,11°W) is found on the eastern margin of Rockall Trough
extending in depth from 2520 m to 2710 m and situated between
the Barra and Donegal Fans. These waves are seen on the
only track passing through this region. Airgun records sug-
gest they have migrated to the east (upslope).

Small patches of sediment waves are present on the nose
of the sediment drift (52°45'N, 21°W)and on the small, south-
ward-trending spur (51°50'N,20°W)(Figure 3.1, 3.5). These
waves are generally of smaller height and wavelength than
those described from the main body of the Feni.

Sediment waves were not observed on any of the available
ship tracks crossing the Rockall Trough north of the Anton
Dohrn Seamount.

Near-bottom studies

Near-bottom investigations were undertaken with the deep
tow to determine the structure of the sediment waves in two
regions of the trough. One area (Profile A, figure 3.1)
crosses the Feni Drift at 54°50'N, while the other (Area 1,

Figure 3.4   Surface-ship 3.5 kHz profiles of Areas 1 and 2.

      a.   Area 1. Surface-ship 3.5 kHz records
          of Areas 1 and 2.

      b.   Area 2. Records courtesy of U. S.
          NAVOCEANO.

      Areas 1 and 2 are indexed on Figures 3.1 and
      3.12. V.E. = 16X

a. S   N

AREA 1

DEPTH (METERS)

2600 —

2700 —

0   5

KILOMETERS

b. S   N

AREA 2

2800 —

2900 —
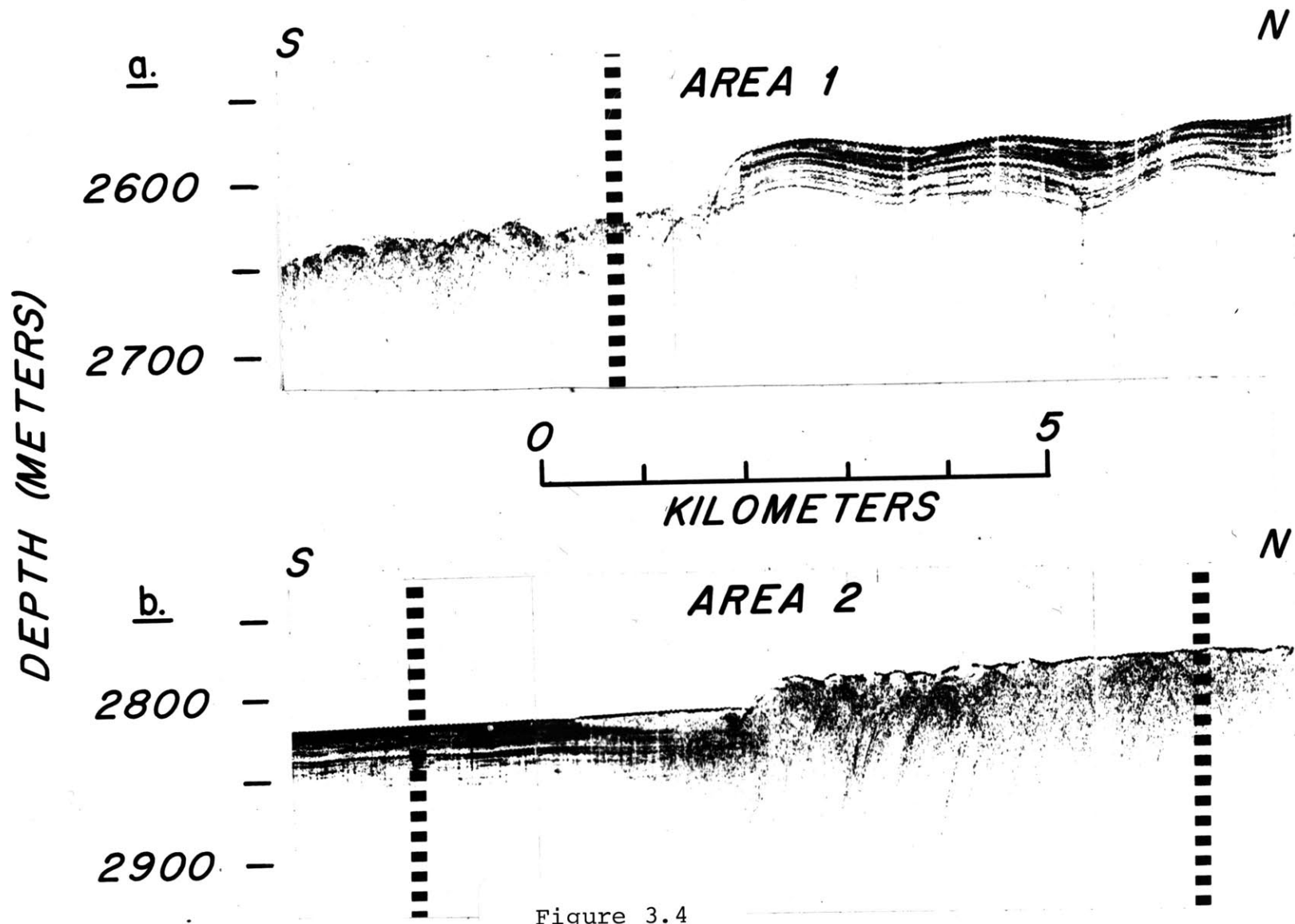
Figure 3.4

Figure 3.5   Surface-ship 3.5 kHz profile showing transition
                    between small sediment waves and hyperbolic
                    echoes. Profile indexed on Figure 3.1. Record
                    courtesy of U.S. NAVOCEANO. V.E. = 11X.
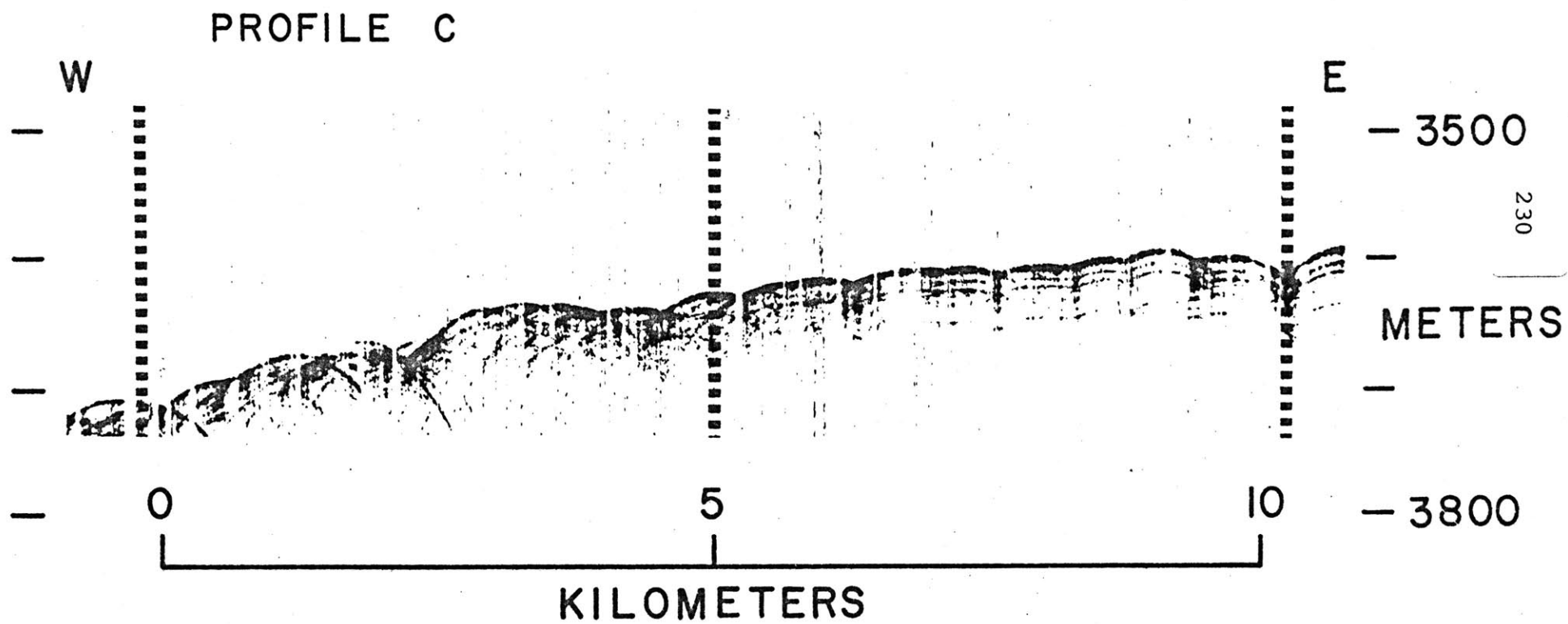
Figure 3.5

Figure 3.1) is at the southern limit of the northern area of sediment waves.

SOUTHERN WAVES (PROFILE A)

Investigation of the southern area of sediment waves was limited to a single long tow and no bottom transponders or current meters were deployed. This tow crossed the Feni Drift on a northwest - southeast line (Figure 3.1) and collected photographic, bathymetric and 4 kHz reflection data on the sediment waves. Lonsdale and Hollister (in press) have discussed some results from this crossing.

Sediment waves were observed with the deep tow on both the northwest and southeast flanks of the Feni. The waves present on the northwest flank are quite subdued, with heights of three to five meters and apparent wavelengths of about 700 m. Those on the southeast flank are more pronounced, with heights of 10 m to 20 m and apparent wavelengths of 1.5 to 2.5 km (Figure 3.3).

All of the layers observed by both the surface-ship 3.5 kHz echo sounder and the near-bottom 4 kHz sediment profiler display a thinning and thickening consistent with the upslope migration of the sediment waves. This indicates that the sediment waves have been actively migrating for the period of time sampled by this profile. By comparison with nearby sediment cores, Lonsdale and Hollister (in press) determined the deepest reflector observed on the near-bottom

profile is 660,000 years old, indicating that the waves have been active features since at least that time. Individual wave crests can be traced on surface-ship airgun profiles (see Lonsdale and Hollister, in press; Roberts, 1975) to a depth of 500 meters indicating that any given wave may have been active for the last 35 million years (Roberts, 1975).

Although the survey conducted was not detailed enough to establish an unambiguous trend for the sediment waves, some estimates can be made as to their orientation. Profiles made perpendicular to the regional contours (profiles NNW-SSW) indicate that the sediment waves are migrating toward the crest of the ridge. Profiles running parallel to the regional contours of the southeastern side of the ridge (profiles ENE-WSW) show sediment waves which are migrating toward the WSW, or downcurrent. The sediment waves must therefore trend roughly NE-SW, at an angle to the regional contours and to the currents, and migrate toward the northwest. D.G. Roberts (personal communication) has determined a similar orientation for these sediment waves using GLORIA, a large side-scan sonar unit operated from the surface (Rushby, 1970). In contrast to the sediment waves of the Blake-Bahama Outer Ridge (section II.B.1), these waves are migrating downcurrent.

Comparison between deeply-towed 4 kHz records and surface-ship 3.5 kHz records obtained in this area provides a good illustration of the distortion that can be encountered

(Figure 3.3). Although these records do not insonify the
same area of the sea floor, the sediment waves do not change
radically over a distance of several kilometers. These
sediment waves have S values of 0.5 to 1.5 (Appendix I).
The disagreements between the actual bathymetry and the
surface-ship echo trace are similar to those between the true
bathymetry and the echogram of Figures Al.3 c and d which
sought to model a migrating sediment wave.

NORTHERN WAVES (AREA 1)

   Area 1 is straddling the 30 m high step-like contact
between a zone of hyperbolic echoes and the northern zone of
sediment waves (Figure 3.4a). Hyperbolic echoes are on the
deep side of the step. The mud waves present on the north
side of the step show evidence of migration toward the
north. This survey consisted of 2.5 day lowering of the
deep-tow fish within a four-transponder net. Current meters
were deployed on three of the transponder moorings. The
two successful current meters showed average currents of 3
to 4 cm/sec toward 290° and strong tidal components (Figure
3.2). Three giant piston cores, five large-diameter cores,
and five free-fall cores were recovered from accurately
known locations (100 m radius) within this transponder net.

   A bathymetric map (Figure 3.6) of the survey area, con-
structed from transponder-navigated bathymetric profiles,
was contoured with the aid of data collected by the side-scan

Figure 3.6   Bathymetric map of sediment waves, scarp, and debris flow (Area 1). Areas of complex topography were contoured with the aid of side-scan sonar (Figure 3.7). Contour interval 10 m.

ROCKALL TROUGH SURVEY AREA 1
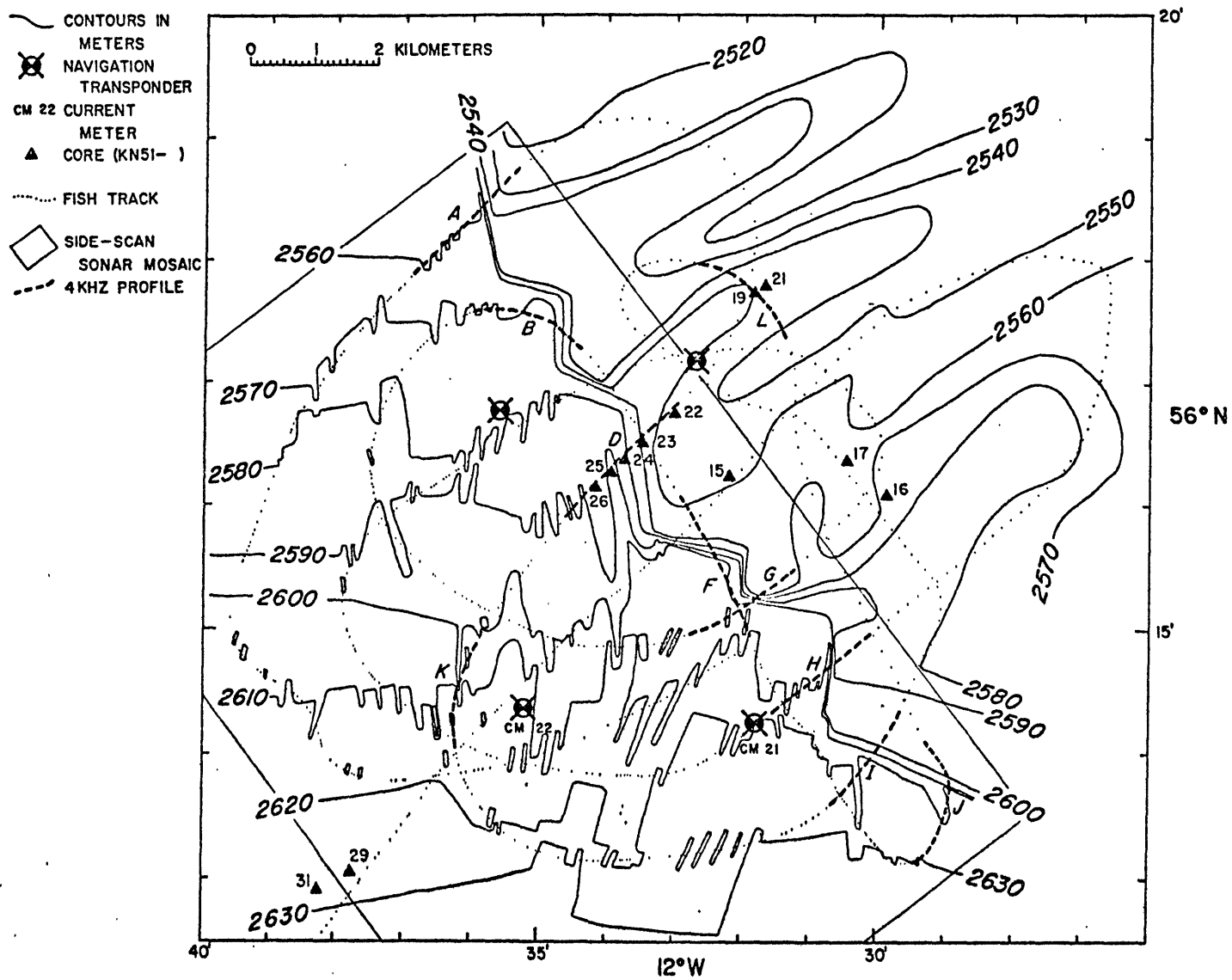
Figure 3.6

sonar units attached to the deep tow (Figure 3.7). These side-scan sonar data proved essential for a realistic bathymetric map.

The sediment waves developed on the northeast side of the scarp do not have the regular topographic expression observed in other areas where sediment waves have been mapped by similar methods (section II.B.1). Instead, the waves have a suprisingly complex topographic expression. Sub-bottom penetration records taken with the deep-tow's 4 kHz transducer (Figure 3.8) indicate that the complex topography can be accounted for by the recent preferential deposition of almost flat-lying, strong reflectors in the wave troughs, smoothing the wave topography. Deeper reflectors show sinusoidal sediment waves. Near-bottom 4 kHz and surface-ship 3.5 kHz sub-bottom profiles indicate that there has been preferential deposition on the northwest (upslope) sides of the wave crests during those time intervals when no preferential deposition was occurring in the wave troughs (Figure 3.4a and 3.8).

A contour map of the depth of the deepest observable reflector (reflector H, which can easily be followed throughout the survey area) shows that the sediment waves had a regular topographic expression at the time this reflector was deposited (Figure 3.9). Extrapolating sedimentation rates in KN51-19GPC gives an age of 400,000 years for reflector H. These relict waves trend at 060° but have heights of 5-30 m.

Figure 3.7   Side-scan sonar mosaic of rugged$_\wedge$topography
              debris-flow
              (Area 1).. Side-scan sonar records have
              been placed in their correct position relative
              to each other (at the correct scale, except
              no correction for slant range close to the fish)
              in order to give an accurate representation of
              the topographic expression present in the area.
              The portion of Area 1 which is included in this
              figure is shown on Figure 3.6. The scarp is
              indicated by the dotted line.

SIDE—SCAN SONAR MOSAIC
ROCKALL TROUGH SCARP SURVEY

⊗ NAVIGATION TRANSPONDER

0   1000   2000 M

56°12'N   12°35'W
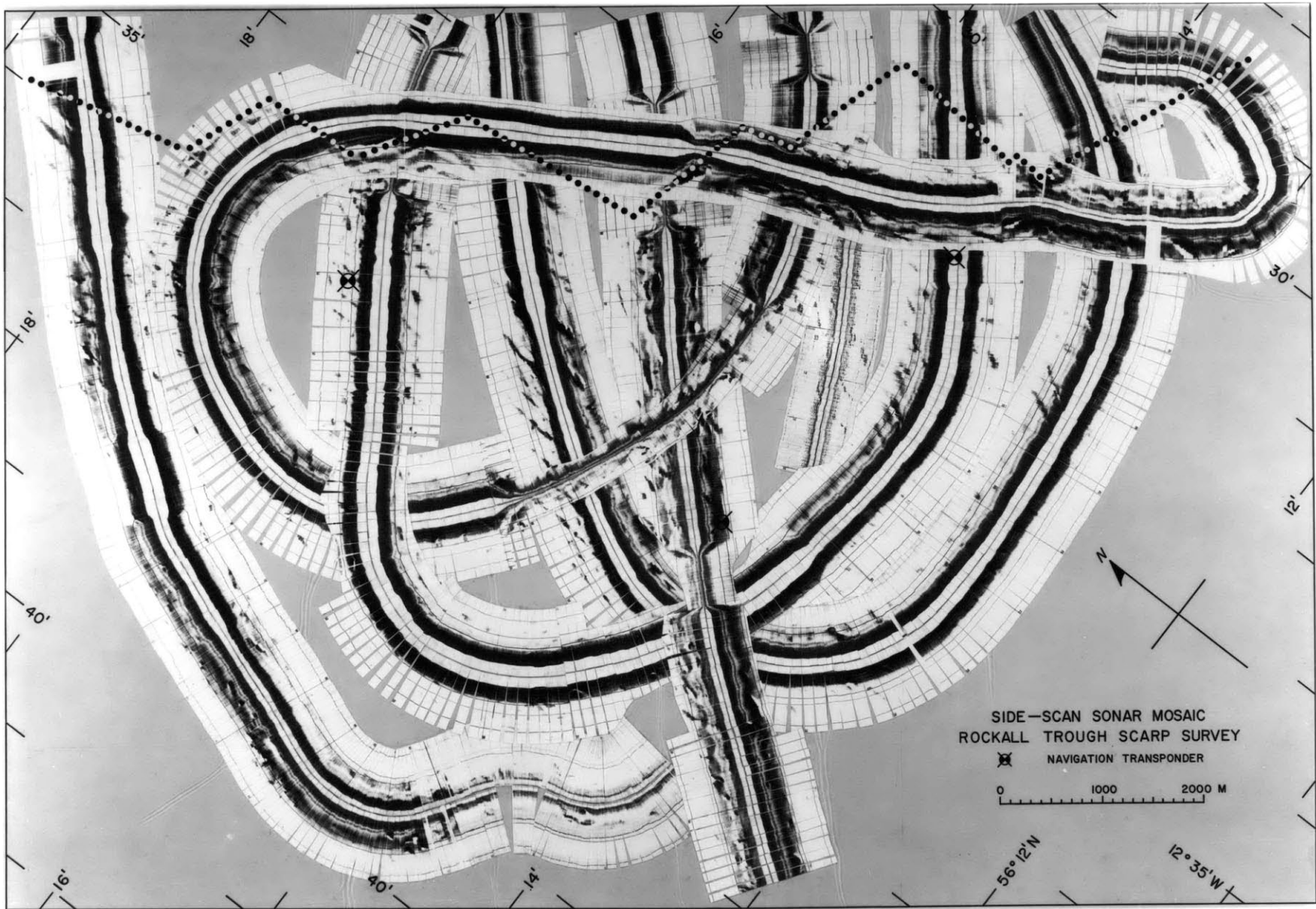
Figure 3.7

Figure 3.8   Near-bottom profile of sediment wave (Area 1).
               Profile indexed on Figure 3.6. The upper
               trace shows the record uncorrected for the
               height of the fish above the bottom while in
               the lower profile, the bottom return is cor-
               rected for the elevation of the fish. Arrows
               indicate the position of core KN 51-19 GPC and
               Reflector H.   (Compare with Figure 3.4a)
               V.E. = 4X

NW   SE

KN51—19GPC

4 KHZ RECORD
(NO DEPTH
CORRECTION)

REFLECTOR H

FISH DEPTH

0515   0530   0545

2550 m

4 KHZ RECORD
(DEPTH
CORRECTED)

2600 m

REFLECTOR H

O   I KILOMETER

Figure 3.8

240
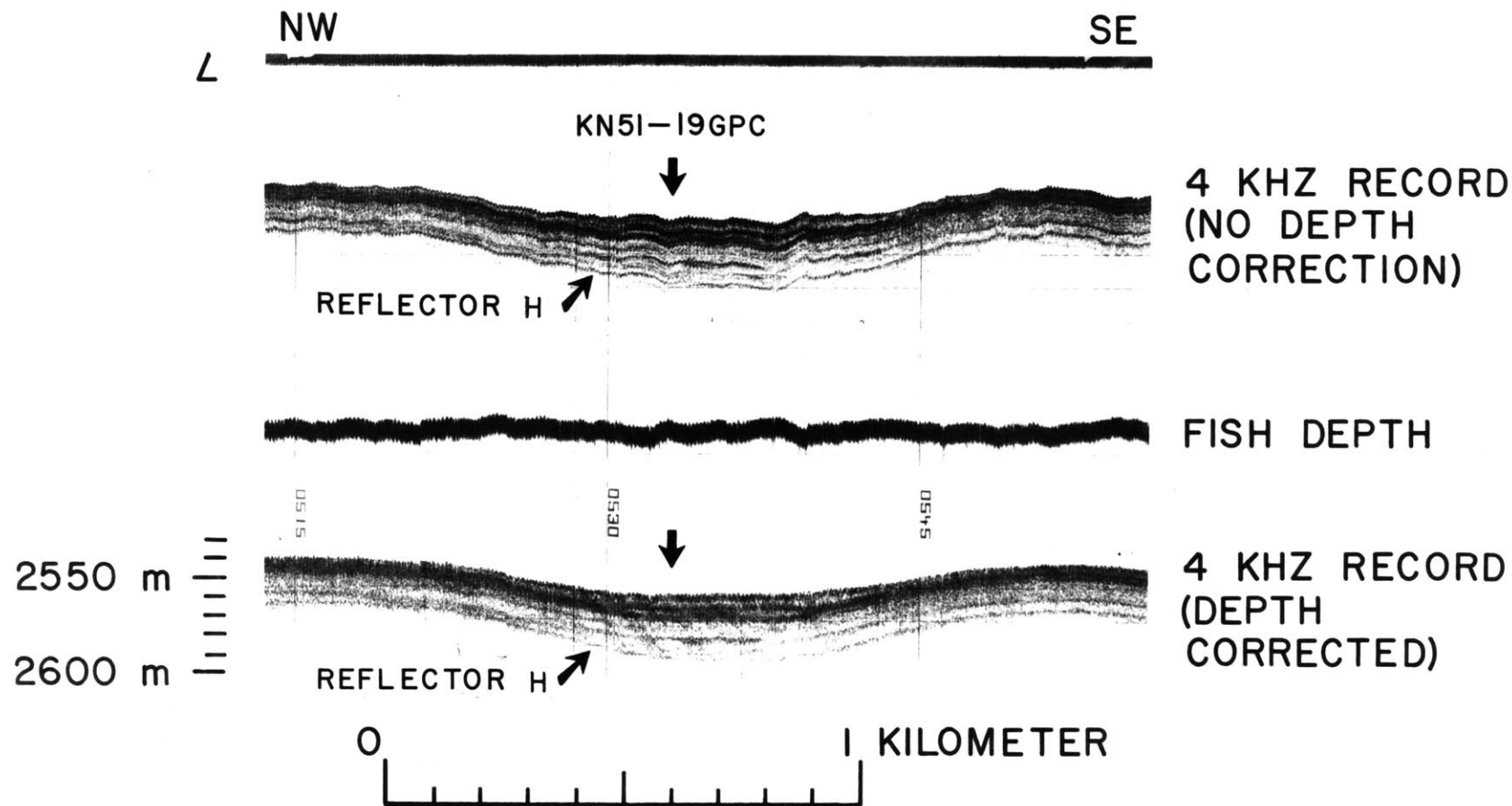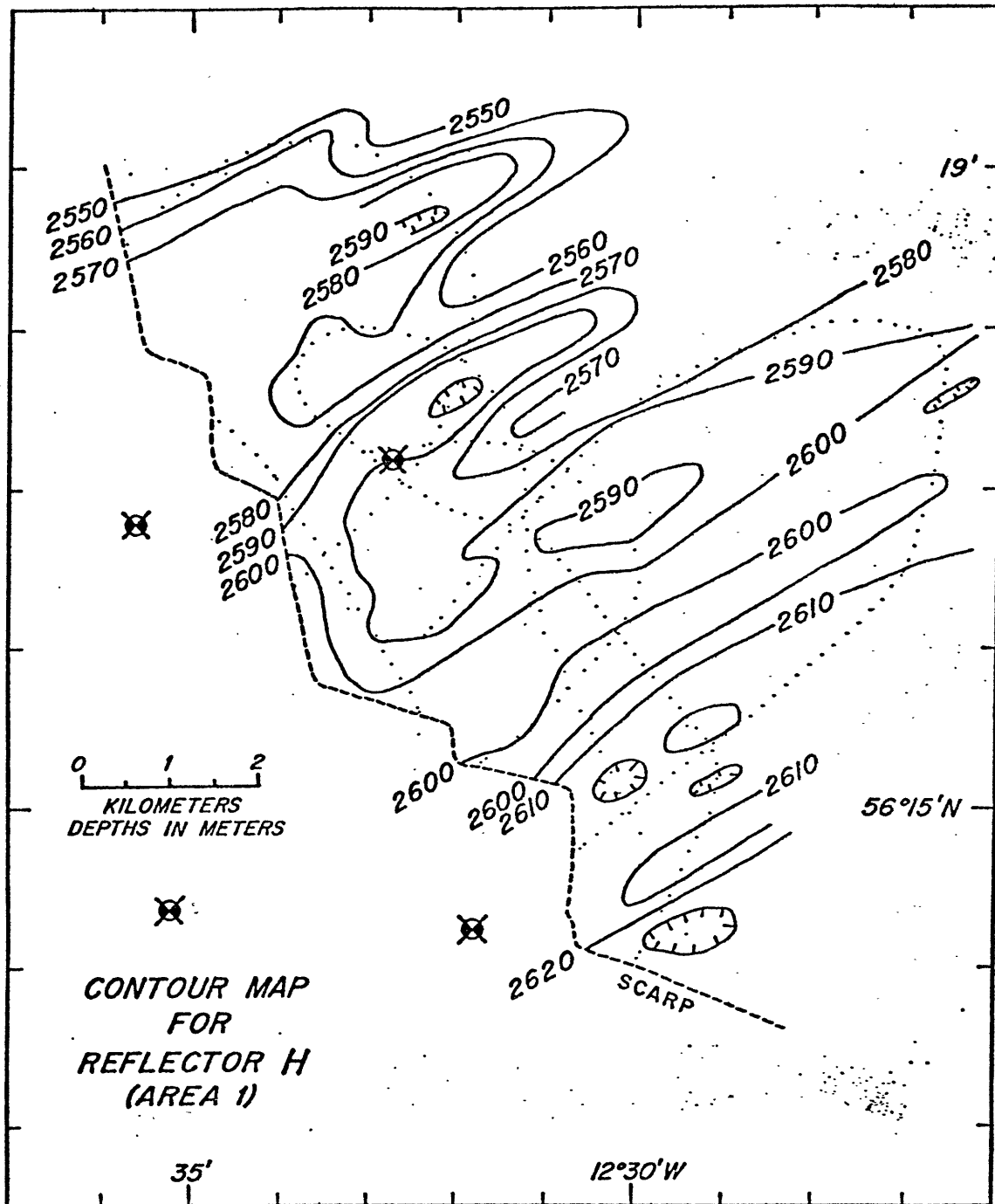
Figure 3.9

Figure 3.9   Contour map of reflector H. Regular sediment
waves are evident at this time (400,000 ybp);
compare with Figure 3.6.

When these wave trends are compared with the measured currents, the waves are migrating downstream; however, the waves are parallel to the trend of the sediment wave zone (Figure 3.1).

Relationship to circulation pattern

Previous studies of sediment waves have suggested that they are developed in regions of available sediment supply and steady bottom currents (e.g., Chapter II). The distribution of sediment waves in the Rockall Trough is consistent with the circulation patterns suggested for the trough and reflects the primary sources of sediment for the Feni Drift.

As Northeast Atlantic Deep Water flows northward along the base of Porcupine Bank at a depth of 2600 to 2950 m, it may erode sediments and transport them to the north (Lonsdale and Hollister, in press). Additional sediments may be injected into the bottom current by turbidity currents moving down canyons on the edge of Porcupine Bank or crossing the Donegal, Fan. After passing over the Donegal Fan, the current appears to lose some of its sediment and to construct the sediment waves observed between the Donegal and Barra Fans. The current then passes over the Barra Fan, picks up more sediments, and turns and crosses the trough to the western margin. As the current crosses the trough, more of the suspended load is deposited, creating the northern zone of sediment waves. These sediment waves have been inactive at times in the past, as preferential deposition has occurred in the troughs of the

waves. The field of sediment waves ends abruptly where it is truncated by a large field of hyperbolic echoes, a debris flow (described below).

As the current continues to the south, it joins with the southward flowing Norwegian Sea Overflow Water and gives rise to the complex circulation pattern which has developed the Feni Drift (Lonsdale and Hollister, in press), here existing as a ridge separate from the western margin of the Rockall Trough. These waves have been active for most of the last 660,000 years.

C. HYPERBOLIC ECHOES

Distribution

Hyperbolic echoes were observed concentrated in three major areas of Rockall Trough, as well as in several scattered patches (Figure 3.1). Hyperbolic echoes were not found developed on any of the sediment waves observed.

Hyperbolic echoes are characteristic of several zones at the nose of the Feni Drift (Figures 3.1, 3.5, 3.10), where a deeper sedimentary ridge strikes due south (Johnson et al., 1971). Three zones of hyperbolic echoes, elongated parallel to the contours, are seen in this area. Two of the zones (51°-52°N,21°W and 51°-52°N,19°W), which may be part of the same large area, extend from a depth of 3650 m to 4520 m on the eastern and western sides of the ridge. A third zone, located

Figure 3.10   Hyperbolic echoes on west flank of Feni
Drift. Sub-bottom profile (3.5 kHz)
indexed on Figure 3.1. Record courtesy
of U.S. NAVOCEANO. V.E. = 13x

PROFILE D
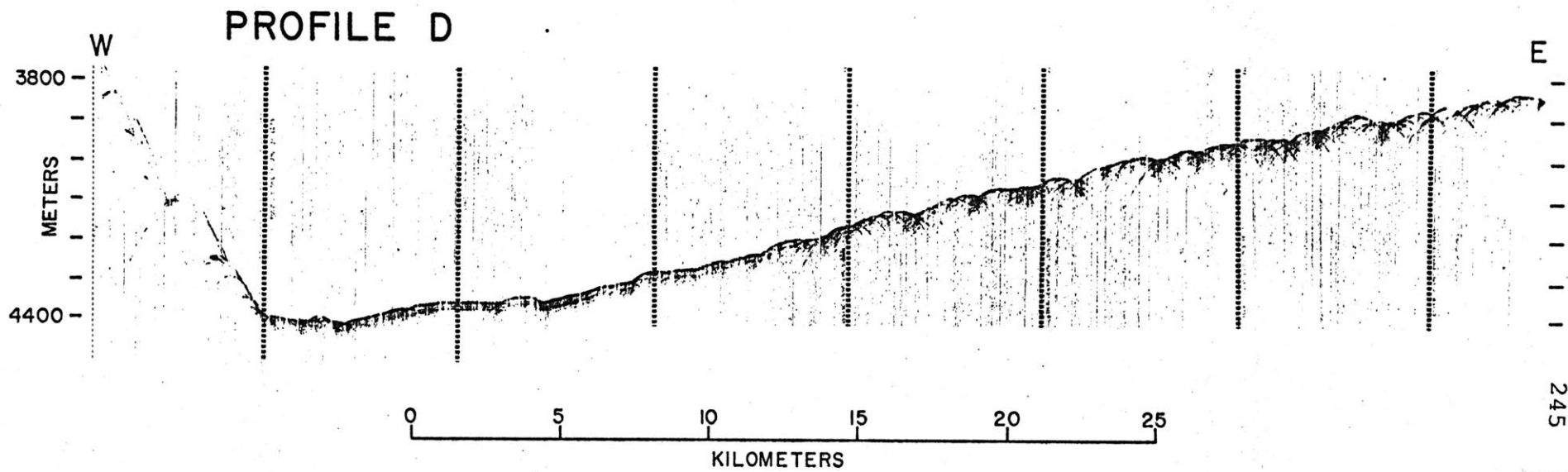
Figure 3.10

on the western flank of the Feni Drift after the drift takes

a 90° turn to the north (53°N,21°W), ranges in depth from

2805 m to 3750 m. These hyperbolic echoes appear quite

similar in character to those observed in regions of the Blake-

Bahama Outer Ridge, where furrows have been mapped on the sea

floor (Chapter II). The zones of hyperbolic echoes trend

parallel to the regional contours and the linear features

responsible for the hyperbolic echoes also appear to trend

parallel to the contours. These hyperbolic echoes may indi-

cate a region of current-controlled topography, or bed forms,

like the furrows. Unfortunately, no near-bottom investigations

were made in this region. The current system that may have

been responsible for these features is as yet unknown.

The deeper parts of the Barra Fan and the Donegal Fan are

characterized by many zones of hyperbolic echoes as well as

a complex echo character in general. Ship tracks were too

widely spaced in these regions to delineate the zones of

hyperbolic echoes.

A zone of hyperbolic echoes cuts across the Feni Drift

in the vicinity of 56°N, 13°W, abruptly terminating a field

of sediment waves (Figures 3.1, 3.4a). These hyperbolic

echoes (Figure 3.11) are more irregular in character than

those resulting from current-produced furrows on the Blake-

Bahama Outer Ridge and are similar to the hyperbolic echoes

found in regions which have been affected by sediment slumps

and slides and resulting debris flows (e.g., Embley, 1976).

Figure 3.11   Hyperbolic echoes in debris flow zone.
               Surface-ship 3.5 kHz profile courtesy
               of U.S. NAVOCEANO. Profile located in
               Figure 3.12. V.E. = 20X

PROFILE E

S

N

2650 m —

—1420 fm

2700 m —

2750 m —

—1460 fm

0   5 KM

248
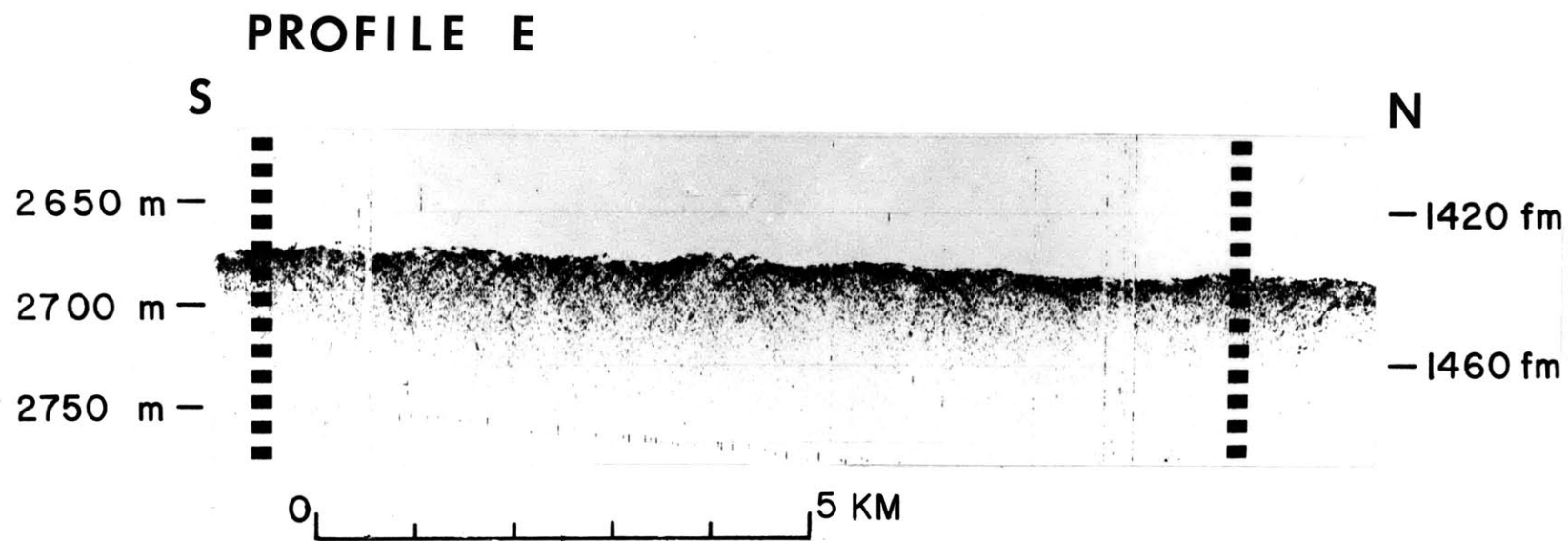
Figure 3.11

These hyperbolic echoes show several features which distinguish them from those related to current-produced furrows. The hyperbolic echoes are not all similar in form, but have different slopes on the flanks of adjacent echoes indicating that the bottom features are not parallel to each other (Appendix I). Near-bottom investigations show these features are generally elongated perpendicular to the contours, as is the entire zone of hyperbolic echoes. There are also variations in the character of the returned echo from different parts of the zone (e.g., hyperbolic echoes of Figure 3.4a and 3.4b) indicating that the nature of the bottom topography also varies over this zone. Detailed investigations show that this region is covered by a large debris flow.

The zone of hyperbolic echoes is located directly downslope from the southern end of a series of slump blocks on the eastern margin of Rockall Bank (Roberts, 1972) (Figure 3.12). The contacts between this area of hyperbolic echoes and the surrounding echo types are often quite abrupt and in the form of a step-like change in echo character (Figure 3.4a and 3.4b). Several zones within the flow area show undeformed sediments with a normal echo return. These changes in echo character within the slide are also often associated with step-like changes in depth.

Surface-ship 3.5 kHz echo-sounding records do not record the base of the debris flow deposit. Airgun records, while indicating the presence of a rough surface within the slide

Figure 3.12   Detailed map of debris flow area. Contours
(in corrected fathoms) are from Roberts(1975)
and indicate that sediments have been removed
at depths shallower than 1400 fm (roughly
2600 m) and deposited at depths greater than
1400 fm.
(1 fathom = 1.8288 meters)

SURFACE SHIP ECHO RETURN

∿∿∿∿ HYPERBOLIC

∿∿ WAVY

── FLAT

★ CORE (NOT IN SURVEY AREA)

SLUMP SCAR OF
ROBERTS, 1972

OUTLINE OF HYPERBOLIC
ECHO REGION (DEBRIS FLOW)

DEEP TOW SURVEY AREA
AND KN51 CORES

BATHYMETRY FROM
ROBERTS, 1975.
DEPTHS IN·
CORRECTED FATHOMS
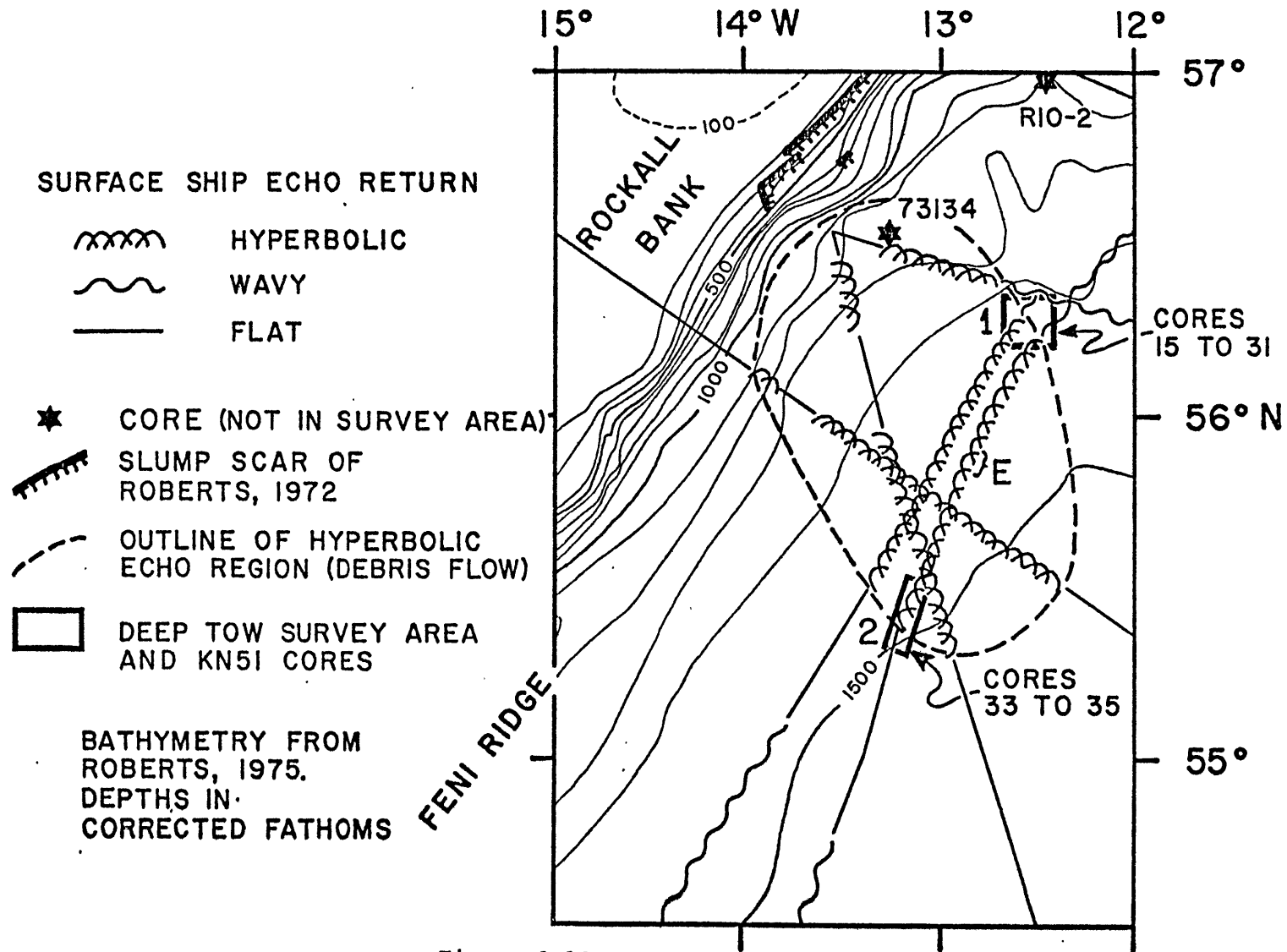
Figure 3.12

area, do not show signs of sediment deformation within the deeper sediments. Any deformation present occurs within the section of the record obscured by the bubble pulse. Thus, the deformed sediments appear to be 20 to 100 m thick.

This debris flow and associated turbidity currents (described below) were formed by the rotational slumps described by Roberts (1972). These gravitational flows probably formed when sediment slumps entrained water at the foot of the 2-4° slope of the Rockall Bank. These flows continued across the Feni Drift with the debris flow crossing the entire 100 km width of the drift (regional slopes 0.2-1.5°), obliterating a field of sediment waves which decorated the drift in this area. Internal layering associated with these sediment waves can sometimes be observed beneath the debris flow on airgun records.

This submarine flow is quite similar to those studied in other areas (e.g., Normark, 1974; Embley, 1975, 1976; and Jacobi, 1977). The following morphological features were noted in those studies. First, the upper part of the sediment flow is ringed by a pronounced sedimentary scarp or series of scarps up to 50 or more meters high. The scarp is often quite irregular along its trend. Second, the deeper side of the scarp often shows hyperbolic echoes on surface-ship echo sounders, indicating the presence of relief below the limit of resolution of the echo sounder. In some cases, flat-lying reflectors are observed underlying these hyperbolic echoes

(e.g. Embley, 1975); however, in many cases no layering is observed (Figure 3.11) possibly indicating the presence of disturbed sediments. Third, the deeper, depositional portions of the flow surface often are characterized by the presence of "hummocky topography", an echo return indicating the presence of subdued irregular relief on the sea floor. And fourth, wedges of acoustically transparent sediments often extend from or make up, the down-slope end of the flow.

The terminology used in this report is as follows: A slide is a slope failure where there is finite shear along a slip plane but with little internal deformation of the slide mass. In a flow no slip plane is present and movement takes place by the continuous deformation of the sediments (Dott, 1963; Sharpe, 1968; Carter, 1975). A slump is a slide where rotational movement has occurred along the slip plane (Dott, 1963).

The term debris flow is used following Carter (1975), to indicate the movement of a fine-grained slurry which contains an appreciable number of clasts suspended by a viscous flow mechanism. These clasts can range in size from pebbles (centimeters) to large blocks (tens to hundreds of meters). These sediment flows can also be termed olistostromes. Olistoliths are inclusions greater than 4 meters (Abbate et al., 1970).

Viscous flows, such as debris flows, are characterized by

poor sorting with large clasts supported by a mud or sand matrix. These flows often have irregular tops with large clasts protruding from both the flow and the deposit (Middleton and Hampton, 1973; Carter, 1975).

Near-bottom studies of the debris flow

Near-bottom studies were undertaken in two areas of the debris flow (Figures 3.1, 3.12). Study Area 1 is located at the contact between the debris flow and the northern area of sediment waves and study Area 2 is located on the southern margin of the debris flow.

EROSIONAL SCARP (AREA 1)

The most prominent feature of this study area (56°16'N, 12°33'W, 2570m) is the 30 m scarp which cuts through the area and separates the sediment waves from the debris flow (hyperbolic echoes) (Figure 3.4a).

The scarp, mapped on the basis of both bathymetric and side-scan sonar data (Figures 3.6 and 3.7), has an overall strike of 325° for the 13 km interval within Area 1. This scarp can be resolved into a series of shorter segments of one to two kilometers in length which intersect at angles of roughly 110°. These smaller scarp sections trend either 350° to 005° or 280° to 290°. There is a possible correlation between the areas where the scarp has cut back farther and the troughs of the relict waves (Figure 3.9). Deep-tow 4 kHz sub-bottom

profiles (Figures 3.13 and 3.14) show that the scarp is quite abrupt, with laminated sediments cropping out on the scarp. The true shape of the scarp may be obscured by the presence of side echoes. The sediments on the deeper side of the scarp has a blocky appearance with some of the blocks faulted (Figure 3.13). The sediments in between the blocks show few coherent reflections. The depth of penetration of the 3.5 or 4 kHz profiles is not adequate to determine if there are deeper reflectors which cross the scarp zone undisturbed. Available airgun reflection profiles show no deformation of the sediments greater than 100 m deep across this boundary. The scarp is quite variable in form, ranging from a steep (Figure 3.14, profiles A, G, H, J) to a more gradual transition (Figure 3.14, profiles B, I). Profiles D and F also show the development of a series of steps. Many of the profiles show evidence of some erosion of the laminated sediments at a distance of up to 1 km from the scarp.

The surface-ship hyperbolic echoes found on the southwest side of the scarp are caused by a number of short (up to a few km long) ridges and blocks (widths of 100 m and heights of 10-20 m). These ridges and blocks trend roughly perpendicular to the regional contours (Figure 3.6 and 3.7). This area is characterized by a jumbled sub-bottom return, with the only coherent reflectors observed when a ridge or block of sediment is crossed (Figure 3.15). Deeper reflectors are sometimes seen in the areas between the blocks, but often have

Figure 3.13   Near-bottom 4 kHz profile over erosional
scarp (Area 1). See caption for Figure
3.8 for an explanation of this figure.
Several large blocks of undeformed sedi-
ments can be seen at the base of the scarp,
one of which is faulted. Compare with
Figure 3.4a. Profile indexed on Figure
3.6. V.E. = 4X

A

4 KHZ RECORD (NO DEPTH CORRECTION)

FISH DEPTH

2520 m

2570 m

4 KHZ RECORD (DEPTH CORRECTED)

0   1 KILOMETER
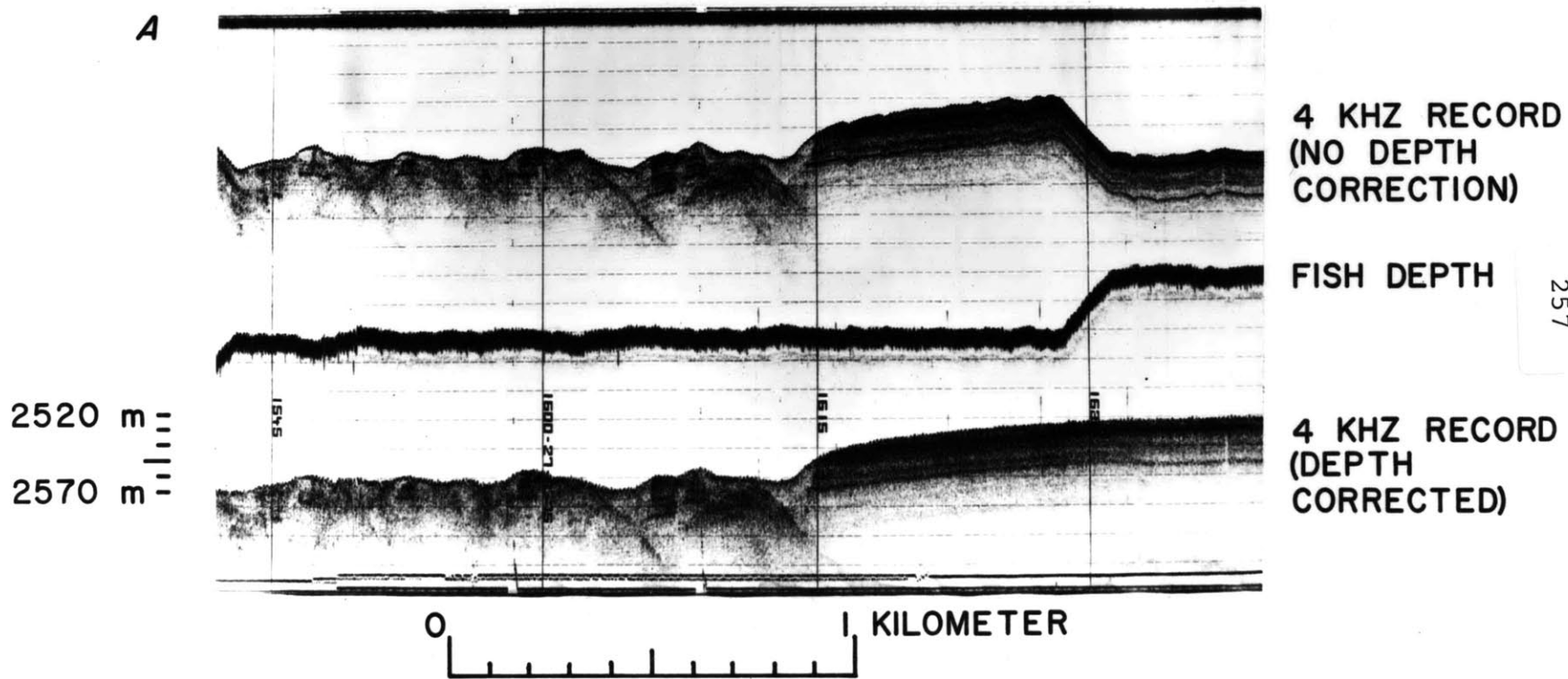
Figure 3.13

Figure 3.14   More near-bottom 4 kHz profiles over scarp,
               Area 1. Deep-tow   profiles A-J (profiles
               C and E not shown) indexed on Figure 3.6.
               Profiles shown are corrected for the depth
               of the deep-tow fish. The form of the scarp
               changes significantly from crossing to
               crossing. V.E. = 4X
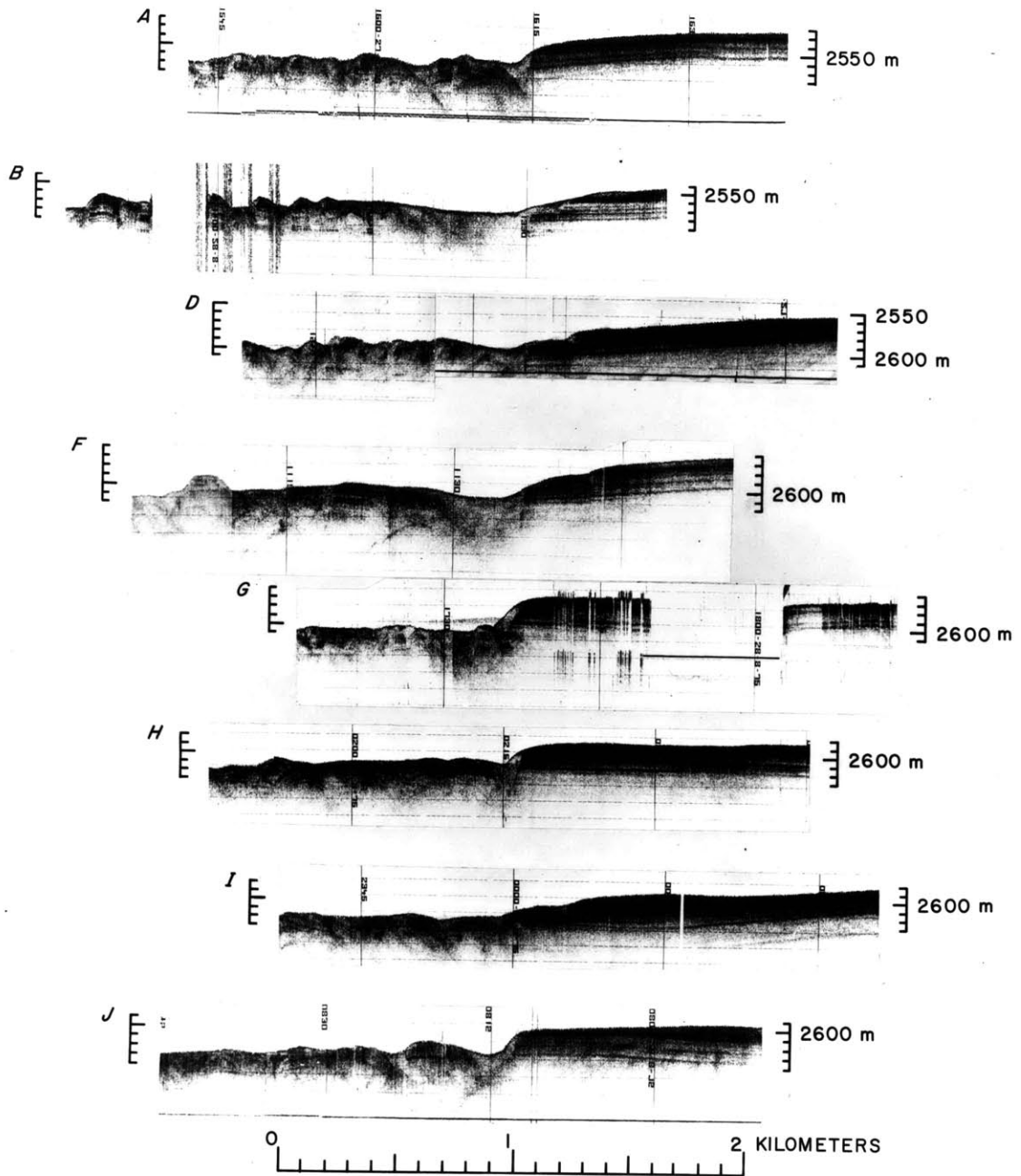
Figure 3.14

Figure 3.15   Near-bottom profile of debris flow surface
(Area 1). Profile K indexed on Figure 3.6.
See caption to Figure 3.8 for an explanation
of the figure. Discrete layers are observed
only beneath the blocks of sediment. Areas
in between the blocks often show steeply-
dipping reflections, which may either be de-
formed sediments or side echoes.

K

4 KHZ RECORD
(NO DEPTH
CORRECTION)

FISH DEPTH

2590 m

2620 m

4 KHZ RECORD
(DEPTH
CORRECTED)

0   1 KILOMETER
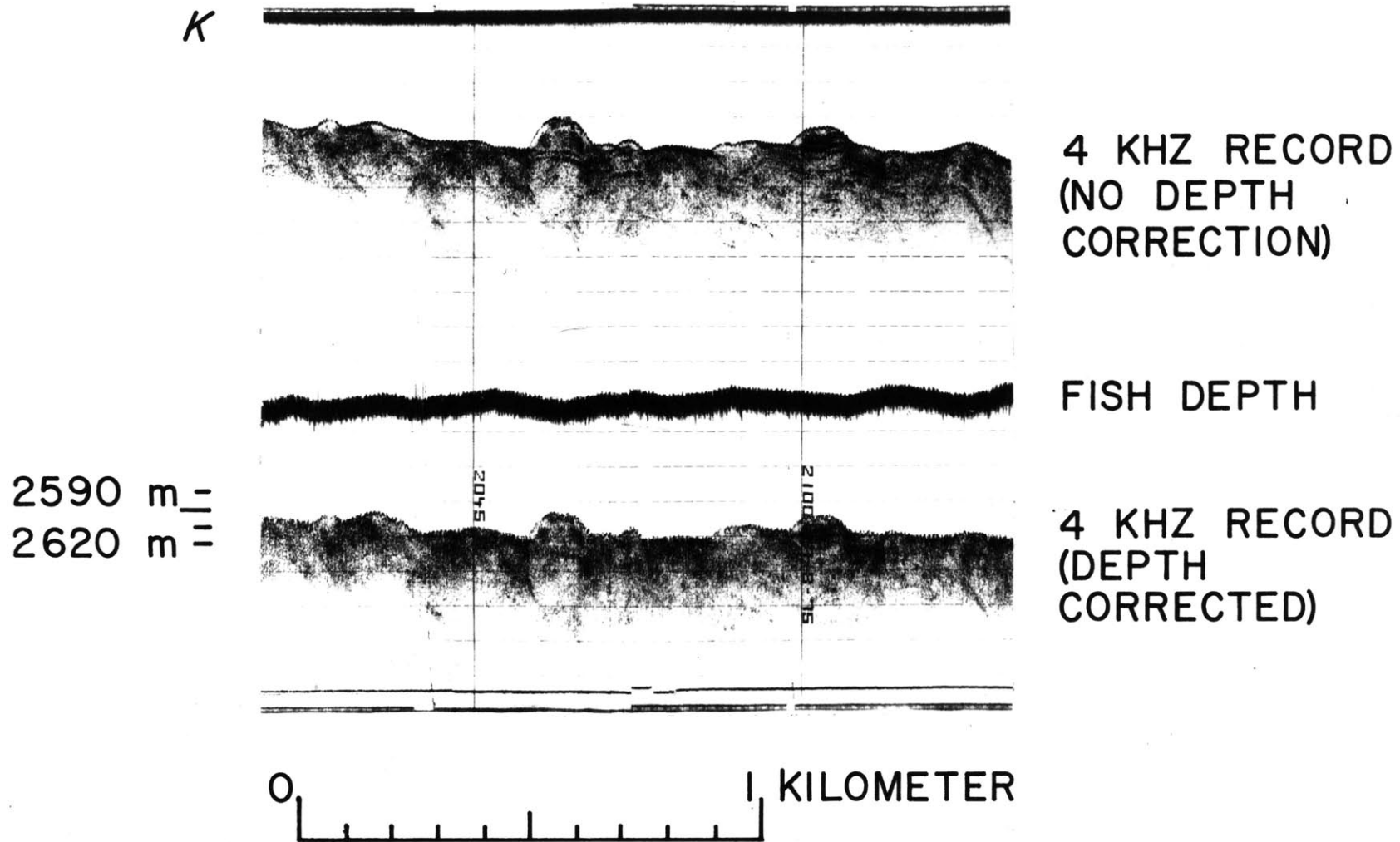
Figure 3.15

large dips or appear to be side echoes. Cores from this region show calcareous sand layers (up to 30 cm thick), which may also limit sound penetration.

Different types of blocks are found in different parts of the debris flow (Figure 3.7). Near the base of the scarp (up to a distance of 2 km), blocks exhibit only a slight north-south orientation (perpendicular to the contours). The shape of these blocks is variable. At a distance of 2 km to 4 km from the scarp, the blocks show a preferred orientation, and parallel ridges strike north-south. These ridges are generally less than 2 km in length and have regular spacings of a few hundred meters. At the outer edge of the survey area, some 5 km from the scarp, only small isolated blocks are seen. These blocks have no preferred orientation. A single long tow extending 8 km away from the scarp suggests that these blocks become less common as distance from the scarp increases. The blocks are mostly buried in this region. Other than the sediment blocks and the scarp, little relief was observed by the side-scan sonar in this survey area. Bottom photographs also showed little sign of activity other than the general evidence of current smoothing and biological activity (Lonsdale and Hollister, in press). A few photographs taken on the sides of particularly steep blocks and near the scarp showed sediments with outcropping sedimentary layers (Figure 3.16). Sessile organisms are often seen on

Figure 3.16   Bottom photographs from debris flow and
scarp, (Area 1).

A.   Ridge on top of debris flow (56°15'N,
12°35'W, 2600 m)

B.   Outcropping layers and organisms on the
scarp (56°17'N,12°34.5'W, 2570 m)

Scale bar is one meter.
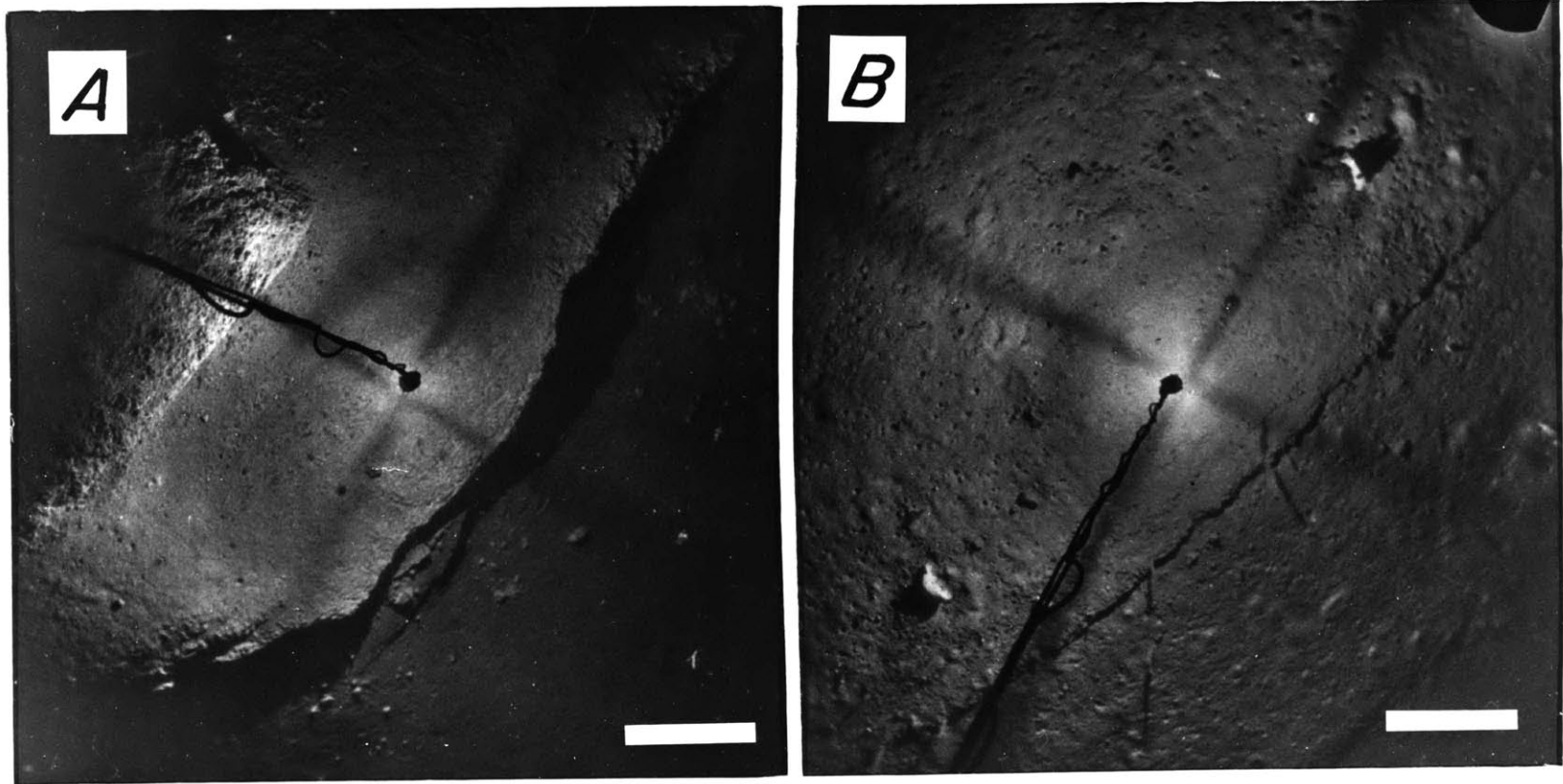
Figure 3.16

these slopes (Figure 3.16b) and may be important in making

sediments available for downslope movement or current re-

moval. Although photographs showed no evidence of sediment

deformation similar to that observed by Embley (1976) for a

debris flow off Northwest Africa, some possible recent de-

formation is observed (Figure 3.16a, lower center). The

smooth sea floor suggests that much of the original relief

has been masked by the deposition of a blanket of sediments

over this area. Sediment studies (described below) confirm

this observation.

DEPOSITIONAL NOSE (AREA2)

A second deep-tow lowering was at the southern margin

of the zone of hyperbolic echoes (55°24'N,13°12'W, 2790 m).

At this contact the echo changes from hyperbolic to coherent

with laminations. These echo types are separated by a 15 m

scarp and a small lens of transparent sediment (Figure 3.4b).

No transponders or current meters were deployed for this 10

hour survey and three large-diameter gravity cores were re-

covered.

Near-bottom investigations in this area were limited to

a single 13 km long pass starting 7 km north of the scarp. The

deep-tow 4 kHz record obtained over this scarp (Figure 3.17)

reveals that the transition is more gradual than indicated on

surface-ship records, extending over a distance of 1.5 km.

The hyperbolic echoes are caused by several 5 m high smooth

Figure 3.17   Near-bottom profile of debris flow nose
(Area 2). Profile indexed on Figures 3.1 and
3.12. See caption to Figure 8 for an
explanation of the figure. The ridges
in this area appear to be due to folded
or faulted blocks of sediment rather than
to blocks of undeformed sediments. Trans-
parent sediments can be seen covering much
of the relief of the area. (Compare with
Figure 3.4). V.E. = 6X
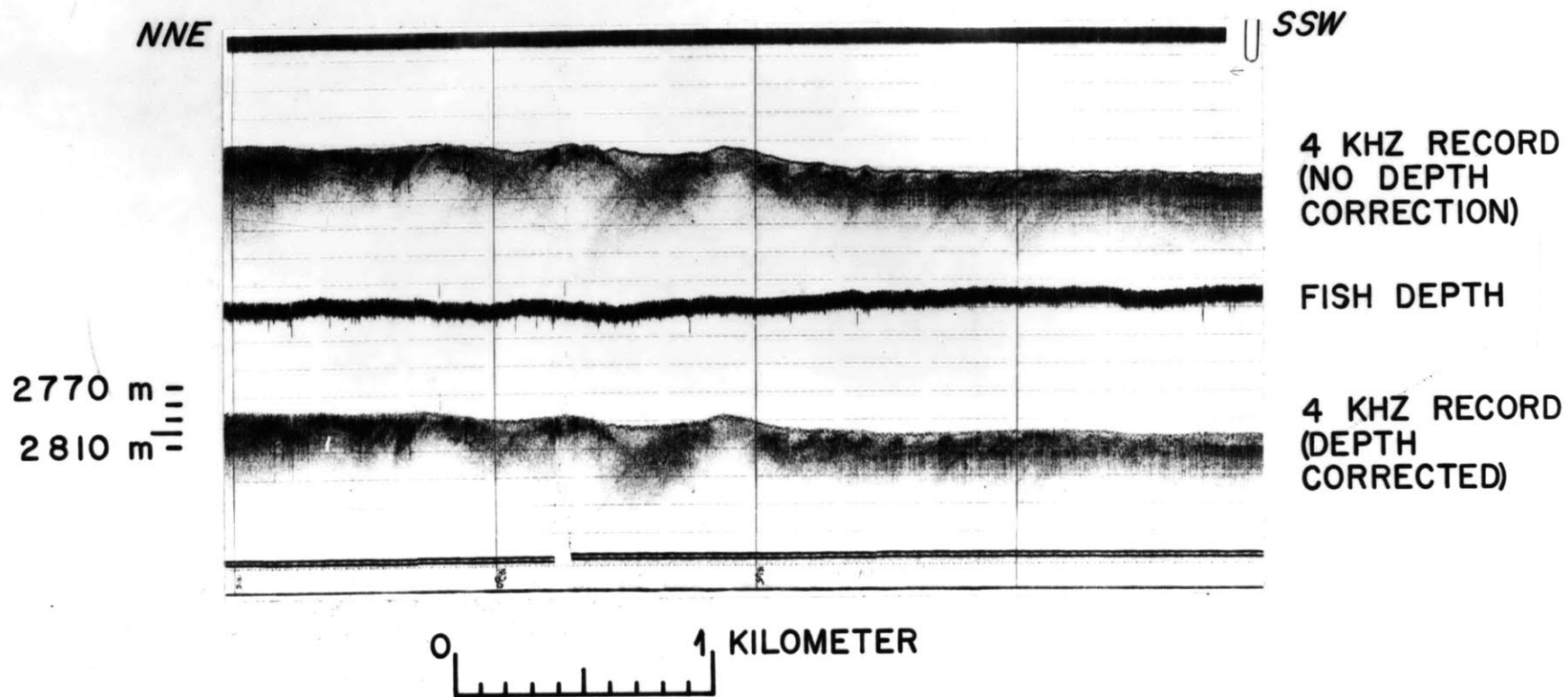
Figure 3.17

ridges near the scarp. Side-scan sonar indicates that the
southernmost ridge strikes 330°. These ridges appear to be
formed by disturbed (possibly folded) sediments at the toe
of the debris-flow deposit, contrasting with the blocks of
undisturbed sediments which form the ridges in Area 1. Some
smaller-scale relief had been developed in the 1.5 km south
of the southernmost ridge (Figure 3.17) but subsequent depo-
sition has smoothed the present sediment surface. The 4 kHz
record indicates that the transparent sediments, clearly seen
on the surface-ship 3.5 kHz record (Figure 3.4b), are overlain
by the same thin layer (<3m) which covers the rough topography
directly to the north (Figure 3.17), suggesting that the
transparent sediments are the same age as the rough debris-
flow nose to the north. The laminated sediments continue
north under the smaller-scale relief for a distance of 1.25
km. Bottom photographs and side-scan sonar show that the
bottom is quite smooth along the entire traverse, with little
surface expression of sediment deformation. The sharp acousti-
cal contrast between the flow and the overlying sediments is
due to a pronounced density (water content) difference between
these two units (described below).

D. SEDIMENT STUDIES

Cores recovered from in and around the Rockall Trough
study areas permit dates to be assigned to major sedimentary
events. These events are the time interval in which preferential

deposition occurred in the sediment wave troughs and the time

of slumping and debris flows on the western margin of Rockall

Plateau (Roberts, 1972). The positions of these cores are

given in Table 3.1 and indicated on Figures 3.1, 3.6 and 3.12.

Sediment waves

Only one good core (KN51-11GC) was recovered from the

southern zone of sediment waves. These waves are developed in

cohesive sediments.

Cores KN51-17 GPC and KN51-19 GPC (Figure 3.18) were re-

covered from adjacent sediment wave troughs in the northern

zone of sediment waves (Area 1). Comparisons between nearby

4 kHz records and cores KN51-17 GPC and 19 GPC indicate that

the thick sequences of gray lutite with abundant silt layers

correspond quite closely to the sub-bottom reflectors deposited

preferentially in the wave troughs (Figure 3.8) (Silva, et al.,

in preparation). KN51-17 GPC has a zone of high carbonate

at its base which may correspond to a prominent reflector fol-

lowing the general shape of the wave and marking a time when

preferential deposition was not occurring in the wave troughs.

KN51-19 GPC did not penetrate into this deeper reflector and

does not show the increase in carbonate at depth.

Carbonate curves of KN51-17 GPC and KN51-19 GPC are

similar to that of core RC9-225, recovered from 250 km to the

southwest on the Feni Drift (McIntyre et al., 1972; Ruddiman

and McIntyre, 1973). The carbonate content decreases from

TABLE 3.1
CORES IN ROCKALL TROUGH STUDY AREAS

CORE #	LAT. (N)	LONG. (W)	SURVEY AREA	LOW m. WATER DEPTH	UNDISTURBED LENGTH (cm)	Depth of Carbonate Change (13,400y)	Sed. Rate (cm/10^3 y) (0-13,400 y)	Depth of Top of Gravity Flow Deposit (cm)	Age of Top of Deposit (ypb)	Depth of 73,000 y Coccolith Event	Sed. Rate (cm/10^3 y) (13,400-73,000 y)
KN51-11GC	54°28.4	15°14.8	A, waves	2680	270	65	3.9	--		--	
15GC	56°16.2	12°32.2	1, waves	2554	45	>35	> 2.6	--		--	
16GC	56°16.1	12°29.9	1, waves	2572	160	45	3.4	90		--	
17GPC	56°16.4	12°30.5	1, waves	2565	1001	60	4.5	87	15,200	950	14.9
19GPC	56°17.7	12°31.9	1, waves	2560	1136	52	3.7	93	>15,600	>1140	>18.3
21GC	56°17.8	12°31.7	1, waves	2557	275	55	4.1	155		--	
22FF	56°16.7	12°33.0	1, waves	2557	84	22	1.6	n.d.		--	
23FF	56°16.5	12°33.5	1, scarp	2570	87	15	1.1	2.8		--	
24FF	56°16.4	12°33.8	1, scarp	2582	86	35	2.6	65		--	
25FF	56°16.3	12°38.9	1, scarp	2596	90	35	2.6	70		--	
26FF	56°16.2	12°34.3	1, flow	2583	50	>50	> 3.8	--		--	
29GC	56°13.1	12°37.7	1, flow	2626	263	100	7.5	180		--	
31PC	56°12.9	12°38.2	1, flow	2619	122	>122	> 9.1	--		--	
31GPC	56°12.9	12°38.2	1, flow	2619	323	n.d.		0		265	
33GC	55°22.6	13°13.0	2, lam.	2813	144	130	9.7	--		--	
34GC	55°24.4	13°12.2	2, flow	2805	264	107	8.0	175		--	
35GC	55°26.6	13°11.4	2, flow	2783	212	51	3.8	107		--	
V28-72	57°44'	11°35'	base of Rockall	1772	442	~39	2.9	257		--	
R10-2	56°59'	12°28'	Bank debris	2305	185	~25	1.9	32		--	
73134	56°31.3	13°15.1	flow	2300	630	~175	13.0	280		--	

n.d. = event not detected in core

--- = core did not penetrate far enough to recover this horizon

Figure 3.18   Lithologic description and carbonate curves
(KN51-17 GPC, 19 GPC and 31 GPC(Area 1)).
Tie-lines connect events of similar age.
Horizontal reflectors found in the wave
troughs (Figure 3.8) correspond to a zone of
abundant silt layers at a depth of about 800
cm in 19 GPC.   Squares along 19 GPC are inter-
vals dated by C^{14} (Table 3.2).
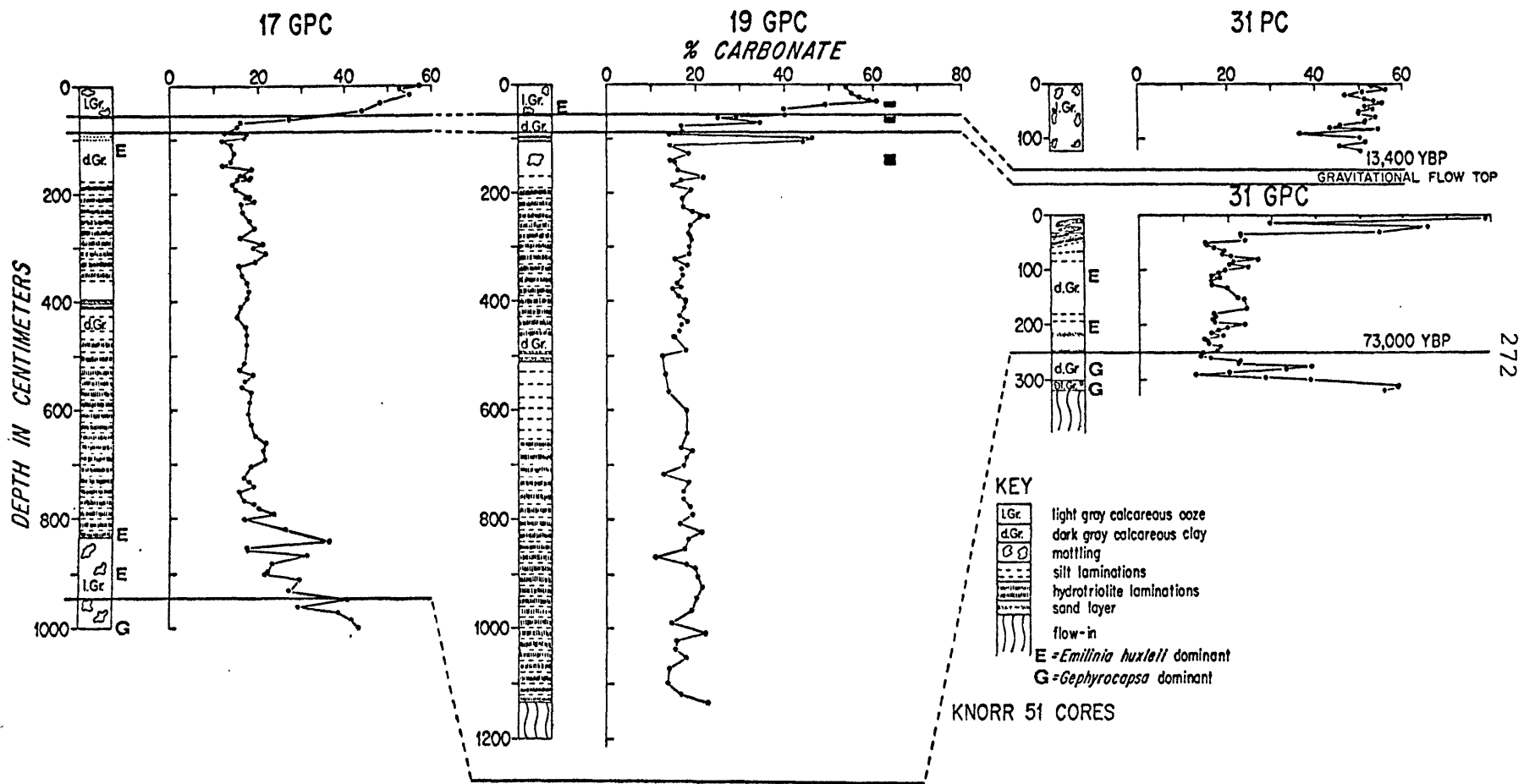
Figure 3.18

55-60% at the top of the core to 15-20% at depth. At depths
greater than 8 m in KN51-17 GPC, higher carbonate values (50%)
are encountered again. Ruddiman and McIntyre (1973) indicate
that the change from high to low carbonate sediment in the
upper parts of the cores corresponds to a faunal change from
a non-polar fauna at the surface to a polar fauna at depth.
They have dated this termination at 13,400 ypb in core RC9-
224. C^{14} dates from KN51-19 GPC support this correlation
(Figure 3.18).

The zone of increased carbonate at the base of KN51-17
GPC corresponds to a similar zone of high carbonate in
RC9-225. Light-microscope investigations of the sediments of
KN51-17 GPC show that a reversal in dominance between the
coccoliths *Gephyrocapsa* and *Emiliania huxleyi* occurs at a
depth of approximately 950 cm in this core (Figure 3.18),
further strengthening the correlation with RC9-225. This
reversal occurs at about 73,000 ybp in this area (McIntyre
et al., 1972; Thierstein et al., 1977). Sediments have thus
been preferentially deposited in the wave troughs since that
time. Sub-bottom penetration records (Figure 3.8) do not
indicate the upper limit of this preferential deposition, and
insufficient sediment samples were recovered to determine the
present-day depositional pattern.

Turbidites and debris flow

Most of the cores recovered from in and around the
northern study areas show sedimentary sequences deposited
as a result of slumping on the western margin of the Rockall
Plateau. Two types of deposits, turbidites and debris-flow
deposits, were cored in similar stratigraphic positions.

Carbonate-rich sand/silt layers, often showing graded
bedding, are present in cores from the laminated sediments
in Area 1 (Cores KN51-16 GC and 19 GPC, Figure 3.19; core
KN51-17 GPC, Figure 3.18), as well as in cores further north,
although still downslope from the slump on Rockall Plateau
(cores R10-2, V28-72; Figures 3.1, 3.12; Table 3.1). Like
many other cores, core R10-2 contains two calcareous sand
layers. The deeper sand layer is 16 cm thick and is graded,
with median grain size increasing from 180 μ at the top to
210 μ at the base (Ericson et al., 1961, p. 222, 251). A
description of V28-72, provided by Lamont-Doherty Geological
Observatory, indicates the presence of a 29 cm thick foram-
iniferal sand in a similar stratigraphic position. The cal-
careous sand layers show up as prominent spikes on carbonate
curves (Figure 3.19) and can be correlated from core to core.

Cores recovered from the debris-flow surface (hyperbolic
echoes) contain debris-flow deposits and/or deformed sedi-
ments. Core KN51-29 GC has two prominent debris-flow
deposits, one containing clasts of white nanno-oozes and gray
lutites suspended in a foram-sand matrix. The other deposit,
immediately below, has similar clasts in a muddy matrix

Figure 3.19   Lithologic descriptions and carbonate curves
for cores KN 51-16 GPC and 29 GC (Area 1)
and cores KN 51-34 GC and 35 GC (Area 2).
The character of the gravitational flow deposit
changes from core to core. Tie-lines connect
events of similar age. Vertical bars along
19 GPC are intervals dated by C^{14} (Table 3.2).

16 GC

19 GPC

% CARBONATE

29 GC

34 GC

35 GC

DEPTH IN CENTIMETERS

13,400 YBP

TOP-GRAVITATIONAL FLOW

KEY

l.Gr.   light gray calcareous ooze

d.Gr.   dark gray calcareous clay

mottling

silt laminations

hydrotriolite laminations

sand layer

graded bedding

debris flow—mudclasts in sand matrix
            —mudclasts in clay matrix

folded or inclined bedding

sand pockets

E = E. huxleii dominant

KNORR 51 CORES

Figure 3.19

276
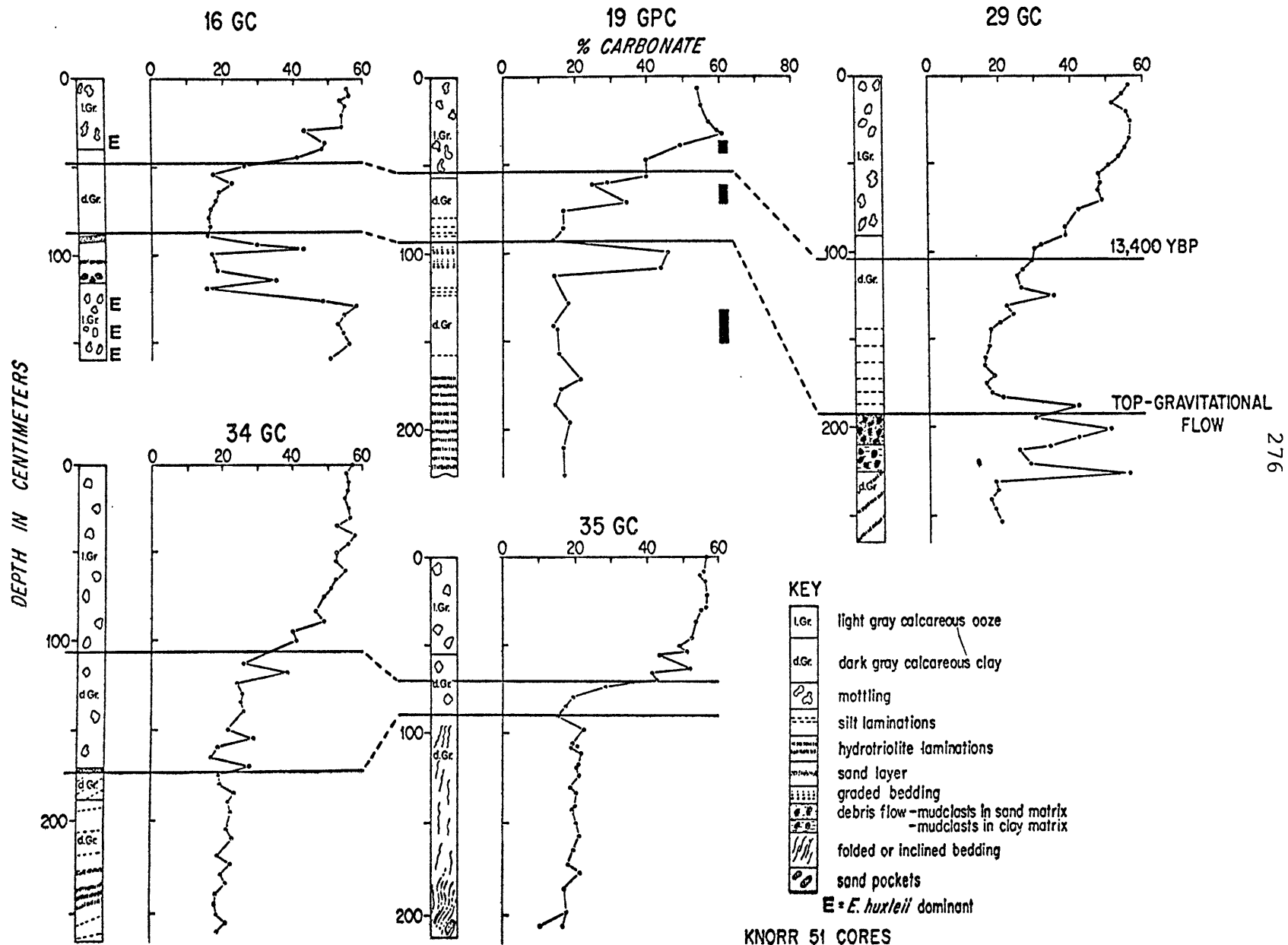
(Figures 3.19, 3.20). These debris-flow deposits apparently lie on disturbed sediments, as vertical hydrotroilite bands were observed below the debris flows. In contrast, cores from the sediment waves have horizontal hydrotroilite bands in this unit. Although core KN 51-31 GPC (Figure 3.18), 500 m from 29 GC (Figure 3.19), apparently did not recover the surface sediments, it shows a disturbed sandy zone overlying sediments similar to those cored by KN51-17 GPC and 19 GPC. The coccolith event (73,000 years ago) is found at a depth of 260 cm, only 230 cm below the sandy zone. This core apparently penetrated a large undeformed sedimentary mass within the debris flow (an olistolith?) and not the sediments which lie below the base of the flow.

Core 73134 (Pujol et al., 1974), from the debris flow area (Figures 3.1, 3.12), contains several calcareous sandy layers, one of which (approx. 1 cm thick) shows normal grading. Also in the core is an interval described as "glide plane", apparently similar to the debris-flow deposit in core KN51-29 GC. This glide plane rests on slightly deformed sediments which in turn grade into a clay sediment with silt layers.

The sandy debris-flow deposits are present as prominent spikes on the carbonate curves (Figure 3.19), and can be correlated with the calcareous sand/silt layers found outside the area of hyperbolic echoes.

Two cores were recovered from the nose of the debris flow (Area 2). Cores KN51-34 GC and 35 GC (Figures 3.19, 3.20)

Figure 3.20   Photographs of debris-flow sediment

R: Gravity Core KN51-35 GC.   (165 to 210 cm).
Folded bedding and silt lenses in debris-
flow deposit.

L: Gravity Core KN51-29GC.   (175 to 220 cm).
Two debris-flow deposits are present
185 to 203 cm: mud clasts in sand matrix
203 to 223 cm: mud clasts in clay matrix

Note: Horizontal and vertical cracks and
gaps due to extrusion method.
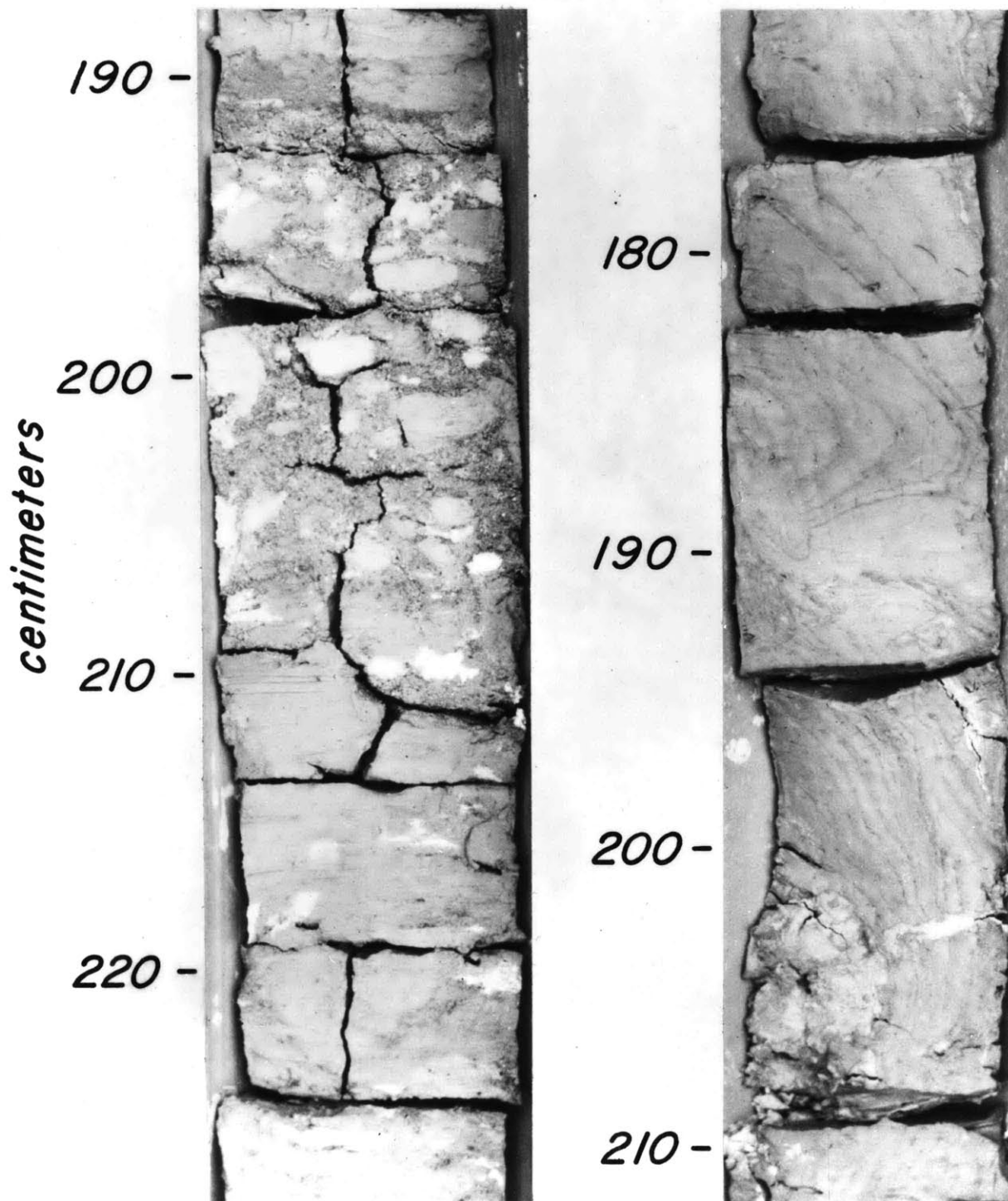
Figure 3.20

show disturbed and folded bedding surfaces in the lower parts of the cores. These disturbed sediments are in the same stratigraphic position as the sand/silt turbidites and debris flows described from Area 1, higher up on the debris flow. No lenses of calcareous sand are found in these cores, and they emphasize the different nature of the debris flow in this area.

The apparent widespread correlation of carbonate-rich sand/silt layers, carbonate turbidites, debris-flow deposits and deformed sediments suggest that these sedimentary horizons are related to the same event, the slumping of sediments on the eastern margin of the Rockall Trough.

The strong reflector at the base of the thin post-debris-flow sediment (Figure 3.17) results from a sharp 5 to 10% change in density (water content) from the debris flow to the overlying sediments (Figure 3.21). The water contents for the upper units in these cores are comparable to those of other surface sediments in the area (Silva et al., in preparation). The low water contents of the debris flow sediments can be due either to the greater age of these sediments or to a loss of water as the sediments were disturbed during emplacement. As the water contents are similar to those of the older sediments in these areas (Silva et al., in preparation) the first choice is taken.

One core, KN51-33 GC, was recovered from the laminated sediments at the base of the debris-flow nose. Although this
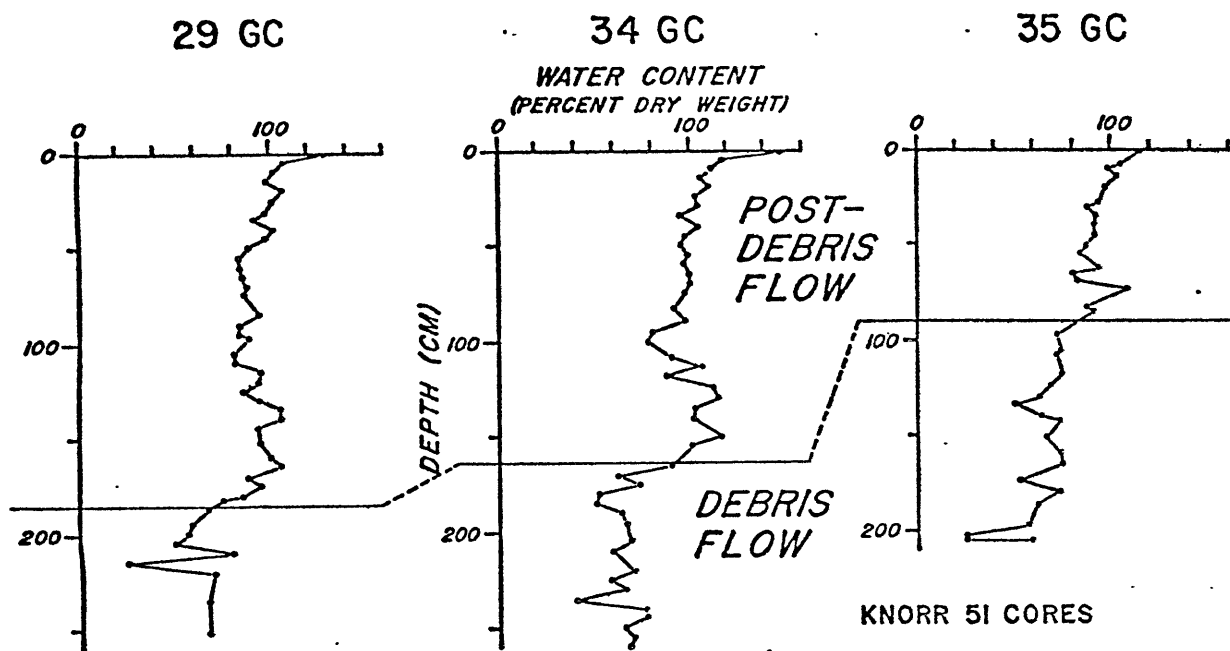
Figure 3.21   Salt-corrected water content profiles for
cores which sampled debris flow. Debris-
flow sediments have lower water content (higher
density) than overlying sediments. Acoustic
contrast creates a strong reflector at the
base of the post-debris flow sediments
(Figure 3.17).

core did not penetrate sediments old enough to be associated
with the slumping on Rockall Plateau, it did penetrate a
series of terrigenous turbidites. As these turbidites are
not present in other cores, they appear to come from south of
the area affected by slumping. These turbidites, which have
crossed the Feni Drift in an area where no sediment waves are
developed (Figure 3.1, 3.12), may be an important source of
sediment for the sediment drift found farther to the south.

Sedimentation rates

Two stratigraphic boundaries have been identified based on
carbonate stratigraphy and on coccolith abundances. These
boundaries are the change from high-carbonate sediments to
low-carbonate sediments at the top of the core (13,400 years)
and the change in dominance between *E. huxleyi* and *Gephyracapsa*
(73,000 years). These two markers allow the calculation of
sedimentation rates for the most recent interglacial period
(13,400-present) and the previous glacial period (73,000-13,400
y). These results have been compiled in Table 3.1 for all
cores studied.

For at least the last 13,400 years, the depositional pat-
terns in the vicinity of the debris flow have been influenced
by the presence of the rough topography. Sedimentation rates
for this time interval range from 3.4 to 4.5 cm/1000 years in
the area of sediment waves (upstream from the flow deposits)
decreasing to less than 1.1 to 2.6 cm/1000 years at the scarp.

At the base of the scarp the sedimentation rates increase to
more than 3.8 cm/1000 years and to 7.5 and greater than 9.1
cm/1000 years for cores recovered from the debris flow surface.
The low sedimentation rates in the vicinity of the scarp may
result from the exposed location and the steep slopes in this
area. High sedimentation rates in the debris flow area may
result from rugged topography providing quiet areas where
material in suspension can deposit quickly.

Sedimentation rates of 3.8, 8.0 and 9.7 cm/1000 years are
found for cores recovered from the nose of the flow. Sub-
bottom profiles of the nose of the debris flow (Figure 3.17)
indicate variable but high sedimentation rates. The highest
sedimentation rate is for KN51-33 GC, which contained tur-
bidites.

Sedimentation rates for 13,400-73,000 years ago can be
determined only for cores KN 51-17 GPC and 19 GPC. These
cores also allow us to estimate the age of the slumping on
Rockall Plateau. Sedimentation rates of 14.9 cm/1000 y and
greater than 18.3 cm/1000 y are determined for the glacial-age
sediments on KN 51-17 GPC and 19 GPC respectively. Linear
interpolation with these sedimentation rates leads to an age
of 15,200 y for the calcareous sandy zone in KN 51-17 GPC and
an age of greater than 15,600 y for the calcareous turbidites
in KN51-19 GPC. The age of the youngest sediments deposited
by the slump is thus 15,000-16,000 years old, suggesting that
slumping ended at this time. Although cores indicate that

several distinct sedimentary events have occurred, the
slumping probably occurred over only a short period of time.
This age is similar to the late Pleistocene age estimated for
the slump by Roberts (1972).

An attempt was made to determine a more accurate date for
the slumping on Rockall Bank by obtaining C-14 dates on the
sediments of KN51-19 GPC. Some dates, determined on the in-
organic carbon fraction, were much older than those predicted
by lithostratigraphic techniques (Table 3.2). Smear slide
examination showed that detrital carbonate rhombs were present
in all intervals dated, and were especially common in the
rapidly deposited sediments below 52 cm (older than 13,400 y).
A sample which contains 50% old carbon will have a C-14 age which
is 5568 years too old (Olsson, 1968). The deeper intervals
dated have significant amounts of old detrital carbonate
(appx. 25% to more than 75%) and those dates are too old. The
shallower C-14 date (36 to 43 cm) is more reliable, since the
sample is predominantly tests of planktonic organisms. This
date suggests either that the upper sediment layers were dis-
turbed by coring, or that there have been changes in sedi-
mentation rate within the last 13,400 y. Lithostratigraphic
ages were used in preference to C-14 ages.

TABLE 3.2

C^{14} Dates - KN51-19GPC

ID#	Depth(cm)	Age (C^{14})[1] years before present	Estimated age[2] years before present
I-10,069	36-43	6580 ± 130	10,200
I-10,070	61-71	$17,880 \pm 330$	>14,200
I-10,071	132-150	>32,500	>18,300

[1] C^{-14} age based on total inorganic carbon

[2] Age estimated assuming 0 years at 0 cm, 13,400 years at 52 cm, and less than 73,000 years at 1140 cm (Table 3.1). These ages are consistent with the carbonate and coccolith stratigraphy. Comparisons with KN51-17 GPC suggest the actual dates are not much older (<1000 years) than those given here (Figure 3.18).

E. SEDIMENTARY HISTORY
Sediment waves

Sediment waves cover large regions of Rockall Trough. Sediment waves studied in the southern zone have remained active apparently since their formation some 35 million years ago. They have certainly been active for most of the last 660,000 years.

Sediment waves in the northern zone have not always been active features. Preferential deposition has occurred in the wave troughs from at least 73,000 to 13,400 years ago. This preferential deposition may have resulted from an increased supply of sediment due to continental glaciations, possibly coupled with a change in deep circulation pattern. Current-sorted layers of coarse silt and sand (contourites of Hollister and Heezen, 1972) present in the trough fill suggest that relatively strong currents were present at this time. The areal extent of localized deposition in the wave troughs is not known, as the fill (less than 15 m thick) is difficult to observe on most surface-ship 3.5 kHz echo sounding records (e.g. Figure 3.4a).

Debris flow

Sediment waves, a continuation of the field present on the north side of the scarp, probably covered much of the Feni Drift now characterized by hyperbolic echoes. The sediment waves north of the debris-flow deposit were inactive at the time of the slide, as preferential deposition had

partially filled in the wave troughs.

Cores indicate that the sediment slumping on the eastern
margin of Rockall Bank (Roberts, 1972), and the resulting debris
flows and turbidity currents, occurred 15,000 to 16,000 years
ago. The cause of this slump is not known. Factors such as
earthquake activity, deposition of large amounts of sediment
during glacial times, or increased wave activity at times of
lowered sea level (the upper scar of the slump is found in
water depths as shallow as 100-200 m; Roberts, 1972) may have
played a major role in triggering the slump. These slumps have
played an important role in forming the morphology of, and
perhaps providing a sediment source for, the Feni Drift in
this area. Over much of the area slumps gave rise to a series
of turbidity currents, and turbidites of this age are found
over a broad area. Directly down-slope from the southern end
of the slump, slumps have triggered a series of debris flows.

The area affected by the debris flow (11,000 km^2, 220 km^3
of sediment affected) is a region of sediment removal at depths
less than 2600 m. Here there are large erosional scarps along
the boundaries (Figure 3.4a) and the bathymetric contours
(Figure 3.12), taken from an independent study of Roberts (1975),
suggest that material has been removed. Area 1 straddles one
of these erosional scarps.

The area affected by the debris flow appears to widen
downslope. North-south blocks (observed in Area 1) are parallel
to the regional slope and at an angle of 65° to 90° to the

average trend of the scarp. If the ridges indicate the direction of local sediment movement, the divergence of these ridges from the scarp may be due to the growth of the area affected by the debris flow. As the distance from the scarp increases, the blocks become smaller and their orientations more variable. Possibly these blocks have been disturbed by additional motion. The blocks very close to the escarpment have little preferred orientation. Less movement may have occurred at the base of the scarp than on other areas of the debris flow.

At depths greater than 2600 m, the debris flow has been depositional rather than erosional. Scarps in this region have hyperbolic echoes and deformed sediments on the higher side (Figure 3.4b, 3.12), indicating that deformed sediments are piled onto undisturbed sea floor. The contours in this region bow out, (Figure 3.12) suggesting that material has been deposited. Area 2 straddles one of these scarps. Cores recovered from this survey area indicate that the nose of the flow is constructed of deformed sediment. Near-bottom acoustic profiles indicate that sediment ridges (possibly folds) are responsible for the hyperbolic echoes. No samples were recovered from a transparent wedge downslope from the nose (Figure 3.4b, 3.17), which acoustic profiles suggest is the same age as the debris flow. This transparent wedge may also be a debris flow as it has acoustic characteristics similar to debris flows described by Embley (1976). A core

from the laminated sediments, downslope from the transparent area, indicates these sediments may be turbidites.

Following the major debris flow event, there were one or more minor debris flows and turbidity currents. These flows may have been generated by subsequent activity of the slumps. As secondary debris flows were not cored on the nose of the major flow, they may be more limited in extent than the major flow.

Sedimentation rates for the last 13,400 years vary in a systematic manner with the highest rates found in areas of rough, debris flow topography. Preferential deposition has smoothed much of the small-scale relief in the rugged flow area. The volume of material affected by the debris flow (220 km^3 for a 20 m thick flow) is comparable to the volume estimated for the slumps on Rockall Bank (300 km^3; Roberts, 1972).

F. CONCLUSIONS

The distribution of sediment waves can be related to a deep counter-clockwise bottom water gyre in the Rockall Trough, rather than to a northern source of bottom water. Much of the sediments which make up the Feni Drift and the sediment waves in other areas of the trough comes from the Barra and Donegal Fans, and from other canyons developed along the eastern side of the Rockall Trough. Except for episodic events, such as that which caused the debris flow studied in this

report, little sediment appears to have come from Rockall
Bank.

Two sets of sediment waves have been studied with a near-
bottom instrument package. One set of waves has always been
active, while the other set has not. The less active waves
are closer to the sediment source and may be buried at times
when coarser sediments are put into the trough at high
rates.

The sediment waves in this region apparently migrate down-
current as well as upslope, in contrast to the waves on the
Bahama Outer Ridge, which migrate upcurrent. One of the major
hydrographic differences between these areas is that tidal
currents are much stronger in the Rockall Trough, even though
average currents are about the same (Lonsdale and Hollister,
in press). Perhaps tidal components are important in determining
the orientation of the sediment waves.

Hyperbolic echoes are observed in areas of (1) deep-sea
fans, (2) suspected deep-current activity, and (3) debris flow
activity. A detailed study of the debris flow shows that the
hyperbolic echoes are caused by blocks and ridges created
during the flow. Other gravity flows resulting from the slump
on Rockall Bank have deposited calcareous sand and silt
turbidites over a large area of the Feni Drift, otherwise un-
affected by the debris flow. The age of slumping, debris flow
formation, and turbidite deposition is roughly 15,000-16,000
years.

This large debris flow, which truncated a field of inactive sediment waves, shows many morphological features used as indicators of gravitational sediment movement. These morphological features include (1) a sediment scarp or series of scarps with (2) hyperbolic echoes developed on the deeper side of the scarp (the surface of the gravitational flow or slide), (3) hummocky topography in the deeper, depositional portions of the flow, and (4) a wedge of transparent sediment extending downslope from the nose of the sediment flow.

As the presence of hyperbolic echoes on surface-ship echo sounding records only indicates the presence of topographic elements below the limit of resolution of the echo-sounding system, observations on the nature of the hyperbolae, the trend, if any, of the topography responsible for the side echoes, the trend of the zone of hyperbolic echoes and the character of the hyperbolic returns themselves must be included before conclusions can be drawn as to the origin of the features which form the rough topography (Appendix I.D).

Hyperbolic echoes on the erosional portion of the debris flow (e.g., Area 1) result from blocks of undeformed sediment riding in a matrix of deformed sediments. These blocks are roughly perpendicular to the regional contours. The hummocky topography at the nose of the debris flow (e.g., Area 2) results from folded or deformed sediments. Near the nose of the flow these deformational ridges are parallel to the trend of the nose.

The area of the debris flow, as outlined by the presence of surface-ship echo sounding records, cuts across the bathymetric contours, whereas large regions of hyperbolic echoes which result from current-produced longitudinal bed forms, such as furrows, are generally elongated parallel to the bathymetric contours (Chapter II).

CHAPTER IV

DISTRIBUTION AND ORIGIN OF BED FORMS STUDIED

A. INTRODUCTION

The aforementioned near-bottom investigations of the sea-floor morphology have shown that current-produced topographic features (bed forms) can be important topographic elements in certain areas of the deep sea. The origins of some of these bed forms can be relatively well understood by comparisons to well-studied analogues in shallow water and experimental flumes (e.g., ripples and sand waves in sand-size incohesive material; (Lonsdale and Spiess, 1977). However, the mechanisms responsible for the formation of bed forms in the fine-grained, cohesive sediments commonly found in the deep sea, those in which interparticle forces are important, are not well understood.

For the purpose of this study, a definition of a bed form will be taken from Allen (1968a). Bed forms can be defined as any deviation from a flat bed (usually spatially quasi-periodic) that depends for its origin on an interaction between a bed material and a fluid flow such that there occurs a spatially nonuniform transfer of material from bed to flow or between bed and flow. The occurrence of bed forms is, in general, independent of the precise nature of the fluid or the nature

of the bed material. Lists of the features which develop as bed forms due to flow of air or water over incohesive substrates such as sand or over cohesive substrates such as clay or snow have been compiled by Allen (1968a).

This study concentrated on the bed forms produced by water flow over cohesive sediments. In all, five kinds of bed forms ranging in scale from a few centimeters to several hundred kilometers were described. During the course of these investigations, information was collected on the origin of transverse ripples, longitudinal triangular ripples, furrows, and sediment waves. No data relevant to the formation of the largest bed form, the sediment drift, were collected.

In this section the observational data relevant to the bed form are briefly summarized. They are compared with similar features reported from other areas of the deep sea and from shallow water, when possible. Possible origins of these bed forms and the factors which control their distribution are discussed.

B. *RIPPLES IN COHESIVE SEDIMENT*

During the course of these investigations, ripples were found formed in the cohesive sediments (median deflocculated size 1 μ) of the Bahama Outer Ridge. No ripples were observed

on the Feni Drift in the Rockall Trough (this study, Lonsdale
and Hollister, in press). The ripples are asymmetrical with
steeper downstream sides, and they have spacings of about 20
cm and amplitudes of about 5 cm. Many of the ripples photo-
graphed or observed visually had sharp crests and were well
formed, suggesting that they are maintained by currents which
occur frequently.

Ripples on the steep small-furrow walls in Area 1 are at
an angle of roughly 45° to the mean flow (5 to 15 cm/sec).
The ripples, which have small cornice-like overhangs above
the downstream side, are the best developed on the steepest
portions of the furrow walls. In Area 2 they are found on
slopes within the large furrow troughs, and are generally
transverse to the flow 5-10 cm/sec). Ripples were also photo-
graphed from Area 3, but the relationship between the furrows
and the ripples cannot be determined. Currents range from
about 5 to 10 cm/sec.

Ripples are often photographed in the deep sea (e.g.,
Heezen and Hollister, 1964; Lonsdale and Spiess, 1977) de-
veloped in both noncohesive and cohesive sediments. Where
ripples are developed in noncohesive sediment, usually well-
washed foram oozes, they appear similar to those found in
shallow water environments and in laboratory flumes (Lonsdale
and Spiess, 1977). Ripples have been produced in noncohesive

sediments as fine as 10 μ at apeeds of 30 cm/sec (Rees, 1966).
Experiments by Southard (personal communication) suggest that
similar bed forms could develop in even finer sediments if
cohesive forces were not present.

Since ripples in cohesive sediments similar to the ones
described from these studies have not been described from
shallow water or laboratory flows, their origin is unknown.

Cornice-like overhangs of the downstream side of the
ripple crests resemble cornices developed in snow on the
downstream side of mountain ridges (Seligman, 1963). Snow
cornices are thought to be formed when snow deposits out of
a region of separated flow behind the ridge crest. Similar
flow separation patterns exist for flow over ripples, and
the cohesive-sediment ripple cornices may form in a similar
way. The ripples would then migrate forward as
material is removed from the upstream side and attached to
the downstream side.

The restricted appearance of ripples on slopes suggest
that such slopes may enhance ripple formation. Experiments
with noncohesive sediments have shown that the sediments on
channel walls form ripples at lower velocities than those on
the channel floor (Raudkivi, 1976, p. 115). The ripples in
cohesive sediments may be more easily initiated on slopes
than on levels surfaces.

The angle between the ripple and the furrow may result from secondary circulation produced by the furrow form. This circulation pattern would consist of water flowing up the furrow, and would not necessarily be the flow which was responsible for the furrow itself. Visual observations of the flow along a furrow showed no indication of such a secondary circulation, but the flow may have been disturbed by the presence of the submersible.

C. LONGITUDINAL TRIANGULAR RIPPLES

Longitudinal triangular ripples were mapped only on the abyssal plain in Blake-Bahama Outer Ridge Area 2. These ripples, two to five meters long and spaced two to five meters apart, have a triangular cross-section (base 75 cm, height 15 cm). Sediments recovered from the crest of a longitudinal ripple show that they are developed in sandy muds (8-29% sand). The coarse component may be derived from the erosion of the nearby large furrows. Evidently, none of the sediment is contributed by turbidity current activity. These bed forms show systematic changes in orientation across the abyssal plain embayment (Figure 2.25).

In 1973, currents were steady at 2 cm/sec from the south. In 1977, currents of the same magnitude were directed toward 260°, parallel to the triangular ripples in the dive area.

They are buried in places by more recent sediments and thus appear relict.

Similar features have been reported from other areas of the ocean. Heezen and Hollister (1964) reported longitudinal ripples from just above and to the east of the Mozambique Abyssal Plain. The surface-ship echo sounder showed hyperbolic echoes (Heezen and Hollister, 1964) and a nearby core indicated the presence of abundant current-sorted silt and sand layers (Heezen and Hollister, 1971). These ripples are developed beneath Antarctic Bottom Water as it loops through the Mozambique Basin (Kolla et al., 1976b).

Longitudinal ripples are present and they appear to be constrained to a depth interval of 4600 to 4950 m (bottom-water potential temperature less than 1.82°C) where there are fast currents (highest speed at 4849 m was 24.4 cm/sec; Zimmerman, 1971). The ripples have their long axes parallel to the current flow and to the regional contours (Zimmerman, 1971). Cores recovered from the lower continental rise in this vicinity show abundant current-bedded silt layers (Hollister and Heezen, 1972).

Similar features have also been reported from the Horizon A outcrop area in the western North Atlantic (Ewing and Mouzo, 1968).

Previous investigators (Zimmerman, 1971; Lonsdale and Spiess, 1977) have noted a similarity between these bed forms and the "longitudinal ripple marks" in mud beds reported by van Straaten (1951). The "longitudinal ripple marks" of van Straaten (1951) have, however, been classified by Allen (1968a) as an example of a "longitudinal welt". As defined by Allen (1968a) longitudinal welts are a series of long, fairly evenly spaced ridges eroded parallel to the flow. They are commonly a few centimeters deep and 10-20 cm apart, although larger examples have been described. These longitudinal welts appear more similar to furrows than to longitudinal triangular ripples, as the latter appear to be depositional. It appears these triangular ripples have no counterpart described from shallow water.

The following conclusions can be drawn about the longitudinal triangular ripples. They appear to form parallel to the currents; they are often found in areas characterized by deep-current activity, although only at the greatest depths of those currents; and they appear to form in areas where coarser sediments are available due in part to the extensive erosion of nearby areas (e.g., Horizon A outcrop area or furrowed topography). These bed forms may be created when a strong current event picks up sediment and concentrates the coarser fraction in these short ridges.

They may form rapidly and then lay dormant for long periods
of time.

D. FURROWS

Abyssal Furrows

Furrows were studied in detail in both of the deep tow
survey areas on the Blake-Bahama Outer Ridge (Area 1 and 2).
Although furrows are suspected to exist in portions of the
Feni Drift, no data were collected on those features.

Furrows are long, almost rectilinear grooves observed
to range from 1 to 100 m in width, 0.5 to 20 m in depth, and
spaced 20 to 350 m apart. In any one area the widths, depths
and spacings vary, but, in general, are quite uniform. These
furrows are at least several kilometers in length, aligned
parallel to the measured currents (up to 15 cm/sec) and to
the regional contours, and join in tuning fork junctions which
open into the current flow. The walls of the furrows can be
decorated with small ripples, eroded to expose sedimentary
layers, or smooth.

All furrows in a given region may not have formed at the
same time. The small furrows cover a relatively large range
of sizes (e.g., Figure 2.17) and sub-bottom profiles may
sometimes indicate the presence of an old furrow beneath the
surface while side-scan sonar records show no furrow presently
on the surface (Figure 2.9).

Furrows have been found at a depth of 5800 m in the Samoan Passage where they are eroded into patches of reworked calcareous nannofossil ooze (Lonsdale et al., 1973; Lonsdale, 1974; Lonsdale and Spiess, 1977). The furrows, about one meter deep and are spaced an average of 30 m apart, were observed with deep-tow side-scan sonar. Tuning-fork junctions open to the north, indicating that the furrows were formed by southward flowing currents. Bottom currents in this area measured at the time of the survey averaged only 2.5 cm/sec towards the north, and there is geological evidence that they are relict (Lonsdale, 1974; Lonsdale and Speiss, 1977). Hollister et al. (1974b) report the presence of small hyperbolic echoes on a surface-ship 3.5 kHz record across this patch of furrows (their figure 13). One other small patch of furrows was also observed by Lonsdale (1974) in the Samoan Passage.

Although less well documented, furrows have also been observed in other areas of the ocean basins. Bottom photographs on the Greater Antilles Outer Ridge, a large sedimentary drift in the western North Atlantic located directly north of the Puerto Rico Trench (Tucholke and Ewing, 1974), show the presence of furrows on the northeast side of that bottom current deposit (Figure 4.1a). Photographs indicate that the furrows are present at least from 5311 to 5424 m.

Figure 4.1.   Photographs of deep-sea furrows in other areas
               of the ocean.

               (a)   Greater Antilles Outer Ridge.
                     Sta. AII60 K14.   Lat.   23°19.5' N
                                        Long. 68°05.5' W
                                        Depth 5424 m
                     (Photograph from W.H.O.I.)
               (b)   Brazilian Continental Rise.
                     Sta. RC15 K146   Lat.   13°58.4' S
                                       Long. 34°04.4' W
                                       Depth 4840 m
                     (Photograph courtesy of Larry Sullivan
                     and Lamont-Doherty Geological Observatory.)

GREATER ANTILLES OUTER RIDGE

BRAZILIAN CONTINENTAL RISE

Figure 4.1

A nearby current meter at 5290 m (current meter E, 100 m above the bottom, Tucholke et al., 1973) showed nearly unidirectional currents flowing parallel to the contours and the furrows (to the southeast) for a period of 166 days. Hourly averaged currents ranged from 3 to 17 cm/sec (Tucholke et al., 1973).

Hyperbolic echoes are often seen over much of the eastern Brazil Continental Margin (Damuth and Hayes, 1977). Damuth and Hayes (1977) suggest that many of these hyperbolic echoes are caused by furrows formed by northward-flowing Antarctic Bottom Water, but little direct evidence is given for this broad generalization. One camera station from that rise (not reported by the above authors) has recorded a small furrow from 4840 m (Figure 4.1b). This camera station was in a small patch of hyperbolic echoes surrounding a deep-sea channel (Damuth and Hays, 1977). Although the local hydrography of the area is not known (several large seamounts and a major channel are nearby, Damuth and Hayes, 1977), the furrow is parallel to the nearby channel (east-west) rather than to the regional contours or expected currents (north-south). Furrow morphology indicates that the current flow in this area is to the east (downslope). This raises the possibility that the furrow was formed by a downslope current event rather than

along-slope currents related to the northward flow of Antarctic Bottom Water. However, it must be emphasized that details of the local hydrography, microtopography or structure of the bed form have not as yet been determined.

Furrow - like erosional lineations have been reported from the insular rise off southern Iceland (Lonsdale and Hollister, 1976). These lineations, observed only by side-scan sonar, are associated with a large meander in a submarine canyon that is being cut off by erosive turbidity currents. These lineations are shallow (less than 2 m), narrow (less than 5 m) and oriented roughly perpendicular to the strong current (greater than 20 cm/sec) which crosses this rise (Lonsdale and Hollister, in preparation). Further investigation will be required before any similarity between these erosional lineations and the contour-current furrows can be established.

Thus, furrows appear to be common bed forms in clayey deep-sea sediments and often produce regular hyperbolic echoes on surface-ship echo sounders. Some form of furrow might be related to turbidity currents.

Furrows are thought to exist in areas of the ocean basins where no direct evidence exists, but where a pattern of regular hyperbolic echoes on an otherwise smooth sea floor is observed (e.g., Figure 2.3). On the basis of echo-sounding

records, furrows are thought to be developed in the Guiana

Basin (Embley and Hayes, 1972; Damuth, 1975a); Embley, 1975),

the East Brazilian Continental Margin (Damuth and Hayes,

1977), the Madeira Rise (Laughton, 1962; Clay and Leong,

1974; Embley, 1975), the continental rise south of the

Canary Islands (Embley, 1975), the Northeast American Lower

Continental Rise (Hollister and Heezen, 1972), the northern

Bermuda Rise (Silva et al., 1976), the southern Rockall

Trough (this study), near the Mozambique Abyssal Plain

(Heezen and Hollister, 1971), and on the continental rise

off Antarctica (Schroeder, 1976).

Furrows in other Environments

Bed forms similar to abyssal furrows have been described

from several locations on the continental shelf. Dyer (1970)

reported furrows 5 m wide, 1 m deep, 4 km long and 10-25 m

apart in 1-10 m deep water. These furrows, developed in the

muds of Southampton Water, have tuning-fork junctions which

open into the stronger ebb tide. Velocities exceed 70 cm/sec

at 1 m above the bottom in the center of the furrow patch

(Dyer, 1970).

Stride et al., (1972) and Belderson et al. (1972) discuss

occurrences of furrows in the English Channel and in other

locations around the UK. Furrows develop in the coarse sedi-

ments (mainly gravel) of the English Channel (water depth
45 m) in where maximum near-surface velocity is greater than
3 knots (150 cm/sec) (Stride et al., 1972) and furrows have
been described from sandy sediments on the Spanish Saharah
continental shelf (Newton et al., 1973).

Although not enough is known about the formation of
these shallow-water features to relate them in detail to
deep-sea furrows, it does appear they are similar features
and that furrows are common bed forms in natural systems.

Origin of Furrows

Some insight into the way in which the furrows are
produced can be gotten by comparison with longitudinal bed
forms found in other environments. They are widespread in
many natural sedimentary environments and have been pro-
duced in laboratory experiments involving a variety of flow
conditions and sediment sizes. Such bed forms tend to be
a ubiquitous feature in sedimentary environments character-
ized by unidirectional flows over erodible substrates.
Examples of longitudinal bed forms in a variety of environ-
ments are given by Allen (1968a), and new kinds of longitu-
dinal bed forms are continually being found in the marine
environment, mainly through the use of side-scan sonar
(McKinney et al., 1974; Lonsdale, 1974; Lonsdale and Spiess,
1977; Werner and Newton, 1975).

Many of these longitudinal bed forms are thought to result from the interaction of large-scale helical secondary circulations within the fluid flow interacting with and modifying the sediment bed (Karcz, 1970; Jackson, 1976). For example, extensive regions of longitudinal seif sand dunes exist in areas where steady winds blow over hot, dry, loose sand. These large dunes result from large helical-vortex circualtions in the unstable layer of heated air (Hanna, 1969; Folk, 1971). The seif dunes are characterized by tuning-fork junctions opening into the prevailing wind direction (Folk, 1971). Large vortices have been observed in the atmosphere (Angell et al., 1968), and they may be responsible for banded cloud patterns often observed in the atmosphere (Kuettner, 1959; 1971). Helical circulations, present in the surface layers of the ocean, form windows or wind slicks on the sea surface (Langmuir, 1938). However, windslicks are formed when surface waves interact with a wind-induced surface drift (Faller and Capona, 1977).

Large scale organized secondary circulations have been observed and predicted in turbulent flows. Small pinpoint vortices exist in the inner part of a turbulent boundary layer (e.g., Kline et al., 1967; Kim et al., 1971). These vortices are associated with ejections (bursts) of slow-moving fluid from near the boundary into the flow followed by a sweep of higher-velocity fluid from the interior of the

flow to the boundary. The pairs of counter-rotating vortices can be identified as such for a distance only of about one-quarter of their mean spacing into the flow (Kline et al., 1967). A similar organized secondary flow structure exists in large-scale, high-Reynolds-number flows. (Gordon and Witting, 1977). Instabilities of the Ekman layer which take the form of organized secondary circulations were first reported by Faller (1963). Subsequent investigations have indicated that these well-organized secondary circulations are widespread in laminar and turbulent Ekman layers. Brown (1970) suggests that these rolls have characteristic thicknesses of 5 to 7 times the Ekman depth and wavelengths of 4π times the Ekman depth. The resulting roll pair is one-half as high as it is wide. Similar rolls are reported for the turbulent Ekman layer (Deardorff, 1972).

The well-mixed constant temperature layer found at the bottom of the ocean may be the site of these secondary circulations. Armi and Millard (1976) and Armi (1977) report that this layer is six times the Ekman depth for stations on the Hatteras Abyssal Plain.

The secondary flows predicted by such models are generally at some angle (ca. 20°) to the mean flow and cross-stream velocities are 2 to 20% of the mean velocity (e.g., Brown, 1970). Similar flow structures can also be developed in a stably stratified flow at angles other than those observed

for neutrally stratified flows (Faller and Kaylor, 1966).

Experiments on the instability of the three-dimensional boundary of a rotating disk (Gregory et al., 1955) indicate these instabilities can produce steady-state longitudinal patterns in sedimentary materials placed in the flow. The sediment may fix the positions of these instabilities. Similar experiments with turbulent Ekman layers have not been reported.

The existence of large-scale secondary circulations in high-Reynolds-number geophysical flows appears relatively well established. Few studies have determined how these flows are modified by the presence of a sedimentary substrate.

Experiments with cohesive sediments in laboratory flumes have produced features with similarities to the abyssal furrows. Allen (1969) produced "longitudinal erosional grooves" during flume experiments with cohesive muds. The grooves, 1 mm deep and spaced 6 mm apart, have the same average spacing as longitudinal streaks (secondary circulations) in a turbulent boundary flow. These grooves trap sedimentary particles moving along the bed. The particles enhanced the groove's erosion.

In another experiment, a zone of localized erosion in a laboratory flume resulted from a secondary circulation which encompassed its entire cross section (Figure 4.2a; Partheniades, 1965). In this case, the circulation pattern is related to the flume's geometry. The erosion of cohesive sediments was restricted to a region near the center of the flume where the secondary flow lines departed the bed (a zone of flow conver-

Figure 4.2.   Flow patterns around furrows.

(a, upper) Velocity contours in a laboratory
flume where cohesive sediments have been locally
eroded (a furrow?). After Partheniades (1965).

(a, lower) Secondary circulations within flume
implied by the velocity distribution above.
Locallized erosion occures where the secondary
flow lines converge on the bed.

(b) Predicted relationship between furrows
and the secondary circulations in the well-
mixed bottom boundary layer which formed them.
Furrows are expected to occur where the secon-
dary flow lines converge on the bed.

(c) Possible secondary circulations within a
small furrow. Secondary circulations shown
are similar to those found in a trapazoidal
duct by Nikuradse (1930).

a, upper

2.8 3.0 3.2 3.4 3.4

3.6

3.2

2.6
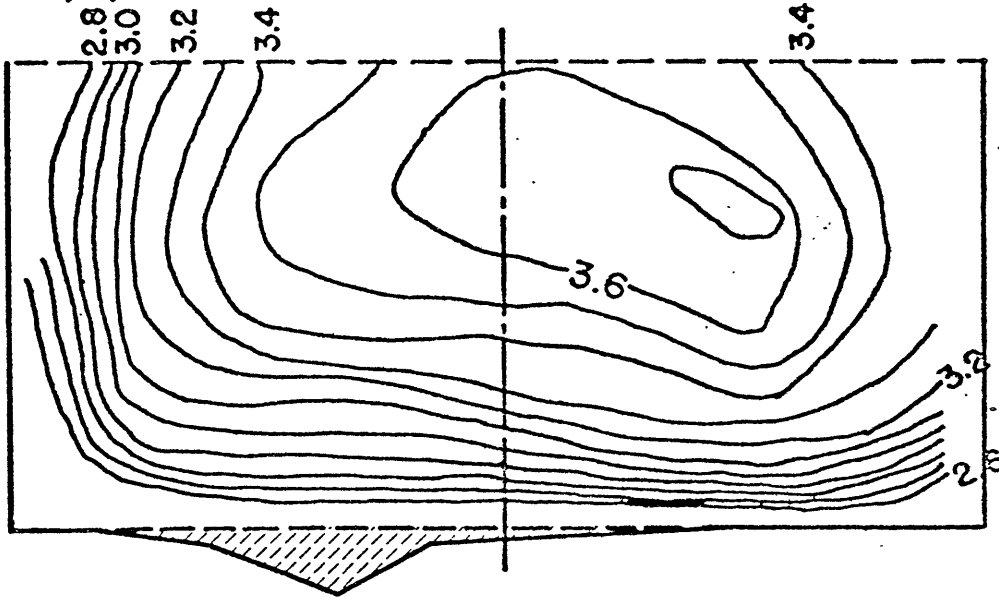
LOCALIZED EROSION (FURROW?)

VELOCITY (Contours in ft./sec.)

⊢————⌐ 0.2 ft.

a, lower

FLOW CONVERGENCE
ON BED
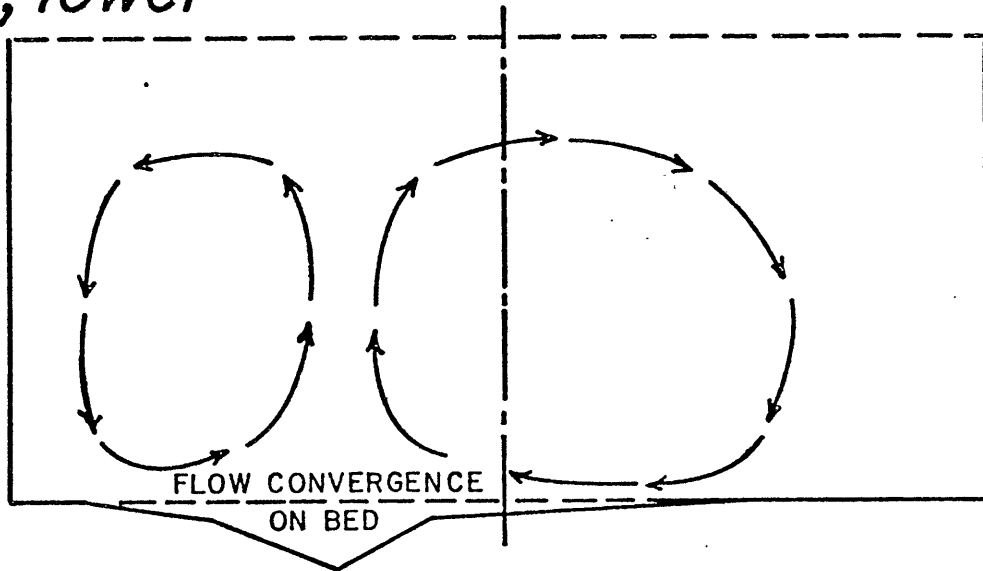
SECONDARY CIRCULATIONS

Figure 4.2

b.

BENTHIC THERMOCLINE

COARSER SEDIMENTS
IN FURROW

c.

1m

0

0   1m
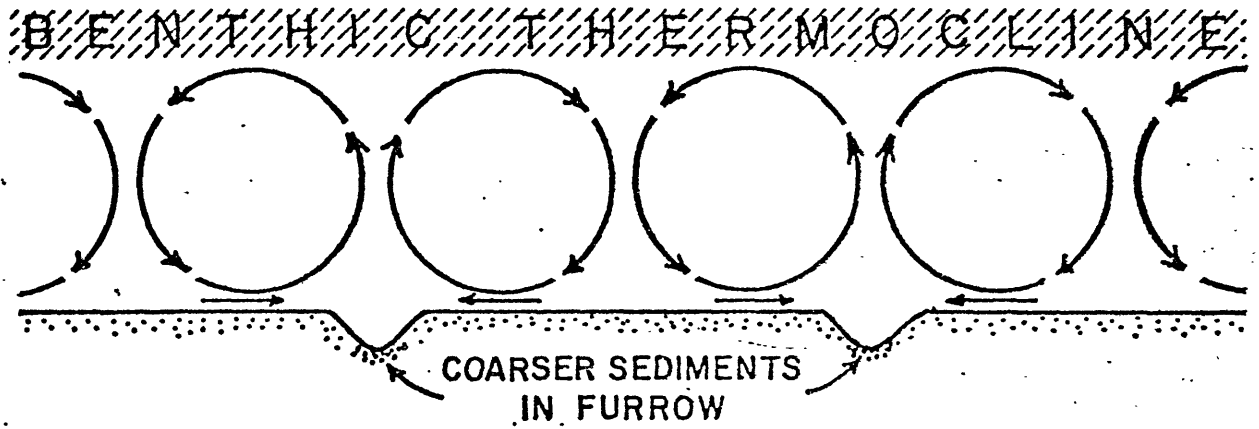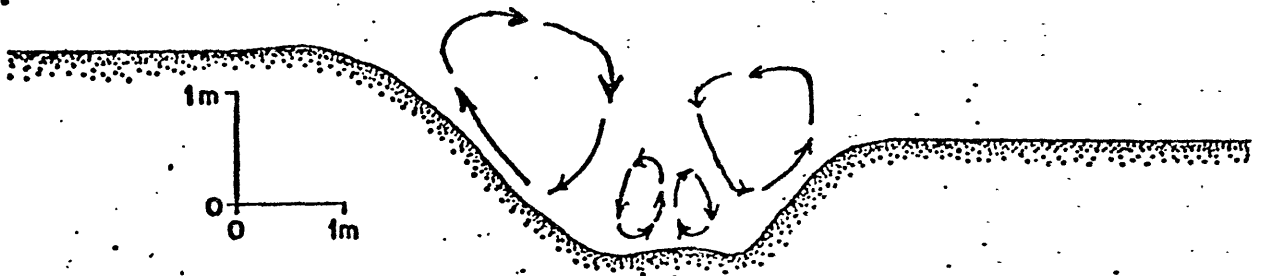
Figure 4.2

gence on the bed). As a similar flow pattern was

present when no furrow was developed, the flow determined the

position of the eroded zone.

On the basis of these experiments, two hypotheses of

furrow formation are discussed. One hypothesis emphasizes the

role of secondary-flow induced variations in bed shear stress,

while the other is mainly concerned with the role of grain

impacts on the bed. The actual situation is most likely a

combination of the two hypotheses.

Secondary flows are commonly developed in turbulent, non-

circular channel flows (e.g., Nikuradse, 1930; Kennedy and

Fulton, 1961; and Melling and Whitelaw, 1976). The center of

the channel generally corresponds to a region where secondary

flow departs the bed (e.g., Figure 4.2a). Near the center of

the flume, there is a velocity component away from the bed.

The magnitude of this component increases, and the magnitude

of the component parallel to the bed decreases as the center

of the flume is approached. The decrease of the horizontal

flow component is equivalent to an adverse pressure gradient.

This results in a higher shear stress in the region of flow

convergence (Kline et al., 1967; Gordon, 1975). Measurements

of shear stress near the wall of a duct in which a turbulent

flow and secondary circulations is present have shown that the

largest shear stresses are developed along the centerline of

the duct (flow convergence on the bed; Melling and Whitelaw,

1976). As the rate of fine-grained cohesive sediment deposition decreases when the shear stress on the bed increases (e.g., McCave and Swift, 1976), less sediment will be deposited in the center of the flume. For high velocities, the critical shear stress for erosion may be exceeded only at the center of the channel, resulting in locallized erosion.

This model may be extended to naturally-occuring secondary flow patterns (Figure 4.2b). Similar pressure gradients will be developed in the regions of flow convergence, and less sediment will be deposited there, or more will be eroded, forming a furrow.

This mode of formation would require that a given circulation pattern be fixed in position, or at least reoccupy the same position, for relatively long periods of time. Any nearby linear features, such as previously-existing furrows, may help to stabilize the circulation pattern.

A furrow could be formed in a shorter period of time if the role of particles impinging on the bed is included. Secondary circulations will sweep sediments into lines aligned with the flow somewhat similar to windrows on the ocean surface. The coarser fraction of this material may be swept along the bottom, repeatedly impacting the bed. There may be preferential erosion or nondeposition along these lines, and these places could develop into furrows.

Allen (1969) reported that small streaks of concentrated

suspended sediment were present on the bed before the erosion

of the rectilinear grooves. These streaks, while they were

not fixed in position, had the same spacing as the resulting

grooves. The streaks could have concentrated the coarser

sediment and locally eroded the flume bed, and thus fixed

the position of the subsequent groove.

Once a depression is formed parallel to the flow, a

different interaction may take place between the bed and the

flow. The furrow may be able to control the circulation

pattern in its vicinity, and thus control its own growth

(Figure 4.2c). Coarse materials will easily be trapped in the

furrow once they fall in, especially very large objects such

as *Sargassum* sea weed.

At present, insufficient evidence is available to

determine how the various furrows were formed. Clearly some

of the furrows are presently erosional and some are presently

depositional. It is possible that the furrows formed in dif-

ferent ways, although their morphologies can also be explained

by furrows following different routes of development once they

are formed.

Secondary flows in the geophysical boundary layer appear

to initially control the position of the furrows. These second-

ary flows may result from instabilities in the turbulent Ekman

layer, or they may result from the structure of turbulent flows

in general. The flow should be unidirectional (tidal component

smaller than mean flow) during the time intervals the furrows are forming in order to allow these organized flow patterns to develop (Figure 4.2b).

After a depression has been formed by the interaction between the fluid flow and the sediments, significantly lower flow velocities may be able to maintain them. A large groove parallel to the flow should be able to generate its own secondary flow. This flow, which is not necessarily similar to the one which formed the furrow, may be responsible for the skewed ripples on the furrow wall (Figure 4.2c).

If the well-mixed layer is the site of large-scale secondary circulations, it should be one-half to one-fourth of the spacing of the furrows. This relationship is observed over the large furrows on the BBOR. As these furrows are quite large (15 m deep), they may determine the thickness of the well-mixed layer. Once a bed form is this well developed, it is difficult to seperate the initial interaction from one created by the bed form.

E. SEDIMENT WAVES

A variety of large surface undulations are developed in deep sea sediments. The particular sediment waves under discussion in this section are only one form these quasi-periodic undulations can take. The important points in the morphology of these sediment waves are their regular, almost sinusoidal

nature and the tendency for internal reflectors to indicate that the waves have migrated with time. This discription excludes from discussion other forms of periodic topography which are more irregular, such as the sediment swells and layered valleys of the Greater Antilles Outer Ridge (Tucholke and Ewing, 1975) and the irregular sediment swells on the southeastern flank of the Blake-Bahama Outer Ridge (section II.A). Insufficient data are available on the nature of these features to include them in this discussion.

Sediment waves on the western flank of the Bahama Outer Ridge (Chapter II) are oriented 35° to the regional contours. Those developed on the steeper portions of the ridge are found at greater angles to the contours than those on the more gradual flanks of the ridge. The waves have wavelengths of about 2 km and heights of 10 to 100 m. They are developed in cohesive clayey sediments with only 20 to 40% silt-sized material and currents averaged 5 to 10 cm/sec with small tidal components. The waves have migrated both uplsope and upcurrent.

Sediment waves in the Rockall Trough have similar wavelengths, but heights are generally smaller. They are also oriented at an angle to the contours, and have migrated upslope and down current. Currents are estimated at 10 to 15 cm/sec and tidal components are large.

Sea floor features with similar characteristics have been reported from a number of areas in the ocean. They have been

reported from the abundant sediment drifts in the eastern

North Atlantic (Jones et al., 1970; Johnson et al., 1971; Davies

and Laughton, 1972); the lower continental rise of eastern

North America (Ballard, 1966; Fox et al., 1968; Rona, 1969);

the Blake-Bahama Outer Ridge (Bryan and Markl, 1966; this

study); the Greater Antilles Outer Ridge (Tucholke and Ewing,

1975); the continental rise of northeastern South America

Damuth, 1975; Embley, 1975a; Embley and Langseth, 1977); the

Argentine Basin (Ewing et al.,1971); the Antarctic Continental

Rise (Tucholke and Houtz, 1976); the Mozambique Basin (Ewing

et al., 1968); the western Bay of Bengal (Kolla et al., 1976a);

and from the Amirante Passage (Johnson and Bunce, 1977).

Similar features have also been reported from the levees

of turbidity-current channels in the Gulf of Alaska (Embley,

1975), from a possible deep channel crossing the Columbian

Continental Rise (Bouma and Treadwell, 1975), and from channels

on the Antarctic Continental Rise (Tucholke and Houtz, 1976).

While all of these features are sometimes lumped together

under the general classification of sediment waves, there do

appear to be differences in their distribution patterns.

Sediment waves follow one of two distinct distribution patterns.

Either waves are found in restricted depth ranges, but extending

large distances parallel to the contours, or they occur in

isolated areas, but with a large depth range. Waves in the

first category are often associated with contour-following

current activity, while those in the second may be the result of turbidity-current activity.

Although the observational data are poor, most sediment waves appear to be formed at some angle to the currents. There are few if any well-documented cases where waves are parallel to the currents. While the waves generally migrate up any regional slope, they apparently can migrate either upstream or downstream. The only documented case of downstream wave migration is in the Rockall Trough where wave trends have been determined by Roberts (personnal communication). Upstream sediment wave migration is observed along the eastern North American Continental Rise (this study, Fox et al., 1968), on the northeastern South American Continental Rise (Embley and Langseth, 1977), and along the continental rise of Antarctica (Tucholke and Houtz, 1976). At present, data is only available on the water flow over the upstream-migrating sediment waves on the Bahama Outer Ridge.

At present, no features similar to these sediment waves are described from cohesive shallow-water sediments.

Early studies of upcurrent-migrating sediment waves (Fox et al., 1968) suggested that they were similar in structure to antidunes. Antidunes are bed forms formed when shallow, high-velocity water flows over loose, unconsolidated sediments. Antidunes, which can migrate either upstream or downstream, occur in supercritical flows (water speed equal to or greater

than the surface wave speed) and can be recognized in ancient sediments by the tendency of internal layering to parallel the antidune surface (Allen, 1966). Such antidunes can only occur in noncohesive sediments with a free surface.

Temperature sections over the BBOR sediment waves indicate the presence of stationary internal waves over the sediment waves (section II.B.3; Figure 4.3a). As the frequency of these internal waves is less that the buoyancy frequency of the fluid, the flow is subcritical. The internal waves take the form of lee waves. The flow patterns associated with those lee waves imply a higher current velocity near the bed on the downstream side of the wave.

The magnitude of the velocity variation over the wave can be estimated from the furrow trends (Figure 2.21), if the furrows are assumed to represent flow lines in the wave surface and if the flow component parallel to the wave does not change over the wave (Figure 4.3b). If θ_u and θ_d are the angles between the furrows and the wave crest and v_x is the flow component parallel to the wave, the flow velocity on the upstream side is $V_u = v_x / \cos \theta_u$, and that on the downstream side is $V_d = v_x / \cos \theta_d$ (Figure 4.3b). The ratio between the downstream velocity and the upstream velocity is

$V_d/V_u = \cos \theta_u/\cos \theta_d$, and that between the flow components perpendicular to the wave is $v_{y,d}/v_{y,u} = \tan \theta_d/\tan \theta_u$. For a typical wave crest, $\theta_u = 20°$ and $\theta_d = 35°$ (Figure 2.21).

Figure 4.3. Flow patterns over sediment wave.

     (a)   Cartoon showing flow pattern expected when lee waves are being generated in the flow. Higher velocities are expected on the downstream side of the wave leading to lower sedimentation rates. As a result, the sediment wave will migrate upstream.

     (b)   Using furrow trends over sediment wave to calculate the velocity distribution on the bed. Furrows represent flowlines on the bed. See text for a description of the calculation.
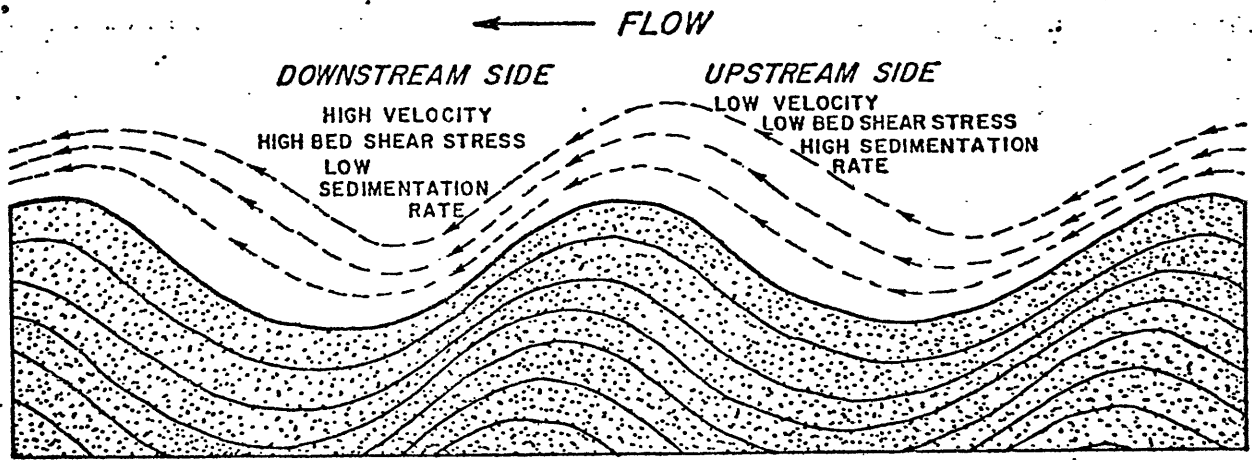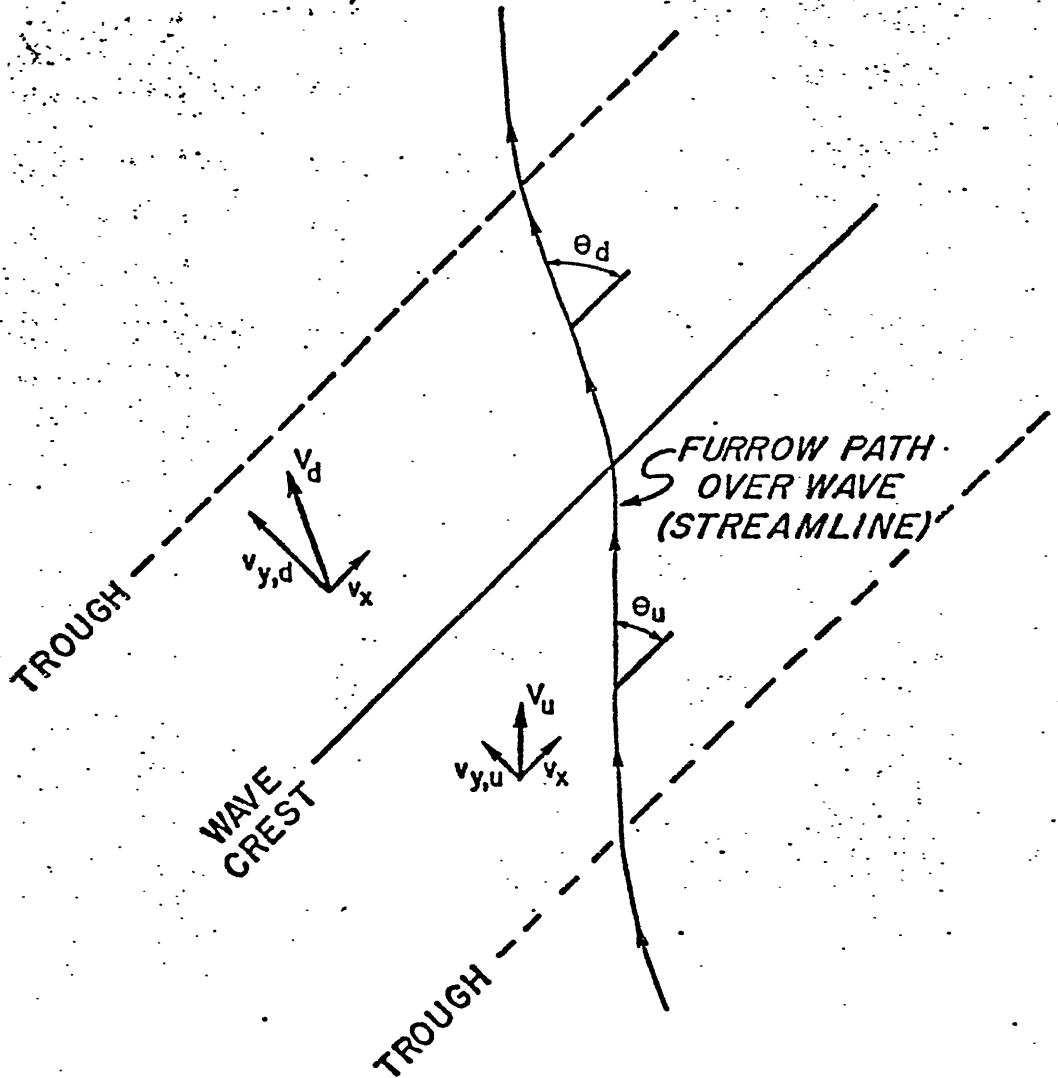
Figure 4.3

Therefore, $V_d/V_u = 1.15$ and $v_{y,d}/v_{y,u} = 1.9$. Thus the flow component over the wave will change by a factor of two (the flow affected by the generation of lee waves), but the current velocity will only change by a factor of about 20%. Although the current measurements are inconclusive, the velocity at a wave crest (KN31-CM 7, Figure 2.47) is often about 10% higher than that measured in the trough (KN31-CM 4 or CM 6).

Investigations of the deposition rate of fine-grained cohesive sediments have shown that the rate of deposition decreases as the bed shear stress increases (Krone, 1962; Einstein and Krone, 1962; McCave and Swift, 1976; Owen, 1977). McCave and Swift (1976) relate the deposition rate (R) of deep-sea sediments to the suspended sediment concentration (C_s), the particle fall velocity (w_s), and the bed shear stress (τ) by

$$R = C_s w_s (1 - \frac{\tau}{\tau_c}) p$$

where p accounts for unquantified factors, such as biological activity, and τ_c is the critical deposition stress on the bed. No sediment is deposited for τ greater than τ_c. Experimental values for τ_c fall in the range of 0.41 to 0.81 dynes/cm^2; however, smaller values may be expected (McCave and Swift, 1976).

An estimate of the shear stress, and therefore the sedimentation rate, variations over a sediment wave can be made for the flow pattern described above. Since the furrows indicate the flow direction on the sediment surface, the velocities calculated by the above method will be taken as representative

of those near the bed (specifically at a height of 1 m above the bed, V_{100}). The quadratic stress law relates V_{100} to the boundary shear stress , $\tau = C_d \rho V_{100}^2$, where C_d is a drag coefficient (taken as 3×10^{-3}, Sternberg, 1968) and ρ is the fluid density. The shear stress ratio between the two sides of the wave is $\tau_d/\tau_u = (\cos \theta_u/\cos \theta_d)^2$. For the parameters above, $\tau_d/\tau_u = 1.3$.

For C_s, w_s, and p constant (no changes in suspended sediment concentration, particle fall velocity or other factors over the sediment wave) , the ratio between the upstream sedimentation rate and the downstream rate is

$$\frac{R_u}{R_d} = \frac{\tau_c - \tau_d}{\tau_c - \tau_u}$$

Using the above expressions for τ and V_d, the sedimentation rate ratio can be expressed in terms of V_u, θ_u, and θ_d only.

$$\frac{R_u}{R_d} = \frac{\tau_c - C_d V_u^2}{\tau_c - C_d V_u^2 (\frac{\cos \theta_u}{\cos \theta_d})^2}$$

For the reasonable choices of $V_u = 8$ cm/sec and $\tau_c = 0.6$ dynes/cm^2, a sedimentation rate ratio of 1.2 is obtained. This is the same ratio as that derived for the last 11,000 years on the basis of core samples (Figure 2.43).

This simple model suggests that the waves are indeed active features today, and that they migrate when the flow velocity parallel to the contours is about 8 cm/sec. The sedimentation pattern may be explained solely on the basis of the water flow

pattern over a wave (figure 4.3 a and b).

In addition, the depositional nature of the small furrows superimposed on the sediment waves in Area 1 is emphasized by the view that they represent flow conditions during times when the depositional sediment waves are migrating.

While this model sucessfully predicts how the flow pattern over a sediment wave results in the upstream migration of that wave, it does not tell us what initially formed the waves. The lee waves were presumably originally formed when the flow encountered an obstacle of some type. The sediment waves then form when a sufficient sediment source is present nearby. Once a few sediment waves have formed, they will also generate lee waves and create more sediment waves downstream. Since sediment waves are often found on the downstream side of turbidity current channels, these channels may both generate the lee waves and provide the sediment source. Areas where there are well-documented sediment waves on the downstream side of turbidity current channels are in the Rockall Trough (section III.B), off northwest Africa (Jacobi et al., 1976), and off northeastern South America (Embley and Langseth, 1977). As far as is known, no such channel is present on the Blake-Bahama Outer Ridge, but some pre-drift topography may have been present. The presence of sediment waves therefore indicates that both steady currents and an abundant sediment source have been present for long periods of time.

Lee waves formed as water flows on to the continental shelf off Brittany appear to have generated a train of sand waves on La Chapelle Bank (Cartwright, 1959; Stride and Tucker, 1960). A similar mechanism appears to be responsible for the regular sediment waves.

As mentioned above, a similar lee-wave mechanism may be responsible for the downcurrent-migrating sediment waves in the Rockall Trough. Although the dynamics of the flow over an individual sediment wave is not known, it may be different from that observed in the upstream-migration case. For instance, tidal velocity fluctuations in the Rockall Trough are as large as the mean velocity, whereas on the Bahama Outer Ridge, tidal fluctuations are only about one third of the mean velocity. The flow direction over the wave will change more often in Rockall Trough, and flows like the ones observed on the BBOR may not have time to develop. The actual flow pattern could deposit more sediment on the downstream side, but the waves would have been triggered by a lee wave phenomena of some type.

The persistant upslope migration of the sediment waves is not explained by the lee-wave mechanism proposed. It is likely that the trends of the waves are related to the development of the sedimentary body on which they are found, much in the same that ripples are affected by the furrows and furrows by the sediment waves. Studies of the flow around these sedimentary bodies will be necessary in order to better understand the waves.

CHAPTER V

CONCLUSIONS

The following conclusions can be drawn from this study.

(1) Much of the microtopography of sedimentary areas under the influence of contour-following currents is controlled by those currents. Other important influences are downslope gravitational sediment movement and, in some areas, water seepage from the sediments.

(2) Furrows are widespread bed forms in the deep sea. These furrows, which may not be detected at all by surface-ship echo sounders if they are less than 1 to 2 m wide, often appear as regular hyperbolic echo traces superimposed on the sea-floor return. These furrows are an indication of current activity.

(3) All furrows are not the same. There are distinct differences between depositional and erosional furrows. Linear bed forms of some type (furrows?) are also associated with turbidity current channels. It is suggested that all furrows start as erosional features and some subsequently develop into depositional features. Once formed, furrows may continue as primarily depositional features under the influence of steady currents and with a sufficient sediment supply. If the sedi-mentation rate is higher on the wall of a depositional furrow than it is in the trough, the furrow will change shape with time, and will eventually close up. Thus

erosional and depositional furrows may be different stages in furrow evolution, with the life cycle proceeding from furrow erosion to a depositional furrow, to a smooth sea floor. This cycle may take many 100,000's of years for the largest features.

(4) Furrows are initially formed by the activity of large, organized secondary circulations (within the fluid flow) interacting with the sea-floor sediments. These circulations may be due to instabilities of the Ekman boundary layer or to the structure of turbulent flows in general. According to the model presented, furrows may mainly be formed rapidly during high-velocity current episodes. The nature or timing of such events is not known, although they may be related to glacial/ interglacial cycles in bottom water production.

(5) All hyperbolic echoes are not furrows. A large region of hyperbolic echoes in Rockall Trough is due to a debris flow. Similar debris flows have been mapped in other areas of the deep sea. Also, features described as hyperbolic echoes may result from sinusoidal topography with a small wavelength and a large amplitude.

(6) However, characteristics of hyperbolic echoes recorded on wide-beam surface echo-sounder recors can be used to distinguish between furrows and debris flows. Such charac- teristics include the regular spacing between and similar form of adjacent hyperbolic echoes over furrowed topography. Both the linear topographic elements and the zone of hyperbolic

echoes are parallel to the regional contours. Echoes from debris flows tend to be more variable in form and have irregular spacings. While the zone of hyperbolae cuts across the contours, the linear features (if any) can be aligned perpendicular to or parallel to the direction of flow movement.

(7) In the area affected by the Rockall Trough debris flow, the highest post-debris flow sedimentation rates are in areas of rough topography. This topography may create still regions where suspended sediments may fall out rapidly.

(8) Regular sediment waves found in zones parallel to the regional contours are formed by the interaction between steady currents and sea-floor sediments. They may be formed in equilibrium with lee waves generated by topographic features, such as submarine canyons, that the flow crosses, or with some type of unknown instability of contour-current flow. The sediment waves are found downstream of a sediment source, such as a submarine canyon. Once a few waves are developed, they may generate more lee waves downstream, thus extending the sediment wave field.

(9) Although many regular sediment waves follow similar distribution patterns, they do not all behave in a similar fashion. The waves on the BBOR are migrating upcurrent and upslope, while those on the Feni Drift appear to be migrating downcurrent and upslope. A major difference in the hydrography of these regions is the presence of relatively strong tidal

component superimposed on the mean flow on the Feni. The
sediment waves of the BBOR appear to be generating lee waves
in the overlying fluid. These lee waves and the associated
flow pattern influence sediment deposition over the wave, and
the waves migrate upstream. On the Feni, steady internal waves
may not develop as current directions are often changing. The
resulting flow pattern may lead to downstream migration.

(10) All sediment waves, and all bed forms in general, may
not have followed the same pattern of development, even in a
relatively restricted area. Some sediment waves in the Rockall
Trough have been active for most of the period under investiga-
tion, while others have almost been buried. On the BBOR, some
of the waves have been severely eroded, while others have not.

(11) A more complete understanding of the sediment waves
will have to include the sediment bodies on which the waves are
found. It is likely that the wave patterns are related to the
development of the next larger bed form. In the same way the
furrows are affected by the sediment waves, and the current
ripples by the furrows.

(12) Current ripples are developed as depositional
features in cohesive sediments. In areas under investigation,
the ripples occur on steep slopes. These ripples, oriented at
an angle to the mean flow when developed on the side of a fur-
row, may reflect secondary circulations within the furrows which
are due to the form of the trough.

(13) Longitudinal triangular ripples are developed in sandy muds. High velocities are probably required in order to form them.

(14) Understanding the ways in which the various bed forms are developed provides some information on the nature of the structure of the bottom boundary layer of the ocean. Assessing the dynamics and history of bed form development leads to a measure of how important, and how fast, deep currents have been in the past, and how they are presently shaping the form of the sediment surface.

REFERENCES CITED

Abbate, E., Bortolli, V., and Passerini, P., 1970. Olisto-
    stromes and olistoliths. Sediment. Geol., 4:521-557.

Allen, J.R.L., 1966. On bed forms and paleocurrents.
    Sedimentology, 6:153-190.

Allen, J.R.L., 1968a. On the character and classification
    of bed forms. Geologie en Mijnbouw, 47:173-185.

Allen, J.R.L., 1968b. Current Ripples; Their Relations to
    Patterns of Water and Sediment Movement. North Holland
    Publ. Co., Amsterdam, 433pp.

Allen, J.R.L., 1969. Erosional current marks of weakly
    cohesive mud beds. J. Sediment. Petrol., 39: 607-623.

Angell, J.K., Pack, D.H., and Dickson, C.R., 1968. A
    Lagrangian study of helical circulations in the planetary
    boundary layer. J. Atmos. Sci., 25: 707-717.

Amos, A.F., Gordon, A.L., and Schneider, E.D., 1971. Water
    masses and curculation patterns in the region of the
    Blake-Bahama Outer Ridge. Deep-Sea Res., 18: 145-165.

Andrews, J.E., 1967. Blake Outer Ridge: development by
    gravity tectonics. Science, 156: 642-645.

Armi, L., 1977. The dynamics of the bottom boundary layer of
    the deep sea. In: J.C.J. Nihoul (Editor), Bottom
    Turbulence, Elsevier, New York, pp. 153-164.

Armi, L., and Millard, R.C., 1976. The bottom boundary layer
    of the deep ocean. J. Geophys. Res., 81: 4983-4990.

Ballard, J.A., 1966. Structure of the lower continental rise
    hills of the western North Atlantic. Geophysics, 31:
    506-523.

Barrett, J.R., Jr., 1965. Subsurface currents off Cape
    Hatteras. Deep-Sea Res., 12: 173-184.

Belderson, R.H., Kenyon, N.H., Stride, A.H., and Stubbs, A.R.,
    1972. Sonographs of the Sea Floor, Elsevier, New York,
    185pp.

Benson, W.E., Sheridan, R.E., et. al., 1976. In the North
    Atlantic: deep-sea drilling. Geotimes, 21(2): 23-26.

Beverly, B.E., 1975. Consolidation characteristics of deep-sea sediments recovered with a giant piston corer: Blake-Bahama Outer Ridge area. M.S. Thesis, Dept. Civil Eng., Worcester Polytech. Inst. (Unpublished manuscript.)

Biscaye, P.E. and Eittreim, S.L., 1974. Variations in benthic boundary layer phenomena: nepheloid layer in the North American Basin. In: R.J. Gibbs (Editor), Suspended Solids in Water, Plenum, New York, pp. 227-260.

Bornhold, B.D. and Pilkey, O.H., 1971. Bioclastic turbidite sedimentation in the Columbus Basin, Bahamas. Geol. Soc. Am. Bull., 82: 1341-1354.

Bouma, A.H. and Treadwell, T.K., 1975. Deep-sea dune-like features. Mar. Geol., 19: M53-M59.

Broecker, W.S. and van Donk, J., 1970. Insolation changes, ice volumes, and the O^{18} record in deep sea cores. Rev. Geophys. and Space Physics, 8: 169-198.

Brown, R.A., 1970. A secondary flow model for the planetary boundary layer. J. Atmos. Sci., 27: 742-757.

Bryan, G.M., 1970. Hydrodynamic model of the Blake Outer Ridge. J. Geophys. Res., 75: 4530-4537.

Bryan, G.M. and Markl, R.G., 1966. Microtopography of the Blake-Bahama Region. Lamont-Doherty tech. rept. no.8 CU-8-66-NObsr 85077, 26pp.

Bush, P.A., 1976. Bathymetry of the MODE-I Region. Deep-Sea Res., 23: 1105-1113.

Carter, R.M., 1975. A discussion and classification of subaqueous transport with particular application to grain-flow,slurry-flow and fluxoturbidites. Earth-Sci. Rev., 11: 145-177, 1975.

Cartwright, D.E., 1959. On submarine sand waves and tidal lee waves. Proc. Royal Soc. Lond. A, 253: 218-241.

Clay, C.S. and Leong, W.K., 1974. Acoustic estimates of the topography and roughness spectrum of the sea floor south-west of Iberian Peninsula. In: L. Hampton (Editor), Physics of Sound in Marine Sediments, Plenum, New York, pp. 373-446.

Clay, C.S. and Rona, P.A., 1964. On the existence of bottom corregations in the Blake-Bahama Basin. J. Geophys. Res., 69: 231-234.

Cook, H.E., Johnson, P.D., Matti, J.C., and Zemmels, I., 1975. Methods of sample preparation and X-ray diffraction analysis, X-ray Mineralogy Laboratory, Deep-Sea Drilling Project, University of California, Riverside. In: Hayes, D.E., Frakes, L.A., et al., Initial Reports of the Deep-Sea Drilling Project, vol. 28, Washington (U.S. Gov't Printing Office), pp. 999-1007.

Damuth, J.E., 1975a. Echo character of the western Equatorial Atlantic floor and its relationship to the dispersal and distribution of terrigenous sediments. Mar. Geol., 18:17-45.

Damuth, J.E., 1975b. Quaternary climate change as revealed by calcium carbonate fluctuations in western Equatorial Atlantic sediments. Deep-Sea Res., 22: 725-743.

Damuth, J.E. and Hayes, D.E., 1977. Echo character of the east Brazilian Continental Margin and its relationship to sedimentary processes. Mar. Geol., 24: 73-95.

Davies, T.A. and Laughton, A.S., 1972. Sedimentary processes in the North Atlantic. In: Laughton, A.S., Berggren, W.A., et al., Initial Reports of the Deep-Sea Drilling Project, vol. 12, Washington (U.S. Gov't Printing Office), pp. 905-934.

Deardorff, J.W., 1972. Numerical investigation of neutral and unstable planetary boundary layers. J. Atmos. Sci., 29: 91-115.

de Vanssay de Blavous, P., 1930. Slope corrections for echo sounding. Hyd. Rev., 7(2): 50-63.

Dott, R.H. Jr., 1963. Dynamics of subaqueous gravity depositional processes. Bull. Am. Assoc. Petrol. Geologists, 47: 104-128.

Dyer, K.R., 1970. Linear erosional furrows in Southampton Water. Nature, 225: 56-58, 1970.

Einstein, H.A. and Krone, R.B., 1962. Experiments to determine the modes of cohesive sediment transport in salt water. J. Geophys. Res., 67: 1451-1461.

Eittreim, S.L., Biscaye, P.E., and Amos, A.F., 1975. Benthic nepheloid layers and the Ekman thermal pump. J. Geophys. Res., 80: 5061-5067.

Eittreim, S.L., Thorndike, E.M., and Sullivan, L., 1976.
Turbidity distribution in the Atlantic Ocean. Deep-Sea
Res., 23: 1115-1127, 1976.

Ekman, V.W., 1908. Die Zusammendruechbarkeit des Meerwassers
nebst einigen Werten fuer Wasser und Queksilber. Publs
Circonst. Cons. Perm. int. Explor. Mer, 43: 1-47.

Ellett, D.J. and Roberts, D.G., 1973. The overflow of Nor-
wegian Sea Deep Water across the Wyville-Thompson Ridge.
Deep-Sea Res., 20: 819-835.

Embley, R.W., 1975. Studies of deep-sea sedimentation proces-
ses using high-frequency seismic data. Ph.D. Thesis,
Columbia University, New York, 334pp. (Unpublished
manuscript.)

Embley, R.W., 1976. New evidence for occurence of debris
flow deposits in the deep sea. Geology, 4: 371-374.

Embley, R.W. and Hayes, D.E., 1972. Site survey report for
Site 142. In: Hayes, D.E., Pimm, A.C., et al., Initial
Reports of the Deep-Sea Drilling Project, vol. 14,
Washington (U.S. Gov't Printing Office), pp. 377-388.

Embley, R.W. and Jacobi, R., in press. Distribution and
morphology of large sediment slides and slumps on
Atlantic continental margins. Marine Geotech.

Embley, R.W. and Langseth, M.G., 1977. Sedimentation processes
on the continental rise of northeastern South America.
Mar. Geol., 25: 279-297.

Emery, K.O., 1974. Pagoda structures in marine sediments.
In: I. Kaplan (Editor), Natural Gasses in Marine Sediments,
Plenum, New York, pp. 309-317.

Ericson, D.B., Ewing, M., Wollin, G., and Heezen, B.C., 1961.
Atlantic deep-sea cores. Bull. Geol. Soc. Am., 72: 193-286.

Ericson, D.B. and Wollin, G., 1968. Pleistocene climatic
and chronology in deep-sea sediments. Science, 162: 1227-1234.

Ewing, J.I., Ewing, M., and Leyden, R., 1966. Seismic profiler
survey of Blake Plateau. Amer. Assoc. Petrol. Geol. Bull.,
50: 1948-1971.

Ewing, J.I. and Hollister, C.D., 1972. Regional aspects of deep
sea drilling in the western North Atlantic. In: Hollister,
C.D., Ewing, J.I., et al., Initial Reports of the Deep-

Sea Drilling Project, vol. 11, Washington (U.S. Gov't Printing Office), pp. 951-973.

Ewing, M., Aitken, T., and Eittreim, S., 1968. Giant Ripples in the Madagascar Basin (abstract). Trans. Amer. Geophys. Un., 49: 218.

Ewing, M., Eittreim, S.L., Ewing, J.I., and LePichon, X., 1971. Sediment transport and distribution in the Argentine Basin. 3. Nepheloid layer and process of sedimentation. Phys. and Chem. of the Earth, 8: 48-77.

Ewing, M., Embley, R.W., and Shipley, T.H., 1973. Observations of shallow layering utilizing the pingerprobe echo-sounding system. Mar. Geol., 14: M55-M65.

Ewing, M. and Mouzo, F., 1968. Ocean bottom photographs in the area of oldest known outcrops, North Atlantic Ocean. Proc. Nat. Acad. Sci., 61: 787-793.

Ewing, M. and Ewing, J.I., 1964. Distribution of oceanic sediments. In: Studies in Oceanography, Tokyo (Geophys. Institute, U. Tokyo), pp. 525-537.

Faller, A.J., 1963. An experimental study of the instability of the laminar Ekman boundary layer. J. Fluid Mech., 5: 560-576.

Faller, A.J. and Caponi, E.A., 1977. A laboratory study of wind-driven Langmuir circulations. Tech. note BN-861, Univ. of Maryland, 57pp.

Faller, A.J. and Kaylor, R., 1967. Instability of the Ekman spiral with applications to the planetary boundary layers. Phys. of Fluids, 10: S212-S219.

Flood, R.D., in press. X-ray mineralogy of DSDP Legs 44 and 44A, western North Atlantic: lower continental rise hills, Blake Nose and Blake-Bahama Basin. In: Benson, W.E., Sheridon, R.E., et al., Initial Reports of the Deep-Sea Drilling Project, vol 44, Washington (U.S. Gov't Printing Office).

Flood, R.D. and Hollister, C.D., 1974. Current-controlled topography on the continental margin off the Eastern United States. In: C.A. Burk and C.L. Drake (Editors), The Geology of Continental Margins, Springer-Verlag, New York, pp197-205.

Fofonoff, N.P., 1977. Computation of potential temperature of seawater for an arbitrary reference pressure. Deep-Sea Res., 24: 489-491.

Folk, R.L., 1971. Longitudinal dunes of the Northwestern edge of the Simpson Desert, Northern Territory, Australia, 1. Geomorphology and grain size relationships. Sedimentology, 16: 5-54.

Folk, R.L., 1974. Petrology of Sedimentary Rocks, Hemphill Publishing Co., Austin, 182pp.

Fox, P.J., Heezen, B.C., and Harian, A.M., 1968. Abyssal antidunes. Nature, 220: 470-472.

Glenn, M.F., 1970. Introducing an operational multi-beam array sonar. Int. Hyd. Rev., 67(1): 35-39.

Gordon, C.M., 1975. Sediment entrainment and suspension in a turbulent tidal flow. Mar. Geol., 18: M57-M64.

Gordon, C.M. and Witting, J., 1977. Turbulent structure in a benthic boundary layer. In: J.C.J. Nihoul (Editor), Bottom Turbulence, Elsevier, New York, pp. 59-81.

Gregory, N., Stuart, J.T., and Walker, W.S.R., 1955. On the stability of three-dimensional boundary layers with application to the flow due to a rotating disk. Phil. Trans. Royal Soc. Lond., A, 248: 155-199.

Hagedoorn, J.G., 1954. A process of seismic reflection interpretation. Geophys. Prosp., 2: 85-127.

Hanna, S.R., 1969. The formation of longitudinal sand dunes by large helical eddies in the atmosphere. J. Appl. Met., 8: 874-883.

Harms, J.C., 1969. Hydraulic significance of some sand ripples. Geol. Soc. Am. Bull., 80: 363-396.

Hathaway, J.C., 1972. Regional clay mineral facies in estuaries and continental margin of the United States east coast. Geol. Soc. Am. Memoir 133, pp 293-315.

Hays, J.D., Imbrie, J., and Shackleton, N.J., 1976. Variations in the earth's orbit: pacemaker of the ice ages. Science, 194: 1121-1132.

Heezen, B.C. and Hollister, C.D., 1964. Deep-sea current evidence from abyssal sediments. Mar. Geol., 1:141-174.

Heezen, B.C. and Hollister, C.D., 1971. The Face of the Deep, Oxford University Press, New York, 695 pp.

Heezen, B.C., Hollister, C.D., and Ruddiman, W.F., 1966. Shaping of the continental ride by deep geostrophic contour currents. Science, 152: 502-508.

Heezen, B.C., Tharp, M., and Ewing, M., 1959. The Floors of the Oceans -- I. The North Atlantic. Geol. Soc. Am. Special Paper 65, 122 pp.

Hersey, J.B., Bunce, E.T., Wyrick, R.F., and Dietz, F.T., 1959. Geophysical investigation of the continental margin between Cape Henry, Virginia, and Jacksonville, Florida. Geol. Soc. Am. Bull., 70: 437-466.

Hilterman, F.J., 1970. Three-dimensional seismic modeling. Geophysics, 35: 1020-1037.

Hoffman, J., 1957. Hyperbolic curves applied to echo sounding. Int. Hyd. Rev., 34(2): 45-55.

Hollister, C.D., 1967. Sediment distribution and deep circulation in the western North Atlantic. Ph.D. Thesis, Columbia University, New York. (Unpublished manuscript.)

Hollister, C.D., Flood, R.D., Johnson, D.A., Lonsdale, P.F., and Southard, J.B., 1974a. Abyssal furrows and hyperbolic echo traces on the Bahama Outer Ridge. Geology, 2: 395-400.

Hollister, C.D. and Heezen, B.C., 1972. Geologic effects of ocean bottom currents: western North Atlantic. In: A.L. Gordon (Editor), Studies in Physical Oceanography, Gordon and Breach, New York, 2: 37-66.

Hollister, C.D., Johnson, D.A., and Lonsdale, P.F., 1974b. Current-controlled abyssal sedimentation: Samoan Passage, Equatorial West Pacific. J. Geol., 82: 275-300.

Hollister, C.D., Silva, A.J., and Driscoll, A., 1973. A giant piston corer. Ocean Engng., 2: 159-168.

Hollister, C.D., Southard, J.B., Flood, R.D., and Lonsdale, P.F., 1976. Flow phenomena in the benthic boundary layer and bed forms beneath deep current systems. In: I.N. McCave (Editor), The Benthic Boundary Layer, Plenum, New York, pp. 183-204.

Huppert, H.E., 1968. Appendix to paper by J.W. Miles. J. Fluid Mech., 33: 803-814.

Ivers, W., 1975. The deep circulation in the North Atlantic. Ph.D. Thesis, Univ. of California, San Diego, Calif., 179 pp. (Unpublished manuscript.)

Jackson, R.G., 1976. Sedimentological and fluid-dynamic implications of the turbulent bursting phenomenon in geophysical flows. J. Fluid Mech., 77: 531-560.

Jacobi, R.D., 1976. Sediment slides on the northwestern continental margin of Africa. Mar. Geol., 22: 157-173.

Jacobi, R.D., Rabinowitz, P.D., and Embley, R.W., 1975. Sediment waves on the Moroccan Continental Rise. Mar. Geol., 19: M61-M67.

Johnson, D.A. and Bunce, E.T., 1977. Abyssal sediment waves in the Amirante Passage, western Indian Ocean. Woods Hole Oceanogr. Inst. Tech Rept. No. 77-7, 46 pp. (Unpublished manuscript.)

Johnson, G.L., Vogt, P.R., and Schneider, E.D., 1971. Morphology of the northeastern Atlantic and Labrador Sea. Deutsche Hydrographische Zietschrift, 24: 49-74.

Jones, E.J.W., Ewing, M., Ewing, J.I., and Eittreim, S., 1970. Influences of Norwegian Sea Overflow Water on sedimentation on the northern North Atlantic and Labrador Sea. J. Geophys. Res., 75: 1655-1680.

Karcz, I., 1970. Possible significance of transitional flow patterns in interpretations of origin of some natural bed forms. J. Geophys. Res., 75: 2869-2873.

Kennedy, R.J. and Fulton, J.F., 1961. Effect of secondary currents upon the capacity of a straight open channel. Transactions of the E.I.C., 5: 12-18.

Kennett, J.P. and Huddlestun, P., 1972. Abrupt climatic change at 90,000 YBP: faunal evidence from Gulf of Mexico cores. Quat. Res., 2: 384-395.

Kim, H.T., Kline, S.J., and Reynolds, W.C., 1971. The production of turbulence near a smooth wall in a turbulent boundary layer. J. Fluid Mech., 50: 133-160.

King, L.H. and MacLean, B., 1970. Pockmarks on the Scotian Shelf. Geol. Soc. Am. Bull., 81: 3141-3148.

Kline, S.J., Reynolds, W.C., Schraub, F.A. and Runstadler, P.W., 1967. The structure of turbulent boundary layers. J. Fluid Mech., 30: 741-773.

Knott, S.T., and Hersey, J.B., 1956. Interpretation of high-resolution echo-sounding techniques and their use in bathymetry, marine geophysics, and biology. Deep-Sea Res., 4: 36-44.

Knox, R.A. and Millard, R.C., 1973. Bottom sensing device for use with STD systems. Deep-Sea Res., 21: 419-421.

Kolla, V., Moore, D.G., and Curray, J.R., 1976a. Recent bottom-current activity in the deep western Bay of Bengal. Mar. Geol., 21: 255-270.

Kolla, V., Sullivan, L., Streeter, S.S., and Langseth, M.G., 1976b. Spreading of AABW and its effects on the floor of the Indian Ocean inferred from bottom water potential temperature, turbidity, and sea-floor photography. Mar. Geol., 21: 171-189.

Krause, D.C., 1962. Interpretation of echo sounding profiles. Int. Hyd. Rev., 39(1): 65-123.

Krone, R.B., 1962. Flume studies of the transport of sediment in estuarial shoaling processes. University of Californai Hydraulic Engineering Laboratory and Sanitation Res. Laboratory, Berkley, Calif. 110 pp.

Kuettner, J., 1959. The band structure of the atmosphere. Tellus, 11: 267-294.

Kuettner, J. 1971. Cloud bands in the earth's atmosphere. Tellus, 23: 404-426.

Laine, E.P., 1977. Geological effects of the Gulf Stream system in the North American Basin. Ph.D. Thesis, Mass. Inst. of Tech.-Woods Hole Oceanogr. Inst. Joint Program in Oceanogr., Woods Hole, Mass., 147pp. (Unpublished manuscript.)

Lahee, F.H., 1952. Field Geology. McGraw-Hill, New York, 883 pp.

Langmuir, I., 1938. Surface water motions induced by wind. Science, 87: 119-123.

Laughton, A.S., 1962. Discrete hyperbolic echoes from an otherwise smooth sea floor. Deep-Sea Res., 9: 218.

Laughton, A.S., 1975. Tectonic evolution of the northeast Atlantic: a review. Norges. Geol. Unders., 316: 169-193.

Lohmann, G.P., 1974. Paleo-oceanography of the Oceanic Formation, Barbados, West Indies. Ph.D. Thesis, Brown Univ., Providence, R.I., 130 pp. (Unpublished manuscript.)

Lohmann, G.P., 1977. Increased and decreased production of Atlantic deep waters during ice ages: benthonic foraminifera evidence from the Vema Channel (abstract). EOS, Trans. Amer. Geophys. Un., 58: 416.

Lonsdale, P.F., 1974. Abyssal geomorphology of a depositional environment at the exit of the Samoan Passage. Ph.D. Thesis, Univ. of California, San Diego, Calif., 106 pp. (Unpublished manuscript.)

Lonsdale, P. and Hollister, C.D., 1976. Cut-off of an abyssal meander in the Icelandic insular rise (abstract). EOS, Trans. Amer. Geophys. Un., 57: 269.

Lonsdale, P. and Hollister, C.D., in press. A near-bottom traverse of Rockall Trough: hydrographic and geological inferences. Deep-Sea Res.

Lonsdale, P. and Spiess, F.N., 1977. Abyssal bed forms explored with a deeply towed instrument package. Mar. Geol., 23: 57-75.

Lonsdale, P.F., Spiess, F.N., and Mudie, J.D., 1973. Erosional furrows across the abyssal Pacific floor (abstract). EOS, Trans, Amer. Geophys. Un., 54: 1110.

Luskin, B., Heezen, B.C., Ewing, M., and Lansidman, M., 1954. Precision measurement of ocean depth. Deep-Sea Res., 1: 131-140.

Markl, R.G., Bryan, G.M., and Ewing, J.I., 1970. Structure of the Blake-Bahama Outer Ridge. J. Geophys. Res., 75: 4539-4555.

Matthews, D.J., 1939. Tables of the vleocity of sound in pure water and sea water for use in echo-sounding and sound ranging. H.D. 382, Hydrographic Department, Admiralty, 52pp.

Maul, G.A., Precise echo sounding in deep water. Int. Hyd. Rev., 47(2): 93-106.

McCave, I.N. and Swift, S.A., 1976. A physical model for the rate of deposition of fine-grained sediments in the deep sea. Geol. Soc. Am. Bull., 87: 541-546.

McGeary, D.F.R., and Damuth, J.E., 1973. Postglacial iron-rich crusts in hemipelagic deep-sea sediments. Geol. Soc. Am. Bull., 84: 1201-1212.

McIntyre, A., Ruddiman, W.F., and Jantzen, R., 1972. South-ward penetration of the North Atlantic Polar Front: faunal and floral evidence of large-scale surface water mass movements over the last 225,000 years. Deep-Sea Res., 19: 61-77.

McKinney, T.F., Stubblefield, W.L., and Swift, D.J.P., 1974. Large-scale current lineations on the central New Jersey shelf: investigation by side-scan sonar. Mar. Geol., 17: 79-102.

Melling, A. and Whitelaw, J.H., 1976. Turbulent flow in a rectangular duct. J. Fluid Mech., 78: 289-315.

Middleton, G.V. and Hampton, M.A., 1973. Sediment gravity flows: mechanics of flow and deposition. In: Middleton, G.V., and Bouma, A.H. (Editors), Turbidites and Deep-Water Sedimentation. Pacific Section SEPM, Los Angeles, Calif., pp. 1-38.

Milliman, J.D., 1974. Marine Carbonates, Springer-Verlag, New York, 375 pp.

Milliman, J.D., 1976. Late Quaternary sedimentation on Atlantic continental margins and the deep sea. An. Acad. bras. Ciênc., 48(Suppl.): 199-206.

Newton, R.S., Seibold, E., and Werner, F., 1973. Facies dist-ribution on the Spanish Sahara continental shelf mapped with side-scan sonar. Meteor Forsch., C(15): 55-77.

Nikuradse, J., 1950. Untersuchungen über turbulente Strömungen in nicht kreisförmigen Rohren. Ing. Arch., 1: 306-332.

Normark, W.R., 1974. Ranger submarine slide, northern Sebastian Vizcaino Bay, Baja California, Mexico. Geol. Soc. Am. Bull., 85: 781-784.

Olsson, I.D., 1968. Modern aspects of radiocarbon dating. Earth-Sci. Rev., 4: 203-218.

Owen, M.N., 1977. Problems in the modeling of transport, erosion, and deposition of cohesive sediments. In: E.D. Goldberg (Editor), The Sea, vol 6, Interscience, New York, pp. 515-537.

Partheniades, E., 1965. Erosion and deposition of cohesive soils. Proc. Am. Soc. Civil Eng., 91(HY1): 105-139.

Pekeris, C.L. and Accad, Y., 1969. Solution of Laplace's equation for the M_2 tide in the world oceans. Phil. Trans. Royal Soc. Lond., A, 265: 413-436.

Pratt, R.M. and Heezen, B.C., 1964. Topography of the Blake Plateau. Deep-Sea Res., 11: 721-728.

Prell, W.L. and Hays, J.D., 1976. Late pleistocene faunal and temperature patterns of the Columbian Basin, Carribbean Sea. In: R.M. Cline and J.D. Hays (Editors), Investigations of Late Quaternary Paleoceanography and Paleoclimatology. Geol. Soc. Am. Memoir 145, pp. 201-220.

Pujol, C., Duprat, J., Gonthier, E., Peypouquet, J-P, and Pujos-Lamy, A., 1974. Résultats préliminaires de l'étude effectuée par l'Institute de Géologie du Bassin d'Aquitaine concernant la mission Faegas (25 Jiun-17 Juillet 1973) dans l'Atlantique Nord-Est. Bull.Inst. Géol. Bassin Aquitaine, 16: 65-94.

Raudkivi, A.J., 1976. Loose Boundary Hydraulics, (2nd Edition), Pergamon, New York, 397 pp.

Rees, A.I., 1966. Some flume experiments with a fine silt. Sedimentology, 6: 209-240.

Richardson, P.L., 1977. On the crossover between the Gulf Stream and the Western Boundary Undercurrent. Deep-Sea Res., 24: 139-159.

Roberts, D.G., 1972. Slumping on the eastern margin of Rockall Bank, North Atlantic Ocean. Mar. Geol., 13: 225-237.

Roberts, D.G., 1975. Marine geology of the Rockall Plateau and Trough. Phil. Trans. Royal Soc. Lond., A, 278: 447-509.

Roberts, D.G., Hogg, N.G., Bishop, D.G., and Flewellen, C.G., 1974. Sediment distribution around moated seamounts in the Rockall Trough. Deep-Sea Res., 21: 175-184.

Rona, P.A., 1969. Linear "lower continental rise hills" off Cape Hatteras. J. Sediment. Petrol., 39: 1132-1141.

Ruddiman, W.F. and McIntyre, A., 1973. Time-transgressive retreat of polar waters from the North Atlantic. Quat. Res., 3: 117-130.

Rushby, J.S.M., 1970. A long-range side-scan sonar for use in the deep sea. Int. Hyd. Rev., 47: 25-39.

Schick, G.B., Issacs, J.D., and Sessions, M.N., 1968. Autonomous instruments in oceanographic research. Marine Sciences Instrumentation, vol 4, Plenum, New York, pp. 203-230.

Schroeder, F.W., 1976. A geophysical survey at Site 325 in the Bellingshausen Basin. In: Hollister, C.D., Craddok, C. et al., Initial Reports of the Deep-Sea Drilling Project, vol 35, Washington (U.S. Gov't Printing Office), pp. 251-261.

Seligman, G., 1963. Snow Structures and Ski Fields, Jos. Adams, Brussels, 555 pp.

Sharpe, C.F.S., 1968. Landslides and Related Phenomena, Cooper Square Publishers, New York, 137 pp.

Sheridan, R.E., Golovenko, X., and Ewing, J.I., 1974. Late Miocene turbidite horizon in Blake-Bahama Basin. Bull. Amer. Assoc. Petrol. Geologists., 58: 1797-1805.

Silva, A.J. and Hollister, C.D., in press. Geotechnical properties of ocean sediments recovered by a giant piston corer: Blake-Bahama Outer Ridge. Mar. Geol.

Silva, A.J. Hollister, C.D., Laine, E.P., and Beverly, B.E., 1976. Geotechnical properties of deep sea sediments: Bermuda Rise. Mar. Geotechnology, 1: 195-232.

Smith, S.G., 1977. A reflection profile modelling system. Geophys. J. R. Astr. Soc., 49: 723-737.

Spiess, F.N. and Mudie, J.D., 1970. Small-scale topographic and magnetic features. In: A.E. Maxwell (Editor), The Sea, vol.4, Wiley, New York, pp. 205-250.

Spiess, F.N. and Tyce, R.C., 1973. Marine Physical Laboratory deep tow instrumentation system. Scripps Institution of Oceanogr. Ref. 73-4. 37 pp.

Sternberg, R.W., 1968. Friction factors in tidal channels with differing bed roughness. Mar. Geol., 6: 243-260.

Stommel, H., 1958. The abyssal circulation, Deep-Sea Res., 5: 80-82.

Stommel, H. and Arons, A.B., 1960. On the abyssal circulation of the worlds oceans-II. An idealized model of the circulation pattern and amplitude in oceanic basins. Deep-Sea Res., 6: 217-233.

Stride, A.H., Belderson, R.H., and Kenyon, N.H., 1972. Longitudinal furrows and depositional sand bodies of the English Channel. Mémoire du B.R.G.M., 79: 233-240.

Stride, A.H. and Tucker, M.J., 1960. Internal waves and waves of sand. Nature, 188: 933.

Swallow, J.C. and Worthington, L.V., 1961. An observation of a deep counter current in the western North Atlantic. Deep-Sea Res., 8: 1-19.

Thierstein, H.R., Geitzenauer, K.R., Molfino, B., and Shackleton, N.J., 1977. Global syncroneity of late Quaternary coccolith datum levels: validation by oxygen isotopes. Geology, 5: 400-404.

Tucholke, B.E., 1974. Determination of montmorillonite in small samples and implications for suspended-matter studies. J. Sediment. Petrol., 44: 254-258.

Tucholke, B.E., 1975. Sediment distribution and deposition by the Western Boundary Undercurrent: the Greater Antilles Outer Ridge. J. Geol., 83: 177-207.

Tucholke, B.E., Bryan, G.M., and Ewing, J.I., 1977. Gas-hydrate horizons detected in seismic profiler data from the western North Atlantic. Bull. Amer. Assoc. Petrol. Geologists, 61: 698-707.

Tucholke, B.E. and Ewing, J.I., 1974. Bathymetry and sediment geometry of the Greater Antilles Outer Ridge and vicinity. Geol. Soc. Am. Bull., 85: 1789-1802.

Tucholke, B.E. and Houtz, R.E., 1976. Sedimentary framework of the Bellingshausen Basin from seismic profiler data. In: Hollister, C.D., Craddok, C., et al., Initial Reports of the Deep-Sea Drilling Project, vol 35, Washington (U.S. Gov't Printing Office), pp. 197-228.

Tucholke, B.E., Wright, W.R., and Hollister, C.D., 1973. Abyssal curculation over the Greater Antilles Outer Ridge. Deep-Sea Res., 20: 973-995.

Turner, J.S., 1973. Buoyancy Effects in Fluids, Cambridge Univ. Press, New York, 368 pp.

Tyce, R.C., 1976. Near-bottom observations of 4 kHz acoustic reflectivity and attenuation. Geophysics, 41: 673-699.

van Straaten, L.M.J.U., 1951. Longitudinal ripple marks in mud and sand. J. Sediment. Petrol., 21: 47-54.

van Weering, T., Jansen, J.H.F., and Eisma, D., 1973. Acoustic reflection profiles of the Norwegian channel between Oslo and Bergen. Neth. J. of Sea Res., 6: 241-263.

Walker, J.R. and Massingill, J.V., 1970. Slump features on the Mississippi Fan, northeastern Gulf of Mexico. Geol. Soc. Am. Bull., 81: 3101-3108.

Werner, F. and Newton, R.S., 1975. The pattern of large-scale bed forms in the Langland Belt (Baltic Sea). Mar. Geol., 19: 29-59.

Worthington, L.V., 1976. On the North Atlantic Circulation, Johns Hopkins Oceanographic Series, no. 6, Johns Hopkins Univ. Press, Baltimore, 110pp.

Worthington, L.V. and Wright, W.R., 1970. North Atlantic Ocean atlas of potential temperature and salinity in the deep water, including the temperature, salinity, and oxygen profiles from the Erika Dan cruise of 1962. Woods Hole Oceanogr. Inst. Atlas, Ser. 2, 58 plates.

Wüst, G., 1936. Das Bodenwasser und die Gliederung der Atlansischen Tiefsee: Deutsche Atlantische Exped. METEOR 1925-1927, Wiss. Erg., Bd. 6, 1 Teil, Berlin, Walter de Gruyter and Co.

Young, R.A., 1975. Flow and sediment properties influencing erosion of fine-grained marine sediments: sea floor and laboratory experiments. Ph.D. Thesis, Mass. Inst. of Tech.-Woods Hole Oceanogr. Inst. Joint Prog. in Oceanogr., Woods Hole, Mass., 202pp. (Unpublished manuscript.)

Young, R.A., 1977. Seaflume: a device for in-situ studies of threshold velocity and erosional behavior of undisturbed muds. Mar. Geol., 23: M11-M18.

Zemmels, I. and Cook, H.E., 1976. X-ray mineralogy from the Nazca Plate-Leg 34 Deep Sea Drilling Project. In: Yeats, R.S., Hart, S.R., et al., Initial Reports of the Deep-Sea Drilling Project, vol. 34, Washington (U.S. Gov't Printing Office), pp. 589-600.

Zimmerman, H.B., 1971. Bottom currents on the New England Continental Rise. J. Geophys. Res., 76: 5865-5876.

APPENDIX I

MECHANICS OF SIDE ECHOES FROM TOPOGRAPHIC FEATURES
AND INTERPRETATION OF ECHO-SOUNDING PROFILES

Many of the features described in this work were

first observed on surface-ship echo-sounding profiles as

ambiguous types of echo returns. Some of the difficulties

in studying these features have been due to the deep water in

which these features are found and to the large beam angle

(30° to 60°) of conventional surface-ship echo sounders.

This combination results in an echo-sounding profile which

can be quite different from the true sea-floor morphology.

Many areas of the deep sea have been mapped on the basis of

their distinctive echo character; but unless detailed near-

bottom investigations are undertaken, the nature of the

topography responsible for these echo characters remains un-

known.

A number of echo-character classifications have been

developed for surface-ship echo-sounding profiles (e.g.,

Damuth, 1975a); however, knowledge of the relationship between

the sea-floor morphology and the surface echo trace is needed

in order to relate the echo character to the form and

structure of the features on the sea floor. The purpose of

this section is to review the mechanics of formation of side

echoes from topographic features, to point out some of the

difficulties in determining the structure of relatively small

sedimentary features in the deep sea by surface echo sounders, to give some examples of sub-bottom echo-sounding profiles over certain types of structural features, and to provide some realistic criteria for the interpretation of these profiles.

A. HYPERBOLIC ECHOES

Many types of echo returns are included in the category of hyperbolic echoes. Strictly, hyperbolic echoes are formed only when the surface ship passes near or over a point re-flector of sound energy. In instances where the topographic elements of the sea floor do not act as point reflectors, for example the large sediment waves, the resulting echo is more properly described just as a side echo. Side echoes of this type will be discussed in a subsequent section.

Hoffman (1957) has shown that any peak or sharp change in slope on the bottom will give a hyperbolic echo trace. The dimensions of the hyperbola will depend on water depth as well as on ship speed, paper feed rate, and depth scale of the echo sounder. If the feature responsible for the hyper-bolic echo is linear rather than a point, the form of the echo will also depend on the angle at which the linear feature is crossed (Bryan and Markl, 1966). One can calcu-late the angle that such a linear feature makes with the ship track from the form of the hyperbola. There is an ambiguity

in the solution, as the linear feature may lie at an angle either to the right or to the left of the ship track. Two or more intersecting tracks are needed in order to determine the actual orientation (Figure A1.1a).

A form of the equation presented by Bryan and Markl (1966) determined for a speed of sound in water of 800 fm/sec is as follows:

$$\sin \theta = \frac{24}{v_o} \frac{T}{(T^2 - T_m^2)} \frac{dT}{dt}$$

Where: θ = angle between linear feature and ship track

v_o = ship's speed (knots)

T_m = two-way travel time to apex of hyperbola (sec)

T = two-way travel time to a point on the side of the hyperbola (sec)

$\frac{dT}{dt}$ = slope of the side of the hyperbola at the point where T is measured (dT in seconds, dt in minutes)

The trend of the linear feature responsible for the hyperbolic echo can be determined more directly if there is a surface ship available. If the ship travels in a circle with a diameter of a few hundred meters, the ship will alternately run parallel to and perpendicular to the linear features. If the ship's heading is recorded during this maneuver, the heading which corresponds to the ship running parallel to the linear features, and thus the trend of the linear features,

A. HYPERBOLIC ECHO

B. VARIABLE SLOPE SIDE ECHO
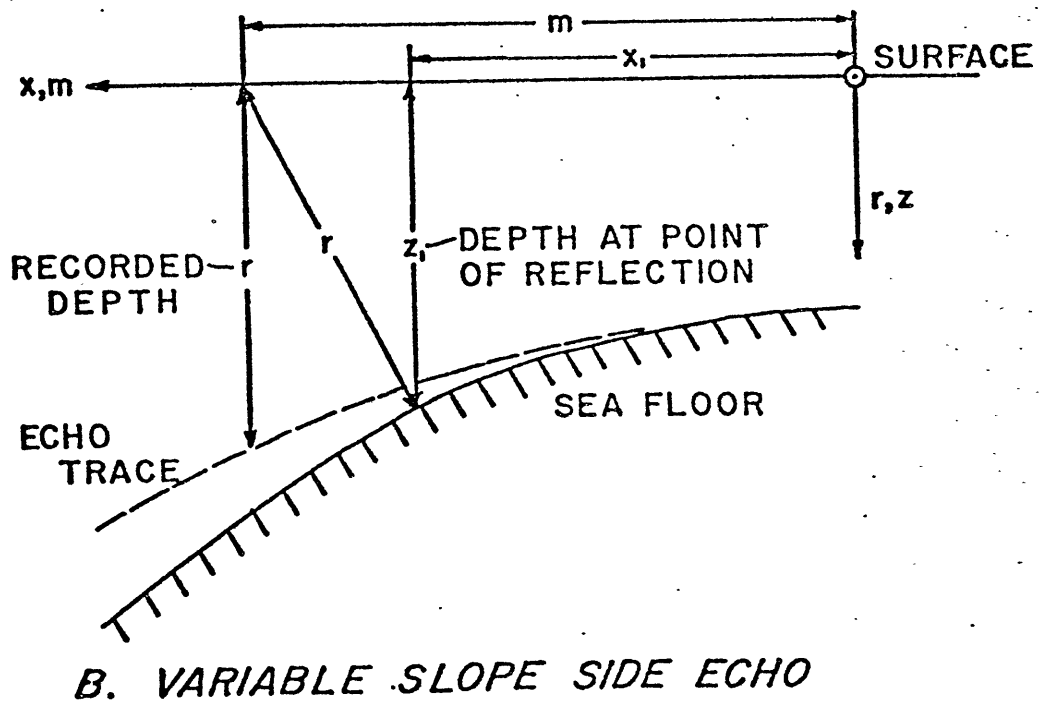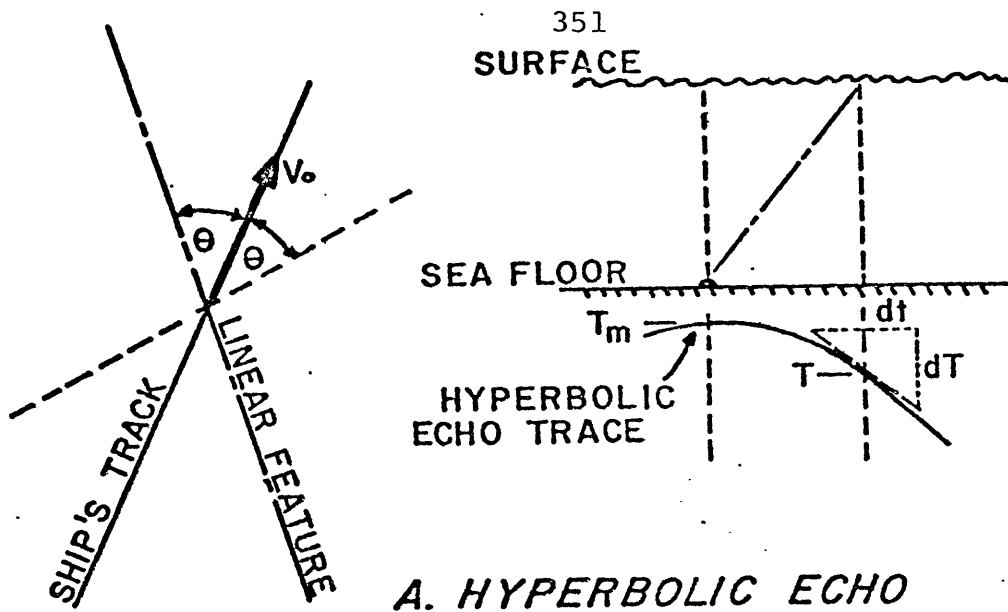
Figure A1.1   Parameters involved in the calculation of an echo-sounding profile.

(a) Hyperbolic echo from a linear feature. (After Bryan and Markl, 1966).

(b) Side echo over a feature of arbitrary slope. (After Krause, 1962.)

can be determined. This method was successfully used by Embley (1975) to determine the orientation of linear features off N. W. Africa and in Section II.B.1 of this work to determine the orientation of linear features on the Blake-Bahama Ourter Ridge.

B. SIDE ECHOES FROM SINUSOIDAL TOPOGRAPHY

The role of side echoes from surface echo sounders in obscuring the true shape of the sea floor has long been appreciated. Many investigators have modelled echo-sounding profiles which can result from various sea floor topographies (e.g., de Vanssay de Blavous, 1930; Hoffman, 1957; Krause, 1962) and have studied the related problem of interpreting seismic profiles on land as well as at sea (e.g., Hagedoorn, 1954; Hilterman, 1970; Smith, 1977). The objective of this section is to derive the shape of an echo-sounding profile over a two-dimensional, sinusoidal sea floor (an easily used function which is fairly close to the sea-floor shape in some situations of interest in this study), to determine how that echo-sounding profile changes as the dimensions of the wave and the water depth change, to observe how the problem is complicated by the addition of sub-bottom reflectors, and to point out some of the pitfalls in interpreting the resulting echograms.

The relationships used for determination of the shape of

the side echo come from Krause (1962). The quantities used in the following equations are shown in Figure Al.lb. For a sea floor represented by an equation of the form z = f(x), the echogram will be given by the following equations:

$$m(x) = x + f(x) \ f'(x) \qquad (Al.1)$$

$$r(x) = f(x) \ (1 + (f' \ (x))^2)^{\frac{1}{2}} \qquad (Al.2)$$

where m(x) and r(x) are parametric expressions for the echo trace. These equations will predict the shape of the echo returned from any two-dimensional sea floor shape for which the depth (f(x)) and the slope (f'(x)) can be specified for a sufficient number of values of x. The assumptions involved in this treatment are that the bottom is two-dimensional, the reflection is specular, and the feature is crossed perpendicular to its strike.

For two-dimensional features, the shape of the surface echo will vary as the feature is crossed at different angles. As the character of the returned echo is due primarily to the large diameter of the sea-floor area insonified (diameter of insonified area is 2 A tan ϕ, where A is water depth and ϕ is echo-sounding beam half-width, usually about 30°), the basic characteristics of the echo returned over the trough will be independent of the angle at which the feature is crossed. However, the wavelength of the feature on the echogram will vary as the cosecant of the angle between the ship's track and the long axis of the feature. The wavelength of the recorded

echogram will therefore be a minimum when the ship is crossing normal to the feature, and will approach infinity when the ship runs parallel to the features. This dependence of the apparent wavelength on the ship's heading can also be used to determine the strike of the sea-floor feature.

The equations of Krause (1962) are readily applied to a sinusoidal feature of the form $f(x) = A - B \cos (\frac{2\pi}{\lambda}x)$, a wave of amplitude B (one-half peak-to-peak) and wavelength λ at an average depth of A (Appendix II). Depth is taken as positive in the down direction. The slope of the wave surface is $f'(x) = \frac{2\pi B}{\lambda} \sin (\frac{2\pi}{\lambda} x)$. Equations derived for $\frac{m(x)}{\lambda}$ and $\frac{r(x) - A}{B}$ (normalized by the wavelength and amplitude of the sine wave, equations A2.3 and A2.4, Appendix II) show that, for B less than about ten percent of A, the shape of the echo-sounding profile depends only on the quantity $\frac{AB}{\lambda^2}$. For reasons which will be clear below, the parameter S, where $S = \frac{4\pi^2 A B}{\lambda^2}$, will be used to specify the shape of the resulting echo-sounding profile. If two different combinations of A, B, and λ have the same value of S, the echo-sounding profiles will be similar. Doubling the wave amplitude or the water depth will double the value of S, while doubling the wavelength will quarter the value of S. Examples of surface echo-sounding profiles and the related bathymetric profile calculated for various values of the parameter S are shown

in Figure Al.2a-f.

An important change in the character of the returned echo occurs when the radius of curvature of the wave trough is equal to the water depth (S=1). If the radius of curvature of the wave trough is greater than the water depth (S ≤1), only one echo will be received at the surface at any given time. If the radius of curvature of the wave trough is less than the water depth (S>1), side echoes from the wave crests will cross in the troughs and echoes can be received from more than one point of the wave at a time.

If the sea floor surface is not sinusoidal, but has a broader trough than a sine wave with the same amplitude and wavelength, overlapping side echoes will occur in the wave trough at larger values of S. The converse is true for waves with narrow troughs.

The convex wave crests and the concave wave troughs respectively defocus and focus the reflected sound waves, thus reflections from wave crests are weak while those from wave troughs are strong. Triangular tick marks on the echograms of Figure Al.2a-f indicate points which are reflections from the regularly spaced circular tick marks on the associated bathymetric profile. These tick marks give a rough indication of the way sound waves are focused and defocused by the topographic forms under discussion. Where the

Figure A1.2. Echo-sounding profiles for a sine wave with different values of S, where

$$S = \frac{4\pi^2\ AB}{\lambda^2}$$

Profiles normalized to unit wavelength and amplitude. V.E. = 10x.

a: S = 0.25
b: S = 0.5
c: S = 1.0
d: S = 2.0
e: S = 4.0
f: S = 8.0

S=0.25
a

S=0.5
b

S=1.0
c

S=2.0
d

S=4.0
e

S=8.0
f

▲—▲—▲ ECHOGRAM
⊶—⊶—⊶ BATHYMETRY
V.E.=10X

$$S = \frac{4\pi^2 AB}{\lambda^2} ;$$

A=WATER DEPTH
B=WAVE AMPLITUDE
(1/2 PEAK-TO-PEAK)
λ=WAVELENGTH

Figure A1.2

357
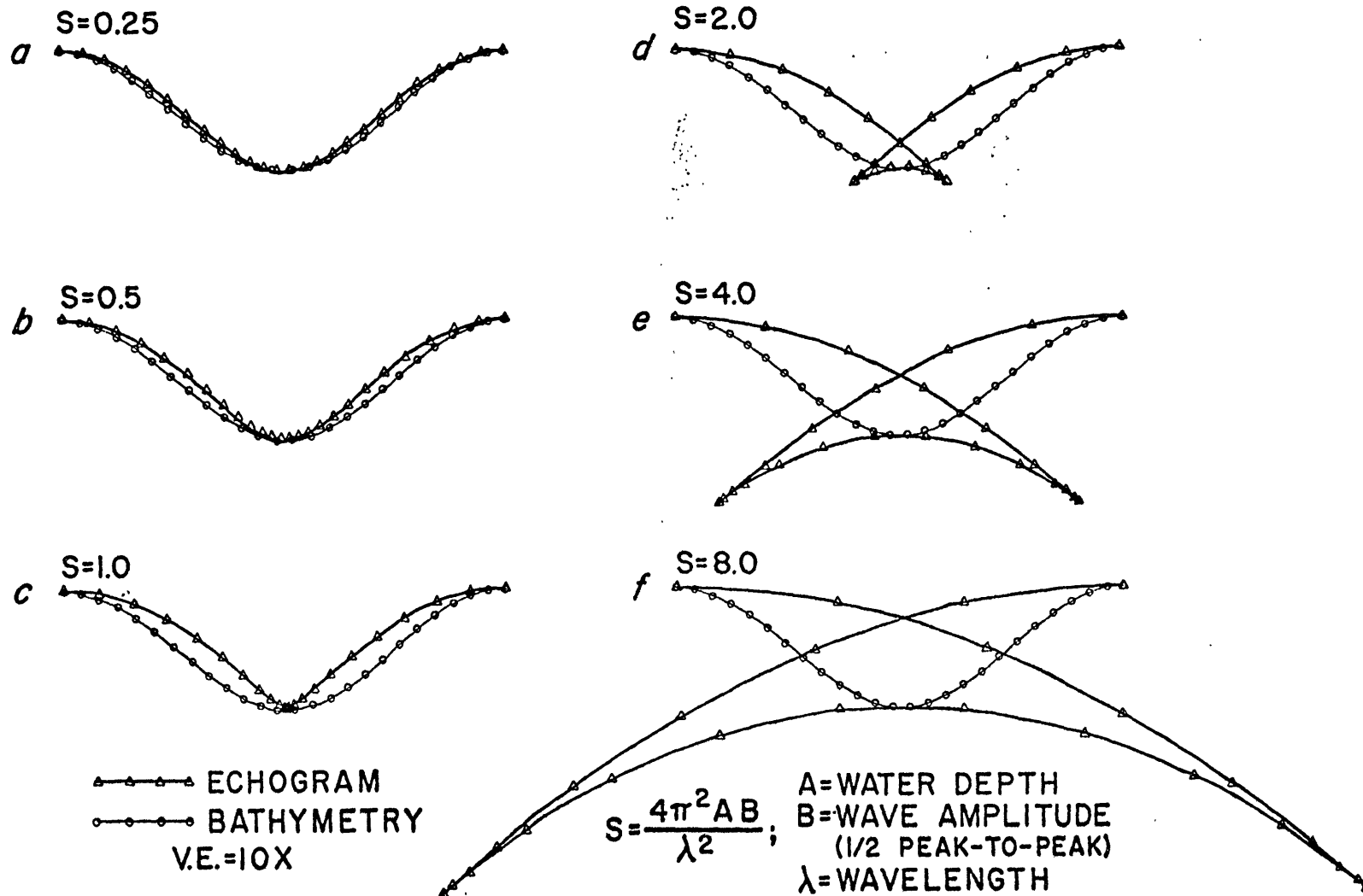
triangular tick marks are far apart, the intensity of the reflected sound is low, and, conversely, where the tick marks are close together, the intensity of the reflected sound is high. For S less than or equal to 1, the reflected echo is weaker over wave crests and stronger over wave troughs (Figure Al.2 a-c). In cases where side echoes from crests cross in the troughs (S greater than 1) (Figure Al.2 d-f)the intensity of the reflected sound is greatest at ends of the side-echo arms, weaker in the center of the wave trough, and weakest over the wave crest. Quantitative estimates of effects of focusing and defocusing on the intensity of the reflected echo have been made by Tyce (1976) for cases of concave and convex cylindrical and spherical sediment surfaces.

A regular sea-floor pattern, like these sinusoidal waves, can thus create an echo pattern showing characteristics which could be interpreted as variations in the nature of sea-floor sediments. Interpretation of variations in intensity of the reflected energy must therefore be treated with caution.

C. SIDE ECHOES AND SUB-BOTTOM PROFILES

The high-frequency echo sounders in use on many oceanographic ships today are designed to show reflections from buried reflecting horizons within the sediments. Since these 3.5 kHz echo sounders generally have beam widths which are

comparable to those of conventional higher-frequency echo sounders (e.g., 12 kHz), the relationship between the shape of a reflecting horizon and the shape of the resulting sub-bottom profile will be similar.

As a rough approximation (valid because of the small velocity gradients in near-surface sediments), the profile which results from a particular combination of sub-bottom layers will be similar to the superposition of the echoes from each layer, where each layer is in turn treated as the sediment surface. However, in order to approach the problem more rigorously, and to develop techniques which may be applicable to a more general range of problems, a computer program was written which includes the effects of sound refraction between layers of constant, but different, sound velocity. A description of the FORTRAN IV program, which converts a given depth section into a reflection record, is in Appendix II.

As presently configured, the program requires that the bottom and up to four sub-bottoms be sinusoidal waves of the same wavelength and the same regional gradient. The amplitudes of the various interfaces, their phase relationships, thicknesses, and sound velocities can be independently specified. As output, the program draws two plots. The first plot is labled "TRUE BATHYMETRY" and is the given depth section. The second plot, labeled "ECHOGRAM", shows the profile

calculated for the given depth section with time on the vertical axis. Both plots have vertical exaggerations of ten to one and are similar in proportions to a typical 3.5 kHz echo-sounding record. Triangular tick marks are drawn on the echogram to show positions of reflections at the water surface for sound reflected from evenly-spaced circular tick marks on the true bathymetry plot. The spacing between the triangular tick marks indicate variations in reflected energy over the sea floor.

This program can, in principal, be generalized to apply to sea-floor features of arbitrary shape, as well as to other specific bathymetric functions of interest.

Sub-bottom profiles have been calculated for four hypothetical sea-floor structures. The first three situations, a migrating sediment wave, (Figure A1.3) a filling trough (Figure A1.4), and a stationary sediment wave (Figure A1.5 a,b), appear to be represented in the oceans. In the first two cases, an echogram was calculated for the given structure for each of two different water depths. At the shallower depth, the structure of the sea floor, while slightly distorted, is still evident on the acoustic profile. At the deeper depth, the structure of the sea bottom has been significantly obscured by side echoes, and some care is required in order to interpret the resulting profile. Where appropriate, examples of 3.5 kHz records which show features similar to those

Figure A1.3. Sub-bottom profiles of a migrating ridge
(V.E.= 10X).

Shallow Water
(a) True Bathymetry
(b) Echogram
     Depth   = 2500 m
     Wavelength   = 2100 m
     Amplitude   =   30 m
     Layer Spacing   =   10 m
     Gradient   = 1:100
     S   =   0.67 to 0.68

Deep Water
(c) True Bathymetry
(d) Echogram
     Same parameters as a,b, except depth =
     5500 m and S = 1.48 to 1.49.
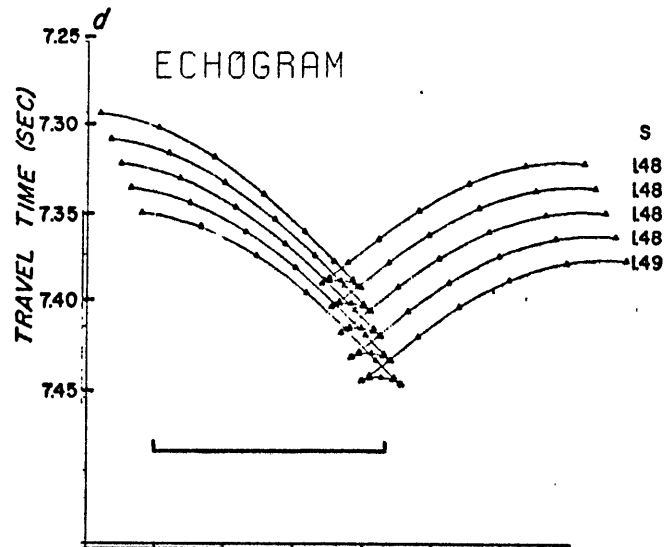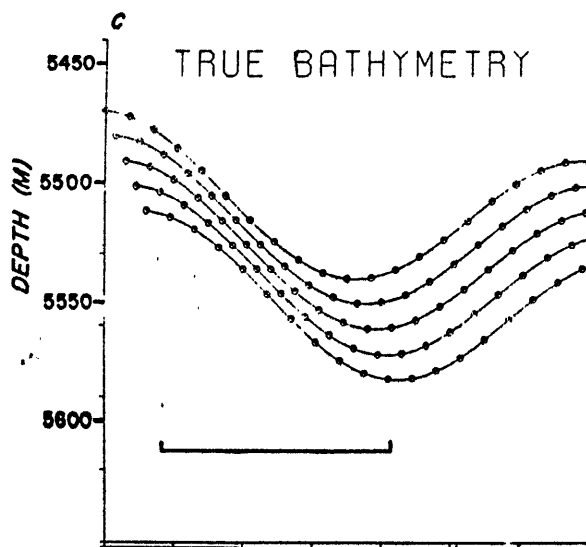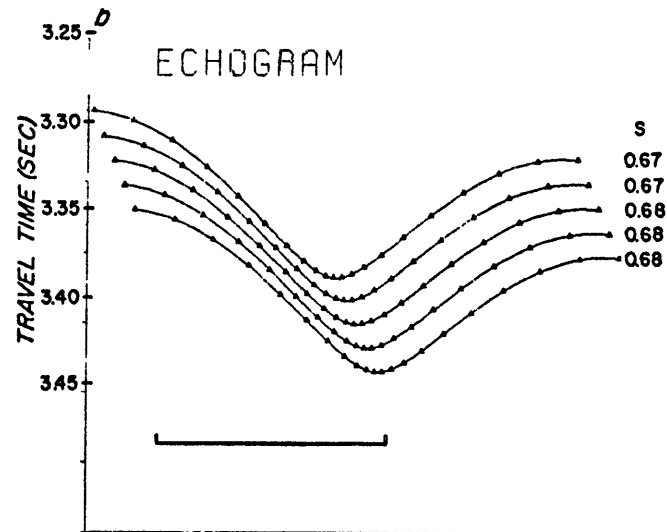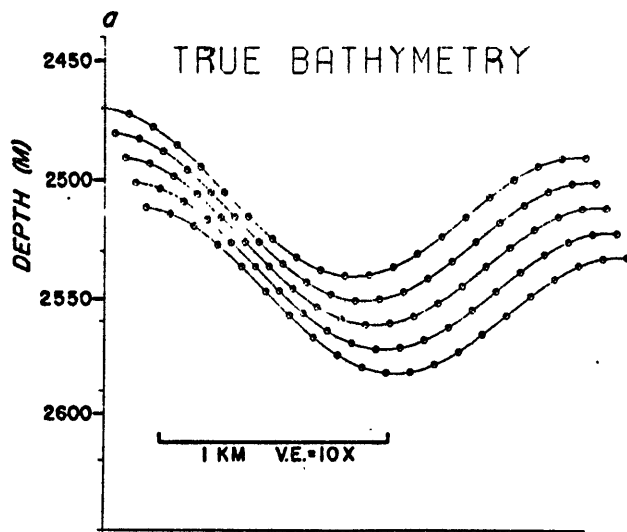
Figure Al.3

Figure A1.4. Sub-bottom profiles of a filling trough.
(V.E. = 10X).

Shallow Water
(a) True Bathymetry
(b) Echogram
    Depth   = 1000 m
    Wavelength   = 700 m
    Layer Spacing =   4 m
    Gradient   =   0

Amplitude	S
3	0.24
5	0.70
7	0.57
9	0.73
11	0.90

Deep Water
(c) True Bathymetry
(d) Echogram
    Same as above, depth = 4000 m

Amplitude	S
3	0.97
5	1.61
7	2.26
9	2.91
11	3.56
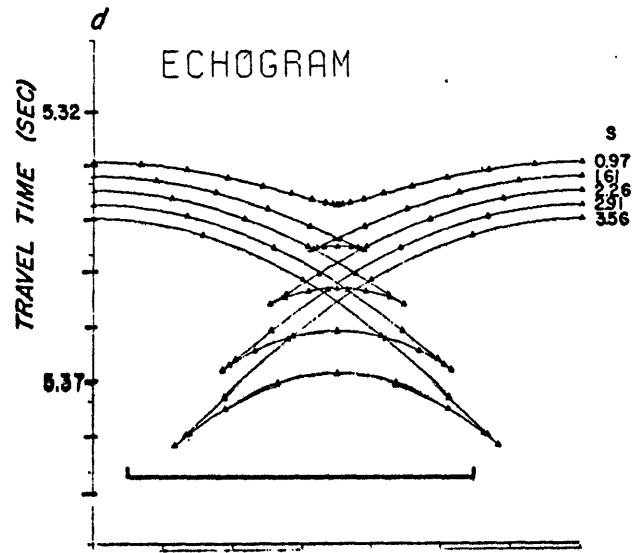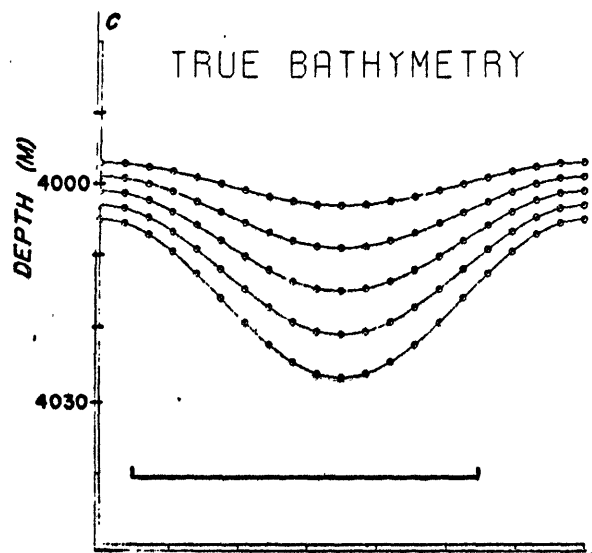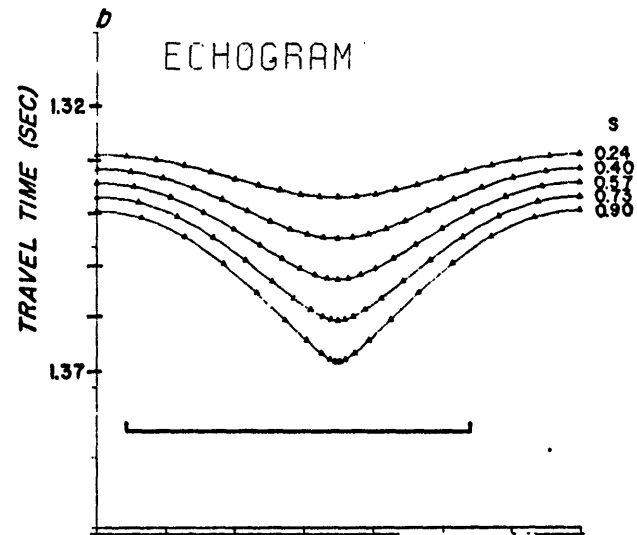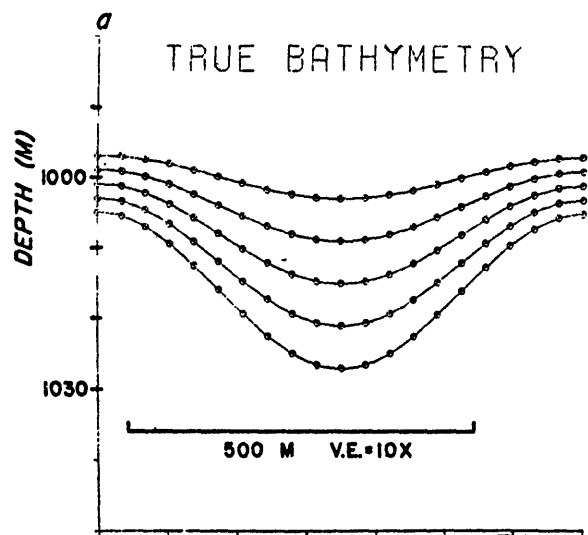
Figure A1.4

Figure A1.5. Sub-bottom profiles for a stationary wave and for growing ridges.

Stationary Wave
(a)   True Bathymetry
(b)   Echogram
      Depth   =   4000 m
      Wavelength   =   700 m
      Layer Spacing =   4 m
      Gradient   =   0
      Amplitude   =   7 m
      S   =   2.25 to 2.26
Growing Ridge
(c)   True Bathymetry
(d)   Echogram
      Depth   =   4000 m
      Wavelength   =   700 m
      Layer Spacing =   8 m
      Gradient   =   0
      Amplitude   S
         11   3.54
          9   2.91
          7   2.25
          5   1.62
          3   0.97
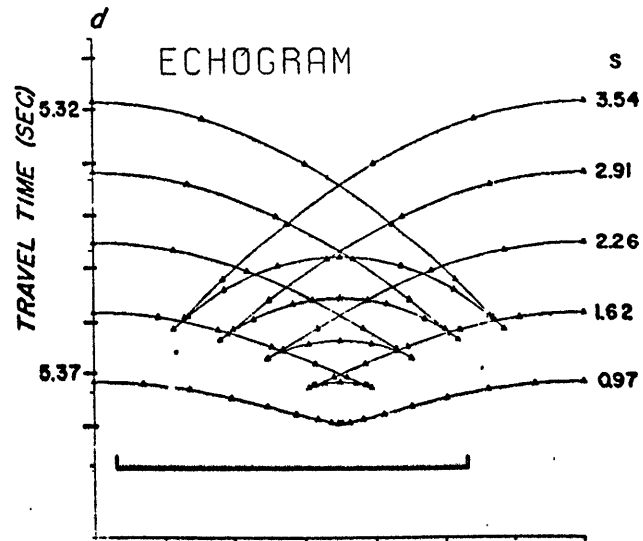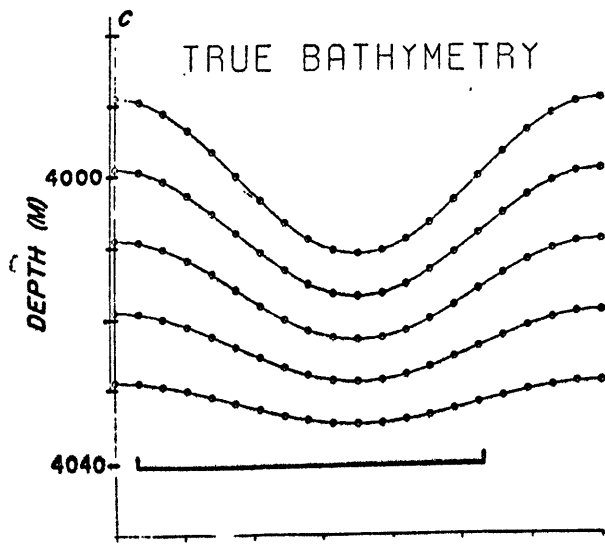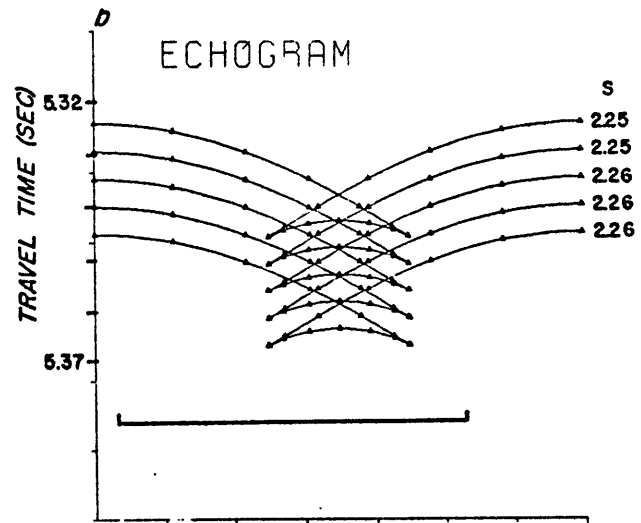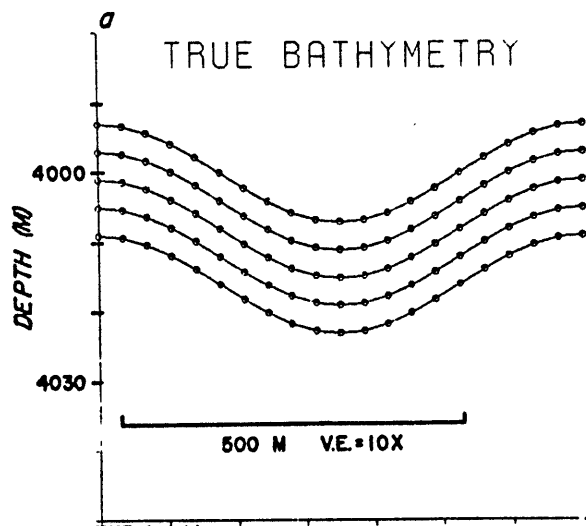
Figure A1.5

modelled here are cited.

A sub-bottom profile is also calculated for one situation which, although it appears to be unrealistic, does give some insight into the role played by side echoes in the deep sea. This is the case of a pair of growing ridges (Figure A1.5 c,d). The profiles calculated for a filling trough, a stationary sediment wave, and a pair of growing ridges all involve sine waves of the same wavelength at the same water depth. The effect of varying the layer amplitudes can be clearly seen.

In all of the following examples, sound velocity in the water column is taken as 1500 m/sec and velocities of all the sedimentary layers are taken as 1525 m/sec. At present, not enough information is available on the velocity structure of the upper sediment layers to justify the use of a specific velocity profile.

Migrating Sediment Wave

The first example is that of a large sediment wave (amplitude 30 m, wavelength 2100 m) migrating up a regional slope of 1:100. The migration is simulated by a phase shift of the deeper layers with respect to the surface. Echograms are plotted for the sediment surface and for four sub-bottom layers spaced at intervals of 10 m (Figure A1.3 a,d). Echograms were calculated for water depths of 2500 m (Figure A1.3 b)

and 5500 m(Figure Al.3 d).

At a water depth of 2500 m (S = 0.67) the echogram retains many of the structural relationships present in the bathymetry; however,the crests of the waves are considerably broader and the troughs are narrower and sharper than is actually the case. In addition, tick marks on the echogram inidicate that the intensity of the returned echo in the wave trough is greater than that from the wave crest. Careful examination of the plot reveals that the tick marks are slightly closer together on the upslope side of the wave than on the downslope side. Thus, for this particular geometry, the echo from one side of the wave will be slightly stronger than that from the other side. Aside from these complications, the echogram gives a fairly accurate rendition of the sea-floor structure.

If the same sediment wave is profiled at a depth of 5500 m (S = 1.48), the echo pattern is changed. The wave crests are even broader and the wave troughs sharper than in the case of the shallower water. The side echoes overlap in the wave troughs, resulting in a zone of confused echo return. Individual layers are difficult to trace across the wave trough and appear to intersect at a large angle, perhaps suggesting faulting.

Migrating sediment waves are often observed on 3.5 kHz echo sounding records. A good example of this type of profile is shown in Section III B, where near-bottom bathymetric profiles indicate a nearly sinusoidal topography with a uniform reflecting sequence. Surface-ship 3.5 kHz profiles show bands of strong echo return in the trough, with overlapping side echoes clearly visible in some cases. Examples of 3.5 kHz echograms which show similar features have been published by other investigators. Jacobi et al. (1976) show a good example of strong echo returns from wave troughs. Bouma and Treadwell (1976) also show examples of this phenomena. However, they suggested that, since zones of strong echo return did not disappear when the ship's course was reversed, the zones were not acoustic artifacts. Instead, they suggested that this phenomenon and other "reflectivity" changes, on these sediment waves, were due to textural variations over the sediment waves. The modelling experiments described here suggest that many of the details of the echograms are, in fact, acoustic artifacts. Some of their profiles may be situations where the side echoes cross in the wave trough; but careful examination of the original record is often necessary to determine the nature of the reflection.

Filling Trough

The second example is that of a trough which is filling in. This structure is created by stacking up waves whose amplitudes increase with depth (Figures A1.4 a and c). The wavelength of the trough is 700 m and the amplitude of the surface is 3 m. The amplitude of the deepest layer is 11 m. Each layer has an average thickness of four meters. Echograms are calculated for a water depth of 1000 m (Figure A1.4 b) and 4000 m (Figure A1.4 d).

At a depth of 1000 m (S ranging from 0.24 at the surface to 0.90 at depth), the structural relationships between the various layers are, by and large, correctly displayed on the echogram. The deeper layers are somewhat distorted due to their larger amplitudes and, in the case of the deepest layer, the trough looks more like a V-shaped valley than a sinusoidal depression. With increasing depth into the sediment, the reflections from the sides of the trough become weaker, while those from the bottom of the trough become stronger. An echogram of this type might be interpreted as a V-shaped valley which is filling in. One might speculate as to the origin of the highly reflective (coarse?) sediments at the base of the valley. This would contrast with the actual sinusoidal valley which has no reflective sediments at its base. No examples of this type of record are known to the author at this time.

If the same structure is observed at a depth of 4000 m (Figure A1.4d; S ranging from 0.97 at the surface to 3.56 at depth), the situation is quite different. The profile now bears little relationship to the actual structure. Instead, a complex pattern of side echoes is seen. The center of the trough is a zone of strong reflection and on many inter-secting side echoes. The intense reflections at the end of the side-echo arms form two sharp bands which slope at a sharp angle to the sea floor. These bands abruptly terminate the side echoes from the wave crests. The many crossing echo traces between these two dark bands may result in a confused echo return.

Echograms which appear similar to Figure A1.4d have been observed in many areas of the oceans. Good examples of this pattern are shown by Damuth (1975a, p.27) and by Damuth and Hayes (1977, p.83). The dark bands in the wave troughs diverge with depth into the sediment, suggesting that the sea-floor features are troughs which have been filling in.

The echogram in Figure A1.4d also has some similarities to patterns shown by Emery (1974, p. 312). Emery (1974) has termed these features "pagoda structures" and has postulated that they indicate the presence of gas hydrates in the sediments. These models suggest that the patterns in question may be produced by a series of troughs or depressions which have been filling in. The nature or origin of the sea-floor

features is not known.

George Bryan (Lamont-Doherty Geological Observatory, personal communication) has used a similar technique to construct the echo-sounding profile of features similar to the trough of Figure A1.4c. He has used a more complicated model of the sea-floor structure, but has come to similar conclusions about the origin of "pagoda structures" (see Emery, 1974, p. 315).

Stationary Sediment Wave

The echo-sounding profile of a stationary sediment wave was modelled by offsetting a sinusoidal wave (amplitude seven meters, wavelength 700 m) vertically to form layers with a thickness of four meters. Only one water depth is shown here, as previous examples adequately indicate the effects of changing water depth on the character of the resulting echogram.

Figure A1.5a shows the bathymetric profile for such a structure at a depth of 4000 m; Figure A1.5b shows the resulting echo-sounding profile (S = 2.25). In this case, side echoes are clearly developed on each layer. These side echoes all cross in the trough. As all layers have the same value of S, the width of the overlapping echo zone remains constant with depth, and two vertical bands of strong echo should be recorded in the wave trough.

If this profile is compared to that determined for a migrating sediment wave (Figure A1.3d) some similarities are noted. The greatest difference is in the angle that the zone of strong reflection in the wave trough makes with the sediment surface. For the migrating wave, this zone dips in the direction opposite to the migration direction of the waves, while for stationary waves, the zone is vertical. This zone increases with depth into the sediment for a filling trough (Figure A1.4d).

Examples of this type of record might be thought to be common in the deep sea. Close examination of surface-ship profiles often show that the zone of overlapping side echoes either is not vertical or becomes slightly wider with depth. This is evidence for either waves which are migrating or troughs which are filling in.

Growing Ridges

A series of ridges which are growing with time (i.e., higher sedimentation rates on the crests of the ridges than in the troughs) was modelled by decreasing the amplitudes of a series of layers with increasing sediment depth. The wavelength and amplitudes of the layers used in this example are the same as those used in the case of a filling trough (Figure A1.4c,d), except that the layers have been inverted to put the

largest-amplitude wave on the top. The spacing between the layers has been doubled to eight meters to separate the reflections from the various horizons. Again, only one water depth has been shown.

Figure A1.5c shows this structure for a water depth of 4000 m (S varying from 3.54 on the surface to 0.97 at depth). Figure A1.5d shows the resulting echogram. In this case, the width of the overlapping side-echo zone decreases with depth to form a downward-pointing triangle. The widest portion of the triangle does not intercept the sediment surface for this particular geometry. To the author's knowledge, examples of this type of echogram have not been observed. This example was included for the sake of thoroughness, and to encourage the close examination of echo-sounding records to discern features of this sort.

The echo-sounding profiles shown above are by no means an exhaustive set, but were chosen (1) to illustrate specific examples of 3.5 kHz records often seen in the deep sea, (2) to indicate from a set of structures with the same wavelength and water depth, how changes in the arrangement and amplitude of the layers can change the observed profile, and (3) to point out some of the pitfalls of interpreting these wide-beam surface-ship echo-sounding records. The similarity between the 3.5 kHz records cited and the models shown certainly

does not prove the origin of these echoes, but it does suggest types of sea-floor structures which may be responsible for these common echo-sounding patterns.

In this section, no attempt was made to construct synthetic seismograms which would model in detail the responses of a sedimentary structure to a specified pulse of 3.5 kHz sound. Such a model would include effects of three-dimensional structures, a detailed velocity profile for the sediments, a knowledge of the mechanics of reflection from horizons within the sediments,and constructive and destructive interference between echoes from different portions of the structure. All of this would be necessary in order to predict, in detail, the 3.5 kHz (or other frequency) echogram of a particular sea-floor structure.

D. IDENTIFICATION OF SEA-FLOOR FEATURES FROM SURFACE ECHO-SOUNDING PROFILES

As large areas of the sea floor can often be characterized by a similar type of echo return, it is often of considerable interest to determine the type of topographic or structural features which create certain echo patterns. As is evident from the foregoing discussion, there is often no obvious relationship between echo pattern and bottom topographic and structural features. Other kinds of information are usually needed in order to determine the true nature of the topography.

Techniques available for determination of the sea floor

topography from a scale of a few meters to several kilometers

include side-scan sonar (Rushby, 1970), narrow-beam echo

sounders (Maul, 1970), multiple-beam echo sounders (Glenn,

1970), and near-bottom instrument packages (Spiess and Mudie,

1970). The migration of wide-beam echo-sounding data record-

ed at 12 or 3.5 kHz should be a practical method for deter-

mining the shape and structure of the sea floor in cases

where the assumption of two-dimensional structure holds. At

present, the author knows of no work in this area.

Characteristics of echo-sounding profiles recorded by

conventional wide-beam profilers can be used to discern some

properties of the sea-floor relief. The following character-

istics of the surface echoes from topographic features are

easily determined and may permit identification, or at least

classification, of the topographic features in question.

Hyperbolic Echoes

Several characteristics are important in describing the

types of hyperbolic echoes recorded over different areas of

the sea floor.

(1) Similarity between adjacent echoes. If the features

on the sea floor are point reflectors to parallel linear fea-

tures of similar shape, adjacent echoes will also be similar

in shape. For linear features, the shapes of the echoes will all change, but will remain similar to each other, when the ship's course changes. If there are variations in the shape of adjacent hyperbolic echoes, the features on the sea floor are not parallel to each other and possibly not linear.

(2) Depth of vertices of adjacent hyperbolic echoes and comparison between this depth and the large-scale sea-floor relief. If the hyperbolae are nearly tangent to the sea floor, the features responsible for the hyperbolae are small compared to the overall relief of the sea floor. If the height of the vertices varies considerably, the features responsible for the hyperbolae are major relief features on the sea floor. If the height of the vertices does vary considerably, the echo pattern should be closely scrutinized to determine if the echoes are true hyperbolic echoes from features of various heights, or if there could be a wave-like topography with a large value of S responsible for the echo.

(3) Spacing between adjacent echoes. A regular spacing will indicate that the features on the sea floor may also be regularly spaced.

(4) Nature of any deep reflectors observable beneath the side echoes. If properly evaluated, these reflections can give insight into the structure of the topographic feature.

(5)   Orientation of the linear features. If linear features are thought to be responsible for the hyperbolae, their orientation should be determined.

(6)   Size and shape of the area of sea floor characterized by any given echo pattern and the relationship between this area and the major topographic features in the area. This information may suggest various mechanisms for the formation of the features on the sea floor.

Side Echoes from Larger Topographic Features

The characteristics of echoes from a point source can be equally applied to the echo patterns of larger features.

(1)   Linearity, nature of side echoes, similarity between adjacent forms.

(2)   Amplitude.

(3)   Spacing, regularity of spacing.

(4)   Character of deep reflectors, form of side echoes.

(5)   Orientation of the features, if linear.

(6)   Size, shape, and location of the area characterized by these features.

These characteristics of the echo type can be compared with those of an echo type which has been correlated with a specific topographic or structural feature. Identification

of similarities and differences in the details of the pro-
files in question can aid in determining the similarities and
differences between the topographic elements in the areas
under investigation.

At present, too little information is available on the
range of features which can exist on the sea floor to provide
the basis for a general correlation between echo type and
sea-floor morphology. For the present, one must be content
with a careful study of the echo received from the sea floor
and the comparison of that echo with the few echo patterns
studied in detail, such as the various features discussed in
Chapters 2 and 3, to determine the nature of the sea floor
from wide-beam echo-sounding data.

APPENDIX II

CALCULATION OF SIDE ECHOES
FOR SINUSOIDAL TOPOGRAPHY

A. SURFACE ECHO TRACE

The equations of Krause (1962), equations Al.2 and Al.3,

can be applied to a sinusoidal sea floor f(x), where

$$f(x) = A - B \cos \frac{2\pi}{\lambda} x$$

A = Water Depth

λ = Wavelength

B = Wave Amplitude

to give the surface echo trace (m(x), r(x))

$$m(x) = x + (A-B \cos \frac{2\pi}{\lambda} x) (\frac{2\pi}{\lambda} B \sin \frac{2\pi}{\lambda} x)$$

$$r(x) = (A-B \cos \frac{2\pi}{\lambda} x) (1 + (\frac{2\pi}{\lambda} B \sin \frac{2\pi}{\lambda} x)^2)^{\frac{1}{2}}$$

These expressions for m(x) and r(x) can be normalized by

the wavelength, water depth and amplitude of the sea floor to

give the normalized echo trace

$$M(\frac{x}{\lambda}) = \frac{m(x)}{\lambda}$$

$$R(\frac{x}{\lambda}) = \frac{r(x)-A}{B}$$

Expanding $M(\frac{x}{\lambda})$,

$$M(\frac{x}{\lambda}) = \frac{x}{\lambda} + 2\pi \frac{AB}{\lambda^2}(\sin 2\pi\frac{x}{\lambda}) (1-\frac{B}{A} \cos 2\pi \frac{x}{\lambda})$$

or $$M(\frac{x}{\lambda}) = \frac{x}{\lambda} + \frac{S}{2\pi}(\sin 2\pi \frac{x}{\lambda}) (1-\frac{B}{A} \cos 2\pi \frac{x}{\lambda})$$ (A2.1)

Where $$S = \frac{4\pi^2 AB}{\lambda^2}.$$

Expanding $R(\frac{x}{\lambda})$, using the approximation that, for small y,

$(1+y)^{\frac{1}{2}} \cong 1 + y/2$,

$$R(\frac{x}{\lambda}) = 2\pi^2 \frac{AB}{\lambda^2} (\sin^2 2\pi \frac{x}{\lambda})(1- \frac{B}{A} \cos 2\pi \frac{x}{\lambda}) - \cos 2\pi\frac{x}{\lambda}$$

or $\quad R(\frac{x}{\lambda}) = \frac{S}{2} (\sin^2 2\pi \frac{x}{\lambda})(1- \frac{B}{A} \cos 2\pi \frac{x}{\lambda}) - \cos 2\pi\frac{x}{\lambda} \qquad$ (A2.2)

The approximation for the square root term has an error of

less than 2% for $B/\lambda \le 0.5$.

For A<<B (small-amplitude wave in deep water), the terms

of equations A2.1 and A2.2 multiplied by B/A become negligle.

The resulting expressions

$$M(\frac{x}{\lambda}) = \frac{x}{\lambda} + \frac{S}{2\pi} \sin 2\pi \frac{x}{\lambda} \qquad \text{(A2.3)}$$

$$R(\frac{x}{\lambda}) = \frac{S}{2} \sin^2 2\pi \frac{x}{\lambda} - \cos 2\pi \frac{x}{\lambda} \qquad \text{(A2.4)}$$

show that, in this case, the echo trace depends only on the

value of S.

B. SUB-BOTTOM PROFILES

Sub-bottom porfiles can be calculated for two-dimensional

features whose interfaces are sinusoidal waves by the follow-

ing FORTRAN IV program. This program determines the path and

travel time of the echo-sounding pulse in a manner similar to

that by Smith (1977).

```
1.    C  SINE WAVE SIDE ECHO CALCULATION AND PLOTTING PROGRAM   R. FLOOD-MARCH 23,1977
2.    C
3.    C  FIRST CARD INDICATES THE NUMBER OF TIMES THE PROGRAM IS TO BE EXECUTED FOR A
4.    C  DIFFERENT SET OF VARIABLES (NRUN).  THE PROGRAM THEN READS A CARD WHICH
5.    C  SPECIFIES THE MEAN DEPTH OF WATER (A)(M), TOPOGRAPHY WAVELENGTH (W)(M),
6.    C  NUMBER OF LAYERS WITH THE FIRST LAYER THE WATER COLUMN (NLAYER)(5 MAXIMUM),
7.    C  WAVE AMPLITUDES (MEAN DEPTH TO PEAK)(B(I))(M), WAVE OFFSETS (WITH RESPECT TO
8.    C  A COSINE WAVE, + OFFSETS TO THE LEFT)(XO(I))(M), LAYER THICKNESSES (MEAN
9.    C  DEPTH TO MEAN DEPTH)(D(I),D(1)=A)(M), AND LAYER VELOCITIES (V(I))(M/SEC) FOR
10.   C  ALL FIVE LAYERS.  THE MEAN SLOPE (SIMILAR FOR ALL LAYERS) IS ALSO SPECIFIED
11.   C  (+ SLOPES UP TO THE RIGHT)(S)(M/M).  VALUES FOR FIVE LAYERS MUST BE SUBMITTED
12.   C  EVEN IF LESS THAN FIVE LAYERS ARE CALCULATED.
13.   C  A DIFFERENT CARD IS USED FOR EACH ITERATION OF THE PROGRAM.  A 'TRUE
14.   C  BATHYMETRY' AND AN 'ECHOGRAM' ARE PLOTTED FOR THE INPUT CONDITIONS.  THE
15.   C  PLOTS ARE MADE WITH A VERTICAL EXAGGERATION OF TEN TO ONE.
16.   C
17.         DIMENSION IBUF(1000),FPL(103),XMPL(103),RPL(103),XPL(103)
18.         INTEGER  RUN
19.         DOUBLE PRECISION A,W,W1,XI,X1,X10,   ELP0,EL2  ,ELP1,ELP2,EL0,EL1,
20.        1SUMD,X2,THETA1,SL1,ES1,B(5),XO(5),D(5),X(103),V(5),F(5,103),XM(5,1
21.        203),R(5,103),A1,FP,TOL,S   ,XL
22.   C  INPUT NUMBER OF TIMES PROGRAM IS TO BE EXECUTED
23.         INPUT NRUN
24.         CALL PLOTS (IBUF,-1000)
25.         CALL PLOT (0.0,1.0,-3)
26.         TOL=0.0001
27.         DO 500 RUN=1,NRUN
28.   C  INPUT RUN PARAMETERS SEPERATED BY COMMAS.  FIVE VALUES OF B,XO,D AND V
29.   C  AND ONE VALUE OF S MUST BE SPECIFIED.  PROGRAM SETS D(1)=A,
30.         INPUT A,W,NLAYER,B,XO,D,V,S
31.         D(1)=A
32.         DO 10 M=1,2
33.         OUTPUT '  '
34.         OUTPUT  RUN
35.         OUTPUT 'INPUT PARAMETERS'
36.    10   OUTPUT A,W,NLAYER,B,XO,D,V,S
37.         OUTPUT '  '
38.   C  CHANGE LAYER VELOCITIES TO TWO-WAY VELOCITIES.
39.         DO 20 M=1,NLAYER
40.    20   V(M)=V(M)/2.
41.         W1=6.28318530718/W; XI=W/100.
42.         DO 100 N=1,101
43.   100   X(N)=(N-1)*XI
44.         A1=0
45.   C  CALCULATE 'TRUE BATHYMETRY' (F(M,N)).
46.         DO 120 M=1,NLAYER
47.         A1=A1+D(M)
48.         DO 120 N=1,101
49.         XL=X(N)-XO(M)
50.   120   F(M,N)=A1-B(M)*DCOS(W1*(XL +XO(M)))-S  *XL
51.   C  CALCULATE SURFACE 'ECHOGRAM' (XM(1,N),R(1,N)).
52.         M=1
53.         DO 125 N=1,101
54.         XL=X(N)-XO(M)
55.         FP=B(M)*W1*DSIN(W1*(XL +XO(M)))-S
56.         XM(M,N)=XL +F(M,N)*FP
57.   125   R(M,N)=(F(M,N)*DSQRT(1+FP**2)/V(1))*1000
58.   C  CALCULATE SUBBOTTOM 'ECHOGRAM' (XM(M,N),R(M,N)).
59.         REPEAT 300, FOR M=(2,NLAYER)
```

```
60.          DO 300 N=1,101
61.          X10=X(N)=XO(M)
62.          SUMD=0
63.          ELPO=W1*R(M)*DSIN(W1*(X10+XO(M)))=S
64.   C  CALCULATE REFRACTION AT LAYER INTERFACES.  EL'S ARE INTERFACE DEPTHS (TIMES),
65.   C  ELP'S ARE INTERFACE SLOPES, O IS ON BOTTOM, 1,2 ARE ON TOP.  ITERATE UNTILL
66.   C  ELP1 = ELP2,
67.          DO 290 MM=H,2,-1
68.          ELO=(B(MM)*DCOS(W1*(X10+XO(MM)))-D(MM ))/V(MM)+S     *X10/V(MM)
69.          ELP2=W1*B(MM-1)*DSIN(W1*(X10+XO(MM-1)))=S
70.          IF (DABS(ELPO).LT.TOL)  X2=X10                   , GO TO 275
71.          X1=X10
72.      150 EL1=B(MM-1)*DCOS(W1*(X1+XO(MM-1)))/V(MM-1)+S      *X1/V(MM-1)
73.          X2=X10-(ELO-EL1)*ELPO*V(MM)
74.          ELP1=ELP2
75.          ELP2=W1*B(MM-1)*DSIN(W1*(X2+XO(MM-1)))=S
76.          IF (DABS(ELP1)-DABS(ELP2) .LT. TOL   ) GO TO 275
77.          X1=X2 ,GO TO 150
78.      275 EL2=B(MM-1)*DCOS(W1*(X2+XO(MM-1)))/V(MM-1)+S      *X2/V(MM-1)
79.          SUMD=SUMD+DSQRT((((X1C-X2)/V(MM))**2+(ELO-EL2)**2)
80.          THETA1=DASIN((V(MM-1)/V(MM))*DSIN(DATAN(-1,ELPO)-DATAN(-1,ELP2)))
81.          SL1=DTAN(DATAN(ELP2)+THETA1)
82.          X10=X2
83.      290 ELPO=SL1
84.          ES1= A-B(1)*DCOS(W1*(X2+XO(1)))=S    *X2
85.          XM(H,N)=X2+ES1*SL1
86.      300 R(M,N)=(ES1*DSQRT(1+SL1**2)/V(1)+SUMD)*1000
87.   C  DETERMINE SCALES FOR PLOTS (V*E.=10X),
88.          WINCR=W/7
89.          AINCR=-WINCR/10
90.          AL=A-AINCR*5
91.          VINCR=AINCR*1000/V(1)
92.          VL=A*1000/V(1)-VINCR*5
93.          XPL(102)=0, XPL(103)=WINCR
94.          XMPL(102)=0, XMPL(103)=WINCR
95.          RPL(102)=VL, RPL(103)=VINCR
96.          FPL(102)=AL, FPL(103)=AINCR
97.   C  PLOT 'TRUE BATHYMETRY',
98.          CALL AXIS (0.0,0.0,'DISTANCE-M',-10,7.0,0.0,0.0,WINCR)
99.          CALL AXIS (0.0,0.0,'DEPTH-M',+7,7.0,90.0,AL,AINCR)
100.         DO 350 M=1,NLAYER
101.         DO 325 N=1,101
102.         XPL(N)=X(N)-XO(M)
103.     325 FPL(N)=F(H,N)
104.     350 CALL LINE (XPL,FPL,101,1, 5,1)
105.         CALL SYMBOL (1.0,6.5,0.35,'TRUE BATHYMETRY',0.0,15)
106.         CALL PLOT (10.0, 0.0,999)
107.   C  PLOT 'ECHOGRAM',
108.         CALL AXIS (0.0,0.0,'DISTANCE-M',-10,7.0,0.0,0.0,WINCR)
109.         CALL AXIS (0.0,0.0,'TWO-WAY TRAVEL TIME (MILLISECONDS)',+34,7.0,
110.        1 90.0,  VL,VINCR)
111.         DO 450 M=1,NLAYER
112.         DO 425 N=1,101
113.         XMPL(N)=XM(M,N)
114.     425 RPL(N)=R(M,N)
115.     450 CALL LINE (XMPL,RPL,101,1, 5,2)
116.         CALL SYMBOL (1.0,6.5,0.35,'ECHOGRAM',0.0,8)
117.     500 CALL PLOT (10.0, 0.0,999)
118.         STOP
119.         END
```

APPENDIX III

BULK X-RAY MINERALOGY

METHODS

Bulk samples were analyzed with an X-ray diffractometer
in order to obtain semi-quantitative determinations of the
mineral composition of the sediments samples. The analyses
were performed in the manner of Cook et al. (1975).

Briefly, the method is as follows: Bulk samples are
prepared by washing with distilled water to remove sea salts
and are ground to less than 10 μ under butanol. The samples
are then treated with trihexylamine acetate to expand smectite
minerals and X-rayed as random powders. Bulk samples are X-
rayed with Cu-K radiation at 2° 2θ/min with a 1° divergence
slit, an 0.01 inch receiving slit, and a curved crystal mono-
cromator.

For this study, diffraction patterns were recorded on
chart paper at 1 inch/min with a full scale reading of 1000
counts per 2θ step (0.6 sec counting time for each 0.02°2θ
step). The chart full scale was automatically increased to
10,000 counts per increment for intense peaks, thus peak
heights could be determined for scarce as well as abundant
species.

Mineral identifications were made manually on the basis
of a peak present within one of the windows indicated by

Cook et al. (1975) and verified by the presence of secondary peaks. Diffraction traces were manually smoothed and the diagnostic peak heights were measured. When high-magnesian calcite was present in the sample, the ratio of high-magnesian calcite to low-magnesian calcite was determined on the basis of their combined peak areas (Milliman, 1974). This ratio was then used to determine a "peak height" for high-magnesian calcite. This peak height was used in the calculation of mineral abundances. The total of all minerals identified was set equal to 100%, and relative mineral composition computed. Abundances are reported to the nearest percent.

Peak areas, rather than peak heights, were used to determine the ratio of dolomite to calcite (Milliman, 1974) on samples used to correct the Carbon-14 ages (Section II.B.2) in order to increase the accuracy of the mineral determinations.

Several factors combine to limit the accuracy and precision of the measurements made here. The limitation on accuracy is mainly in the use of the weighting factors (derived by Cook, et al., 1975). As they pointed out, these factors were determined by ratioing the diagnostic peak of the mineral in question to the major quartz peak in mixtures of known composition. Differences in crystallinity between

the mineral standards and the mineral samples and the inter-
ference from other diffraction peaks often keep the accuracy
of the method below the implied precision. Zemmels and Cook
(1976) report that the errors could be as much as ±50% for
smectites; ±20% for micas, chlorites, cristobalite, tridy-
mite and geothite; ±10% for kaolinite, amphibole, augite,
feldspar, zeolite, palygorskite, sepiolite and apatite and
±5% for minerals which have stable crystal lattices and are
not members of solid solution series (or typically have
limited crystal-lattice substitution in the sedimentary en-
vironment) such as quartz, low-magnesian calcite, aragonite,
dolomite, rhodochrosite, siderite, gibbsite, talc, barite,
anatase, gypsum, anhydrite, halite, pyrite, hematite and mag-
netite.

Strictly speaking, the weighting factors are only valid
when used with the X-ray diffraction system for which they
were derived. However, due to the similarity of the instru-
ments involved, it was thought that these factors should apply
to this work. The use of these weighting factors also re-
duces the accuracy of these calculations to less than the
implied precision.

The sensitivity of the method is limited mainly by the effectiveness of the random background noise in masking the diagnostic and secondary peaks of a mineral. In general, a mineral has to make up 1-2% of a sample before it will be recorded on an X-ray diffractogram.

RESULTS

In using these data one should bear in mind two things. First, the reported values are not absolute concentrations, i.e., some adjustment must be made for the amount of amorphous material and any unquantified minerals. Second, the trends seen within a homogeneous set of minerals are valid, but, in order to compare mineral concentrations between lithologic units or geographical regions, information on the crystallinity is required.

As the factors used in the determination of the percentages of the minerals were not derived with the diffractometer used during these studies, some method was sought to assess the reliability of these compositions. If one plots the percent carbonate determined for a sample by the gasometric method of Lohmann (1974) against the percentage of carbonate minerals determined by the X-ray diffraction method, one obtains a straight line (Figure A3.1). The X-ray carbonate is, however, consistently greater than the gasometric
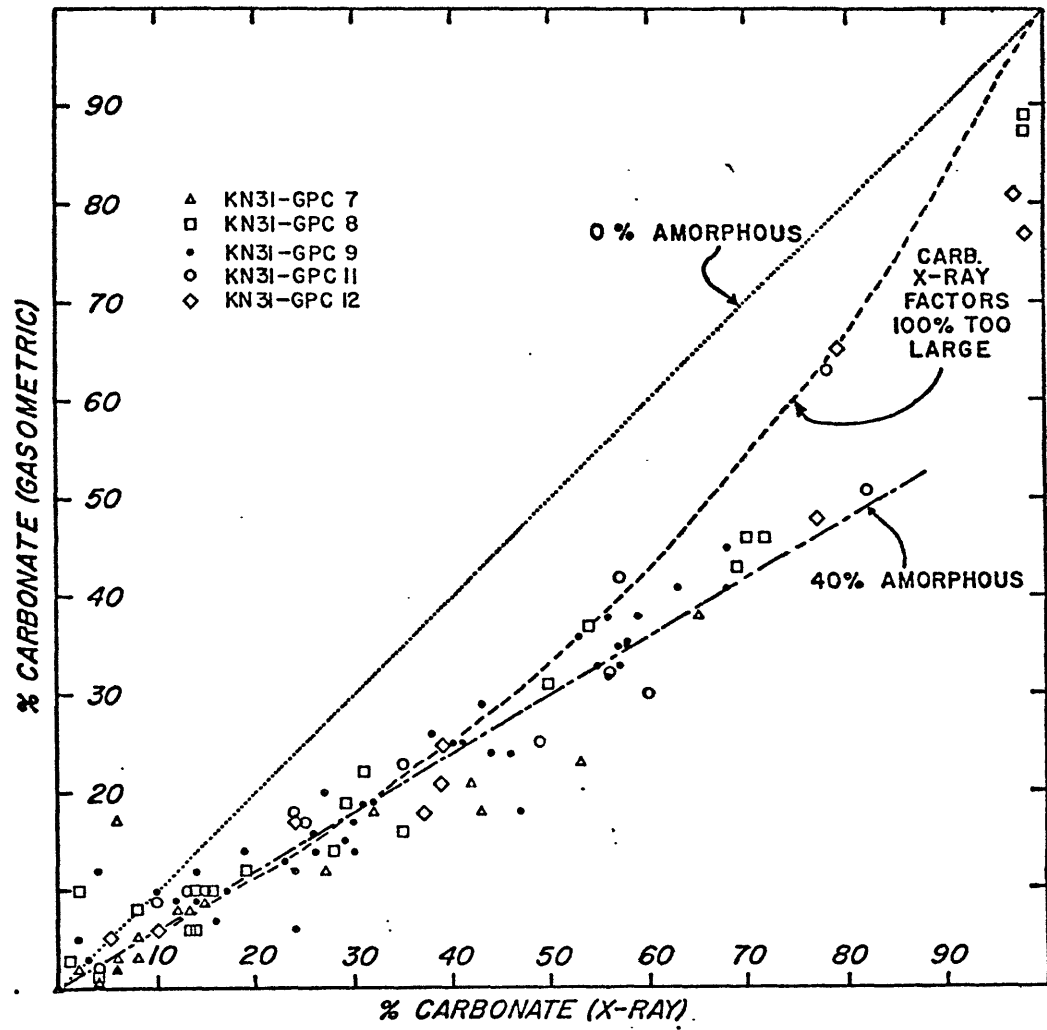
Figure A3.1. X-ray vs. gasometric carbonate content.

carbonate. The straight-line relationship shows that the variations of carbonate mineral abundance, and thus hopefully in the abundances of all minerals, determined by the X-ray method reflect actual carbonate mineral variations in the sediments.

The consistently higher X-ray carbonate value may indicate that the factors used in these computations were not correct. If all the carbonate X-ray factors were 100% too large, the points would fall on the dashed line of Figure A3.1. The points appear to diverge from this line. Thus, not all of the discrepancy between the two measures of carbonate abundance can be accounted for by this assumption. A straight line relationship of the type observed would also be expected if there was a significant amount (about 40%) of unquantified material in the X-ray samples (Figure A3.1). The unquantified material may either be an unidentified or unquantified mineral phase or amorphous material. Estimates of the amount of amorphous material in deep-sea sediments vary widely, but the range of estimated values includes that determined for these samples. If an average of 40% of the sediment is amorphous, the factors relating the intensity of the X-ray peak to the amount of material present are good, and the amount of amorphous material must be taken into account when converting from X-ray composition to the actual composition.

Bulk X-ray compositions, determined by the peak height method, are reported in tables A3.1 to A3.5 for samples from cores KN31-GPC 7, 8, 9, 11, and 12 respectively. Carbonate content determined on the same or nearby samples by the gasometric method are also included.

TABLES A3.1 AND A3.2

BULK X-RAY MINERALOGY

(WEIGHT PERCENT)

TABLE A3.1 — KN31-GPC 7

SAMPLE DEPTH (CM)	CALCITE	QUARTZ	MICA	CHLORITE	KAOLINITE	PLAGIOCLASE	K-FELDSPAR	AMPHILBOLE	HEMATITE	PYRITE	DOLOMITE	ARAGONITE	Mg-CALCITE	CARBONATE (GASOMETRIC)
10	5	31	17	2	7	27	6	1	3	--	1	--	--	17.0
148	4	41	23	4	9	14	--	--	3	--	2	--	--	2.0
210	10	41	20	1	11	13	--	--	2	--	2	--	--	8.0
504	--	41	24	-	9	16	7	--	1	--	2	--	--	0.5
554	13	38	12	3	5	19	6	--	2	--	2	--	--	9.0
1000	41	21	9	-	4	11	11	--	2	--	1	--	--	21.0
1110	2	49	13	3	4	14	5	--	4	--	6	--	--	3.0
1275	29	29	11	3	4	16	3	2	-	--	3	--	--	18.0
1406	9	39	11	4	5	18	4	2	4	--	4	--	--	8.0
1524	39	24	9	-	5	17	2	--	-	--	4	--	--	18.0
2000	--	47	16	2	6	19	3	2	3	--	2	--	--	2.0
2205	--	33	18	-	7	36	3	--	3	--	-	--	--	---
2297	52	19	6	-	3	17	2	-	-	-	1	--	--	23.0
2411	3	44	15	-	4	26	3	-	2	-	3	--	--	3.0
2481	67	15	8	-	3	7	-	-	-	-	-	--	--	38.0
2605	27	29	16	-	7	18	1	-	2	-	-	--	--	12.0
3005	6	37	9	-	5	32	6	-	3	-	2	--	--	5.0

TABLE A3.2 — KN31-GPC 8

SAMPLE DEPTH (CM)	CALCITE	QUARTZ	MICA	CHLORITE	KAOLINITE	PLAGIOCLASE	K-FELDSPAR	AMPHILBOLE	HEMATITE	PYRITE	DOLOMITE	ARAGONITE	Mg-CALCITE	CARBONATE (GASOMETRIC)
35	12	40	18	5	6	11	6	-	-	-	2	--	--	(10.0)[1]
215	15	32	22	2	7	13	6	-	2	-	1	--	--	(10.0)
320	44	13	8	3	2	5	-	-	-	-	-	19	6	(43.0)
335	13	32	21	3	7	14	6	-	3	-	1	--	--	6.0
449	--	36	29	4	9	13	6	-	2	-	1	--	--	(2.0)
977	49	18	10	1	3	8	3	-	3	-	2	3	--	(37.0)
1090	25	34	15	2	4	12	4	-	-	-	4	--	--	(19.0)
1195	10	39	15	2	6	19	4	1	1	-	3	--	--	6.0
1644	17	35	18	2	6	13	4	1	2	-	2	--	--	(12.0)
2001	--	35	16	2	5	26	9	3	2	-	2	--	--	1.0
2060	26	29	16	3	2	13	5	-	4	-	2	--	--	14.0
2090	54	14	4	-	2	8	1	1	-	-	1	15	--	46.0
2203	26	2	-	-	-	-	-	-	-	-	-	60	12	87.0
2250	47	22	9	-	3	10	5	1	-	-	3	--	--	(31.0)
2300	43	2	-	-	-	1	-	-	-	-	-	49	5	89.0
2362	6	39	15	-	5	22	11	-	-	-	2	--	7	8.0
2524	28	30	11	4	4	12	5	-	3	-	3	--	--	(22.0)
2655	--	40	16	3	5	19	8	-	-	7	2	--	--	(10.0)
2887	33	28	13	2	4	13	4	-	1	-	2	--	--	(16.0)
2905	70	11	6	1	2	6	2	-	-	-	2	--	--	46.0

- = not present

( )[1] Sample within 5 cm of X-ray sample depth

TABLE A3.3

BULK X-RAY MINERALOGY, KN31-GPC 9

(WEIGHT PERCENT)

SAMPLE DEPTH (CM)	CALCITE	QUARTZ	MICA	CHLORITE	KAOLINITE	PLAGIOCLASE	K-FELDSPAR	AMPHIBOLE	HEMATITE	PYRITE	DOLOMITE	ARAGONITE	Mg-CALCITE	CARBONATE (GASOMETRIC)
3	57	14	11	-	3	9	5	-	1	-	-	--	--	35
15	58	14	10	-	3	8	4	-	2	-	1	--	--	38
34	55	18	7	1	3	8	5	-	2	-	1	--	--	33
57	41	21	10	3	4	11	6	1	2	-	1	--	--	25
67	29	34	14	-	5	12	5	-	-	-	1	--	--	14
75	32	24	16	3	6	11	7	-	1	-	-	--	--	19
115	43	21	14	-	5	8	5	-	3	-	1	--	--	24
185	10	34	19	4	6	14	8	1	2	-	2	--	--	9
300	23	31	20	2	7	12	2	-	2	-	1	--	--	12
465	19	31	12	2	5	15	9	2	1	-	4	--	--	(6)[1]
595	8	42	12	5	5	18	4	-	-	-	6	--	--	9
785	51	16	12	2	4	8	3	-	2	-	2	--	--	36
855	10	38	17	4	6	15	10	-	-	-	-	--	--	10
1040	37	22	11	3	5	11	6	1	1	-	3	--	--	25
1095	2	40	23	4	8	15	5	-	2	-	1	--	--	12
1291	21	30	15	4	5	15	7	-	2	-	1	--	--	13
1370	46	19	9	2	4	11	7	-	1	-	1	--	--	28
1595	14	31	20	-	5	17	8	-	3	-	2	--	--	7
1665	1	39	16	4	7	20	7	1	2	-	3	--	--	2
1762	36	24	7	2	3	16	7	1	2	-	2	--	--	(26)
1775	--	35	15	2	5	24	13	2	2	-	2	--	--	5
1820	55	13	7	-	3	8	5	-	1	-	1	7	--	41
1835	29	25	15	4	4	13	5	1	2	-	2	--	--	19
1850	67	14	7	-	2	7	2	-	1	-	-	--	--	41
1885	41	23	11	4	3	10	5	-	2	-	1	--	--	29
1900	24	35	16	1	5	11	5	1	1	-	1	--	--	14
1945	54	16	9	3	2	11	3	-	1	-	1	--	--	38
1985	55	21	5	-	4	9	5	-	-	-	1	--	--	32
2025	28	30	11	3	3	14	8	-	2	-	1	--	--	15
2035	53	16	7	3	3	9	5	-	2	-	2	--	--	33
2068	57	15	10	2	3	7	4	1	-	-	1	--	--	35
2082	67	12	9	-	3	5	2	-	1	-	1	--	--	(45)
2095	56	18	9	-	4	7	3	-	1	-	2	--	--	(35)
2109	44	23	8	-	4	9	7	2	1	-	2	--	--	24
2132	28	30	18	4	5	8	5	-	-	-	2	--	--	17
2158	14	31	21	4	8	11	5	-	3	-	3	--	--	10
2195	14	31	21	4	8	11	5	-	3	-	3	--	--	16
2270	15	36	16	6	4	11	7	-	1	-	4	--	--	14
2334	11	36	20	4	6	12	7	1	1	-	3	--	--	12
2411	27	24	17	2	4	16	7	1	1	-	1	--	--	20
2458	1	36	14	3	5	22	12	2	3	-	2	--	--	3

( )[1] Sample within 5 cm of X-ray sample depth

- = not present

TABLES A3.4 AND A 3.5

BULK X-RAY MINERALOGY

(WEIGHT PERCENT)

	SAMPLE DEPTH (CM)	CALCITE	QUARTZ	MICA	CHLORITE	KAOLINITE	PLAGIOCLASE	K-FELDSPAR	AMPHIBOLE	HEMATITE	PYRITE	DOLOMITE	ARAGONITE	Mg-CALCITE	CARBONATE (GASOMETRIC)
TABLE A3.4 — KN31-GPC 11	45	21	27	9	1	3	22	10	2	2	-	3	-	-	(18)[2]
	220	9	30	14	2	5	24	10	1	4	-	1	-	-	(9)
	435	43	21	9	2	2	12	3	1	1	-	6	-	-	(25)
	605	55	15	7	1	1	9	8	1	1	-	2	-	-	(42)
	703	13	39	14	3	5	15	4	1	2	2	2	-	-	(10)
	842	33	27	14	3	4	12	3	1	1	-	2	-	-	23
	990	12	41	16	-	6	16	8	-	-	-	1	-	-	(10)
	1080	55	20	6	2	2	10	3	-	1	-	1	-	-	(32)
	1217	22	34	16	4	3	12	5	-	1	-	3	-	-	17
	1315	56	9	4	-	2	3	-	-	-	-	1	25	-	51
	1498	-	36	12	2	4	29	9	2	4	-	2	-	-	4
	1535	55	16	9	-	3	7	4	-	1	-	1	4	-	(30)
	1680	38	12	5	-	1	4	-	-	-	-	-	37	3	(63)
TABLE A3.5 — KN31-GPC 12	8[1]	38	26	12	2	4	10	4	1	1	-	2	-	-	n.d.
	15	37	28	12	2	5	9	3	-	2	-	2	-	-	21
	60	54	14	-	-	-	7	-	-	-	-	1	24	-	65
	89	76	11	4	-	2	6	-	-	-	-	1	-	-	48
	152	36	26	14	4	4	9	5	-	1	-	1	-	-	18
	225	36	22	12	3	4	17	4	-	1	-	1	-	-	25
	330	21	32	17	2	7	10	6	1	1	-	3	-	-	17
	465	7	34	18	2	7	19	7	-	3	-	3	-	-	6
	535	43	3	3	-	-	2	-	-	-	-	-	33	16	77
	601	3	33	13	3	3	26	13	2	2	-	2	-	-	5
	635	45	3	-	-	-	-	-	-	-	-	-	52	-	81

[1] KN-31-13KC sample used as surface sample since top of KN31-GPC 12 is disturbed.

( )[2] Sample within 5 cm of X-ray sample depth.

- = not present

n.d. = not determined

BIOGRAPHICAL NOTE

Born: July 19, 1950, Framingham, Massachusetts

1968   Graduated Natick High School, Natick, Massachusetts.
                An account of one project undertaken in high
                school is in Amateur Scientist, Scientific
                American, July, 1970.

1971 (summer)   Summer Student Fellow, Woods Hole Oceanographic
                Institution.

1972   S.B. in Earth and Planetary Sciences, Massachusetts
                Institute of Technology. Nominated to Sigma Xi.

1972-1977   Graduate Research Assistant, Woods Hole
                Oceanographic Institution.

PUBLICATIONS

Southard, J.D., Cacchione, D.A., and Flood, R.D., 1971.
    Experiments on bottom sediment movement by breaking
    internal waves (abstract). EOS, Trans. Amer. Geophys.
    Un., 52: 258.

Flood, R.D., Hollister, C.D., Johnson, D.A., Southard, J.B.,
    and Lonsdale, P.F., 1974. Hyperbolic echoes and
    erosional furrows on the Blake-Bahama Outer Ridge
    (abstract). EOS, Trans. Amer. Geophys. Un., 55:284.

Hollister, C.D., Flood, R.D., Johnson, D.A., Lonsdale, P.F.,
    and Southard, J.B., 1974. Abyssal furrows and hyperbolic
    echo traces on the Bahama Outer Ridge. Geology, 2: 395-400.

Flood, R.D. and Hollister, C.D., 1974. Current controlled
    topography on the continental margin off the Eastern
    United States. In: C.A. Burk and C.L. Drake (Editors),
    The Geology of Continental Margins, Springer-Verlag,
    New York, pp. 197-205.

Flood, R.D. and Hollister, C.D., 1975. Microphysiography
    of the abrupt contact between the Bahama Outer Ridge
    and the Bahama Abyssal Plain (abstract). EOS, Trans.
    Amer. Geophys. Un., 56: 371.

Hollister, C.D., Flood, R.D., Southard, J.B., and Lonsdale,
    P.F., 1975. Dimensions, distribution and origin of
    abyssal bed forms on the Blake-Bahama Outer Ridge
    (abstract). EOS, Trans. Amer. Geophys. Un., 56:372.

Flood, R.D. and Hollister, C.D., 1975. Studies and significance of deep-sea bed forms in the North Atlantic (abstract). Abstracts with Programs, GSA 1975 Annual Meeting, 7:1076.

Flood, R.D., Lohmann, G.P., and Hollister, C.D., 1976. Warming of deep water in the North Atlantic during the last glacial period: evidence from benthonic foraminifera in core KN31-GPC 9, Bahama Outer Ridge (abstract), EOS, Trans. Amer. Geophys. Un., 57: 258.

Hollister, C.D., Southard, J.B., Flood, R.D., and Lonsdale, P.F., 1976. Flow phenomena in the benthic boundary layer and bed forms beneath deep current systems. In: I.N. McCave (Editor), The Benthic Boundary Layer, Plenum, New York, pp. 183-204.

Silva, A.J., Hollister, C.D., Laine, E.P., and Flood, R.D., 1976. Lateral coherence of geotechnical and acoustic properties at two giant piston core sites in the northeastern North Atlantic (abstract). EOS, Trans. Amer. Geophys. Un., 57: 269.

Flood, R.D., Lonsdale, P.F., and Hollister, C.D., 1976. Microtopography studies in the Rockall Trough, northeastern Atlantic (abstract). Abstracts with Programs, GSA 1976 Annual Meeting, 8: 868.

Flood, R.D., in press. X-ray mineralogy of DSDP Legs 44 and 44A, western North Atlantic: Lower Continental Rise Hills, Blake Nose, and Blake-Bahama Basin. In: Benson, W.E., Sheridan, R.E., et al., Initial Reports of the Deep-Sea Drilling Project, v. 44, Washington (U.S. Gov't Printing Office).

Flood, R.D., Hollister, C.D., and Lonsdale, P.F., in preparation. Distruption of the Feni Sediment Drift by debris flows from Rockall Bank. Marine Geology.